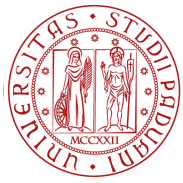

UNIVERSITÀ
DEGLI STUDI
DI PADOVA

Sede Amministrativa: Università degli Studi di Padova

Dipartimento di Ingegneria Civile, Edile ed Ambientale

SCUOLA DI DOTTORATO DI RICERCA IN: Scienze dell'Ingegneria Civile ed Ambientale
INDIRIZZO: Via Loredan 20, 35131 Padova
CICLO XXVII

TECHNIQUES FOR SUSTAINABLE BUILDING MATERIALS PRODUCTION: RECYCLING IN CONCRETE INDUSTRY

Direttore della Scuola: Ch.mo Prof. Stefano Lanzoni
Supervisore: Ch.mo Prof. Carlo Pellegrino

Dottorando: Flora Faleschini

Acknowledgements

The author gratefully acknowledges Prof. Carlo Pellegrino (University of Padova) for giving her the opportunity to work on this topic during the PhD studies. The author would like to thank Prof. Enric Vázquez, Prof. Marilda Barra and Dr. Diego Aponte (UPC Barcelona) for their guidance and for giving the opportunity to work with them in Barcelona. Prof. Enzo Martinelli and Prof. Ioanna Papayanni are also gratefully thanked for their helpful comments and revisions of this thesis. The author would like to express her appreciation to the Italian companies which provided the financial support for the experimental campaigns and for providing the materials used: Zerocento S.r.l., Calcestruzzi Zillo S.p.A, Enel S.p.A., Egap S.r.l. Lastly, special thanks to my family, friends and colleagues for giving all their support, encouragement and patience during the last years.

Abstract

The excellent mechanical and durability properties, with its large availability and affordable costs, make concrete the most used engineered material, with an estimated worldwide consumption about 6 billion tons per year. The prices of this wide diffusion lie into the relevant environmental emissions associated to concrete industry: concrete production is in fact one of the main responsible of carbon emission in atmosphere, mainly due to cement manufacturing and natural aggregates extraction. Together with the energy requirements, water consumption and generation of construction and demolition waste, these factors contribute to the general appearance that concrete is not particularly compatible with the demands of sustainable development.

Several operations can be applied to limit concrete impacts: the replacement of Portland cement with supplementary cementing materials (SCMs) and the use of recycled aggregates in place of natural resources are solutions that may achieve the aim of reducing concrete emissions during all its life cycle. Between the various recycled materials which can be suitable in concrete applications, promising results were obtained when limited quantities of recycled aggregates from construction and demolition wastes (C&DWs) and from electric arc furnace (EAF) slag are used, generally not affecting mechanical properties and environmental compatibility. Nevertheless, in the most of cases a lack of standardized rules hinder their use at market level, in particular when recycled aggregates or mineral additions come from metallurgical industry.

In this thesis the use of two types of recycled aggregates for structural concrete production is explored: EAF slag as recycled aggregates and recycled aggregates from C&DW. In addition, the use of supplementary cementing materials is analyzed, paying particular attention on the suitability of the application of co-combustion fly ash in structural concrete.

Two extensive experimental campaigns were carried out to analyze the main mechanical and durability-related properties of recycled concrete with EAF slag. Several mixes with increasing substitution ratios were produced, using both the coarse and the fine aggregates. A specific chemical and micro-structural in-depth examination was carried out in order to evaluate the actual stability of the material, the influence of the substitution ratio on hardened concrete properties and to study the aggregates-matrix bond when detrimental cycles were applied to concrete specimens. Once determined the suitability of some of the substitution ratios used, for the first time real-scale reinforced concrete beams with EAF slag were realized and tested for bending and shear failure, and their structural behavior is analyzed and discussed.

The second part of the thesis deals with the use of recycled aggregates coming from C&DWs, to assess their influence on the rheological behavior of fresh concrete. An experimental campaign was conducted, and since slump value is often operator-sensitive, a more quantitative estimate was derived in terms of fundamental physical quantities, such as plastic viscosity and yield stress, by means of viscometer measures. The variables analyzed were the aggregates substitution ratio and proportioning method, the super-plasticizer content and the water/cement ratio.

Lastly, an experimental campaign was performed to compare the effects of two different (SCMs) on mechanical and durability-related properties of structural concrete. Three mixes were produced, where coal and co-combustion fly ashes were used as partial substitute of cement (20% in volume) and compared with a reference concrete.

An environmental impacts' assessment was also performed, through a Life Cycle Analysis (LCA) framework specifically developed for concrete emissions evaluation, using a cradle-to-gate approach. Assessment is based on Italian LCI data, collected directly from local EAF slag treatment plant, a natural aggregate extractive plant and a C&DW processing plant.

Sommario

Le eccellenti proprietà meccaniche e di durabilità, unitamente alla sua grande disponibilità ed il suo basso costo, fanno del calcestruzzo il materiale da costruzione più utilizzato al mondo, con un consumo globale di circa 6 miliardi di tonnellate all'anno. A fronte di tale diffusione, il prezzo a livello di emissioni ambientali risulta essere gravoso: l'industria del calcestruzzo è infatti una delle principali responsabili delle emissioni di anidride carbonica in atmosfera, in particolare dovute alla produzione di cemento ed all'estrazione di inerti naturali. Inoltre i grandi consumi energetici e di acqua, e la generazione di scarti dalle attività di demolizione, rendono il calcestruzzo, nella sua forma tradizionale, un materiale non adatto al concetto di sviluppo sostenibile.

Al fine di ridurre i grandi impatti ambientali associati all'industria del calcestruzzo, è possibile ricorrere a varie opzioni, tra cui la sostituzione dei leganti tradizionali (cemento Portland) con materiali innovativi oppure l'utilizzo di aggregati riciclati. Queste due soluzioni permettono di ridurre il consumo delle risorse naturali ed incrementano la vita utile di materiali altrimenti destinati a conferimento in discarica. In particolar modo, l'attuale letteratura ha evidenziato come buoni risultati possano essere ottenuti qualora aggregati riciclati provenienti da scarti demolizione (noti con la sigla C&DWs) e scorie di acciaieria da forno elettrico ad arco (EAF slag) siano utilizzati in limitati rapporti di sostituzione rispetto l'inerte naturale.

Nel corso di questo lavoro di tesi si illustreranno i risultati ottenuti nel corso di due campagne sperimentali, nelle quali sono state analizzate le potenzialità relative all'utilizzo di scorie EAF e aggregati provenienti da scarti C&DWs, per la produzione di calcestruzzi strutturali. Inoltre sono stati analizzati gli effetti legati all'utilizzo di leganti non tradizionali, come le ceneri di co-combustione, sulle proprietà meccaniche e di durabilità di calcestruzzi strutturali.

Sono state svolte prove meccaniche e di durabilità su calcestruzzi contenenti scorie EAF, producendo varie miscele, con rapporto di sostituzione dell'inerte crescente, utilizzando sia la frazione fina che grossa dell'aggregato riciclato. Sono state condotte prove chimiche e microstrutturali al fine di valutare la compatibilità ambientale del materiale, la sua stabilità dimensionale, l'influenza del rapporto di sostituzione sulle proprietà meccaniche ed infine per studiare il legame di aderenza fra la matrice cementizia e l'inerte, in particolare una volta che i provini sono stati soggetti a cicli ambientali. Una volta determinata l'efficacia di talune miscele, sono state realizzate per la prima volta delle travi a scala reale, armate a flessione e taglio, e ne è stato studiato il comportamento strutturale tramite prove a flessione a quattro punti.

La seconda parte della tesi riguarda l'utilizzo di aggregati riciclati provenienti da scarti di demolizione (C&DWs), e l'influenza del loro utilizzo rispetto le proprietà di lavorabilità dei calcestruzzi freschi. Una ulteriore campagna sperimentale è stata realizzata al fine di valutare le proprietà reologiche di diverse miscele, utilizzando un reometro cilindrico concentrico (reometro di Couette). I parametri di indagine sono stati il rapporto di sostituzione dell'inerte, il metodo di proporzionamento dello stesso, il contenuto di additivo fluidificante ed il rapporto acqua/cemento.

Per quanto riguarda le soluzioni volte alla riduzione degli impatti ambientali legate alla riduzione della quantità di leganti tradizionali nei mix design, è stata condotta una campagna sperimentale volta al confronto di alcune proprietà meccaniche e di trasporto di calcestruzzi strutturali contenenti due tipologie di ceneri volanti, sia di carbone che di co-combustione, con un rapporto di sostituzione pari al 20% in volume del dosaggio nominale di cemento

È stata inoltre redatta una procedura per la valutazione comparativa degli impatti ambientali dovuti alla produzione delle scorie EAF, degli inerti naturali, e di quelli riciclati da C&DWs. Tale procedura permette anche il confronto degli impatti dei calcestruzzi prodotti con tali materiali, tramite una analisi a ciclo di vita del materiale, utilizzando un approccio dalla culla al cancello. L'analisi è stata condotta utilizzando un inventario di dati italiano, direttamente raccolto presso gli impianti di produzione delle scorie EAF, degli aggregati riciclati ed una cava di aggregati naturali.

Table of Content

List of Figures

List of Tables

1 Introduction

The recycling of building materials has relatively ancient origins, since when Romans use construction waste such as ceramics in the so-called opus caementicium, the roman concrete. However, from long time ago until nowadays, actual recycling of mineral fraction of demolition wastes is more an exception than a rule, due to the fact that generally those materials have weaker mechanical properties than the virgin aggregates, if not properly treated and processed. For centuries, the construction industry has been a voracious consumer of raw materials, causing also great stream of wastes, which needed to be landfilled. An enormous amount of space was dedicated to the disposal of those materials, leading to the increasing of the ecological footprint of construction market.

In the last decades the research community was pushed to study new fields of application for the wastes coming from construction and demolition operations, driven both by the arise of an environmental consciousness in the society, and also by the realization of the possible depletion of non-renewable natural resources, at least at local scale. Therefore, the concrete industry is being encouraged to improve its efforts for a sustainable development, improving the use of supplementary cementing materials (SCMs) for the reduction of ordinary Portland cement use, and in addition to improve the use of by-products from other industries and aggregates coming from construction and demolition waste (C&DWs) in place of virgin ones. As a consequence, nowadays it is almost everywhere recognized the environmental necessity of recycled aggregates use, even if in several countries, also in the UE, their implementation in the market still remains a challenge. Similarly to construction and demolition waste, also refuses from the metallurgical industry can be applied for building materials production, even though their suitability is limited by a number of factors, including environmental compatibility, dimensional stability, mechanical strength and chemical reactivity.

Concerning the scientific research related to the investigation of recycled materials for building products, promising results have been obtained in the last decades, which lead to the development of green concretes which can be potentially ready-applied into the market, even though the current research has mainly been focused on small specimens. Literature regarding non-structural applications of those materials is abundant, and also the current design codes/recommendations/ guidelines allow the use of recycled aggregates in a number of applications. However, a limited number of real structural applications were studied in

literature, and they were principally related to concretes with C&DW as recycled aggregate. The use of recycled aggregate for structural purposes is also accepted by the current design codes, but generally aggregates origin and the strength class of the structure where it will be placed limit its maximum content (i.e. Table 11.2.III, Italian Code D.M. 14/01/2008). In addition, often research studies have been focused on limited concrete properties, i.e. mechanical strength or some durability-related properties, but a huge gap of knowledge remain still open on a number of aspects, such as concrete rheology or deterioration in aggressive environments. Very limited research exists about the application of metallurgical slag for building material applications.

In this work the use of recycled aggregates both coming from metallurgical industry and C&DWs is explored for structural purposes. The main physical-chemical and micro-structural characteristics of the aggregates have been analyzed. An extensive experimental campaign has been conducted with the aim of analyzing both the mechanical and the durability-related properties of concretes with electric arc furnace (EAF) slag as aggregates. The exposure of the produced concretes in detrimental environments was thoroughly analyzed. In addition, the structural behavior of real-scale reinforced concrete beams made by EAF concrete was for the first time investigated. The main result of this work is that the use of steel slag as aggregate in RC structural elements is, in principle, possible, and the rate of substitution could reach the entire part of coarse aggregates, obtaining benefits both from an economical and environmental point of view. Those benefits were quantified by means of an assessment of the environmental emissions through a life cycle assessment approach: a LCA framework was properly developed to compare the aggregates productive processes and their use in concrete.

Concerning the use of C&DWs in concrete, an experimental campaign with the aim of study the rheology of fresh recycled concretes was for the first time performed. This research was specifically intended to analyze a limited property of fresh concrete, often analyzed in a simplified manner by means of operator-sensitive test methods, and which has a fundamental impact on the placement operations of real structure. A numerical model was used to compare the results, and to verify the potential occurrence of phenomena such as plug flow and gravel migration inside the batches.

Lastly, the use of two types of SCMs was also analyzed: a light-brown coal-fly ash (CFA) and a dark-grey co-combustion fly ash (CCFA), both produced in a full-scale coal-fired power plant. Performances investigated included fresh concrete properties, compressive and tensile strength, elastic modulus, permeability, capillarity and drying/wetting resistance.

This thesis is subdivided in four main sections: the first presents the state-of-the-art about the use of recycled components for concrete

production; the second deals with the use of EAF slag as recycled aggregates; the third is about rheology of fresh recycled concrete; the last one investigates the suitability of new recycled binders application in structural concrete. At the end of each chapter, the main derived conclusions are reported, within the list of references cited in each section. Lastly, future developments and the on-going work are reported.

2 State-of-the-art

In recent years, problems linked to industrial material landfill disposal has become more and more relevant to society, with cost increases for environment and municipalities. Directive 2008/98/EC of European Parliament and Council established the legislative framework for handling of waste in Europe [2.1]: the first objective was the minimization of negative impact of waste management on human health and environment, applying waste hierarchy, and supporting reduction of natural resources. As a consequence, waste reutilization becomes attractive to reduce economical costs and potential pollution problems, and preserve natural raw resources. In this context, construction materials are very significant because they represent the 3 to 4% of the total product in Europe and their environmental impact related to the use of natural aggregates in traditional concrete could be limited using a series of alternative solutions. Nowadays, there are, among others, two significant possibilities to reduce the use of natural aggregates: the use of recycled concrete from construction and demolition waste (C&DWs) [2.2, 2.3, 2.4] and the use of slag from metallurgical industrial production [2.5, 2.6, 2.7, 2.8]. On the other hand, the use of supplementary cementing materials (SCMs) can reduce the great environmental emissions due to cement use.

2.1 C&DWs

All the waste materials coming from construction and demolition operations are known as C&DWs. This material typically comprises large quantities of inert mineral materials, with smaller amounts of a range of other components. Typical materials that can be found inside C&DW are:

- concrete;
- bricks, tiles and ceramics;
- wood;
- glass;
- plastic;
- bituminous mixtures and tars;
- metals (ferrous and non-ferrous);
- soils and stones;
- insulation materials (including asbestos);
- gypsum-based materials (including plasterboards);
- chemicals;
- waste electronic and electrical equipment (WEEE);

- packaging materials;
- hazardous substances.

In this list several hazardous substances appear, which are generally present in building materials because they are used, together with concrete, for completing the structure and for realizing the finishes. These substances are asbestos (found in insulation, roofs and tiles and fire-resistant sealing), lead based paints (found on roofs, tiles and electrical cables), phenols (in resin-based coatings, adhesives and other materials), polychlorinated biphenyls (PCBs) (which can be found in joint sealing and flame-retardant paints / coats, as well as electrical items) and polycyclic aromatic hydrocarbons (PAHs) (frequently present in roofing felt and floorings). The composition of C&DW generally varies highly in relation to the site, because of the local typology and construction technique, climate conditions, economic activities and technologic development of an area, and hence it is difficult to define univocally a composition representative for a large region. As an indicative data, also inside a single Member State, the C&DW composition can be very different: for instance in Northern Italy, soils and stone represent the 17% of the whole waste, but in Central Italy this datum decreases until the 4% [2.9].

The official data regarding the non-hazardous inert wastes' recycling in Italy indicate that there are about 52 million tons of C&DWs produced per year [2.9], even though this number is poorly reliable. Between these, a relevant number of this waste is constituted by contaminated soils, which are generally also sent to inert waste treatment plants. However, during the process of recycled aggregate production, the undesirable fractions are eliminated, and through grading sorting, recycled aggregates are finally obtained. Also at the European level, the statistical significance of figures about C&DWs production is quite poor, and the different available sources are reporting fragmented data and several discrepancies. According to the Eurostat, the C&DWs production of the European countries in 2010 is reported in Table 2-1.

Table 2-1. C&DWs European production [2.10].

State	(x 1000 ton)	State	(x 1000 ton)
Belgium	22 239	Lithuania	357
Bulgaria	2 235	Luxembourg	8 867
Czech Republic	9 354	Hungary	3 072
Denmark	3 176	Malta	988
Germany	190 990	Netherlands	78 064
Estonia	436	Austria	9 010
Ireland	1 610	Poland	20 818
Greece	2 086	Portugal	11 071
Spain	37 497	Romania	238
France	260 226	Slovenia	1 509
Croatia	8	Slovakia	1 786
Italy	59 340	Finland	24 645
Cyprus	1 068	Sweden	9 381
Latvia	22	United Kingdom	105 560
Liechtenstein	0	Norway	1543

2.1.1 Processing procedures for RACs

Two categories of plants are available for treating C&DWs and processing them into recycled aggregates: stationary and mobile ones. In the latter, the same equipment (screens, crushers, magnetic separators, etc.) is furnished by modules that allow recycling operations directly on the site, instead of in the fixed installations. These last may have the disadvantage of being far from the site where demolition takes place, but generally the system is more productive (and therefore the burden of transport is compensated by the quality of the product and the higher capacity of the plant). In both, the processes which are involved are the following:

- separation;
- crushing;
- separation of ferrous elements;
- screening;
- decontamination and removal of impurity (i.e. wood, paper, plastics,...).

A simplified scheme of C&DWs treatment plant is represented in Fig. 2-1.

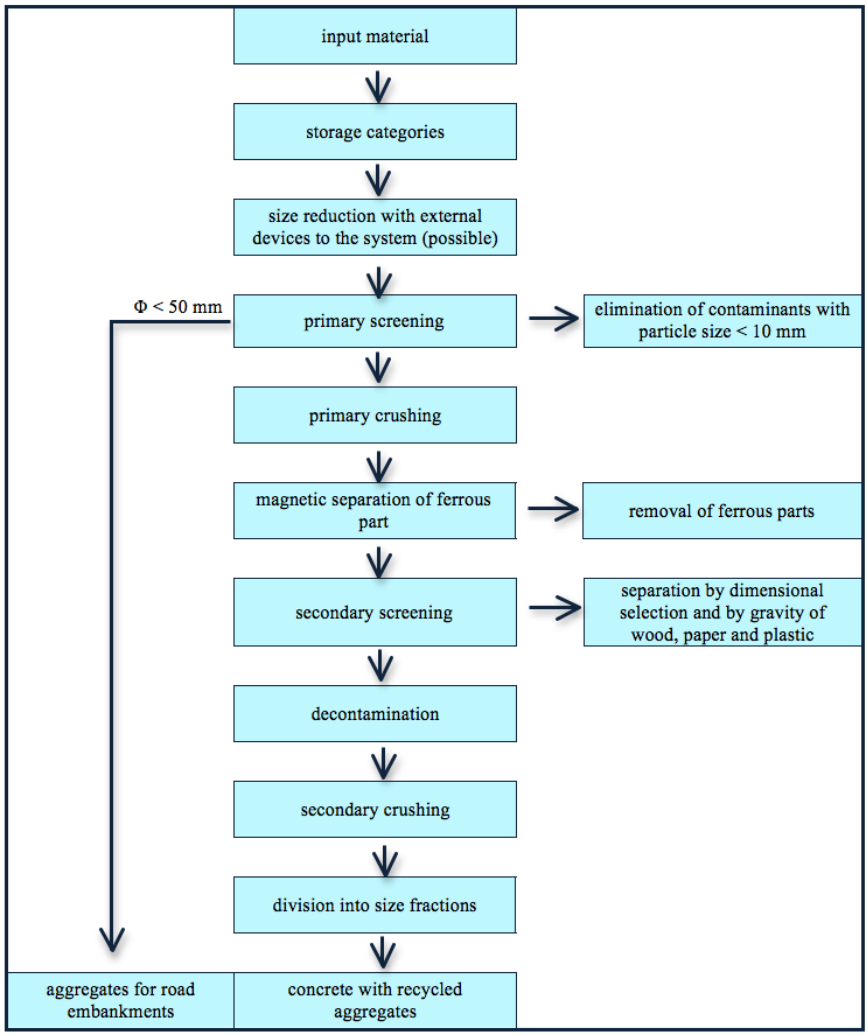

Figure 2-1. Scheme of a C&DWs treatment plant.

Recycled aggregates produced from a C&DWs treatment plant are subjected to regulations which are very different from country to country. The following nomenclature will be used from here on:

- RCA = recycled concrete aggregate;
- RAC = recycled aggregate concrete;
- CRCA = coarse recycled concrete aggregate;
- RA = recycled aggregate;
- NA = natural aggregate;
- NAC = natural aggregate concrete;

2.1.2 International Codes, Guidelines and Regulations

In the Netherlands, the current codes allow the use of recycled aggregate for concrete manufacturing for pre-stressed and reinforced structures. The requirements that the RA should satisfy are reported in the NEN 5905 [2.11] and NEN-EN 12620 [2.12] standards, and relate the coarse aggregate fraction 4/32mm.

In Belgium, recycled concrete aggregates can be used in the exposure class X0 and XC1, and Belgian environmental classes E0 and E1, with a maximum strength class limited to C25/30. For use in other environments and strength classes, the suitability should be experimentally demonstrated. The maximum substitution ratio allowed is about 20% in volume of the total coarse aggregates in the mixture.

Great Britain and the countries of the former Russian Federation limited the use of recycled concrete to the production of road surfaces or underpinning works [2.9].

In the United States there is no regulatory barrier to the use of recycled concrete aggregate in structural concrete: since 1982, ASTM C33 [2.13] has included crushed hydraulic cement concrete in its definition of coarse aggregate, while ASTM 125 [2.14] allowed crushed hydraulic-cement concrete as manufactured sand. However the use of recycled concrete aggregate still remains limited for structural purposes.

In Germany, the use of recycled aggregate is summarized in the standard DIN EN 4226-100 [2.15], where some specifications about the aggregates requirements in relation to the field of application are defined. Only the chipping of concrete according to type 1 and type 2 (as defined in the above standard, and reported in Table 2-2) can be used for concrete production, and the crusher sand is excluded from the reuse as aggregate (minimum RCA diameter: 2 mm). Further limits are reported in the German Committee for Reinforced Concrete (DAFSTB) Code [2.16]: Concrete with Recycled Aggregate, where a limitation on the strength class (C30/37) and on the substitution ratios are given in relation with the exposure class and application (Table 2-3).

Table 2-2. German standards on RA, as defined in DIN EN 4226-100 [2.15].

Constituents (% by mass)	*Type 1 Concrete chipping/ concrete crushed sand*	*Type 2 Construction chipping/ construction crushed sand*	*Type 3 Masonry chipping/ masonry crushed sand*	*Type 4 Mixed chipping/ mixed crushed sand*
Concrete and NA acc. to DIN 4226-1	*≥ 90*	*≥ 70*	*≤ 20*	*≥ 80*
Clinker, non-pored bricks	*≤ 10*	*≤ 30*	*≥ 80*	
Sand-lime bricks			*≤ 5*	
Other mineral materials (i.e. pored bricks, lightweight concrete, no-fines concrete, plaster, mortar, porous slag, pumice)	*≤ 2*	*≤ 3*	*≤ 5*	*≤ 20*
Asphalt	*≤ 1*	*≤ 1*	*≤ 1*	*≤ 1*
Foreign substances i.e. glass, non-ferrous metal slag, lump gypsum, wood, plant residue, paper, ...)	*≤ 0.2*	*≤ 0.5*	*≤ 0.5*	
Oven dry density (kg/m³)	*≥ 2 000*	*≥ 2 000*	*≥ 1 800*	*≥ 1 500*
Maximum water absorption after 10 min (%)	*10*	*15*	*20*	*No requirements*

Table 2-3. Permissible substitution ratio (in % by volume) according to DIN EN 206-1 [2.17] and DIN 1045-2 [2.18].

Field of application		*Type 1*
Dry	*Exposure class XC 1*	*≤ 45*
Humid	*Exposure class X 0*	*≤ 45*
	Exposure class XC 1 to XC 4	*≤ 45*
	Exposure class XF 1 and XF 3	*≤ 35*
	Exposure class XA 1	*≤ 25*

In Italy, there is a similar approach to the German one, and the limitations to the recycled concrete aggregates are reported in the D.M. 14/01/2008 [2.19]. The regulatory does not provide any information about the values of mechanical or physical properties that the recycled aggregates should comply with; although, these limits are present in the EN standards, and in particular in the UNI EN 12620 "Aggregates for Concrete" [2.20]. This standard defines the properties needed by the aggregates to comply with the requirements stated in the UNI EN 206-1 "Concrete - Specification, performance, production and conformity" [2.21]. The Italian UNI 8520-1 [2.22] and UNI 8520-2 [2.23] provide some complementary instructions necessary to apply the above standard. Lastly, UNI EN 13242 "Aggregates for unbound and hydraulically bound materials for use in civil engineering work and road construction" [2.24] provides the possible applications of recycled aggregates in specific fields, i.e. civil engineering work and road construction.

Table 2-4. Percentage of use of recycled aggregates in concrete in Italy [2.19].

Origin of recycled aggregate	*Concrete Class*	*Rate of Use*
Demolition of building (debris)	*= C8/10*	*Up to 100%*
Demolition of concrete or reinforced concrete	*≤ C30/37*	*Up to 30%*
	≤ C20/25	*Up to 60%*
Reuse in certified precast concrete industries - any class of concrete	*≤ C45/55*	*Up to 15%*
Reuse in certified precast concrete industry - class of concrete > C45/55	*Same class of original concrete*	*Up to 5%*

In Portugal the use of recycled aggregates for structural purposes is regulamented by the LNEC E 471 standard [2.25]: this specification classifies coarse recycled aggregates and defines minimum requirements for their use in concrete. Replacement level is defined in accordance with the exposure and strength class of the structures were they will be placed. The use of fine recycled aggregates for concrete production is not allowed. In addition, concrete produced with recycled aggregate could not be used in structures in contact with water for human consumption.

Also in Spain there is a limitation in the substitution ratio for structural concrete applications (about 20% in volume of the whole coarse aggregates), as defined in the Structural Concrete Instruction EHE-08 [2.26], in relation to the strength class of the structure, whereas for non-structural concretes the rate of use can reach the whole percentage of the aggregates.

2.1.3 RAC concrete - Mixture Proportioning

For satisfactorily high quality levels of concrete, recycled aggregate must comply with some minimum requirements, as above reported, mainly concerning chemical stability and physical–mechanical characteristics. However, mix proportions also greatly influence the final performance of concrete. In particular, the design of recycled aggregate concrete (RAC) is usually carried out by simply replacing the Natural Aggregate (NA) of a Natural Aggregate Concrete (NAC) with recycled material, and only taking into account some of the differences in physical properties among aggregates, such as surface texture and water absorption. In general terms, Recycled Aggregate (RA) is taken as NA, and this is the main cause of the poor mechanical performance often reported in the literature when different kinds of RAC mixes are tested [2.27, 2.28, 2.29].

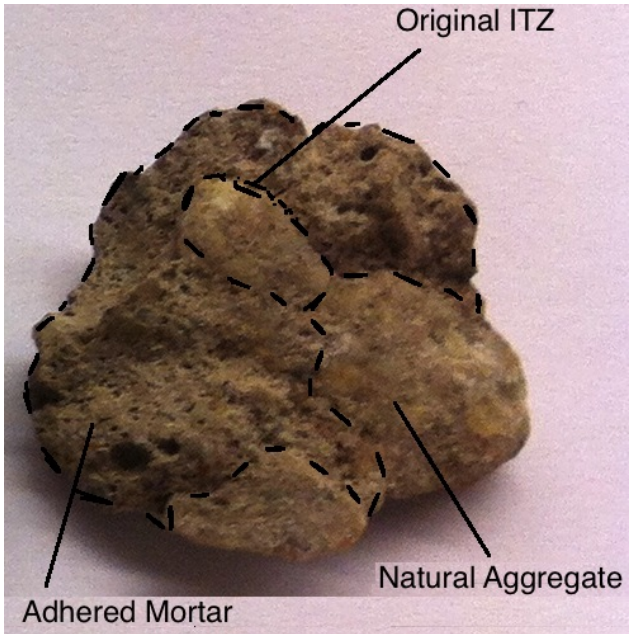

Figure 2-2. Recycled concrete aggregate.

Here, a novel method called Equivalent Mortar Volume (EMV) can be a suitable solution [2.30] to allow the recycled concrete to gain higher strength, because it considers RA as a two-phase material composed of NA and the mortar attached to it, which must be quantified and counted in the proportion. Since the physical properties of RA are affected by the attached mortar quantity and characteristics, this method can directly account for any deficiencies in low-quality aggregate, balancing the mix without affecting the mechanical and durability-related performance of the

final concrete. This allows the RAC mix to be prepared with a similar internal structure to that of NAC [2.30, 2.31, 2.32].

As regards possible workability problems, replacement of NA by RA generally confers greater stiffness, as confirmed by the lower slump values often reported in the literature. Several authors have confirmed this problem [2.33, 2.34], arguing that the reasons for this behavior are closely related to the physical properties of the RA, such as high water absorption, higher angularity, or rough surface texture. This problem can be overcome by the use of water-reducing admixtures in the mix [2.35] or by certain mixing procedures for RACs. The commonly named Mixing Water Compensation Method [2.36] for elaborating concrete, based on added water which recycled aggregate absorbs to the total needed by the mix, allows acceptable workability to be achieved. In the case of EMV methodology, the parameters controlling workability should be carefully taken into account, due to the reduced amount of fresh mortar in the mix in favor of increased coarse aggregate volume.

2.1.4 RAC concrete - Mechanical Properties

Concrete strength is the key mechanical property of structural concrete. Uniaxial strength in compression is accepted as a general index of compressive strength, which is also related to the strength under other stress states, i.e. tensile and flexural strength, elastic modulus, etc. There are several factors affecting concrete strength, starting from the water/cement ratio, which is particularly important because it directly governs concrete porosity and the quality of the interfacial transition zone (ITZ). In addition, aggregate size and mineralogy, and the substitution ratio of recycled aggregates are also particularly relevant in influencing concrete strength: aggregate quality, as also briefly said in the previous section, can highly affect RAC concrete properties due to the quantity of the adhered mortar attached to the virgin aggregates in RCA, which has generally poor mechanical properties. Concerning the quality of the microstructure of ITZ in RAC, as reported in [2.37], SEM observations revealed that the aggregate-cement matrix interfacial zone is very porous with respect to the same ITZ in a conventional concrete, which is denser. Increasing substitution ratio generally decreases mechanical strength, as obtained in numerous research works [2.27, 2.28, 2.29]. A linear relation between RAC density (depending hence on RCA substitution ratio, which has a less specific weight than NA) and compressive strength was also obtained in [2.38]. However, the quality of recycled aggregate, in terms of adhesive mortar strength, affects the strength of recycled aggregate concrete when the water-binder ratio is low. The quality of recycled

aggregate does not affect the strength of recycled aggregate concrete when the water-binder ratio is high. Admixture types and content, within the rate of loading also influence RAC quality and strength.

2.1.5 RAC concrete - Durability

Durability of RAC can be evaluated in a number of ways, depending on the deterioration processes we want to represent at laboratory scale. Generally the lower properties of recycled aggregates, i.e. the lower density and mechanical strength, within the higher absorption, determine RAC to be less durable in terms of carbonation, chloride penetration, permeation, and freezing/thawing resistance [2.39]. Another internal source of possible deterioration arises from the possible contamination of recycled aggregates by gypsum or admixtures and binders, which lead to an increased content of sulfates inside the mix [2.40]. The same may occur if recycled aggregate is contaminated by chlorides, which can lead to an internal source of chlorides inside the mix. In both the cases the addition of mineral admixtures, such as fly ash, can reduce the chloride penetration depth, in particular at low water/cement ratio (a factor which also, per se, improves RAC durability). It has to be recalled that also the mixture proportioning method may affect concrete durability, and recent literature results demonstrated that, when the EMV method is used, durability-related properties are improved, i.e. for the chloride penetration depth.

2.1.6 RAC concrete - Structural Applications

A number of experiments on structural elements have been conducted in literature, with the aim of analyzing structural properties of real-scale elements. One of the most important property that was analyzed is related to the flexural behavior of reinforced recycled concrete beams: a typical load scheme which can be found in many papers involves simply supported beams subjected to four point bending tests. In this test, the specimens are loaded at two points symmetrically about the center of the section. Generally, the flexural behavior is discussed with reference to virgin concrete beams, in which the reinforcement ratio, curing conditions, water/cement ratio are maintained constant. The parameters which are often analyzed are the load, the deflection at the span center, and if it is possible, the tension in the reinforcement.

Flexibility of RAC beams are generally larger than those with NA concrete, under the conditions of same bending moment, w/c ratio, steel reinforcement ratio. In addition, RAC beams experience often wider cracks

and smaller crack spacing, with a lower flexural strength compared to the companion conventional concrete members. This kind of results may discourage the use of this material, because it generates uncertainty with respect to the serviceability and long-term performances of RCA concrete structure [2.41, 2.42]. Nevertheless, when high quality of RAC are used, or when EMV proportioning method is applied, also structural properties highly improve: at both the service and ultimate states, the flexural performance of reinforced RCA-concrete can be comparable or even superior to that of concrete made entirely with natural aggregates. In this last case the general flexural theory based on equilibrium equations and the current code provisions for flexural design of conventional RC beams seem to be satisfying also RAC beams design [2.43].

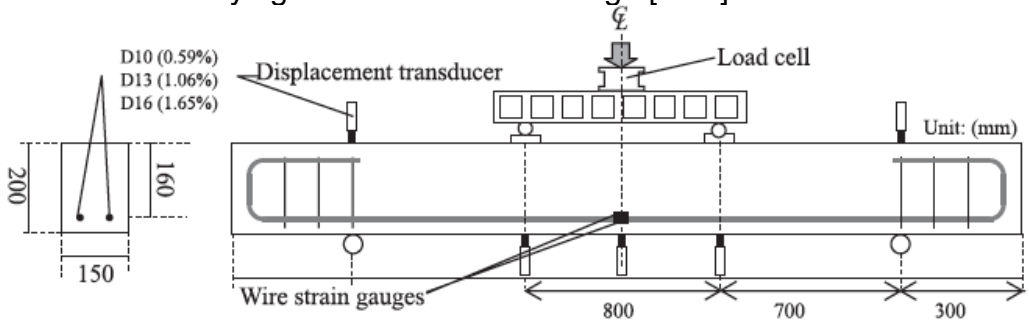

Figure 2-3. Load scheme for flexural behavior analysis of RAC beams [2.41].

Unlike in RC beams subjected to flexure, where longitudinal reinforcement has a prior role in the structural response, concrete plays a more significant role in beams subjected to shear loading. In fact, the shear behavior is governed by the shear capacity of the reinforcement, as well as the concrete shear capacity. Also in this case a number of works have tried to assess the influence of RAC in the response of RC beams subjected to shear, both when transversal reinforcement was present or not.

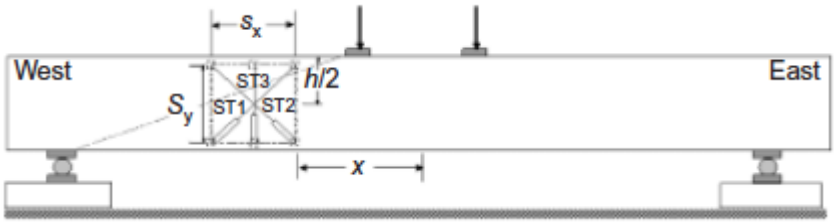

Figure 2-4. Arrangement of LDTV-rosette for sheared deformation measurements.

In general, shear strength of the RAC beams is lower than that of the NAC beams with the same reinforcement ratio and shear span-to-depth ratio [2.44, 2.45]. Nevertheless, as it occurs for almost all the cases, also with NA concrete, current codes and existing models overestimate shear

capacity of RC members; hence, the use of RCA does not primarily determine uncertainty in the predictive shear capacity models. The same consideration given for the flexural behavior can be given if high-quality RA is used.

Lastly, Corinaldesi et al. investigated also the behavior of reinforced beam-column joints under cyclic loading, to assess the seismic performance of the RC frame joints [2.46]. The parameters observed were the failure modes, the hysteresis loops, the ductility and the variation of strength and stiffness under the seismic loads. The joint made of RAC showed adequate structural behavior, however, to achieve safe structural performance, the actual RAC shear strength and stiffness should be considered during the design.

2.2 Metallurgical slag

There are several kinds of slag that could be used in concrete production, depending on their final destination, as cement or aggregate replacement. Among the materials that are currently used, at lab-scale or already regulated, there are Granulated Blast Furnace slag (GBS) and Air-cooled Blast Furnace slag (ABS), both generally used as supplementary cementing material. In addition, Electric Arc Furnace slag - from carbon (EAFC) or stainless/high alloy steel production (EAFS) - can potentially be used as aggregate replacement. Lastly, Basic Oxygen Furnace slag (BOF) has been experimentally used for both the applications. Between these materials, a particular interest emerges about steel by-products, because of the great amount of slag deriving during its production. In fact, the total amount of steel slags generated in 2006 was about 16.9 million tones. In particular, Euroslag divides this amount in: 57.7 % produced as basic oxygen furnace slags, 25.9 % are electric arc furnace slags from carbon steel production, 5.9 % are electric arc furnace slags from high alloy steel production and 11.1 % come form secondary metallurgical slags (Fig. 2-5).

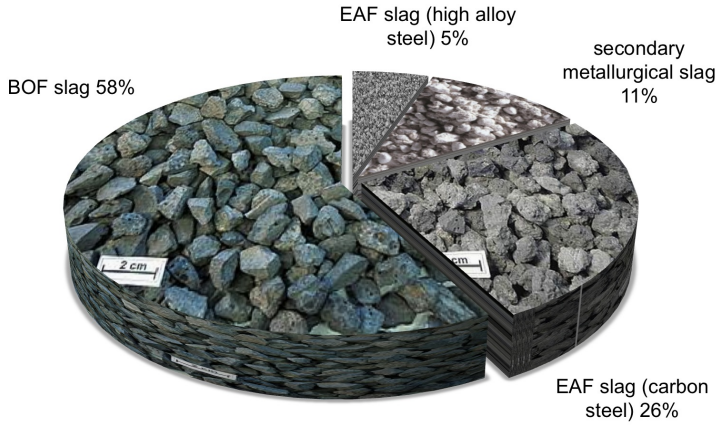

Figure 2-5. Generation of steel slags in Europe in 2006 [2.47].

Steel slag is produced during the separation of molten steel from impurities in steel furnaces. The slag occurs as a molten liquid and is a complex solution of silicates and oxides that solidifies upon cooling. As previously stated, there are several different types of steel slag produced during the steel-making process out of which basic oxygen furnace steel slag (BOF slag), electric arc furnace slag (EAF-slag) and ladle furnace slag (LDF-slag) or refining slag may play an important role in civil engineering applications.

Steel can be produced in electric arc furnaces by melting recycled steel scrap, using heat generated by an arc, created by a large electric current. The slag is formed through the addition of lime, which should remove impurities from within the steel. Slag has a lower density than steel and therefore floats on top of the molten bath of steel.

Basic oxygen furnaces have a different industrial process: hot liquid blast furnace metal, scrap and fluxes, which consist of lime (CaO) and dolomitic lime (CaO-MgO), are initially charged into the furnace. Then, the oxygen, which is injected into the furnace, reacts and removes the impurities in the charge. Those impurities are mainly constituted by carbon as gaseous carbon monoxide, and silicon, manganese, phosphorus and some iron as liquid oxides, which combine with lime and dolomitic lime to form the BOF steel slag.

After being tapped from the furnace, molten steel is transferred in a ladle for further refining to remove additional impurities still contained into the steel. During this operation, known also as ladle refining because it is completed within the transfer ladle, additional steel slags are generated by again adding fluxes to the ladle to melt.

Steel mill scale is produced during processing of iron in steel mills. Here iron oxides, known as mill scale, are formed on the surface of the metal during the continuous casting, reheating and hot rolling operations. Then steel mill scale is removed by water sprays.

According to the specific physical-chemical properties of each kind of slag, a specific use for each type of material can be found: for example, the steel slags are suitable for the amour stone and for air quality control, steel slags and ABS are suitable for gabions manufacture, railway ballast, roofing and for the treatment of waste water, the steel slags and GBS are suitable as sealants and finally the GBS are suitable for sand blasting. In general, both steel slags and blast furnace slag are used for unbound mixtures and hydraulically bound mixtures, for bituminous mixtures, in concrete, in mortar and in embankments. The steel mill scale is similar to steel slag and therefore, like steel slag, it can be used in concrete production. A short list of possible applications is given in Table 2-5.

The use of slag aggregates from iron and steel production in construction has old origins, since when the Romans used crushed slag from the crude iron production for roads building. Nowadays, slag is still used to build roads. Currently they are not only used for road surfaces constructions but also as aggregates of concrete. They must be treated through sieving, crushing and wetting process. These treatments allow their grading, and to fit other related properties in accordance with European product standards or specifications.

Table 2-5. Possible application of steel slags [2.47]

Use	*Blast furnace slag*		*Steel slag (BOS, EAFC and EAFS)*
	GBS	*ABS*	
Unbound and hydraulically bound mixtures	*X*	*X*	*X*
Bituminous mixtures	*X*	*X*	*X*
Concrete	*X*	*X*	*X*
Mortar	*X*	*X*	*X*
Amour-stone			*X*
Gabions		*X*	*X*
Railway ballast		*X*	*X*
Roofing		*X*	*X*
Embankments and fill	*X*	*X*	*X*
Sealants	*X*		*X*
Sand blasting	*X*		
Waste water treatment		*X*	*X*
Air quality control			*X*

From here on, we will refer just to Electric Arc Furnace slag (EAF), because of the great numbers related to its production, which involves approximately 10 million tons every year, and it is destined to grow because of the increase in the use of this technology. In 2009, steel production in Italy represented approximately 14% of the total European steel industry, yielding a considerable quantity of EAF slag during the production cycle [2.47]. EAF slag is the main by-product of steel production, and it could be classified into two types: black basic slag, with a lime content less than 40%, resulting from the cold loading of scrap; and white basic slag, with a lime content higher than 40%, generated during grinding, when more lime is added to remove sulfur and phosphorus from the produced steel [2.48]. An electric arc furnace is a furnace that heats scrap metal or recycled stainless steel by means of an electric arc and it produces steel. The fusion is possible due to an electric arc, which is constituted by three cylindrical electrodes made of graphite, which enter inside the crucible of the furnace from the vault. The components of this type of furnace are three: the first is the hearth, a metal structure lined with refractory material and which is able to oscillate so the inclination of the kiln can be changed (this facilitates the operations of slagging and tapping); the second is the shell, a metal cage which allows to contain the material and then pours it into the oven; finally there is a roof, that can be moved to allow the opening during loading of the material, and it is also envisaged of three holes for the passage of the electrodes, a hole for the extraction of steams produced during the process and a hole to load additives. The first contains both the slag and the molten material or melt. The second and the third components are cooled with water. Additives that may be included are slag formers such as limestone and slag correction agents like bauxites. The operations required to produce steel (and EAF slag) are:

- Furnace charging;
- Melting;
- Refining;
- De-slagging;
- Tapping;
- Furnace turn-around.

Figure 2-6. Slag cooling.

During the steel production, slag is also formed: slag has a lower density than steel and therefore floats on top of the molten bath of steel. Then slag is cooled (generally with water, at least for 24 hours), aged for about two months under the atmospheric conditions, and then it is ready to be treated again for its processing as aggregate. Typical treatments that are made on the EAF slag are:

- Pre-screening;
- Screening;
- Crushing;
- Secondary screening;
- Secondary crushing;
- Magnetic separation;
- Tertiary screening - particle size separation;
- Storage;
- Washing and stabilization.

2.2.1 EAF slag – characterization

EAF slag is a crushed product which generally has very good mechanical properties, constituted by particles with a hard, dense and angular shape. Its characteristics are highly influenced by the productive process and the chemical composition of the metal scraps molted in the furnace.

One of the first research work using this material for concrete production was published in 1997 by Al-Negheimish et al. [2.49], who investigated its potential use by means of tests on the main mechanical properties such as compressive and tensile strength, but no study about the long term concrete properties was done. The slag used was relatively non-porous, with a low absorption rate and with an angular shape that helped in developing very strong interlocking properties. The same characteristics in terms of shape and texture of the aggregates were derived by the further works of Anastasiou and Papayianni [2.50, 2.7], Manso et al. [2.51], Xue et al. [2.52], Ahmedzade and Sengoz [2.53], Pellegrino and Gaddo [2.54]. EAF slag has generally a black color stone appearance, with a rough surface texture, and it is characterized by high abrasion resistance, low crushing value, and a generally excellent resistance to fragmentation. It has a higher bulk density than natural aggregates, and in general, a higher porosity, as also revealed by SEM images taken in [2.49]. Some physical properties of different types of steel slag used as aggregate both in concrete and asphalt mixtures are reported in Table 2-6.

The processing techniques of EAF slag are fundamental to obtain a high-performances material: hence, an adequate grading of the slag is necessary to obtain the required particle grading curves for the intended use. Fig. 2-7 shows two grading curves of coarse and fine EAF slag, within the limits of the ASTM C33 [2.13], as reported in [2.56, 2.56].

Table 2-6. Physical properties of steel slag ([1]: basalt; [2]: granite; [3] quartzite; [4] limestone).

Property	*EAF slag*	*N.A.*	*Reference*
Specific gravity (t/m³)	*3.5*	*2.95¹* *2.70²*	*Manso et al. [2.51]*
Los Angeles (%)	*15-20*	*9-20 ¹* *12-27 ²*	*Manso et al. [2.51]*
Water absorption (%)	*0.3-0.9*	*< 0.5 ¹* *0.3-1.2 ²*	*Manso et al. [2.51]*
Compressive strength (MPa)	*> 130 MPa*	*> 250 MPa ¹* *> 160 MPa ²*	*Manso et al. [2.51]*
Specific gravity (t/m³)	*3.51*	*2.713 ³*	*Almusallam et al. [2.53]*
Los Angeles (%)	*11.6*	*19.2 ³*	*Almusallam et al. [2.53]*
Water absorption (%)	*0.85*	*1.60 ³*	*Almusallam et al. [2.53]*
Specific gravity (t/m³)	*3.51*	*2.54 ⁴*	*Maslehuddin et al. [2.8]*
Los Angeles (%)	*11.6*	*24.2 ⁴*	*Maslehuddin et al. [2.8]*
Water absorption (%)	*0.85*	*2.20 ⁴*	*Maslehuddin et al. [2.8]*
Specific gravity (t/m³)	*3.33*	*2.68 ⁴*	*Papayianni et al. [2.7]*
Percentage of voids (%)	*55.5*	*48.3 ⁴*	*Papayianni et al. [2.7]*
Water absorption (%)	*2.50*	*0.75 ⁴*	*Papayianni et al. [2.7]*
Flakiness Index (&)	*8.0*	*38.4 ⁴*	*Papayianni et al. [2.7]*

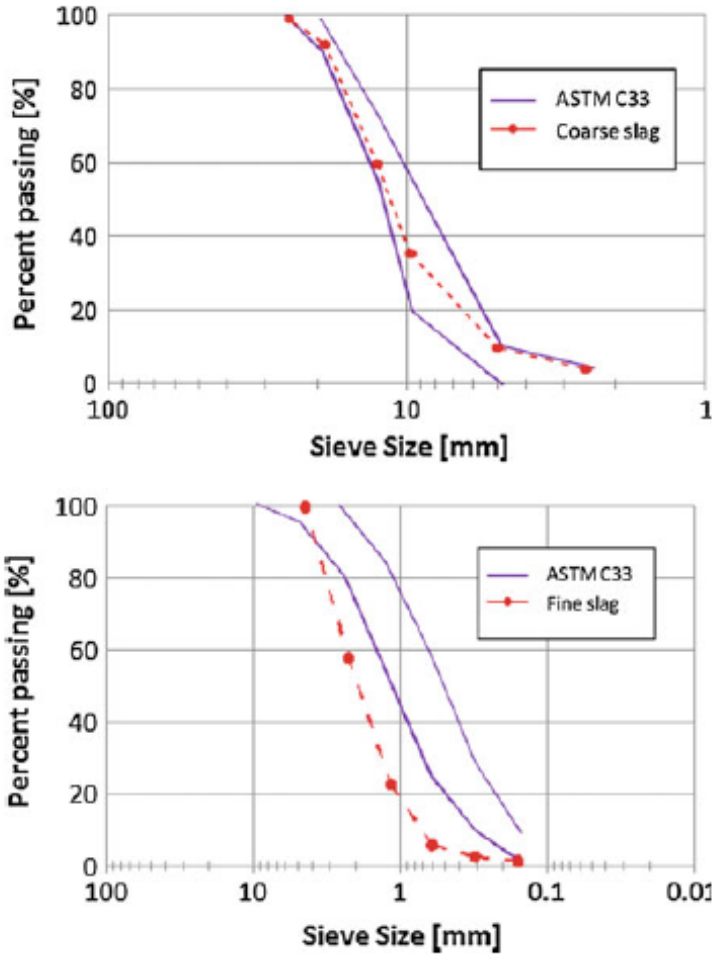

Figure 2-7. EAF aggregate grading curve (coarse and fine) [2.56].

Concerning slag chemical composition, it is very important to define the content of some components such as free lime (CaO) and periclase (MgO), which can lead to aggregates expansion and hence hinder the potential use of those materials in construction industry. In reality those components are often detected in BOF slag, whereas their content is limited in EAF type slag. In every cases, pretreatment operations are recommended to lower the potential presence of these expansive compounds. Ageing and weathering of slag are often applied, as also steam or autoclave curing. Several works in literature have demonstrated the effectiveness of pretreatment operations in reducing the content of potential expansive compounds [2.51, 2.54, 2.56, 2.57].

Table 2-7 lists the chemical composition of some EAF slag used in literature. Steel slag is basic, which means that:

$$(CaO + MgO)/(SiO_2 + Al_2O_3) > 1 \qquad \textbf{2-1}$$

However, in general EAF slag is less basic than LDF and BOF slag. It should be noted that the reactivity of CaO increases with the basicity [2.58], and hence problems of expansion linked to EAF slag seem to be very limited. This result is also confirmed by the mineralogical composition of the slag often reported in literature, which is mainly constituted by the following mineral forms: wustite, hematite, magnetite, merwinite, etc.

Table 2-7. Chemical composition of EAF slag.

	Manso et al. [2.56]	*Pellegrino et al. [2.54]*	*Tossavainen [2.59]*
	Spain	*Italy*	*Sweden*
SiO_2 (%)	*15.30*	*10.1*	*32.2*
Al_2O_3 (%)	*7.40*	*5.70*	*3.70*
CaO (%)	*23.90*	*24.20*	*45.50*
MnO (%)	*4.50*	*5.10*	*2.0*
MgO (%)	*5.10*	*1.90*	*5.20*
Fe_xO_y (%)	*42.50*	*37.20*	*27.41*

2.2.2 EAF slag concrete

Since a long time the use of steel slag in the preparation of blended cement, cement clinker, as aggregate or hydraulic binder in road construction, has been proposed by several authors. However, not much is reported on the use of steel slag as aggregate in preparation of cement mortar and concrete, and when some references are present, they involve mainly the use of EAF slag. Nevertheless, concrete properties analyzed were limited to mechanical characterization or simple fresh concrete workability measurement.

The first complete chemical analysis on EAF slag was conducted in 1999 in Spain [2.48], whereas the firsts works were approached in Germany in 1994 and subsequently in France in 1998. The studies were carried out using optical microscopy, inductively coupled plasma spectroscopy (ICP) for the chemical part, X – ray diffraction (XRD) and infrared (IR) absorption spectroscopy for the mineralogical ones. Also scanning electron microscopy was used to furnish images of the material media. Results obtained present a material with a high porosity, dense and compact, with a surface rich in iron content. Its unit weight appeared high, and with a low water absorption, according to the standard DIN 40 301 “Ferrous and non – ferrous blast furnace slags for building uses” which was active at that time. Also stability was evaluated, because of the

increasing necessity to reveal the potentiality of slag to be used as a building material. Disintegration or expansive compounds represent the main risks for an aggregate to be incorporated in binders: the potential to hydrate expansively becomes a meaningful parameter for the experimentation. Presence of free CaO, MgO, sulphides could lead to this reaction, hence revealing the necessity to monitor the mineralogical phases of calcium and magnesium.

After a couple of years, studies were shifted from the chemical characterization to the evaluation of the suitability of this material as a building material, hence with the aim to establish if slag could be used as an aggregate for concrete. In addition, also its feasibility in asphalt mixtures was often a research topic. In the Arabian areas, where the availability of good-quality aggregate is scarce, a number of researches on slag arose, focusing on the possibility to use the slag as partial replacement of natural gravel. For example, in [2.8] all the coarse aggregates were substituted with EAF slag, maintaining the dune sand constant in both recycled and traditional specimens, in order to evaluate only the coarse fraction substitution effect. Results highlighted that as the substitution ratio increased, compressive strength increased ceteris paribus, fixing the same aggregates grading curve. At the same time, also flexural strength increased, whereas the absorption, volume of permeable voids and pulse velocity decreased, revealing a denser concrete. Furthermore durability tests performed have shown good results, because of the higher impermeability of slag concrete.

One of the most important work on slag appears in 2005 in Spain [2.56], with the aim of analyzing the durability of slag concrete, and in particular it focused about the possible expansion in EAF concrete due to internal compounds (periclase and free lime) by accelerated ageing tests. A study about the effects of this expansion on the mechanical strength was done. In addition, the slag pre – treating processes were analyzed: reduction to standard aggregate sizes following an appropriate crushing, and the successive exposure to weathering over several weeks was found to be a necessary two-phases process to obtain a stabilized product. The correctly performed treatment requires a permanent wetting, homogenization through a periodic turning of the heaps and a minimum weathering period of 90 days, and it provides a significant improvement in stabilizing the slag, both dimensionally and chemically. Another suggestion derived from this study is related to the use of an air-entrainer agent for slag concrete, because of the too high porosity shown, which could deteriorate the concrete in environments subjected to freezing and thawing cycles. A number of specimens were casted, using different substitution ratio for slag and limestone aggregates: in all cases, the mechanical resistance was comparable to the results obtained for the

conventional/traditional concrete, except for the only one made just by slag (100% EAF aggregates), which collapsed and could not be practicable. Accelerated ageing tests were made using American ASTM standards: one was performed in autoclave, one in a moist room, one providing freezing and thawing cycles, one with wetting and drying conditions and the latter was a leaching simulation. Results have shown that the higher is the mechanical strength obtained, and the higher the impermeability performed, with better characteristics. In this work the use of air-entrainer admixture was recommended, because of the losses in strength recorded after thawing/freezing cycles. EAF concrete revealed a high cohesion between cementitious matrix and aggregates, which limited the micro – cracking behavior during ageing.

Another research theme is represented by the possibility to use slag in some percentage as a raw material for Portland cement clinker production. Starting from the knowledge that cement with slag may be weaker than Portland cement, some tests were performed in Greece [2.60], following the experience of BOF slag - cements. EAF slag has a chemical composition similar to that of cement, like most of metallurgical slags. The main difference is the high iron oxide content, which exists in both di- and trivalent states; another difference was evidenced by previous researches, which stated that pozzolanic activity is low if slag is not pre-treated. So, no mechanical differences would be expected in hydration, and only the possible expansion of slag must be evaluated. Specimens with a substitution ratio of about 10.5% were performed, to allow the slag not to affect the hydraulic behavior of the cement produced. XRD analyses were performed, to detect hydration products, and mechanical tests were conducted on small specimens. Results were promising: expansion was under EN 197-3 limit, compressive strength was as good as traditional Portland cement (no significant differences), and the reduction of material costs was high.

Some other works were performed in order to obtain results on the possibility to use slag as fine aggregates in concrete [2.6]. The results have shown a potential use of this material, but an increase of cement content is necessary to do not affect the mechanical strength of EAF concretes.

Also at the University of Padova an initial research work was conducted to assess the potential use of EAF slag [2.54] in structural concrete. The work was focused on the full replacement of the coarse fraction of the aggregates with the slag, and the experimental campaign aimed to analyze the most common mechanical properties and some durability-related properties, i.e. resistance against wetting/drying and freezing/thawing cycles, and accelerated ageing. Results were promising for concrete exposed to those environmental conditions.

2.3 Fly Ash

The use of alternative binders is very common in the concrete industry. Particularly, fly ash (FA) is widely employed as partial replacement of normal Portland cement in concrete, and nowadays around 15–25 % of cement is generally replaced by FA in normal structural concrete mixes. Coal fly ash has been successfully used in concrete industry since more than 50 years, primarily as mineral admixture in Portland cement concrete and also as a component of blended cement [2.61]. Concerning its first use, fly ash can either partially substitute Portland cement or be applied as an addition into ready-mix concrete at the batch plant [2.62, 2.63]. It is generally accepted that the use of those Supplementary Cementing Materials (SCMs) promotes sustainability of concrete industry. Usual structural and durability-related properties were widely analyzed in literature [2.64, 2.65, 2.66]. In addition, several authors have attempted to relate some properties of SCM-concretes with parameters such as fly ash fineness [2.67], glass phase content soluble [2.68] and reactive silica content [2.69], water to powder ratio [2.70] and curing conditions [2.71].

Much higher quantities of FA can be used in concrete if fly ash can partially replace the fine sand fraction in concrete mix, and used as a filler material. This replacement can be made by low quality fly ash too, which has low pozzolanic properties. Although many references are available on the use of fly ash as a SCM in concrete, the number of available references about the use of fly ash as partial replacement of fine aggregates is not very large.

Fly ash represents the most important coal combustion by-product: approximately 6 million tones are actually used in the EU 15 member states as concrete additions. Nevertheless, FA production reaches 1Mt/y in Italy and 40 Mt/y in Europe [2.72]. FA is a product of burning finely ground coal in a boiler to produce electricity: it is removed from the plant exhaust gases primarily by electrostatic precipitators or baghouses, and secondarily by scrubber systems. Within a power station, coal is fed to a series of mills that pulverize the coal (or the combustible matter) to a very fine powder. This powder is then fed into a boiler which combusts the coal to produce heat, which is used to produce steam required for power generation. During the coal combustion process, minerals present in the coal fuse to form glassy alumino-silicate spheres. These spheres remain in suspension within the flue gas from the boiler and they are collected downstream by either electrostatic or mechanical precipitation.

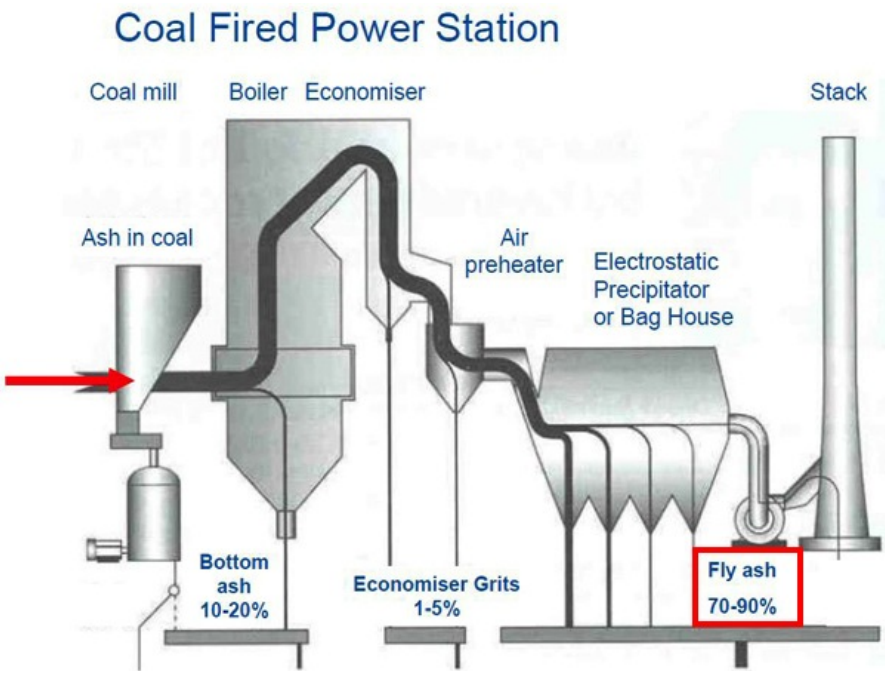

Figure 2-8. Process for the production of FA at a power station.

American Society for Testing and Materials (ASTM) C618-08 [2.73], classifies fly ash into two big categories, according to their chemical composition and other physical properties, and hence from the coal type burned in the coal-fired power plants. Those classes are Class F (low calcium) and Class C (high calcium) fly ash. Combustion of bituminous or anthracite coal normally produces Class F (low calcium) fly ash and combustion of lignite or sub-bituminous coal normally produces Class C (high calcium) fly ash. In Europe, the EN 450-1 standard of 2012 defines the specifics for a correct use of FA in concrete [2.74]. According to the EN 450, FA quality control requirements should be done as defined in Table 2-8.

The chemical composition of fly ash may vary sensibly, as already stated, according to its origin. We have also already seen that there are some limits about the content of some components for its application in concrete. More references are available on the use of low calcium fly ash as a replacement of fine aggregate in concrete than high calcium fly ash. High calcium fly ash contains large amounts of free lime and sulfite than that of low calcium fly ash.

Table 2-8. Fly ash quality control requirements [2.74]. ([1] limit valid on national basis)

Property	*Acceptance limit*	*Test procedure*	*Frequency*
LOI (%)	*≤ 5.0 (≤ 7.0 [1])*	*EN 196-2*	*1/day*
Chloride (%)	*≤ 0.10*	*EN 196-2*	*1/month*
Sulphate (%)	*≤ 3.0*	*EN 196-2*	*1/month*
Free CaO (%)	*≤ 1.0 (≤ 2.5)*	*EN 451-1*	*1/week*
Expansion (mm)	*≤ 10.0*	*EN 196-3*	*1/week*
Fineness (%)	*≤ 40.0*	*EN 451-2*	*1/day*
Fineness uniformity (%)	*Mean value ± 5.0*	*EN 451-2*	*1/day*
Pozzolanic activity	*≥ 75.0 at 28 d*	*EN 450 &*	*1/2 weeks*
index (%)	*≥ 85.0 at 90 d*	*EN 196-1*	
Density (kg/m³)	*Mean value ± 150*	*EN 196-6*	*1/month*

The mineralogical composition of fly ash is also very complex. Mineralogically, FAs are a heterogeneous mixture of mineral phases and amorphous glassy phases with small amount of unburned carbon. The glassy phase of low calcium fly ash is alumino-silicate type whereas that of high calcium fly ash is a mixture of calcium aluminates and ferrous alumino-silicates. High calcium fly ash contains large amounts of calcium-bearing minerals like lime, anhydrite, gypsum, tricalcium aluminate, alite, gehlenite, akermanite, portlandite and larnite. Some other minerals like quartz, hematite and magnetite are also present in high calcium fly ash. On the other hand, low calcium fly ash mainly contains quartz, mullite, hematite, magnetite and small amounts of calcite [2.75].

Concerning the physical properties of FAs, also in this case a huge variability was reported in literature. The specific gravity of fly ash may vary from 1.3 to 4.8 t/m^3, and the shape is generally roundish (which depends by the spherical glassy phase shape). However, large sized or irregular shaped particles can also be formed from the fusion of smaller fragments and incomplete melting. In addition, there could be also hollow spheres (cenospheres) and microsphere-filled spheres (plerosheres): these lasts are cenosphere which have encapsulated a mass of microspheres (1 μm or less in diameter). The formation of such spheres is due to many physical and chemical reactions that occur during coal combustion: initially lignite is heated up to about 950-1000°C and thereafter reactions may occur for some seconds, as the FA is swept towards the stack inlet. The smallest particles are then adhering to the larger ones, thus forming clumps or agglomerate of small particles. Particle size distribution can be very different, and it depends upon the

initial grinding of the coal, the efficiency of the thermal power plant and even fluctuations in power generation. Also the color of coal ash can is an index of chemical and mineral constituents. High lime containing FA is normally tan and light in color. Iron containing FA is brownish in color. The dark grey to black color of FA indicates the presence of a high amount of unburned carbon.

References

[2.1] Oikonomou N.D. Recycled Concrete Aggregates. Cement and Concrete Composites 2005; 27: 315-318.

[2.2] Etxeberria M., Vázquez E., Mari A., Barra M. Influence of Amount of Recycled Coarse Aggregates and Production Process on Properties of Recycled Aggregate Concrete. Cement and Concrete Research 2007; 37: 735-742.

[2.3] Evangelista L., de Brito J. Durability Performances of Concrete Made with Fine Recycled Aggregates. Cement and Concrete Composites 2010; 32: 9-14.

[2.4] Yang K.-H., Chung H.-S., Ashour A.F. Influence of Type and Replacement Level of Recycled Aggregates on Concrete Properties. ACI Materials Journal 2008; 105: 289-296.

[2.5] Wu W., Zhang W., Ma G. Optimum Content of Copper Slag as a Fine Aggregate in High Strength Concrete. Materials & Design 2010; 31: 2878-2883.

[2.6] Qasrawi H., Shalabi F., Asi I. Use of Low CaO Unprocessed Steel Slag in Concrete as Fine Aggregate. Construction & Building Materials 2009; 23: 1118-1125.

[2.7] Papayianni I., Anastasiou E. Production of High-Strength Concrete Using High Volume of Industrial By-products. Construction & Building Materials 2010; 24: 1412-1417.

[2.8] Maslehuddin M., Sharif A.M., Shameem M., Ibrahim M., Barry M.S. Comparison of Properties of Steel Slag and Crushed Limestone Aggregate Concretes. Construction & Building Materials 2003; 17: 105-112.

[2.9] Vázquez E. Progress of Recycling in the Built Environment, Final Report of the RILEM Technical Committee 217-PRE. Springer, 2013.

[2.10] Eurostat, Waste generation by economic activity and households, 2010.

[2.11] NEN 5905: 2010. Dutch supplement to NEN-EN 12620+A1 Aggregates for concrete, 2010; Nederlands Normalisatie-instuut, Delft.

[2.12] NEN 12620: 2011. Aggregates for concrete, 2011; Nederlands Normalisatie-instuut, Delft.

[2.13] ASTM C33 / C33M. Standar Specification for Concrete Aggregates. ASTM International, West Conshohocken, PA, 2013.

[2.14] ASTM C125-14. Standard Terminology Relating to Concrete and Concrete Aggregates, ASTM International, West Conshohocken, PA, 2014.

[2.15] DIN 4226-100:2002-02. Aggregates for concrete and mortar - Part 100: Recycled aggregates.

[2.16] German committee for reinforced concrete (DAFSTB) - Code: Concrete with Recycled Aggregates (in German).

[2.17] DIN EN 206: 2014-07. Concrete - Specification, performance, production and conformity; German version EN 206:2013 (in German).

[2.18] DIN 1045-2:2008-08. Concrete, reinforced and prestressed concrete structures - Part 2: Concrete - Specification, properties, production and conformity - Application rules for DIN EN 206-1 (in German).

[2.19] Technical Standards for Construction, NTC 2008; Italian Ministry of Infrastructures (in Italian).

[2.20] UNI EN 12620: 2013. Aggregati per calcestruzzo; UNI, Ente Italiano di Normazione, Milano (in Italian).

[2.21] UNI EN 206-1:2006. Concrete - Part 1: Specification, performance, production and conformity; UNI, Ente Italiano di Normazione, Milano (in Italian).

[2.22] UNI 8520-1. Aggregati per calcestruzzo - Istruzioni complementari per l'applicazione della EN 12620 – Parte 1: Designazione e criteri di conformità; UNI, Ente Italiano di Normazione, Milano (in Italian).

[2.23] UNI 8520-2. Aggregati per calcestruzzo- Istruzioni complementari per l'applicazione della EN 12620 – Parte 2: Requisiti; UNI, Ente Italiano di Normazione, Milano (in Italian).

[2.24] UNI EN 13242:2013. Aggregati per materiali non legati e legati con leganti idraulici per l'impiego in opere di ingegneria civile e nella costruzione di strade; UNI, Ente Italiano di Normazione, Milano (in Italian).

[2.25] LNEC E 471: 2009. Guide for the use of recycled aggregates in concrete; LNEC, Lisboa, Portugal (in Portuguese).

[2.26] EHE-08: 2011. Comisión Permanente Del Hormigón: Instrucción de Hormigón Estructural, EHE-08. Ministerio de Fomento, Madrid, 2011 (in Spanish).

[2.27] Kou S., Poon C.-S., Agrela F. Comparisons of natural and recycled aggregate concretes prepared with the addition of different mineral admixtures. Cement and Concrete Composites 2011; 33–8: 788–95.

[2.28] Kou S., Poon C.-S., Etxeberria M. Influence of recycled aggregates on long term mechanical properties and pore size distribution of concrete. Cement and Concrete Composites 2011; 33–2: 286–91.

[2.29] Schubert S., Hoffmann C., Leemann A., Moser K., Motavalli M. Recycled aggregate concrete: experimental shear resistance of slabs without shear reinforcement. Engineering Structures 2012; 41: 490–7.

[2.30] Fathifazl G., Abbas A., Razaqpur A.G., Isgor O.B., Fournier B., Foo S. New mixture proportioning method for concrete made with coarse recycled concrete aggregate. Journal of Materials in Civil Engineering 2009: 601–11.

[2.31] Abbas A., Fathifazl G., Isgor O.B., Razaqpur A.G., Fournier B., Foo S. Durability of recycled aggregate concrete designed with equivalent mortar volume method. Cement and Concrete Composites 2009; 31: 555–63.

[2.32] Jiménez C., Aponte D., Vázquez E., Barra M., Valls S. Equivalent mortar volume (EMV) method for proportioning recycled aggregate

concrete: validation under the Spanish context and its adaptation to Bolomey methodology for concrete proportioning. Materials and Construction 2013; 63 – 311: 341–360.

[2.33] Vázquez E., Barra M., Aponte D., Jiménez C., Valls S. Improvement of the durability of concrete with recycled aggregates in chloride exposed environment. Construction and Building Materials 2013; 67: 61-67.

[2.34] Lima C., Caggiano A., Faella C,. Martinelli E., Pepe M., Realfonzo R. Physical properties and mechanical behaviour of concrete made with recycled aggregates and fly ash. Construction and Building Materials 2013; 47: 547–559.

[2.35] Barbudo A., de Brito J., Evangelista L., Bravo M., Agrela F. Influence of water reducing admixtures on the mechanical performance of recycled concrete. Journal of the Cleaner Production 2013; 59: 93–98.

[2.36] Ferreira L., de Brito J., Barra M. Influence of the pre-saturation of recycled coarse concrete aggregates on concrete properties. Magazine of Concrete Research 2012; 63– 8: 617–627.

[2.37] Poon C.S., Shui Z., Lam L. Effect of microstructure of ITZ on compressive strength of concrete prepared with recycled aggregates. Construction and Building Materials 2004; 18(6): 461:468.

[2.38] Li W.X., Zhang X., Liu X. Mechanical properties of recycled aggregate concrete. Study of the impact of factors. Chinese Concrete Journal 2009; 10: 60-63 (in Chinese).

[2.39] Otsuki N., Miyazato S.I., Yodsudjai W. Influence of recycled aggregate on interfacial transition zone, strength, chloride penetration and carbonation of concrete. Journal of Materials in Civili Engineering 2003; 15(5): 443-451.

[2.40] Tovar-Rodríguez G., Barra M., Pialarissi S., Aponte D., Vázquez E. Expansion of mortars with gypsum contaminated fine recycled aggregates. Construction and Building Materials 2013; 38: 1211–1220.

[2.41] Sato R., Maruyama I., Sogabe T., Sogo M. Flexural behavior of reinforced recycled concrete beams. Journal of Advanced Concrete Technology 2007; 5(1): 43-61.

[2.42] Ajdukiewicz A.B., Kliszczewicz A.T. Comparative tests of beams and columns made of recycled aggregate concrete and natural aggregate concrete. Journal of Advanced Concrete Technology 2007; 5(2): 259-273.

[2.43] Fathifazl G., Razaqpur A.G., Isgor O.B., Abbas A., Fournier B., Foo S. Flexural Performance of Steel-Reinforced Recycled Concrete Beams. ACI Structural Journal 2009; 106(6): 858-867.

[2.44] Choi H.B., Yi C.K., Cho H.H., Kang K.I. Experimental study on the shear strength of recycled aggregate concrete beams. Magazine of Concrete Research 2010; 62(2): 103-114.

[2.45] Fathifazl G., Razaqpur A.G., Isgor O.B., Abbas A., Fournier B., Foo S. Shear strength of reinforced recycled concrete beams without stirrups. Magazine of Concrete Research 2009; 61(7): 477-490.

[2.46] Corinaldesi V., Letelier V., Moriconi G. Behaviour of beam–column joints made of recycled-aggregate concrete under cyclic loading. Construction and Building Materials 2011; 25(4): 1877-1882.

[2.47] Euroslag and Eurofer. Position Paper on the Status of Ferrous Slag. European Slag Association, European Steel Association, Duisburg, Germany, 2012.

[2.48] Luxàn M.P., Sotolongo R., Dorrego F., Herrero E. Characteristics of the Slags Produced in the Fusion of Scrap Steel by Electric Arc Furnace. Cement and Concrete Research 2000; 30: 517-519.

[2.49] Al-Negheimish A.I., Al-Sugair F.H., Al-Zaid R.Z. Utilization of local steel making slag in concrete. Journal of King Saud Univerisity - Engineerig Sciences 1997; 9: 39-55.

[2.50] Anastasiou F., Papayianni I. Criteria for the use of steel slag aggregates in concrete. In: Konsta-Gdoutos MS (ed) Measuring, monitoring and modeling concrete properties. Springer, 2006, The Netherlands, 419–426.

[2.51] Manso J.M., Gonzalez J.J., Polanco J.A. Electric arc furnace slag in concrete. Journal of Materials in Civil Engineering 2004; 16(6):639–645.

[2.52] Xue Y., Wu S., Hou H., Zha J. Experimental investigation of basic oxygen furnace slag used as aggregate in asphalt mixture. Journal of Hazardous Materials 2006; 138(2): 261–268.

[2.53] Ahmedzade P., Sengoz B. Evaluation of steel slag coarse aggregate in hot mix asphalt concrete. Journal of Hazardous Materials 2009; 166(1–3): 300–305.

[2.54] Pellegrino C., Gaddo V. Mechanical and durability characteristics of concrete containing EAF slag as aggregate. Cement and Concrete Composites 2009; 31(9): 663–671.

[2.55] Almusallam A.A., Beshr H., Maslehuddin M., Al-Amoudi O.S.B. Effect of silica fume on the mechanical properties of low quality coarse aggregate concrete. Cement and Concrete Composites 2004; 26(7): 891–900.

[2.56] Manso J.M., Polanco J.A., Losanez M., Gonzalez J.J. Durability of concrete made with EAF slag as aggregate. Cement and Concrete Composites 2006; 28(6): 528–534.

[2.57] Faraone N., Tonello G., Furlani E., Maschio S. Steelmaking slag as aggregate for mortars: effects of particle dimension on compression strength. Chemosphere 2009; 77(8): 1152–1156.

[2.58] Shi C., Qian J. High performance cementing materials from industrial slag—a review. Resoures, Conservation, Recycling 2000; 29(2): 195–207.

[2.59] Tossavainen M., Engstrom F., Yang Q., Menad N., Larsson M.L., Bjorkman B. Characteristics of steel slag under different cooling conditions. Waste Management 2007; 27(7): 1335–1344.

[2.60] Tsakiridis P.E., Papadimitriou G.D., Tsivilis S., Koroneos C. Utilization of steel slag for Portland cement clinker production. Journal of Hazardous Materials 2008; 152(2): 805-811.

[2.61] Bouzoubaâ N., Zhang M-H., Malhotra V.M., Golden D.M. Blended Fly Ash Cements - A Review. ACI Materials Journal 1999; 96(6): 641-650.

[2.62] Siddique R. Performance characteristics of high-volume Class F fly ash concrete. Cement and Concrete Research 2004; 34: 487–493.

[2.63] Siddique R., Khatib J.M. Abrasion resistance and mechanical properties of high-volume fly ash concrete. Materials and Structures 2010; 42(5): 709–718.

[2.64] Papadakis V.G., Tsimas S. Supplementary cementing materials in concrete. Part I: efficiency and design. Cement and Concrete Research 2002; 32: 1525-1532.

[2.65] Papadakis V.G., Antiohos S., Tsimas S. Supplementary cementing materials in concrete. Part II: A fundamental estimation of the efficiency factor. Cement and Concrete Research 2002; 32: 1533-1538.

[2.66] Aponte D.F., Barra M., Vàzquez E. Durability and cementing efficiency of fly ash in concrete. Construction and Building Materials 2012; 30: 537-546.

[2.67] Bentz D.P., Garboczi E.J. Simulation Studies of the Effects of Mineral Admixtures on the Cement Paste-Aggregate Interfacial Zone. ACI Materials Journal 1991; 88(5): 518-529.

[2.68] Aughenbaugh K. L., Chancey R.T., Stutzman P., Juenger M.C., Fowler D.W. An examination of the reactivity of fly ash in cementitious pore solutions. Materials and Structures 2013; 46: 869-880.

[2.69] Ranganath R.V., Bhattacharjee B., Krishnsmoorthy S. Influence of size fraction of ponded ash on its pozzolanic activity. Cement and Concrete Research 1998; 28(5): 749-761.

[2.70] Siddique R., Aggarwal P., Aggarwal Y. Influence of water/powder ratio on strength properties of self-compacting concrete containing coal fly ash and bottom ash. Construction and Building Materials 2012; 29: 73-81.

[2.71] Eren O. Strength development of concretes with ordinary Portland cement, slag or fly ash cured at different temperatures. Materials and Structures 2002; 235: 536-540.

[2.72] Belz G., Caramuscio P. Valorizzazione delle ceneri provenienti dagli impianti di combustione a carbone.

[2.73] ASTM C618-08a, Standard Specification for Coal Fly Ash and Raw or Calcined Natural Pozzolan for Use in Concrete; ASTM International, West Conshohocken, PA, 2008.

[2.74] EN 450-1: 2012. Fly ash for concrete - Part 1: Definition, specifications and conformity criteria. Brussels, CEN Comité Européen de Normalisation, Belgium, 2012.

[2.75] de Brito J., Saikia N. Recycled Aggregate in Concrete, Green Energy and Technology, Springer-Verlag, London 2013.

3 Properties of EAF slag concrete

3.1 Abstract

The aim of this section is to comprehensively investigate the possibility of partially substituting natural aggregates with Black/Oxidizing Electric Arc Furnace (EAF) slag in concrete production. Five recycled and one traditional mixes were produced to identify a convenient substitution ratio for the concrete. Main physical and mechanical properties of concrete containing EAF slag as aggregate according to Fuller's grading curve were experimentally investigated. Chemical and durability tests were performed to study the microstructure and analyze the behavior of the conglomerate exposed to detrimental agents. Results showed that high substitution ratios of coarse natural aggregates are possible without decreasing mechanical properties of concrete. Conversely, replacement of fine natural aggregates with recycled ones seems feasible at lower substitution ratios only. Presence of calcium and magnesium oxides in the slag does not seem to represent a limit for the durability of concrete, due to their stabilization in crystalline lattice.

3.2 Introduction

The growing interest in identifying sustainable materials for concrete production, the necessity of establishing a correct management of this kind of slags and the lack of a thorough study on the substitution ratio slag/natural aggregate, induce to deepen this field by means of a comprehensive experimental approach which includes chemical and microstructural analysis of materials, evaluation of durability behavior and mechanical tests on concrete with various percentages of EAF slag as coarse and fine aggregate.

In this section five recycled and one traditional concrete mixtures were produced with the aim of investigating, from a mechanical and chemical point of view and with a particular attention to durability, the possibility of partially substituting natural aggregates with EAF slag and obtain some elements for identifying a convenient (coarse and fine) aggregate substitution ratio. Main physical properties, compressive and tensile strength, elastic modulus of concrete containing EAF slag as aggregate designed according to Fuller's ideal grading curve were experimentally investigated. Durability tests were performed to analyze the behavior of the mixes exposed to detrimental agents, such as frost and moisture, in typical environmental conditions. Chemical and microstructural analyses

were performed by means of four complementary techniques: leaching tests on the slag, Scanning Electroscope Imaging analyses, X-ray Diffraction analysis and Energy Dispersive X-ray Spectroscopy analysis on pulverized slag and concrete.

The present research work is a further stage of a previous research conducted, as a first step, at the University of Padova [3.1], which was focused on a single mix design and where the wholeness of the coarse part was substituted by recycled aggregates. This wide experimental study has the aim of generalizing the previous pilot study introducing, other than mechanical and durability characterization, a specific chemical and microstructural in-depth examination of various mixes with EAF slag. In particular, this work was conducted to assess the suitability of using both coarse and fine recycled aggregates in various replacement ratios, evaluate the effective stability of the material and estimate the effect of the slag/natural aggregate substitution ratio on concrete physical, chemical, mechanical and microstructural characteristics and its durability.

3.3 Materials

Steel slag used in this experimental investigation is obtained from a local steel factory in the North-Eastern part of Italy; it has a black color stone-like appearance, a lime content lower than 40%, a high density and low water absorption and porosity. Two size ranges were used: a fine and a medium/coarse one, with physical characteristics listed in Table 3-1. Fig 3-1 shows the EAF aggregates used in this work.

Table 3-1. Main physical characteristics of EAF slag.

	Medium/coarse EAF slag	*Fine EAF slag*
Size (mm)	*4-22.4*	*0-4*
Apparent specific gravity (t/m³)	*3.850*	*3.780*
Water absorption (%)	*0.53*	*1.613*
Los angeles loss (%)	*< 20*	*-*

Chemical composition is mainly formed by oxides: about 75% is a set of iron, calcium and silicon oxides, plus minor amount of magnesium, aluminum and manganese oxides. The presence of free calcium and magnesium oxides is mainly responsible for hydration and expansion phenomena: the firsts, when in contact with water, rapidly hydrate due to rapid volumetric expansion, whereas the seconds react slower, because the expansion spreads over a longer time [3.2]. Proper treatment, aimed to

stabilize slag by exposing them to outdoor weather and regular spraying for 90 days, was applied to the slag used in this work, allowing to a safer use of the same slag as aggregate in concrete production [3.3]. A specific chemical analysis was performed at the end of the experimental work, to ensure that expansion phenomena will not occur. Leaching tests have been also developed on the slag to verify that the potential toxic compounds were under the limit values reported in the Italian standards, DM 186 [3.4]. Table 3-2 shows the resulting range of obtained quantities; according to the above Italian standards, tested slag is fully admissible.

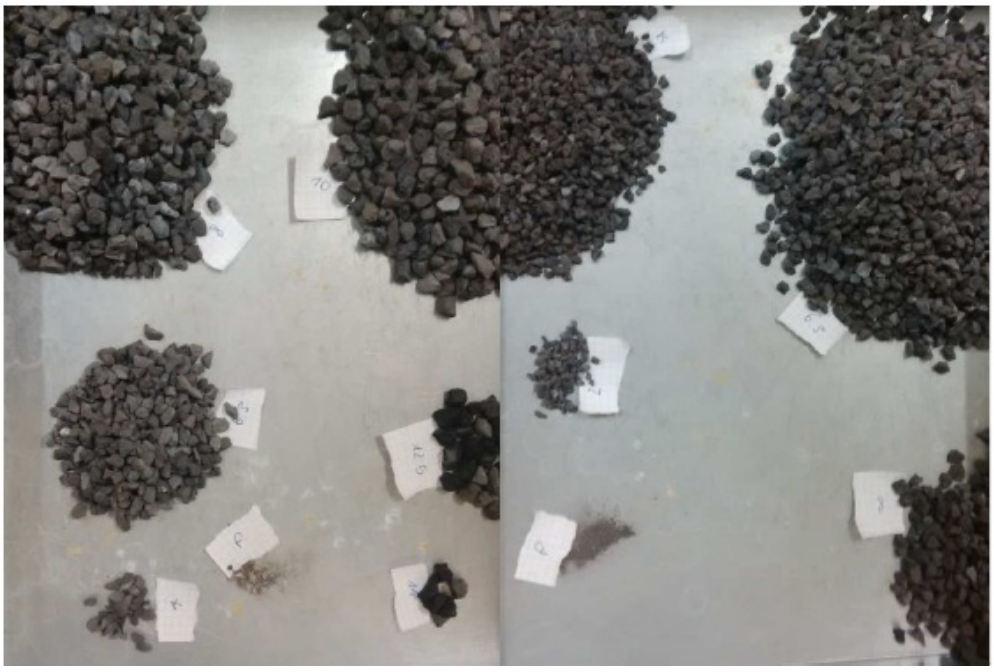

Figure 3-1. EAF aggregates.

Natural aggregates used in this experimentation have carbonate origin, their shape was mainly roundish and the main physical properties are listed in Table 3-3.

A cement mixture type CEM II-A/L 42.5R, commonly used in Italy, was adopted for the conglomerates. This cement has a high percentage content of clinker and limestone. In order to reach a S4 slump class concrete, as defined in EN 206-1 [3.5], it was planned to use a super-plasticizer admixture SP at 0.4% on cement weight, and an air-entrainer admixture AEA at 0.016% on cement weight was introduced to improve durability against freezing/thawing cycles, allowing a 5% percentage of air on the total volume [3.1].

Table 3-2. Leaching test results.

Parameter	*Concentration (mg/l)*	*Limits*
Nitrates	*< 40*	*50*
Fluorides	*< 1.5*	*1.5*
Sulfates	*< 200*	*250*
Chlorides	*< 75*	*100*
Cyanides	*< 0.03*	*0.050*
Barium	*0.0125*	*1*
Copper	*< 0.001*	*0.050*
Zinc	*< 0.03*	*3*
Beryllium	*< 0.005*	*0.010*
Cobalt	*< 0.01*	*0.250*
Nickel	*< 0.005*	*0.010*
Vanadium	*0.103*	*0.250*
Arsenic	*< 0.02*	*0.050*
Cadmium	*< 0.003*	*0.005*
Total chromium	*< 0.002*	*0.050*
Lead	*< 0.04*	*0.050*
Selenium	*< 0.010*	*0.010*
Mercury	*< 0.001*	*0.001*
Amianthus	*< 10*	*30*
COD	*< 25*	*30*
pH	*10.78*	*5.5-12.0*

Table 3-3. Main physical characteristics of natural aggregate.

	Medium/coarse NA gravel	*NA sand*
Size (mm)	*4-22.4*	*0-4*
Apparent specific gravity (t/m³)	*2.732*	*2.724*
Water absorption (%)	*0.75*	*0.8*
Los angeles loss (%)	*18*	*-*

3.4 Mix proportions

One traditional and five experimental mixes with EAF slag were casted, varying the percentage of recycled material on total aggregates. Concerning the concrete production process, the preparation of the mixes was performed to satisfy some specific parameters, such as workability with slump 160–210 mm (S4 slump class), water/cement ratio less or equal than 0.55, and cylindrical compressive strength after 28 days greater than 30 MPa. After the mixing, the specimens were properly compacted and aged in standard temperature and humidity conditions T = 20°C, RH≥95% until the time of testing. The mix proportions are described in Table 3-4.

Aggregate grading curves were obtained according to Fuller ideal curve and are shown in Fig. 3-2.

Table 3-4. Mix details of concretes. Quantities are referred to 1m^3 of concrete.

	Traditional	*Mix 1*	*Mix 2*	*Mix 3*	*Mix 4*	*Mix 5*
NA gravel (%)	*100*	*100*	*100*	*50*	*-*	*-*
NA sand (%)	*100*	*50*	*-*	*50*	*50*	*-*
EAF medium/coarse (%)	*-*	*-*	*-*	*50*	*100*	*100*
EAF fine (%)	*-*	*50*	*100*	*50*	*50*	*100*
D max (mm)	*22.4*	*22.4*	*22.4*	*22.4*	*22.4*	*22.4*
Cement (kg)	*330*	*335*	*340*	*340*	*350*	*355*
Water (l)	*155*	*158*	*167*	*180*	*185*	*195*
w/c	*0.47*	*0.47*	*0.49*	*0.53*	*0.53*	*0.55*
V aggregates (l)	*682*	*678*	*673*	*675*	*662*	*658*
Total EAF s.s.d. fraction (kg)	*-*	*514*	*1019*	*1278*	*1894*	*2508*
Total NA s.s.d. fraction (kg)	*1861*	*1480*	*1102*	*920*	*456*	*-*
Plasticizer admixture (kg)	*1.31*	*1.33*	*1.36*	*1.36*	*1.39*	*1.42*
Air-entrainer (g)	*56*	*56*	*56*	*56*	*56*	*56*

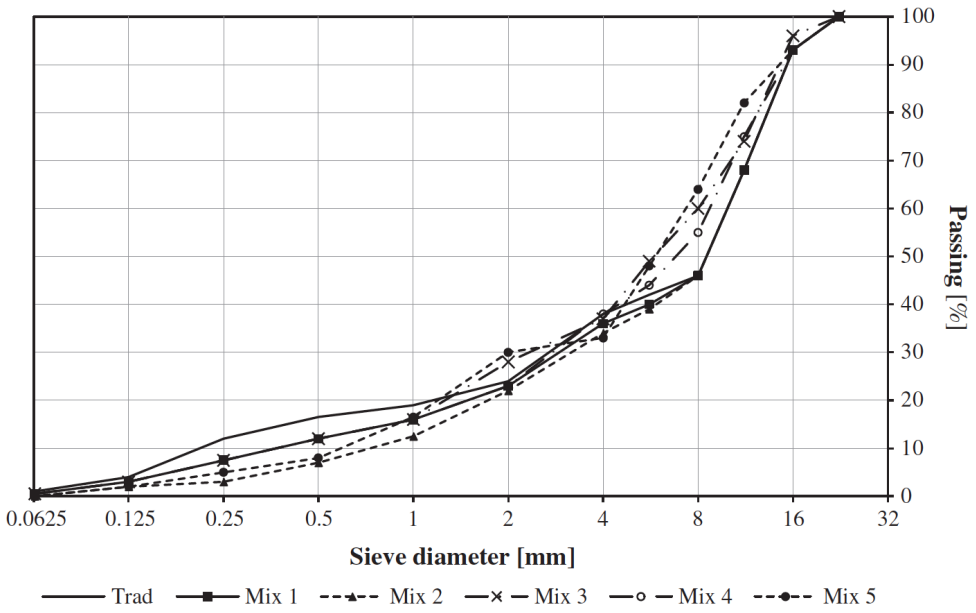

Figure 3-2. Aggregate grading curves.

Water/cement ratio slightly varies in the produced mixes, due to the necessity of reaching S4 slump class concrete for all the fresh concretes. Since fine EAF aggregates have higher absorption capacity than natural sand, it was necessary to slightly increase w/c ratio when the quantity of recycled fine aggregates increases. Moreover w/c slightly increased in EAF conglomerates with respect to traditional ones also because traditional conglomerate has roundish aggregates whereas EAF slag is more angular and, as a consequence, implies less workability for the related mixes [3.1]. During production of Mix 5 (containing only recycled aggregates) some difficulties were experienced, because the paste showed a high water demand, due to the particular smooth and sharp shape of the material. Moreover, the AEA admixture did not seem to work well in this case, causing the development of great diameter bubbles during concrete placement. It should to be noted that, in literature, there are works showing the strong difficulty to produce conglomerates with recycled aggregates only [3.6, 3.7].

3.5 Experimental methods

Mechanical tests and durability analyses were performed on 108 cubic specimens with 150 mm side, 18 cylindrical specimens with 160 mm diameter and 320 mm length for splitting test, according to European Standard EN 12390-1 [3.8], and 18 cylindrical specimens with 160 mm

diameter and 480 mm length for Young modulus calculation, according to UNI EN 6556 [3.9]. Test plan is illustrated in Fig. 3-3: the first phase consists in standard ageing, which concluded after 28 days.

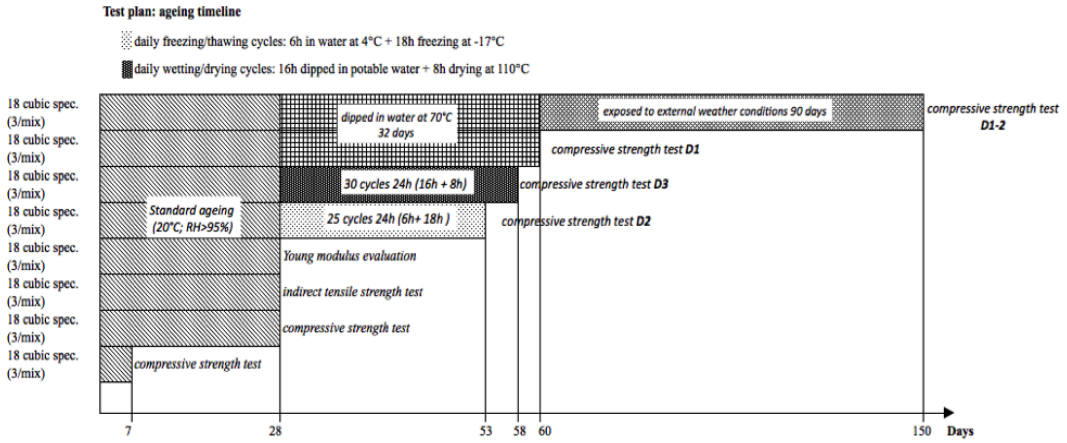

Figure 3-3. Test plan.

Compressive tests have been developed after seven (three specimens for each mix) and 28 days (three specimens for each mix), following the European Standard EN 12390-4 [3.10]. Indirect tensile strength was measured after 28 days by splitting test, following European Standard EN 12390-6 [3.11], and Young modulus was experimentally evaluated according to UNI EN 6556 [3.9]. In the second phase three different types of accelerated ageing (including wetting/drying and freezing/thawing cycles) were developed. The first durability test (*D1*) follows ASTM D-4792 standard [3.12]: specimens were completely dipped in a thermostatic tub containing 70 °C water and properly covered to limit evaporation for a total duration of 32 days. A further set of three specimens for each mix was subjected to the same treatment described above, and then exposed to outdoor weathering for 90 days under atmospheric conditions (*D1-2*), with direct sun and rain exposure. The second accelerated ageing test (*D2*) concerns the investigation of durability of concrete with an alternation of freezing and thawing conditions. Three specimens for each mix were subjected to 25 daily cycles consisting in a first phase with a duration of 18 h in which specimens were frozen at the temperature of -17 °C and a second phase with a duration of 6 h in which they were dipped in 4 °C water. The last durability test (*D3*) was done on three specimens for each mix; they were subjected to 30 wetting/drying daily cycles. Specimens were dipped for 16 h in potable water at room temperature, and then dried for 8 h in a electric oven at 110 °C. The main objective of these tests is to obtain some elements about the durability of the various mixes, comparing compressive strength after standard and accelerated ageing, and

individuating the conditions that mainly affect the mechanical characteristics of concrete containing such recycled aggregates in time.

D1 – 32 DIPPED IN 70°H2O; D2 – 25 FREEZING/THAWING; D3 – 30 WETTING/DRYING

Figure 3-4. Environmental cycles - durability tests.

3.6 Results and discussion

3.6.1 Mechanical strength

The results of compressive and tensile strength tests are listed in Table 3-5. Concerning compressive strength tests, as already obtained in [3.1], observed mean compressive strengths are similar for traditional and recycled concretes, and for some replacement ratios, they result higher than in the traditional mix. The failure mode was similar for specimens made with traditional and recycled aggregates, with exception of Mix 2 and, above all, Mix 5, which showed a more brittle behavior. Results show that the tensile strength in concrete with EAF slag is generally higher than those in traditional concrete; this is probably due to the different cement matrix-aggregate contact surface, which is rougher in recycled concrete and may allow a stronger link between binder and aggregate (this was observed after splitting failure - Fig. 3-5). Splitting surfaces in concrete containing EAF slag are less regular than in the traditional mix, in particular when the coarse aggregates are substituted. On the other hand, substitution of fine aggregates may cause a decrease of the mechanical strength, because cementitious matrix becomes less cohesive.

Table 3-5. Mean specific weight, slump, compressive and tensile strength and Young modulus.

	Trad	*Mix 1*	*Mix 2*	*Mix 3*	*Mix 4*	*Mix 5*
			fresh concrete			
Specific weight (kg/m³)	*2530*	*2660*	*2850*	*2830*	*3000*	*3190*
Slump (cm)	*20.0*	*19.0*	*20.0*	*19.5*	*19.5*	*18.0*
			7 days			
Specific weight (kg/m³)	*2380*	*2530*	*2710*	*2830*	*2900*	*3120*
$f_{cm,cube}$ *(MPa)*	*37.80*	*35.30*	*33.10*	*37.50*	*36.00*	*33.90*
			28 days			
Specific weight (kg/m³)	*2490*	*2610*	*2780*	*2790*	*2940*	*3130*
$f_{cm,cube}$ *(MPa)*	*44.63*	*44.42*	*44.00*	*45.23*	*45.10*	*41.40*
f_{ctm} *(MPa)*	*3.54*	*3.73*	*3.62*	*3.56*	*4.01*	*3.76*
E_{cm} *(GPa)*	*37.51*	*37.36*	*38.68*	*10.39*	*40.04*	*38.47*

As for the other measured mechanical properties, the obtained values of the Young modulus are similar and, in most cases, recycled concrete showed greater moduli. However, the fluctuation in experimental values is more evident for the mixes containing high percentage of EAF slag, in particular for the conglomerates with the whole fine part as recycled aggregate, than for traditional concrete (look at the Appendix to this section). This is mainly due to the higher heterogeneity of the slag with respect to natural aggregates.

Results of mechanical strength tests on each specimen are reported in the Appendix to this section.

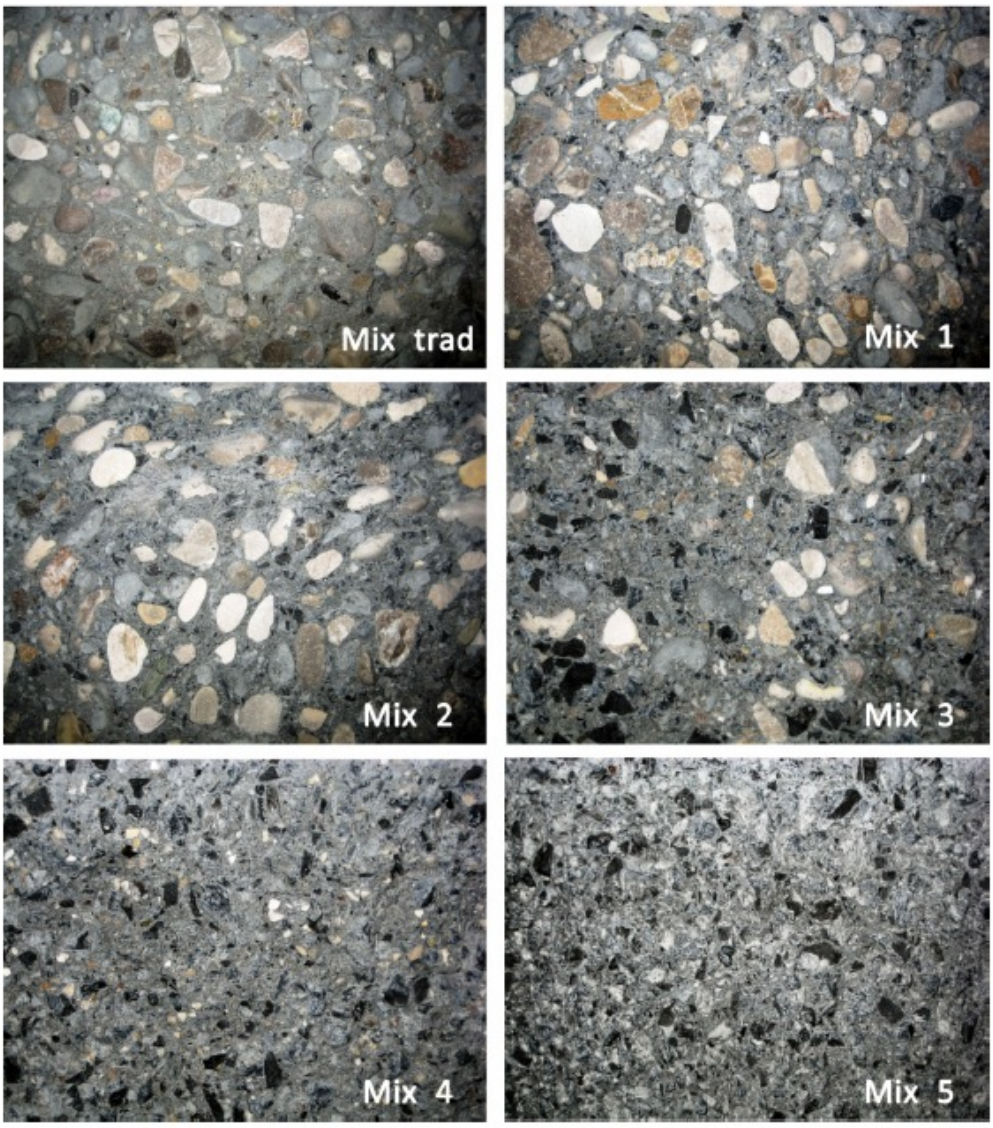

Figure 3-5. Splitting failure of some tested mixes.

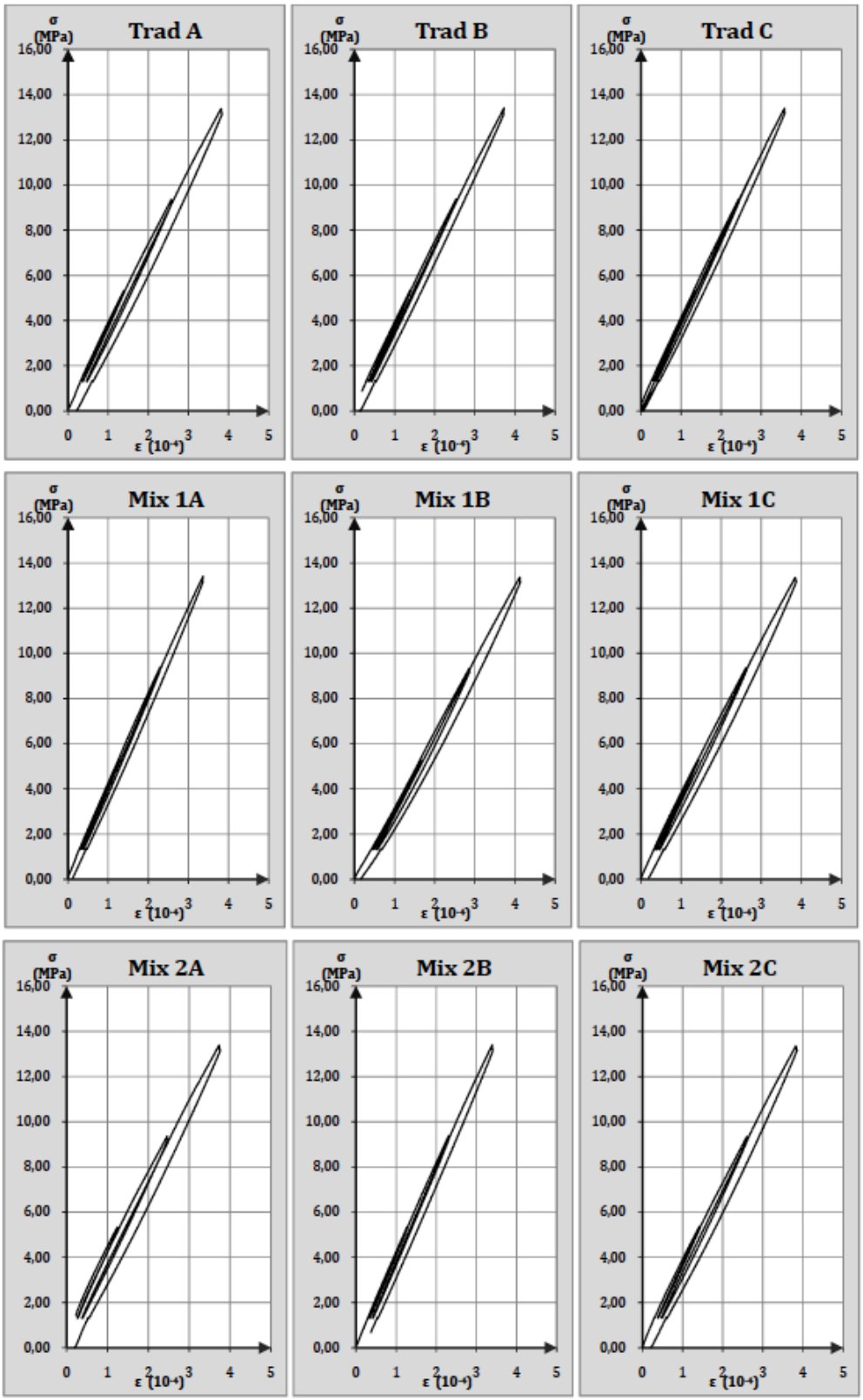

Figure 3-6. Young modulus evaluation.

3.6.2 Durability tests

Once concluded the first part of the experimental work (which was lasting until the 28-days standard maturation), durability tests were performed following the tests plan described in Fig 3-3. Three specimens for each conglomerate have been subjected to three types of accelerated ageing for periods varying from 25 to 32 days.

The first durability test *D1* investigates the potential expansion of dense graded compacted aggregates, which could induce hydration of free lime (CaO) and periclase (MgO) generally contained in most slag used, leading to consequent volume increase. Wang et al. [3.2] have in fact reported that, in some cases, EAF slag can contain high levels of expansive compounds, which can hydrate and increase their volume. This problem, typically recognized for BOF slag, may occur when EAF slag are not pretreated.

After the test, all the specimens, including the traditional ones, showed white powder outcrops, as shown in Fig. 3-7. The formation of this type of efflorescence could be assigned to the cementitious matrix hydration, which leads to the formation of a calcium carbonate powder on specimen surfaces. Specific chemical and microstructural analyses were performed to understand the nature of this phenomenon, revealing a composition mainly consisting in calcium, silicon, magnesium, and aluminum oxides (Fig. 3-8). Iron presence was null, indicating that this material is not connected with EAF slag use, but that it was composed by dissolved salts transported on specimen surface through water evaporation.

Figure 3-7. White powder outcrops on specimens after accelerated ageing treatment.

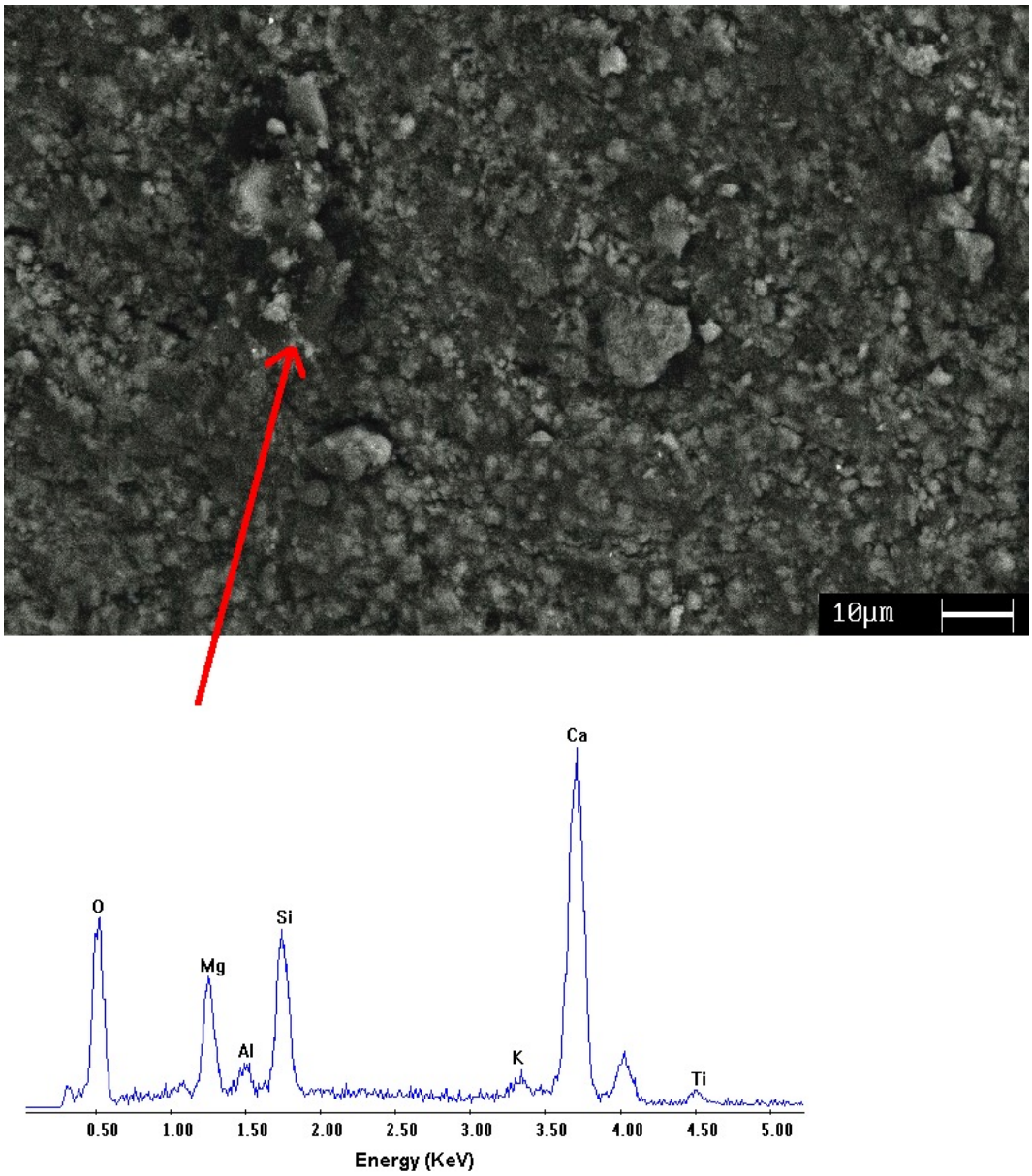

Figure 3-8. BSE-SEM image of the efflorescence + EDS spectrum.

Table 3-6 shows the values of mean compressive strength measured after the above durability test for each mix, compared to the strength after 28 days of natural ageing. All the specimens increased their mechanical strength, even if the treatment in hot water has a worse effect on conglomerates with high content of EAF slag, which were strongly subjected to free oxides hydration and subsequent inner differential micro-expansion. There are no significant differences in specific weight due to this durability test, since the absorption of oxides hydration water only slightly increased the weight of the specimens (the maximum variation is +2.3%).

Table 3-6. Basic properties in specimens after accelerated ageing for 32 days and variation with respect to the same properties before accelerated ageing.

	Mean specific weight			*Mean compressive strength*		
	28 + 32 days	*28 days*	*Δ*	*28 + 32 days*	*28 days*	*Δ*
	(t/m³)	*(t/m³)*	*(%)*	*(MPa)*	*(MPa)*	*(%)*
Mix Trad	*2.49*	*2.49*	*-0.07*	*51.59*	*44.63*	*+13.49*
Mix 1	*2.61*	*2.61*	*-0.19*	*47.02*	*45.42*	*+3.39*
Mix 2	*2.80*	*2.78*	*+0.68*	*44.76*	*44.00*	*+1.70*
Mix 3	*2.85*	*2.79*	*+2.29*	*50.79*	*45.23*	*+10.95*
Mix 4	*2.95*	*2.94*	*+0.38*	*47.52*	*45.10*	*+5.10*
Mix 5	*3.13*	*3.13*	*-0.29*	*42.36*	*41.40*	*+2.28*

A further set of three specimens for each mix produced was subjected to the durability test *D1-2*. Results are reported in Table 3-7: long outdoor weathering is predominant and mitigates the effects of the previous accelerated ageing, allowing a further increase in compressive strength, both in the traditional and experimental conglomerates.

Table 3-7. Basic properties in specimens after accelerated ageing for 32 days plus weathering for 90 days and variation with respect to the same properties before accelerated ageing/ weathering.

	Mean specific weight			*Mean compressive strength*		
	28 + 32 +90 days	*28 days*	*Δ*	*28 + 32 +90 days*	*28 days*	*Δ*
	(t/m³)	*(t/m³)*	*(%)*	*(MPa)*	*(MPa)*	*(%)*
Mix Trad	*2.49*	*2.49*	*-0.17*	*54.50*	*44.63*	*+18.10*
Mix 1	*2.57*	*2.61*	*-1.56*	*53.85*	*45.42*	*+15.65*
Mix 2	*2.78*	*2.78*	*+0.13*	*51.08*	*44.00*	*+13.87*
Mix 3	*2.82*	*2.79*	*+0.97*	*56.24*	*45.23*	*+19.58*
Mix 4	*2.93*	*2.94*	*-0.29*	*53.19*	*45.10*	*+15.21*
Mix 5	*3.12*	*3.13*	*-0.50*	*48.32*	*41.40*	*+14.33*

The second accelerated ageing test *D2* concerns the investigation of durability of concrete with an alternation of freezing and thawing conditions. All the specimens passed this test without showing significant surface deteriorations. This suggests that the AEA admixture contributed to form an air bubble system preventing that a great quantity of water

penetrates in concrete pores, and limiting thermal expansion. After the freezing and thawing cycles, measured compressive strength values increase with respect to the corresponding before cycles both for traditional specimens and specimens with EAF slag (Table 3-8) probably due to further cement hydration occurred by direct contact with water pushed through the frozen saturated surface micro-porosity, and the natural ageing of the material. Mix 3 and Mix 4 showed a reduced increase in compressive strength with respect to Mix 1 and Mix 2, probably due to their higher water/cement ratio. On the other hand, Mix 5, the one containing recycled material only, showed a significant increase in strength after the cycles. All the specimens showed the same failure mode, with the exception of Mix 2 and Mix 5, showing a more brittle failure than the others (particularly for Mix 5).

Table 3-8. Basic properties in specimens after freezing/thawing cycles for 25 days and variation with respect to the same properties before freezing/thawing cycles.

	Mean specific weight			*Mean compressive strength*		
	28 + 25 days	*28 days*	*Δ*	*28 + 25 days*	*28 days*	*Δ*
	(t/m³)	*(t/m³)*	*(%)*	*(MPa)*	*(MPa)*	*(%)*
Mix Trad	*2.50*	*2.49*	*+0.22*	*50.14*	*44.63*	*+10.98*
Mix 1	*2.60*	*2.61*	*-0.32*	*51.74*	*45.42*	*+12.21*
Mix 2	*2.80*	*2.78*	*+0.70*	*50.36*	*44.00*	*+12.63*
Mix 3	*2.82*	*2.79*	*+1.14*	*49.63*	*45.23*	*+8.86*
Mix 4	*2.96*	*2.94*	*+0.51*	*48.83*	*45.10*	*+7.64*
Mix 5	*3.14*	*3.13*	*+0.05*	*50.50*	*41.40*	*+18.03*

The last durability test *D3* has the objective of simulating the behavior of concrete under critical environmental conditions, with intense moisture conditions alternated to drying ones. Mean compressive strength was evaluated at the end of the treatment, and the results are listed in Table 3-9.

Table 3-9. Basic properties in specimens after wetting/drying cycles for 30 days and variation with respect to the same properties before wetting/drying cycles.

	Mean specific weight			*Mean compressive strength*		
	28 + 30 days	*28 days*	*Δ*	*28 + 30 days*	*28 days*	*Δ*
	(t/m³)	*(t/m³)*	*(%)*	*(MPa)*	*(MPa)*	*(%)*
Mix Trad	*2.50*	*2.49*	*+0.33*	*39.24*	*44.63*	*-13.74*
Mix 1	*2.61*	*2.61*	*0.00*	*42.80*	*45.42*	*-6.12*
Mix 2	*2.83*	*2.78*	*+1.66*	*41.65*	*44.00*	*-6.42*
Mix 3	*2.85*	*2.79*	*+2.06*	*37.86*	*45.23*	*-19.48*
Mix 4	*3.01*	*2.94*	*+2.23*	*36.91*	*45.10*	*-22.17*
Mix 5	*3.19*	*3.13*	*+1.65*	*37.35*	*41.40*	*-10.84*

All the mixes (both traditional and recycled) showed a significant decrease in strength, due to the highly harmful conditions of the test combining both the alternating effect of expansion and contraction due to thermal variation plus that due to inner and surface humidity variation. Any goethite type was detected by diffraction test (the results of this test are shown in the following section) and surface damages were not observed in any specimens. Nevertheless strength loss could be assigned to some expansion phenomena occurred during the test. Moreover, the small increase in specific weight in all the conglomerates with respect to that measured before the test, could be due to absorption of hydration water, which probably balances the concomitant expansion, as already obtained in [3.1, 3.13]. Failure mode was similar for all the specimens tested, with the exception of Mix 2 and Mix 5, which showed a more brittle failure, revealing a less cohesive matrix.

Fig. 3-9 summarizes the outcomes of durability analyses in terms of mean compressive strength, showing that Mix 2 and Mix 5 had lower values in almost all the environmental conditions simulated than those of traditional concrete. The complete substitution of coarse and fine aggregates generated the worst conglomerate having the lowest values of compressive strength both in standard conditions and after environmental cycles. On the other hand, partial substitution of natural aggregates with EAF slag does not seem to induce negative effects on the conglomerates, whose behavior remains quite similar to the reference concrete. Specific weight remains almost constant in all the conditions simulated for each conglomerate. As expected, the concrete with EAF slag as aggregate has higher specific weight than traditional concrete and this becomes more evident when the substitution percentage increases.

The results of compressive strength test for each specimen subjected to the analyzed deterioration cycles are reported in the Appendix to this section.

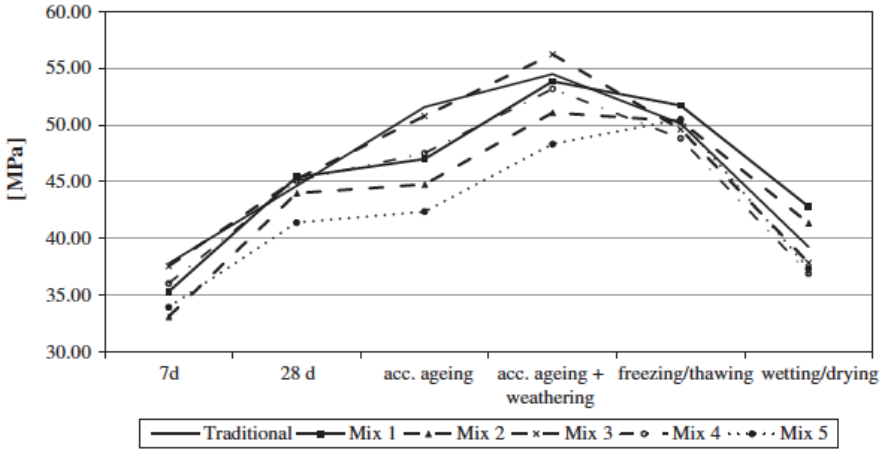

Figure 3-9. Mean compressive strength observed after natural ageing and various durability tests.

3.6.3 Physical–chemical and mineralogical composition

Three complementary techniques were used to investigate the stability of the produced recycled concrete and understand the nature of the variation of the main properties detected after durability tests (specific weight, compressive strength, formation of white powder outcrops): Scanning Electroscope Imaging analyses on concrete samples, X-ray Diffraction analyses and Energy Dispersive X-ray spectroscopy analyses on pulverized slag extracted by concrete specimens.

A Stereoscan Cambridge 440 Scanning Electron Microscopy (SEM) was used to investigate the morphology of the material, applying Secondary Electrons (SE) acquisition technique on samples of concrete extracted from concrete specimens subjected to durability tests and from naturally aged specimens (without environmental cycles). A brief explanation of SEM technique is given in the Appendix to this section. SEM images were taken at 70 magnification aiming at identifying, for traditional and recycled concrete, the development of air bubble systems and analyzing the cementitious matrix appearance.

Fig. 3-10 shows that there are not significant microstructural differences between traditional and recycled concrete for almost all the mixes, with the exception of Mix 5, containing only EAF slag as aggregate. In this last case the number of developed micro-bubbles seems fewer than the other mixes, and micro-pores seem to remain empty, increasing the

probability of having expansion phenomena and reduced strength with respect to the other conglomerates. This result is in agreement with the observed failure mode of Mix 5 that was more brittle probably due to less cohesion in the matrix with respect to the others.

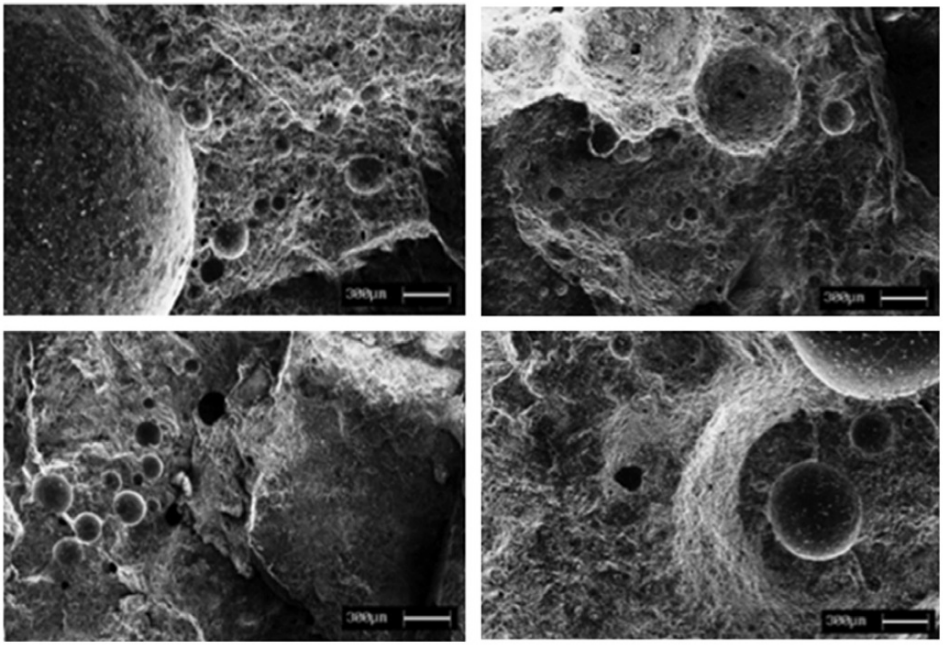

Figure 3-10. SEM images at 70 magnification. Upper left: traditional concrete; upper right: Mix 2; lower left: Mix 4; lower right: Mix 5. All the samples were extracted from specimens subjected to accelerated ageing.

The mineralogy of slag phases was established on pulverized slag extracted from the surface of concrete specimens subjected to durability tests, using Siemens D500 diffractometer, with a stepped and continuous scanning device, with (Cu Kα) radiation emission. The analysis of XRD patterns' is useful to detect the mineralogical phases of a cementitious material: a brief focus of this technique is given in the Appendix to this section. XRD patterns were obtained for samples extracted from Mix 4 concrete specimens, before and after accelerated ageing (*D1)* and wetting/drying cycles (*D3*). In both cases any differences were detected in the crystallographic structure. Fig. 3-11 shows the complex mineralogical system, which is mainly formed by crystalline material, as identified by the graphs. Main crystalline solids are wustite (FeO), calcium silicate (β-Ca_2SiO_4), hematite (Fe_2O_3) and brownmillerite ($Ca_2(Al,Fe)_2O_5$); unassimilated MgO was detected in limited quantities. The high crystalline nature of the examined slag indicates a quite stable material and limits further possibilities of expansion phenomena [3.14].

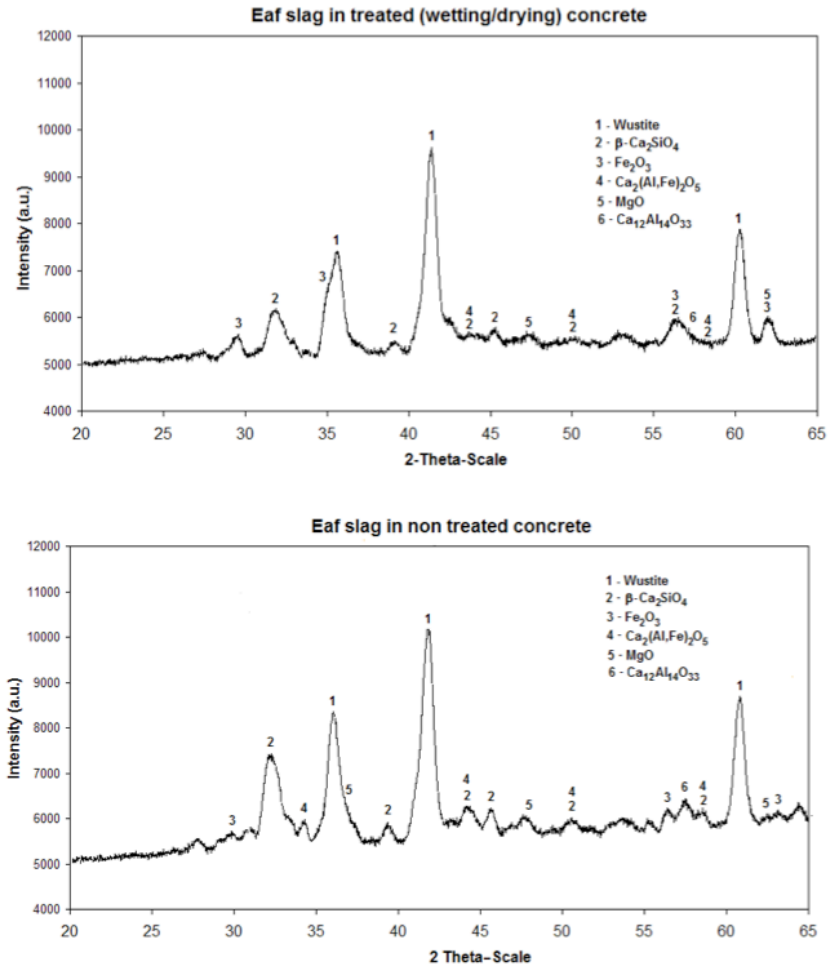

Figure 3-11. XRD patterns of EAF slag extracted from concrete before and after wetting/drying cycles.

Chemical composition and detection of oxides was obtained through the analysis of polished thin samples extracted from the superficial zone of concrete specimens of Mix 4, subjected to accelerated ageing (*D2*), using Philips PV 9800 SEM, with energy dispersive analysis (EDS). Produced spectra applying this analytical technique are similar for all the samples tested, obtaining a maximum fluctuation in quantitative estimation of elements of ±2%, mainly due to the nature of scrap materials in the furnace, during steel production. Fig. 3-12 and Table 3-10 illustrate results of the analyses, firstly defining a qualitative indication of the elements detected inside the slag, and then, after results processing through standardless EDAX ZAF quantification, a quantitative definition of weight percentage of oxides in the material, whose results are similar to those present in [3.15].

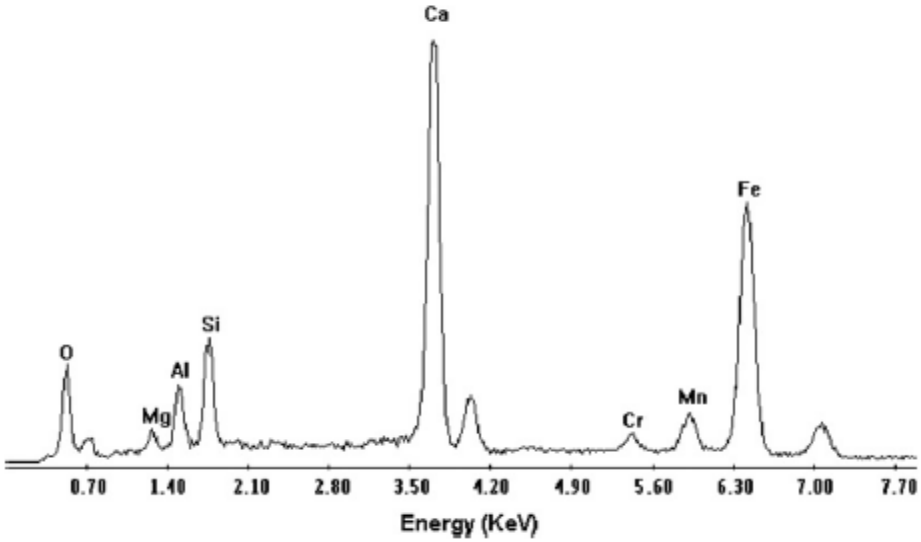

Figure 3-12. EDS spectrum on EAF slag extracted from concrete after accelerated ageing treatment.

Table 3-10. Oxides weight percentage content in EAF slag, detected after EDS-EDAX analysis.

Oxide	*Wt (%)*
MgO	*4.02*
Al_2O_3	*10.99*
SiO_2	*16.61*
CaO	*27.79*
Cr_2O_3	*2.17*
MnO	*4.67*
FeO/Fe_2O_3	*33.75*
Total	*100*

3.7 Conclusions

This experimental campaign dealt with a thorough assessment of the suitability of using both coarse and fine recycled EAF slag aggregates in various replacement ratios for concrete production and the estimation of the effect of the slag/natural aggregate substitution on concrete chemical, physical and mechanical characteristics, durability and microstructure, evaluating the effective stability of the material. According to the results presented in this section, the following conclusions can be drawn:

1. The use of EAF slag has a negative impact on the workability of the mixes when substitution ratio becomes high (more than 50%). It is recommended to maintain at least 50% of fine natural aggregates content, to prevent difficulties in mix preparations.

2. Other than increasing the specific weight of the concrete, the use of EAF slag as a coarse aggregate contributes to increase compressive and tensile strength, and elastic modulus. On the other hand, the effect of EAF slag, when it replaced the wholeness of the fine aggregates (e.g. Mix 2 and Mix 5), has a negative influence on compressive strength, causing, in this case, losses until 7% compared to the traditional mix.

3. The influence of environmental cycles on compressive strength is generally similar for traditional and recycled concrete. Accelerated ageing showed that specimens containing EAF slag as fine aggregates had less significant increase in compressive strength than specimens with EAF slag only as coarse aggregates (average variation of compressive strength in Mix 2 and Mix 5 about +2%; average variation of compressive strength in Mix 3 and Mix 4 about +8%). Both traditional and recycled mixes showed a significant decrease in strength when subjected to wetting and drying cycles: losses were about 15% for traditional concrete and until about 22% for concrete with recycled aggregates.

4. SEM images highlighted a difference between the matrix of Mix 5 (for which both coarse and fine natural aggregates have been replaced by EAF slag) and the other conglomerates in which the use of air-entrainer admixture allowed a well-developed air bubble system and a compact matrix with regular cracks. Mix 5, with recycled materials only, seemed to develop less bubbles with small diameter, showing that the admixture could behave in a different way when EAF fine particles are used and natural sand is not present.

5. Crystalline lattice of EAF slag showed complex mineralogical structures, which seem to improve the stability of the material. Free oxides quantity is limited, and possible further expansion phenomena seemed to be substantially prevented. Furthermore, no significant difference was observed on chemical and mineralogical structure in specimens before and after durability tests.

3.8 Appendix

3.8.1 Compressive strength results

For each mixture, three samples were tested to evaluate compressive strength at 28 days. When possible, also at 7 days three samples were tested. Results are listed in Table 3-11 and Table 3-12.

Table 3-11. Compressive strength at 7 days.

#	Density [kg/m^3]	$f_{c.cube}$ [MPa]	Ultimate Load [kg]	Mix	Density [kg/m^3]	$f_{cm.cube}$ [MPa]
Trad 6B	2249.8	37.00	84862	Trad	2381.2	37.8
Trad 6C	2512.6	38.60	88532			
Mix 1 6B	2526.8	35.30	80963	Mix 1	2526.8	35.3
Mix 2 6B	2710.5	33.10	75917	Mix 2	2710.5	33.1
Mix 3 6A	2848.9	38.30	87844	Mix 3	2827.9	37.5
Mix 3 6B	2806.8	36.80	84403			
Mix 4 6A	2933.9	36.90	84633			
Mix 4 6B	2883.0	36.10	82798	Mix 4	2905.3	36.0
Mix 4 6C	2899.0	35.10	80506			
Mix 5 6A	3146.1	36.70	84174			
Mix 5 6B	3136.3	32.70	75000	Mix 5	3122.1	33.9
Mix 5 6C	3083.9	32.40	74312			

Table 3-12. Compressive strength at 28 days.

#	Density [kg/m^3]	$f_{c.cube}$ [MPa]	Ultimate Load [kg]	Mix	Density [kg/m^3]	$f_{cm.cube}$ [MPa]
Trad 5A	2496.0	45.50	104358			
Trad 5B	2509.6	44.70	102523	Trad	2491.9	44.6
Trad 5C	2469.9	43.70	100229			
Mix 1 5A	2650.4	48.40	111010			
Mix 1 5B	2619.3	44.40	101835	Mix 1	2610.0	45.4
Mix 1 5C	2563.0	43.46	98690			
Mix 2 5A	2776.6	46.70	107110			
Mix 2 5B	2721.5	39.20	89908	Mix 2	2780.0	44.0
Mix 2 5C	2842.1	46.10	105734			
Mix 3 5A	2760.0	40.90	93807			
Mix 3 5B	2764.7	44.30	101606	Mix 3	2789.4	45.2
Mix 3 5C	2843.6	50.50	115826			
Mix 4 5A	2941.0	46.30	106193			
Mix 4 5B	2909.6	45.40	104128	Mix 4	2940.9	45.1
Mix 4 5C	2972.1	43.60	100000			
Mix 5 5A	3185.5	45.00	103211			
Mix 5 5B	3121.8	39.40	90367	Mix 5	3134.7	41.4
Mix 5 5C	3096.9	39.80	91284			

3.8.2 Tensile strength results

For each mixture, three samples were tested to evaluate tensile strength at 28 days. Results are listed in Table 3-13.

Table 3-13. Tensile strength results.

#	Density [kg/m^3]	f_{ct} [MPa]	Ultimate Load [kg]	Mix	f_{ctm} [N/mm^2]
Trad A	2434.3	3.56	25600		
Trad B	2421.6	3.86	27800	Trad	3.54
Trad C	2422.5	3.19	22800		
Mix 1 A	2594.9	3.73	26700		
Mix 1 B	2577.3	4.22	30200	Mix 1	3.73
Mix 1 C	2523.0	3.24	23100		
Mix 2 A	2787.2	3.58	25600		
Mix 2 B	2729.9	3.35	24000	Mix 2	3.62
Mix 2 C	2848.0	3.93	28000		
Mix 3 A	2751.7	3.10	22100		
Mix 3 B	2794.5	4.02	28800	Mix 3	3.56
Mix 3 C	2811.3	2.89	20700		
Mix 4 A	2912.3	4.26	30500		
Mix 4 B	2896.3	3.86	27500	Mix 4	4.01
Mix 4 C	2888.3	3.91	27800		
Mix 5 A	3213.6	4.09	29200		
Mix 5 B	3090.8	4.14	29600	Mix 5	3.76
Mix 5 C	3099.2	3.06	21900		

3.8.3 Elastic modulus results

For each mixture, three samples were tested to evaluate the secant modulus of elasticity. Results are listed in Table 3-14.

Table 3-14. Elastic modulus results.

#	E_c [Mpa]	Mix	$E_{cm.}$ [Mpa]
Trad A	36961		
Trad B	37383	Trad	37507
Trad C	38176		
Mix 1 A	41190		
Mix 1 B	34549	Mix 1	37355
Mix 1 C	36327		
Mix 2 A	37012		
Mix 2 B	41618	Mix 2	38682
Mix 2 C	37416		
Mix 3 A	39116		
Mix 3 B	38793	Mix 3	40393
Mix 3 C	43269		
Mix 4 B	36697	Mix 4	40062
Mix 4 C	43426		
Mix 5 A	36885	Mix 5	38465
Mix 5 B	40044		

3.8.4 Compressive strength results after deteriorating cycles

For each mixture, three samples were tested to evaluate compressive strength after durability tests. Results are listed in Table 3-15, 3-16, 3-17 and 3-18 respectively for *D1*, *D1-2*, *D2* and *D3* tests.

Table 3-15. Compressive strength after *D1* test.

#	Density [kg/m^3]	$f_{c.cube}$ [MPa]	Ultimate Load [kg]	Mix	Density [kg/m^3]	$f_{cm.cube}$ [MPa]
Trad 3A	2481.8	51.45	118000			
Trad 3B	2499.6	53.63	123000	Trad	2490.1	51.6
Trad 3C	2488.9	49.70	114000			
Mix 1 3A	2667.3	49.70	114000			
Mix 1 3B	2618.1	48.83	112000	Mix 1	2605.8	47.0
Mix 1 3C	2532.1	42.51	97500			
Mix 2 3A	2835.6	47.09	108000			
Mix 2 3B	2736.6	41.64	95500	Mix 2	2798.8	44.8
Mix 2 3C	2824.3	45.56	104500			
Mix 3 3A	2835.0	48.61	111500			
Mix 3 3B	2859.3	51.01	117000	Mix 3	2853.3	50.8
Mix 3 3C	2865.8	52.76	121000			
Mix 4 4A	2947.6	48.40	111000			
Mix 4 4B	2951.7	46.22	106000	Mix 4	2952.1	47.5
Mix 4 4C	2957.0	47.96	110000			
Mix 5 3A	3179.9	45.34	104000			
Mix 5 3B	3102.5	40.11	92000	Mix 5	3125.6	42.4
Mix 5 3C	3094.5	41.64	95500			

Table 3-16. Compressive strength after *D1-2* test.

#	Density [kg/m^3]	$f_{c.cube}$ [MPa]	Ultimate Load [kg]	Mix	Density [kg/m^3]	$f_{cm.cube}$ [MPa]
Trad 4A	2487.7	52.97	121500			
Trad 4B	2504.9	56.68	130000	Trad	2487.5	54.5
Trad 4C	2469.9	53.85	123500			
Mix 1 4A	2624.6	57.77	132500			
Mix 1 4B	2576.0	56.24	129000	Mix 1	2570.1	53.8
Mix 1 4C	2509.6	47.52	109000			
Mix 2 4A	2765.6	51.67	118500			
Mix 2 4B	2779.3	47.96	110000	Mix 2	2783.6	51.1
Mix 2 4C	2805.9	53.63	123000			
Mix 3 4A	2815.4	51.88	119000			
Mix 3 4B	2773.3	53.19	122000	Mix 3	2816.6	56.2
Mix 3 4C	2861.0	63.66	146000			
Mix 4 4A	2958.8	54.94	126000			
Mix 4 4B	2952.9	53.63	123000	Mix 4	2932.3	53.2
Mix 4 4C	2885.3	51.01	117000			
Mix 5 3A	3170.4	53.41	122500			
Mix 5 3B	3091.0	44.91	103000	Mix 5	3119.0	48.3
Mix 5 3C	3095.7	46.65	107000			

Table 3-17. Compressive strength after *D2* test.

#	Density [kg/m^3]	$f_{c.cube}$ [MPa]	Ultimate Load [Kg]	Mix	Density [kg/m^3]	$f_{cm.cube}$ [MPa]
Trad 1A	2509.6	51.01	117000			
Trad 1B	2506.7	48.83	112000	Trad	2497.4	50.1
Trad 1C	2475.9	50.58	116000			
Mix 1 1A	2644.1	54.06	124000			
Mix 1 1B	2646.5	54.72	125500	Mix 1	2602.5	51.7
Mix 1 1C	2516.7	46.43	106500			
Mix 2 1A	2800.6	50.14	115000			
Mix 2 1B	2735.7	47.96	110000	Mix 2	2799.5	50.4
Mix 2 1C	2862.2	52.97	121500			
Mix 3 1A	2784.0	46.65	107000			
Mix 3 1B	2823.1	47.74	109500	Mix 3	2821.3	49.6
Mix 3 1C	2856.9	54.50	125000			
Mix 4 1A	2981.3	49.49	113500			
Mix 4 1B	2925.6	47.96	110000	Mix 4	2956.0	48.8
Mix 4 1C	2961.2	49.05	112500			
Mix 5 1A	3192.3	54.94	126000			
Mix 5 1B	3145.5	49.70	114000	Mix 5	3136.2	50.5
Mix 5 1C	3070.8	46.87	107500			

Table 3-18. Compressive strength after *D3* test.

#	Density [kg/m^3]	$f_{c.cube}$ [MPa]	Ultimate Load [Kg]	Mix	Density [kg/m^3]	$f_{cm.cube}$ [MPa]
Trad 2A	2509.6	39.24	90000			
Trad 2B	2510.2	41.42	95000	Trad	2500.1	39.2
Trad 2C	2480.6	37.06	85000			
Mix 1 2A	2632.3	46.87	107500			
Mix 1 2B	2648.9	46.22	106000	Mix 1	2611.0	44.5
Mix 1 2C	2551.7	40.55	93000			
Mix 2 2A	2864.6	42.29	97000			
Mix 2 2B	2775.7	39.46	90500	Mix 2	2826.3	41.3
Mix 2 2C	2838.5	42.29	97000			
Mix 3 2A	2844.4	35.53	81500			
Mix 3 2B	2833.2	36.62	84000	Mix 3	2847.0	37.9
Mix 3 2C	2863.4	41.42	95000			
Mix 4 2A	3024.6	38.59	88500			
Mix 4 2B	3005.6	37.06	85000	Mix 4	3006.6	36.9
Mix 4 2C	2989.6	35.10	80500			
Mix 5 2A	3257.5	39.68	91000			
Mix 5 2B	3155.6	34.88	80000	Mix 5	3186.6	37.4
Mix 5 2C	3146.7	37.50	86000			

3.8.5 Scanning Electron Microscopy, X-Ray Microanalysis and X-Ray Diffraction

A scanning electron microscope (SEM), equipped with an X-ray detector, is one of the most effective equipment for the in-depth analysis of cementitious materials. In the construction industry, the combination of SEM and energy dispersive X-ray microanalysis (EDS) is used for quality control and verification of material composition.

Often, SEM operates at a high vacuum: the basic principle is that a beam of electrons is generated by a suitable source, typically a tungsten filament or a field emission gun. The electron beam is accelerated through a high voltage (typically between 15-30 keV; in this section, 25 keV) and pass through a system of apertures and electromagnetic lenses to produce a thin beam of electrons. The beam scans the surface of the specimen (which can be pulverized or bulk) by means of scan coils. Electrons are emitted from the specimen by the action of the scanning beam and collected by a suitably-positioned detector.

There are different types of electron image. The two most common are the secondary electron image (SE) and the backscattered electron image (BSE). The SE-mode is typically used at high resolution, revealing details in the order of 1 μm. Secondary electrons have low energy (<50eV) and they are ejected from the k-shell of the specimen atoms by inelastic scattering interactions with beam electrons. The BSE-mode uses electrons that are reflected from the sample by elastic scattering. Backscattered electrons are often used in analytical SEM along with the spectra made from the characteristic X-rays, because the intensity of the BSE signal is strongly related to the atomic number of the compounds in the specimen. Hence, BSE images are often used to provide information about the distribution of different elements in the sample. Before the analyses, specimens should be sputtered by a conductive material, which can be gold (used in this case), gold/palladium alloy, platinum, osmium, iridium, tungsten, chromium, and graphite.

Energy-dispersive X-ray microanalysis (EDX) is a complementary analytical technique to SEM. It enables to exactly determine the composition of the features in the SEM image, and possibly quantifying the elemental composition with relative or absolute determination. The principle of EDX is that the electron beam generates X-Rays within the specimen. Many of these X-rays have energies characteristic of the elements that emitted them: measuring the energy of the X-rays, the elements in the specimen can be recognized.

Figure 3-13. SEM – Scanning Electron Microscope, equipped with EDX.

The XRD is a useful technique for the direct identification of crystalline phases present in cementitious materials. X-ray diffraction is based on constructive interference of monochromatic X-rays and a crystalline sample. These X-rays are generated by a cathode ray tube, filtered to produce monochromatic radiation, collimated to concentrate, and directed toward the sample. The interaction of the incident rays with the sample produces constructive interference (and a diffracted ray) if Bragg's Law is satisfied [3.15]. This law relates the wavelength of electromagnetic radiation to the diffraction angle and the lattice spacing in a crystalline sample. The diffracted X-rays could be then detected, processed and counted. By scanning the sample through a range of 2θ angles, all possible diffraction directions of the lattice should be attained due to the random orientation of the powdered material. Conversion of the diffraction peaks to *d-spacing* allows identification of the mineral (each mineral has a set of unique *d-spacing*), via a comparison with standard patterns.

Typically XRD analyses are conducted on pulverized samples, taking the name of XRPD (X-Ray Powder Diffraction), even though this technique can be applied also on properly polished bulk specimens. Copper is the most common target material for single-crystal diffraction, with CuK_{α} radiation = 1.5418Å. These X-rays are collimated and directed onto the sample. As the sample and detector are rotated, the intensity of the

reflected X-rays is recorded. When the geometry of the incident X-rays impinging the sample satisfies the Bragg Equation, constructive interference occurs and a peak in intensity occurs. A detector records and processes this X-ray signal and converts the signal to a count rate which is then output to an output device, such as a computer monitor (patterns as shown in Fig. 3-11). The geometry of an X-ray diffractometer is such that the sample rotates (look at Fig. 3-14 on the left) in the path of the collimated X-ray beam at an angle θ while the X-ray detector is mounted on an arm to collect the diffracted X-rays and rotates at an angle of 2θ. For typical powder patterns, data is collected at 2θ from ~5° to 70°.

Figure 3-14. XRD – left: particular of the goniometer; right: sample holder.

References

[3.1] Pellegrino C., Gaddo V. Mechanical and durability characteristics of concrete containing EAF slag as aggregate. Cement and Concrete Composites 2009; 31(9): 663–671.

[3.2] Wang G., Wang Y., Gao Z. Use of steel slag as a granular material: volume expansion prediction and usability criteria. Journal of Hazardous Materials 2010; 184: 555–560.

[3.3] Luxàn M.P., Sotolongo R., Dorrego F., Herrero E. Characteristics of the slag produced in the fusion of scrap steel by electric arc furnace. Cement and Concrete Research 2000; 30: 517–519.

[3.4] Decreto Ministeriale N. 186 5/04/2006: Test di cessione, 2006 [in Italian].

[3.5] EN 206-1. Concrete – Part 1: Specification, performance, production and conformity; CEN, Comité Europeen de Normalisation, Brussels, Belgium; 2006.

[3.5] Manso J.M., Polanco J.A., Losañez M., González J.J. Durability of concrete made with EAF slag as aggregate. Cement and Concrete Composites 2006; 28: 528–534.

[3.6] Etxeberria M., Pacheco C., Meneses J.M., Berridi I. Properties of concrete using metallurgical industrial by-products as aggregates. Construction and Building Materials 2010; 24: 1594–1600.

[3.7] EN 12390-1. Testing hardened concrete – shape, dimensions and other requirements for specimens and moulds; CEN, Comité Europeen de Normalisation, Brussels, Belgium; 2002.

[3.8] UNI EN 6556. Tests of concretes – determination of static modulus of elasticity in compression; UNI, Ente Nazionale Italiano di Unificazione, Milan, Italy; 1976 [in Italian].

[3.9] EN 12390-4. Testing hardened concrete – compressive strength – specification for testing machines. CEN, Comité Europeen de Normalisation, Brussels, Belgium; 2000.

[3.10] EN 12390-6. Testing hardened concrete – tensile splitting strength of test specimens. CEN, Comité Europeen de Normalisation, Brussels, Belgium; 2009.

[3.11] ASTM 4792-00. Standard test method for potential expansion of aggregates from hydration reactions; ASTM Committee D04 on Road and Paving Materials, West Conshohocken, PA, United States; 2006.

[3.12] Polanco J.A., Manso J.M,. Setién J., Gonzàlez J.J. Strength and durability of concrete made with electric steelmaking slag. ACI Materials Journal 2011; 108: 196–203.

[3.13] Abu-Eishah Samir I., El-Dieb Amr S., Bedir Mostafa S. Performance of concrete mixtures made with electric arc furnace (EAF) steel slag aggregate produced in the Arabian gulf region. Construction and Building Materials 2012; 34: 249–256.

[3.14] Frías M., Sánchez de Rojas M.I. Chemical assessment of the electric arc furnace slag as construction material: expansive compounds. Cement and Concrete Research 2004; 34: 1881–1888.

[3.15] Bragg W.H., Bragg W.L. The Reflexion of X-rays by Crystals. Proceeding of the Royal Society of London, Series A 1913; 88(605): 428-438.

4 Structural behavior of RC EAF concrete

4.1 Abstract

In this section the possibility of partially substituting natural aggregates with black/ oxidizing electric arc furnace slag for reinforced concrete (RC) structural elements is explored. International research has been mainly focused on experimental tests on small specimens rather than investigating the behavior of RC structural elements. In this study, the experimental behavior of RC beams made with EAF slag as aggregate was studied showing that these beams have both ultimate flexural and shear capacity higher than the corresponding reference beams with just natural aggregates. Some comparisons between experimental results and analytical predictions according to the European and U.S. recommendations were also shown. The main result of this work is that the use of steel slag as aggregate in RC structural elements is, in principle, possible, and the rate of substitution could reach the entire part of coarse aggregates, obtaining benefits both from economical and environmental point of view.

4.2 Introduction

In the context of waste reutilization in construction to reduce costs and potential pollution problems, and preserve natural raw resources, some researches have been undertaken to test mechanical and durability properties of concrete containing EAF slag, showing very promising results [4.1]. Nevertheless, international literature has been mainly focused on experimental tests on small specimens rather than investigating the behavior of RC structural elements. Very little research is available on structural elements (for example, beams) made with recycled concrete, and these are mainly related to the use of aggregates derived from building demolition waste. For these reasons, this experimental study aims to increase the knowledge of flexural and shear behavior of RC structural elements made with concrete containing EAF slag as a partial substitution of natural aggregates.

The main purpose of this research is to test a new, sustainable building material allowing to save raw materials, reduce energy consumption, and recycle industrial refuses; and contribute to the existing knowledge on flexural and shear behavior of RC structural elements made with concrete containing EAF slag as a partial substitution of natural aggregates.

In this section first a physical/mechanical and chemical characterization of reference and recycled concrete, designed according to Fuller's ideal grading curve, is presented. Then twelve RC beams were casted, four made by a reference concrete, including just natural aggregates, and eight with EAF as a fully replacement of the coarse aggregates. Four different reinforcement ratios were used, according to the required failure mode. Structural behavior was then investigated by means of four-point bending tests on RC beams made with natural and recycled aggregates, subjected to both flexural and shear failure. Maximum load, deflections, crack patterns, and crack widths were measured. Comparisons between experimental results and analytical predictions according to the European and U.S. recommendations are shown.

4.3 Materials

The first part of the experimental program was related to chemical and physical/mechanical characterization of the materials used in the tests on the structural elements.

The experimental program deals with a black EAF slag with high density and low water absorption, obtained from a local steel factory. Its main physical properties are reported in Table 4-1, and they are evaluated according to [4.2]. Three classes of EAF aggregates were used, depending on their size: 4-8 mm, 8-16 mm, 16-22 mm. Before the use, a stabilization process was applied to the slag: first the slag was externally stored, exposed to atmospheric conditions for about three months, and then it was continuously wetted for a couple of days. This procedure, very simple, allows the stabilization to occur rapidly, due to a sort of crystallization which deactivates the possible internal reagent components. It has also to be highlighted that, even without treatment, risks of expansion are very low.

Leaching tests on slag have been preliminarily developed to verify that the possible presence of toxic compounds remain below Italian standard thresholds [4.3]. Results reported in Table 4-2 show that, from this point of view, the slag used in this work is fully admissible to be used as concrete aggregate.

Table 4-1. Physical properties of EAF slag.

	Medium/coarse EAF slag
Size (mm)	*4-22.4*
Apparent specific gravity (t/m³)	*3.876 - 3900*
Water absorption (%)	*0.4 - 0.5*
Shape	*sharp-pointed*
Fineness modulus	*6.59 - 7.78*
Shape index (4 - 8 mm) (%)	*2.2*
Shape index (8 - 16 mm) (%)	*2.7*
Shape index (16 - 22 mm) (%)	*1.5*
Flakiness index (4 - 8 mm) (%)	*4.4*
Flakiness index (8- 16 mm) (%)	*6.1*
Flakiness index (16 - 22 mm) (%)	*3.6*
Los angeles loss (%)	*< 20*

A chemical characterization on pulverized slag extracted from the concrete used in the experimental tests was performed using an X-ray diffraction (XRD) test and energy dispersive X-ray spectroscopy (EDX) to verify the stability of the material when used for concrete production. On one hand, the extraction of these aggregates from the concrete matrix could lead to the incorporation of cement paste on the tested powders. On the other hand, it allows a better understanding of the behavior of the raw material when included in the concrete matrix. Results obtained are reported in Fig. 4-1 and 4-2, showing a well-developed mineralogical system that improves the stability of the material. The weight percentage of the oxides detected in the slag has about 35% of ferrous/ferric oxides, 28% of calcium oxide, 10% of aluminum oxide, 17% of silicon dioxide, 4% of manganese and 4% of magnesium oxides, plus a minor content of other compounds.

Table 4-2. Leaching test results.

Parameter	*Concentration (mg/l)*	*Limits*
Nitrates	*< 40*	*50*
Fluorides	*< 1.5*	*1.5*
Sulfates	*< 200*	*250*
Chlorides	*< 75*	*100*
Cyanides	*< 0.03*	*0.050*
Barium	*0.0125*	*1*
Copper	*< 0.001*	*0.050*
Zinc	*< 0.03*	*3*
Beryllium	*< 0.005*	*0.010*
Cobalt	*< 0.01*	*0.250*
Nickel	*< 0.005*	*0.010*
Vanadium	*0.103*	*0.250*
Arsenic	*< 0.02*	*0.050*
Cadmium	*< 0.003*	*0.005*
Total chromium	*< 0.002*	*0.050*
Lead	*< 0.04*	*0.050*
Selenium	*< 0.010*	*0.010*
Mercury	*< 0.001*	*0.001*
Amianthus	*< 10*	*30*
COD	*< 25*	*30*
pH	*10.78*	*5.5-12.0*

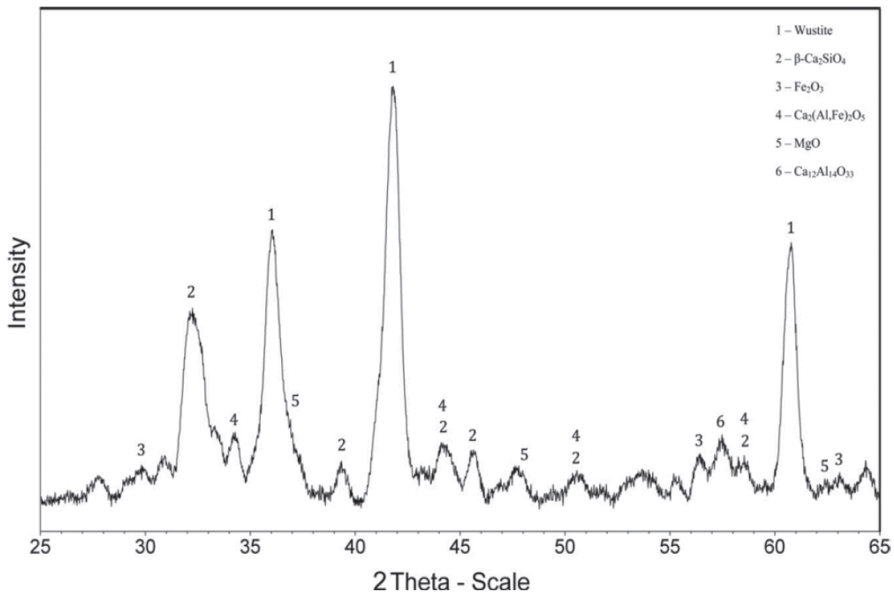

Figure 4-1. XRD spectrum obtained from sample of pulverized EAF slag extracted from concrete.

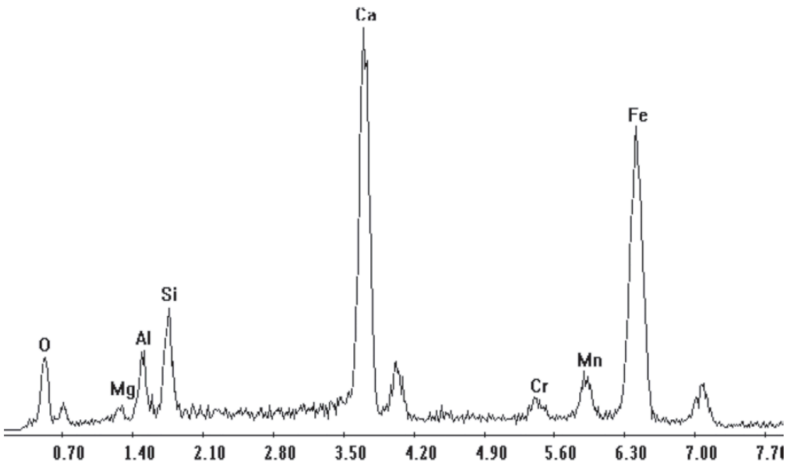

Figure 4-2. EDS spectrum from a pulverized sample of EAF slag.

Natural aggregates used in this experimental campaign have a limestone origin, and their main physical characteristics, according to [4.2], are reported in Table 4-3. Three classes of NA were used, with the following size: 0-4mm (used both for the reference concrete and for the EAF slag mix), 4-16 mm and 16-31.5 mm.

Table 4-3. Physical properties of natural aggregates.

	Medium/coarse NA
Size (mm)	*4-31.5*
Apparent specific gravity (t/m³)	*2.724- 2.736*
Water absorption (%)	*0.8 - 1.16*
Shape	*roundish*
Fineness modulus	*3.15- 7.82*

4.4 Mix proportions

Similarly to a previous research conducted at the University of Padova [4.4], two mixtures were designed for the present study: the first, which contained natural sand filler/medium-coarse EAF slag; and the control, which contained only natural aggregates. The first mixture contains almost 65% by weight of slag with respect to the total aggregate amount. For each mixture, the size fractions correspond to two Fuller's ideal grading curves [4.5], which describes a mixture of aggregates minimizing the void index. The aggregate grading curves are reported in Fig. 4-3.

The objective was to obtain a S4 slump class concrete, as defined in [4.6]. Cement adopted for both mixtures belongs to II/A – L 42.5R class. This cement, with high clinker content, has been chosen because it is very diffused in common applications in Italy. The cement content is slightly different in each mixture in relation to the maximum diameter of the various aggregates. Because maximum slag diameter is smaller than the maximum diameter of traditional aggregate, an increase of 20 kg/m^3 in cement content was necessary in the mixture with slag. The water-cement ratio (w/c) was 0.55 for traditional concrete and 0.53 for concrete with slag. A super-plasticizer SP agent (0.4% of cement weight) and an air-entrainer admixture AEA (0.016% of cement weight) were used to improve the durability and support in bleeding prevention. In Table 4-4, the main characteristics of the two mixtures are listed.

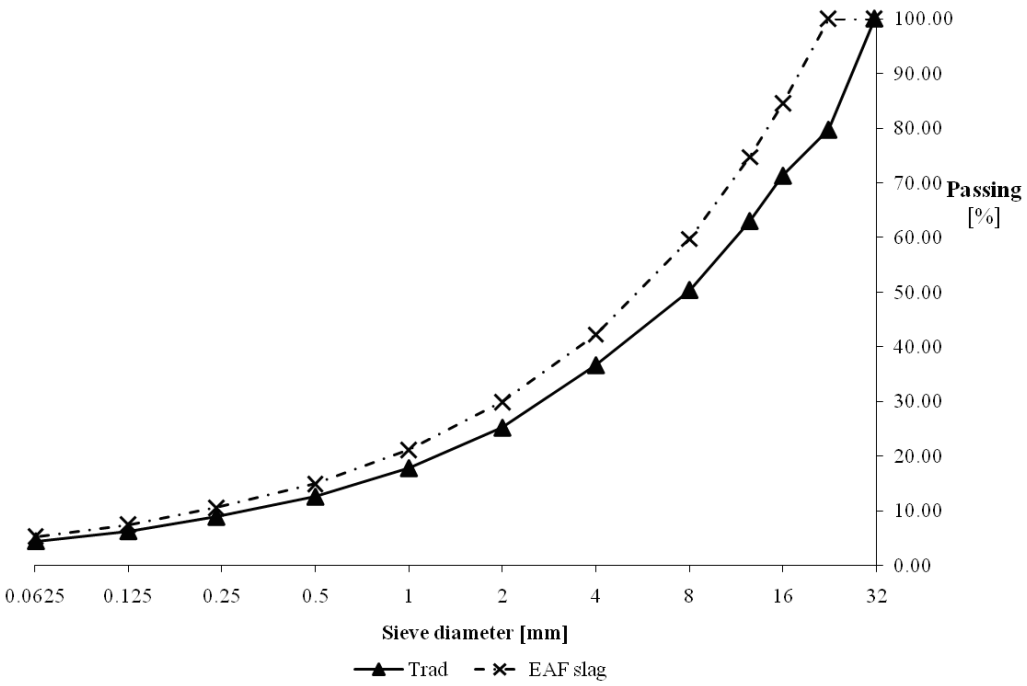

Figure 4-3. Aggregates grading curve.

Table 4-4. Mixtures details.

	EAF concrete	*Reference concrete*
D_{max} (mm)	*22.4*	*31.5*
$V_{aggregates}$ (m^3)	*0.763*	*0.746*
Cement (kg)	*310*	*290*
Water (kg)	*164.3*	*159.5*
w/c	*0.53*	*0.55*
EAF slag SSD(kg)*	*2041*	*-*
NA SSD (kg)*	*617.24*	*2098.43*
Super-plasticizer (kg)	*1.24*	*1.16*
Air entrainer (g)	*49.6*	*46.4*

** SSD= surface saturated dry*

4.5 Experimental methods

The second part of the work deals with flexural and shear behavior of structural elements. Twelve RC beams were casted with the following dimensions: width w = 185 mm; height h = 300 mm; length l = 2000 mm; effective depth d = 270 mm; and shear span a = 750 mm. The beams were designed for obtaining bending or shear failure and were divided in four typologies, according to their steel reinforcement configuration. In the Appendix to this section, the details of the reinforcement in the RC beams is reported.

For each failure type, one specimen was tested with traditional concrete, and two with concrete containing slag as aggregate. Reinforcement descriptions are reported for each specimen in Table 4-5, and geometrical characteristics of the cross sections of the beams are illustrated in Fig. 4-4. Reinforcement steel has a mean yield strength of 535 MPa, and a mean ultimate strength of 650 MPa. Five cubic specimens with 150 mm sides for compressive tests, one cylindrical specimen with a diameter of 150 mm and a length of 300 mm for splitting test and one cylindrical specimen with a diameter of 150 mm and a length of 450 mm for Young's modulus calculation were made for each beam. Compressive tests have been developed on cubic specimens after 7 days (two specimens for each beam) and after 28 days (three specimens for each beam), following the [4.7]. Splitting tests were performed to experimentally evaluate tensile strength, following the European Standard [4.8]. Load cycles were performed on one cylindrical specimen for each beam for the evaluation of elastic modulus, according to [4.9]. Results are listed in Table 4-6.

Table 4-5. Reinforcement details for tested beams.

	Mixture	Reinforcement			Failure
		top	bottom	stirrups	
A1_1	Reference	2ϕ10	3ϕ10	ϕ8/200 mm	Bending
A1_2	EAF slag	2ϕ10	3ϕ10	ϕ8/200 mm	Bending
A1_3	EAF slag	2ϕ10	3ϕ10	ϕ8/200 mm	Bending
A2_1	Reference	2ϕ18	3ϕ18	ϕ8/200 mm	Bending
A2_2	EAF slag	2ϕ18	3ϕ18	ϕ8/200 mm	Bending
A2_3	EAF slag	2ϕ18	3ϕ18	ϕ8/200 mm	Bending
B1_1	Reference	-	2ϕ18+2ϕ14	-	Shear
B1_2	EAF slag	-	2ϕ18+2ϕ14	-	Shear
B1_3	EAF slag	-	2ϕ18+2ϕ14	-	Shear
B2_1	Reference	2ϕ20	4ϕ24	ϕ8/200 mm	Shear
B2_2	EAF slag	2ϕ20	4ϕ24	ϕ8/200 mm	Shear
B2_3	EAF slag	2ϕ20	4ϕ24	ϕ8/200 mm	Shear

It is significant to observe that the compressive strength of concrete containing EAF slag as aggregate is higher than that of the traditional concrete, even if both mixtures were produced with the same aggregates grading curve. This result can be related to higher slag compressive strength with respect to traditional aggregates and also to the slight increase in cement content in concrete with EAF slag.

Specimens made with the reference concrete had lower values of tensile strength than those made with recycled slag, because the shape of natural aggregates is more round and it presents less angularities than EAF slag (this was observed after the splitting failure). These properties could also affect compressive strength and Young's modulus, which are higher in concrete with steel slag.

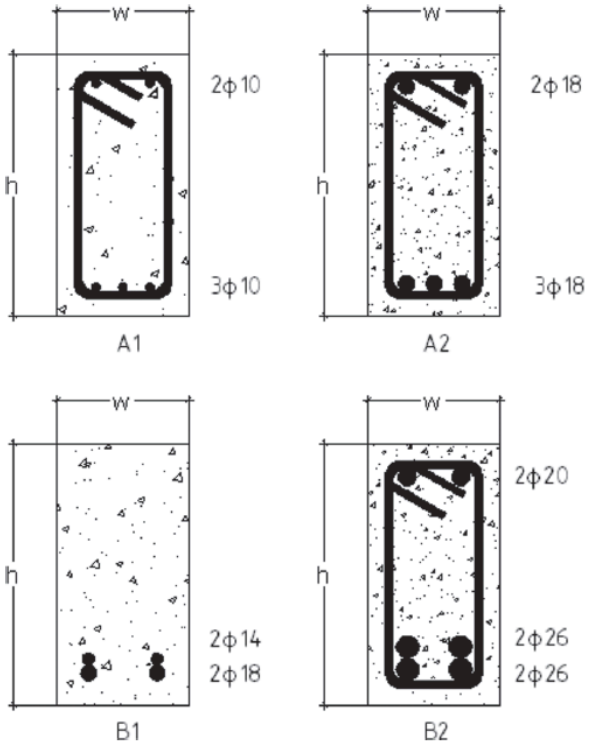

Figure 4-4. Cross sections of beams (Note: diameter of bars are expressed in mm).

Table 4-6. Mechanical properties of experimental concretes.

Mix type	*specific weight after 28 days [kg/m³]*	*slump [cm]*	$f_{c,cube\ 7d}$ *[MPa]*	$f_{c,cube\ 28d}$ *[MPa]*	$f_{ctm,\ exp}$ *[MPa]*	$E_{cm,\ exp}$ *[GPa]*
EAF slag	*3006*	*16.8*	*48.80*	*58.30*	*4.38*	*40.05*
Reference	*2447*	*21.2*	*27.20*	*34.50*	*3.54*	*37.40*

Another important consideration is related to the workability of the mixtures: the presence of EAF slag increases water demand and, hence, a SP admixture and a viscous agent could be used to adjust the fluidity of fresh concrete. Table 4-6 shows that slump value is lower on concrete containing EAF slag compared to a traditional mixture, but this could be due to the choice of maintaining similar w/c and the same plasticizer content in the two mixtures even if this could cause less workability for EAF concretes.

Two different typologies of beams were designed to obtain flexural failure: the first has a low steel reinforcement ratio (three bars with 10 mm

diameter at the tensile side; steel reinforcement ratio $\rho = \frac{A_w}{bd} = 0.157\%$), whereas the second has a high reinforcement ratio (three bars with 18 mm diameter at the tensile side $\rho = \frac{A_w}{bd} = 1.527\%$). Two steel reinforcement ratios have been adopted to obtain flexural failures with different levels of ductility. Deflection was measured at midspan by using ± 0.01mm precision linear variable differential transducers (LVDTs). Cracks widths were measured by using ±0.001mm precision deformation transducers. The instrumentation and load scheme are shown in Fig. 4-5.

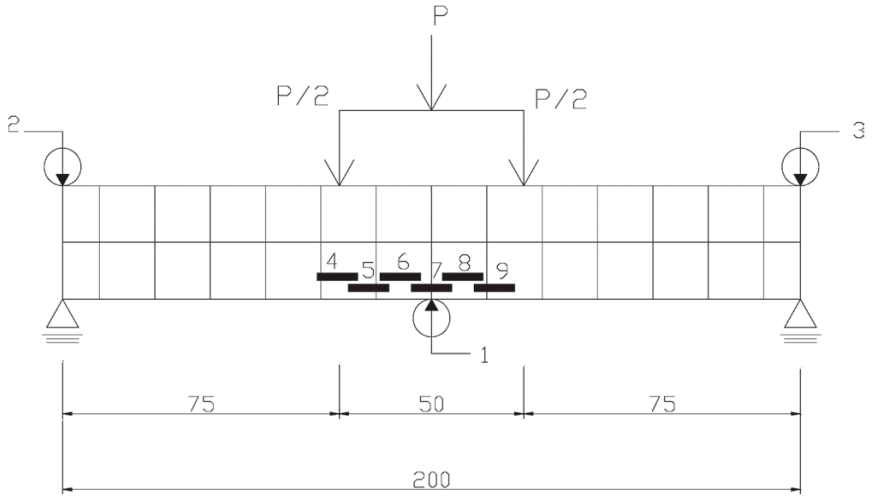

Figure 4-5. Instrumentation and load scheme for beams for which flexural failure was expected. Circles identify LDTV; DD1 are represented by black rectangles. (Note: Measures are expressed in cm).

Two different typologies of beams were designed to obtain a shear failure: the first without shear reinforcement, and the second with stirrups. The first type was designed with the aim of obtaining shear capacity due to concrete only. It was necessary to provide a very high longitudinal reinforcement ratio in both beams to prevent bending failure $\rho = \frac{A_w}{bd} = 1.634\%$ in B1 beams; $\rho = \frac{A_w}{bd} = 3.62\%$ in B2 beams). The instrumentation to measure deflection and crack width is shown in Fig. 4-6.

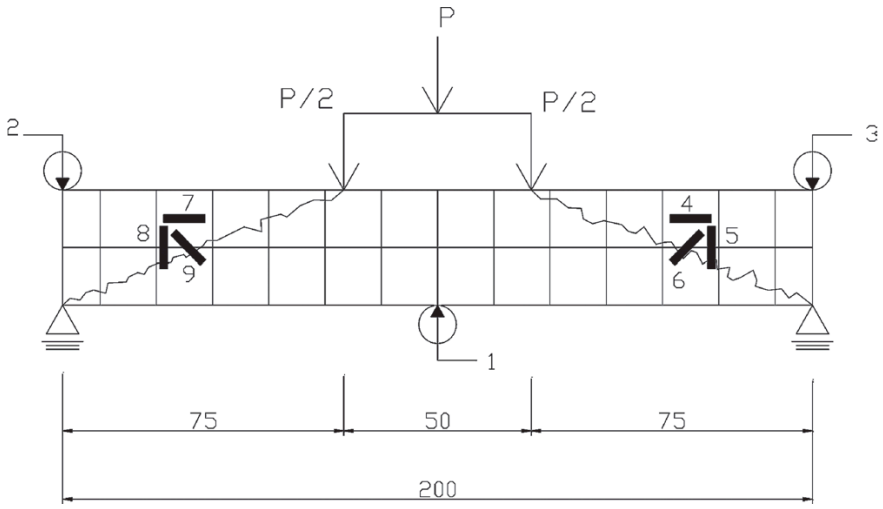

Figure 4-6. Instrumentation and load scheme for beams for which shear failure was expected. Circles identify LDTV; DD1 are represented by black rectangles. (Note: Measures are expressed in cm).

4.6 Results and discussion

Twelve RC flexural elements were subjected to four-point bending tests (refer to Fig. 4-5) with the aim of obtaining values of failure load, deflection at midspan, crack patterns, and crack width. A 150 x 150 mm grid was drawn on the beams to detect cracks formation.

4.6.1 Flexural behavior

Table 4-7 lists the main experimental results. Average mechanical properties and unit safety coefficients were assumed to compare theoretical and experimental results. The theoretical value of ultimate load is calculated by means of equilibrium and strain compatibility equations according to the usual hypotheses of the limit state approach [4.10].

Load-versus-deflection diagrams are illustrated in Fig. 4-7 and load-versus-crack width diagrams are shown in Fig. 4-8. An increase of ultimate flexural capacity is observed for all the beams with EAF slag with respect to beams with traditional aggregates; furthermore, any significant difference in structural behavior in terms of cracking pattern and failure mode is noted. Ultimate capacity and first cracking moment are higher and crack widths are smaller for the beams with recycled concrete due to a combination of factors: slightly higher cement content; slightly lower w/c; higher tensile strength of EAF slag; and higher cohesion in the matrix in beams containing EAF slag with respect to those made with traditional concrete. As described in [4.11], aggregates with angular sharp edges can

improve the cohesion of concrete matrix because of the good abrasion properties due to rough surface and porosity. This phenomenon is observed both in RC beams with low and high reinforcement ratios. Cracks patterns were obtained for all the RC elements tested, and they are represented in Fig. 4-9.

Table 4-7. Experimental and theoretical results in terms of ultimate load P_{ult} and deflection f_{ult}.

Beam	*Mix Type*	$P_{ult,th}$ *(kN)*		$P_{ult,exp}$ *(kN)*	f_{ult} *(mm)*
A1_1	*reference*	*85.25*		*82.37*	*36.7*
A1_2	*with EAF*	*88.66*		*89.85*	*26.17*
A1_3	*with EAF*	*88.66*		*82.88*	*33.57*
A2_1	*reference*	*262.24*		*274.46*	*15.95*
A2_2	*with EAF*	*269.30*		*304.28*	*16.09*
A2_3	*with EAF*	*269.30*		*294.06*	*18.63*
		$P_{ult,EC2}$ *(kN)*	$P_{ult,ACI}$ *(kN)*	$P_{ult,exp}$ *(kN)*	f_{ult} *(mm)*
B1_1	*reference*	*108.04*	*113.24*	*180.44*	*8.65*
B1_2	*with EAF*	*135.22*	*138.95*	*205.90*	*5.27*
B1_3	*with EAF*	*135.22*	*138.95*	*198.06*	*7.23*
B2_1	*reference*	*326.57*	*324.15*	*350.54*	*9.40*
B2_2	*with EAF*	*326.57*	*349.85*	*428.15*	*9.16*
B2_3	*with EAF*	*326.57*	*349.85*	*378.62*	*7.48*

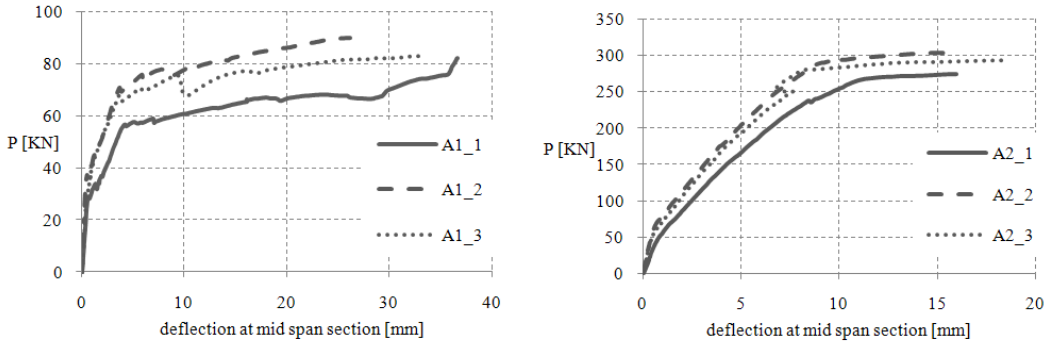

Figure 4-7. Load versus deflection at midspan diagrams for beams of "A" Series.

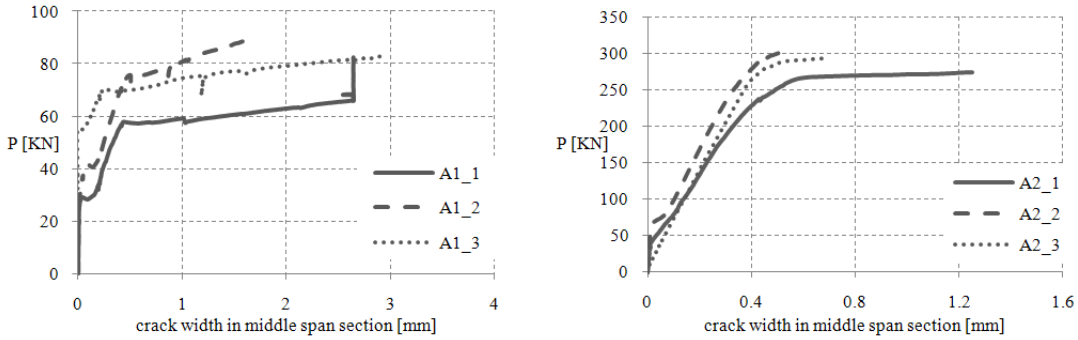

Figure 4-8. Load versus crack width diagrams for beams of "A" Series.

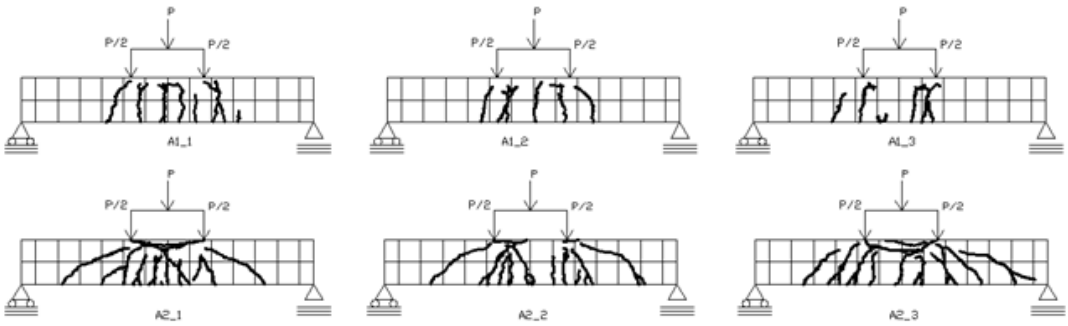

Figure 4-9. Crack patterns in RC structural elements after bending failure.

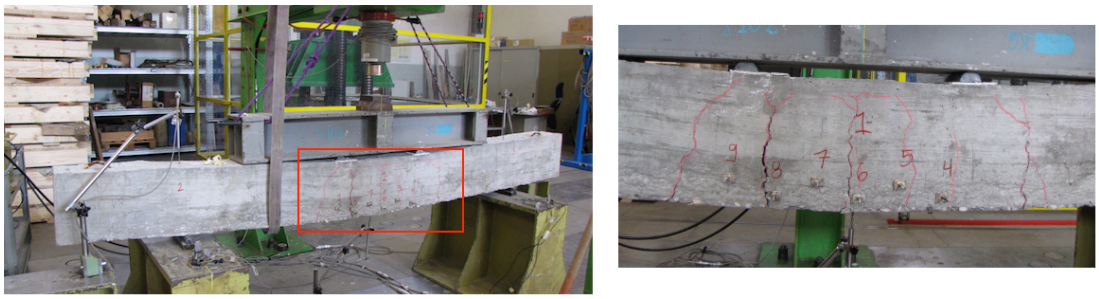

Figure 4-10. Bending Failure: Concrete cracking – "A1" series.

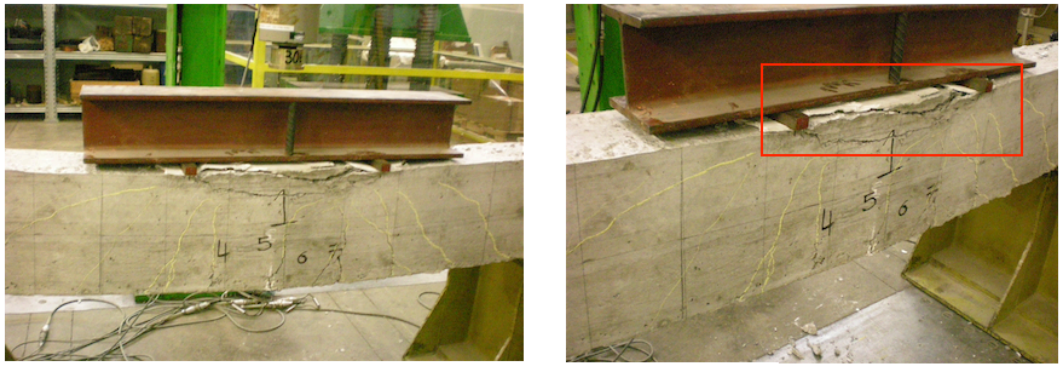

Figure 4-11. Bending Failure: Concrete cracking (bottom) and crushing (top) – "A2" series.

4.6.2 Shear behavior

Eurocode 2 [4.10] and ACI 318 [4.12] formulas were used to calculate theoretical values of ultimate load, both for elements with and without shear reinforcement. Also in this case, average mechanical properties and unit safety coefficients were assumed to compare theoretical and experimental results. For elements without shear reinforcement, shear strength provided by concrete according to the Eurocode 2 formula is:

$$V_{R,c} = C_{R,c} \cdot k \cdot (100 \cdot \rho_l \cdot f_{ck})^{1/3} + k_1 \cdot \sigma_{cp}] \cdot b_w \cdot d \qquad \textbf{4-1}$$

where:
$C_{R,c}$ is basic shear stress strength = 0.18;
$k = 1 + (200/d)^{1/2}$ = size factor, with d in [*mm*];
$\rho_l = A_{sl}/(b_w\, d)$ is the longitudinal reinforcement ratio;
A_{sl} is the area of the longitudinal reinforcement [mm^2];
b_w is the width of the cross-section [*mm*];
d = effective depth of the cross-section [*mm*];
f_{ck} = characteristic value of the concrete cylindrical compressive strength [*MPa*];
$k_1 \cdot \sigma_{cp} = 0$ without pre-stressing forces (as in this case).

The ACI 318 relation is the following:

$$V_c = [0.16 \cdot (f'_c)^{1/2} + 17 \cdot \rho_w \cdot (V_u \cdot d/M_u)] \cdot b_w \cdot d \qquad \textbf{4-2}$$

where:
f'_c = concrete cylindrical compressive strength [*MPa*];
$\rho_w = A_{sw}/(b_w\, d)$ = transverse reinforcement ratio;

A_{sw} = cross sectional area of the stirrups [mm^2];
V_u = shear force at the considered cross-section [*N*];
M_u = bending moment at the considered cross-section [Nm].

Concerning RC beams with stirrups, Eurocode 2 adopts the typical strut-and-tie model, where overall shear strength is given by the minimum of the following two values:

$$V_{Rd,s} = A_{sw} \cdot z \cdot f_{yw} \cdot cot\theta / s \quad \textbf{4-3}$$

$$V_{Rd,max} = \alpha_{cw} \cdot b_w \cdot z \cdot \nu_1 \cdot f_{cd} / (cot\,\theta + tan\theta) \quad \textbf{4-4}$$

where:
s = stirrups' spacing [*mm*];
z = internal level arm that can be assumed equal to 0.9 d [*mm*];
f_{yw} = yielding stress of the stirrups [*MPa*];
θ = angle between concrete strut and longitudinal axis of the beam. In this case, θ=21.8 degrees was adopted (Eurocode 2 allows a variation of this angle between 21.8 and 45 degrees);
α_{cw} = pre-stressing parameter, assumed equal to 1;
ν_1 = efficiency factor, taking into account the reduction of concrete compressive strength due to cracking, equal to 0.6.
f_{cd} = design value of the concrete compressive strength [*MPa*].

The ACI 318 relation for elements with stirrups is:

$$V_n = V_c + V_s \quad \textbf{4-5}$$

where V_c is calculated using Eq. (4.2) and V_s is:

$$V_s = A_{sw} \cdot d \cdot f_{yw} / s \quad \textbf{4-6}$$

where:
A_{sw} = cross sectional area of the stirrups [mm^2];
d = effective depth of the cross-section [*mm*];
f_{yw} = yielding stress of the stirrups [*MPa*];
s = stirrups' spacing [*mm*].

In the beams failing in shear, the typical failure with development of diagonal cracks was observed. Particularly for B1 elements (without shear reinforcement), the experimental ultimate load was higher than the theoretical one (look at Table 4-7), both for traditional and recycled

concrete, showing the conservative nature of both the Eurocode 2 and ACI 318 formulations (Eq. 4-1 and 4-3). Load-versus-deflection diagrams are illustrated in Fig. 4-12 and load versus crack width diagrams are shown in Fig. 4-13. The main crack width of the B1_2 beam could not be measured because it was not intercepted by DD1. The ultimate shear capacity was higher in members containing slag with respect to those made with traditional concrete, again probably due to the higher cohesion of matrix containing slag. In Fig. 4-14, crack patterns at failure are shown. In all the cases, including the specimens with recycled concrete, the main crack direction is that from the bearing axis to the point of application of the load, as expected.

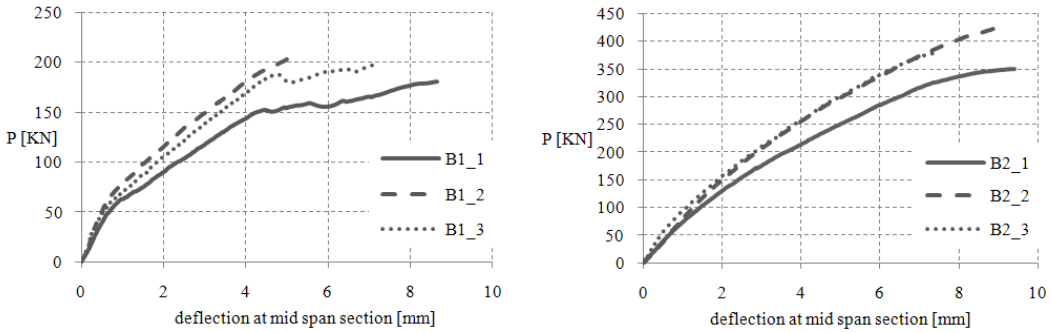

Figure 4-12. Load versus deflection at midspan diagrams for beams of "B" Series.

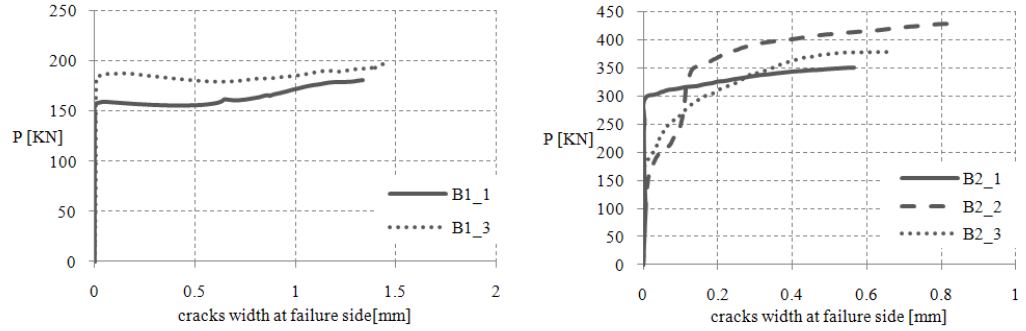

Figure 4-13. Load versus crack width diagrams for beams of "B" Series.

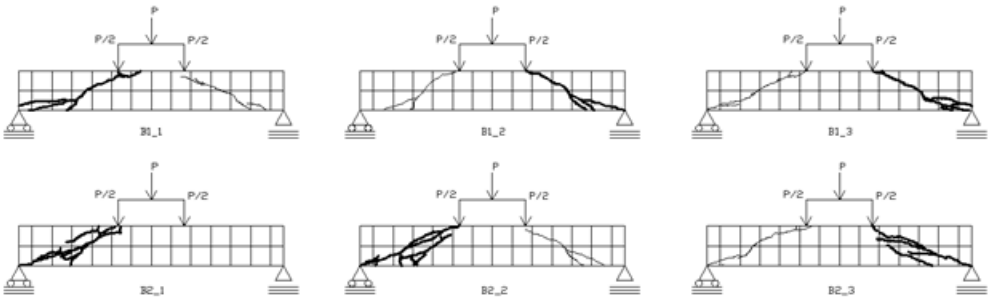

Figure 4-14. Crack patterns in RC structural elements after shear failure.

Figure 4-15. Shear failure - "B1" series.

Figure 4-16. Shear failure - "B2" series.

4.7 Conclusions

In the general context of improving sustainability and waste reutilization in construction, to reduce costs and potential pollution problems, and to preserve natural raw resources, this study aimed at investigating the opportunity of partially substituting natural aggregates for concrete with recycled EAF slag. The experimental behavior of RC flexural elements, made with traditional and EAF slag aggregates and subjected to both flexural and shear failure is studied because international literature had mainly focused on experimental tests on cubic/cylindrical small concrete specimens (without steel reinforcement) made with recycled aggregates. The few available experimental tests on structural elements are mainly related to the use of aggregates derived from building demolition waste. Concerning the results obtained in this section, and referring to the specific test-conditions of this research, the following conclusion can be drawn:

1. Slag used in this work showed a high crystalline nature, and a lot of mineralogical phases were present, thus increasing the stability of the material. Oxides are mainly bound in other compounds, and problems due to expansion or disintegration do not seem to be relevant, as also stated in [4.13]. Durability tests on concrete specimens should integrate these results obtained on raw materials. Moreover, the leaching test has shown that the leachate did not present concentration of unhealthy material over reasonable limits.

2. Concrete tested in this study, which included EAF slag as aggregate, showed higher compressive and tensile strength, elastic modulus, and specific weight than the traditional concrete.

3. The use of EAF slag increases water demand, reducing the workability of fresh concrete. This is not a significant problem because of the possibility of using plasticizers, whose quantity could be adjusted to obtain the required fluidity of the mixture.

4. The experimental behavior of RC beams made with EAF slag as aggregate was studied, showing that these beams have both ultimate flexural and shear capacity higher than the corresponding traditional beams other than higher moment at which first cracking occurs. Generally, crack widths are reduced and crack patterns are similar. For the same load, concretes with EAF slag have a reduced deflection at the mid-span.

5. The flexural capacity of RC beams made with EAF slag can be properly predicted with equilibrium and strain compatibility equations, according to the usual hypotheses of the limit state approach. Conversely, both the Eurocode and the ACI formulations underestimate the ultimate shear capacity of the RC beams, both if they are made with EAF slag and natural aggregates.

6. The use of steel slag as aggregate in RC structural elements, in principle, is possible, and the rate of substitution could reach the entire part of coarse aggregates. Benefits can be obtained both from economic and environmental perspectives: reuse, prevention in discarding materials, and saving natural resources are the main benefits that could be realized. On the other hand, these advantages could be limited by high specific density of slag, which will increase transportation costs.

4.8 Appendix

4.8.1 RC beams design

The aim of this work is to investigate the structural behavior of RC beams, when subjected to flexural loads and shear, to obtain experimental results for a further possible application of this material in building utilizations. To reach such aim, it is important that experimental RC elements made with EAF slag concrete could be comparable to the ones currently used in real applications. This implicates the necessity to cast beams with at least a span of 2 meters. Hence geometrical dimensions of beams were assigned to be 0.185 x 0.3 x 3 m^3, whereas dimension of reinforcement steel depend on the failure chosen for each element. Four types of beams were casted:

- **typology A**: failure under bending moment action:
  - A1: minimum steel reinforcement;
  - A2: medium steel reinforcement;

- **typology B**: failure under shear force action:
  - B1: no shear steel reinforcement;
  - B2: medium shear steel reinforcement.

Twelve beams were produced, three per each typology (also shown in Fig. 4-4): two of these were manufactured with EAF slag concrete, and the last one with traditional concrete, to compare the results obtained. Geometrical parameters are then listed:

w = width = 0.185 m;
h = height = 0.3 m;
l = length = 3 m;
c = concrete cover = 20 mm;
$d' = c + \phi_{st} + \phi_l/2$;
ϕ_{st} = stirrups diameter;
ϕ_l = longitudinal reinforcement diameter;
d=h-d'.

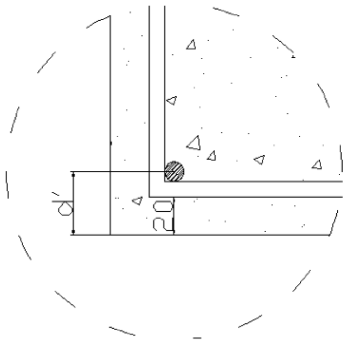

Figure 4-17. Concrete cover detail.

Concerning concrete characteristics, for the design of the RC elements an a priori hypothesis on mechanical performances of the material was made, assuming that a C30/35 class would be reached by the both mixes. Reinforcement steel chosen is a B450C class (with a characteristic yielding stress = 450 MPa). All the calculations refer to Eurocode 2 and Italian NTC 2008, and all the safety coefficients are equal to 1 in order to use the mean values of the design actions and materials' properties (not design values). Mechanical parameters considered in first hypothesis are then listed:

R_{ck} = 35 MPa;
f_{ck}=0.83 R_{ck} = 29.05 MPa;
$f_{ctm} = 0.3 \cdot {f_{ck}}^{2/3}$= 2.835 MPa;
$\beta_1 = 0.8 \ (f_{ck} < 50MPa)$;
$\beta_2 = 0.4 \ (f_{ck} < 50MPa)$.

A1 BEAMS

The first typology has a low reinforcement ratio, to simulate a low reinforced structural element failing for a limited value of load application and developing high deflection, due to the exceedance of bending moment resistance. The cross section of the beam is reported in Fig. 4-18.

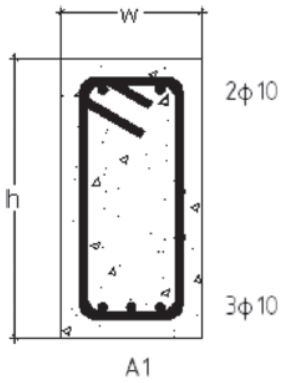

Figure 4-18. A1 - cross section.

Geometrical data are the following ones:

w = width = 18.5 cm;
h = height = 30 cm;
L = effective span length = 200 cm;
c = concrete cover = 2 cm;
$d = H - c + \phi_{st} + \phi_l/2 = 26.7\ cm$;
Longitudinal reinforcement bars=
3Φ10 tense zone (235.5 mm^2) + *2Φ10* compressed zone (157 mm^2);
Shear reinforcement bars = stirrups *Φ8/200* mm;
Lifting hooks = *2Φ12.*

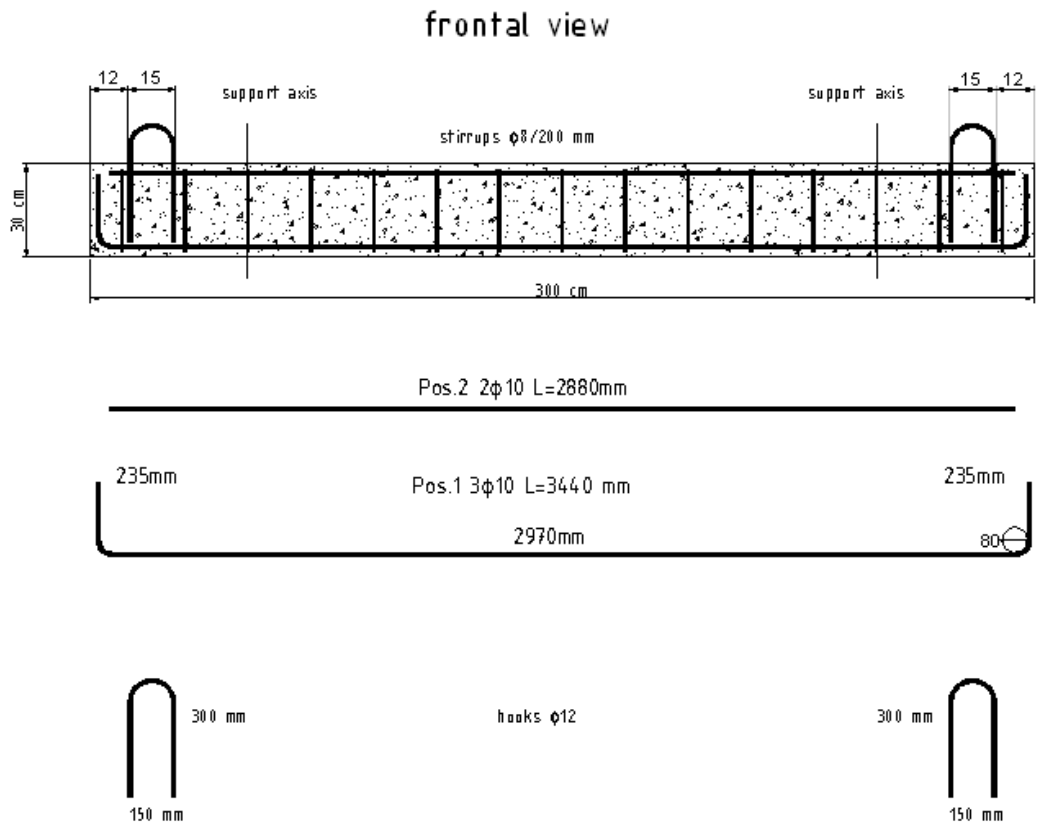

Figure 4-19. Disposition of steel bars in A1 beams.

A2 BEAMS

The second typology presents a medium - high longitudinal reinforcement ratio, to simulate the behavior of a high reinforced structural RC element subjected to high loads, and which would reach failure for bending moment resistance exceedance. Shear reinforcement allows toprevent shear failure, that may occur for the high forces acting at the supports.

Geometrical data are the following ones:

w = width = 18.5 cm;
h = height = 30 cm;
L = effective span length = 200 cm;
c = concrete cover = 2 cm;
$d = H - c + \phi_{st} + \phi_l/2 = 26.3\ cm$;
Longitudinal reinforcement bars=
3Φ18 tense zone (736.02 mm^2) + *2Φ18* compressed zone (508.68 mm^2);
Shear reinforcement bars = stirrups *Φ8/200* mm;
Lifting hooks = *2Φ12.*

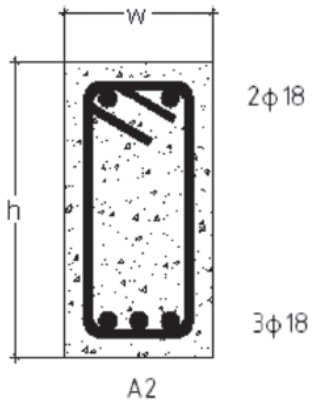

Figure 4-20. A2 - cross section.

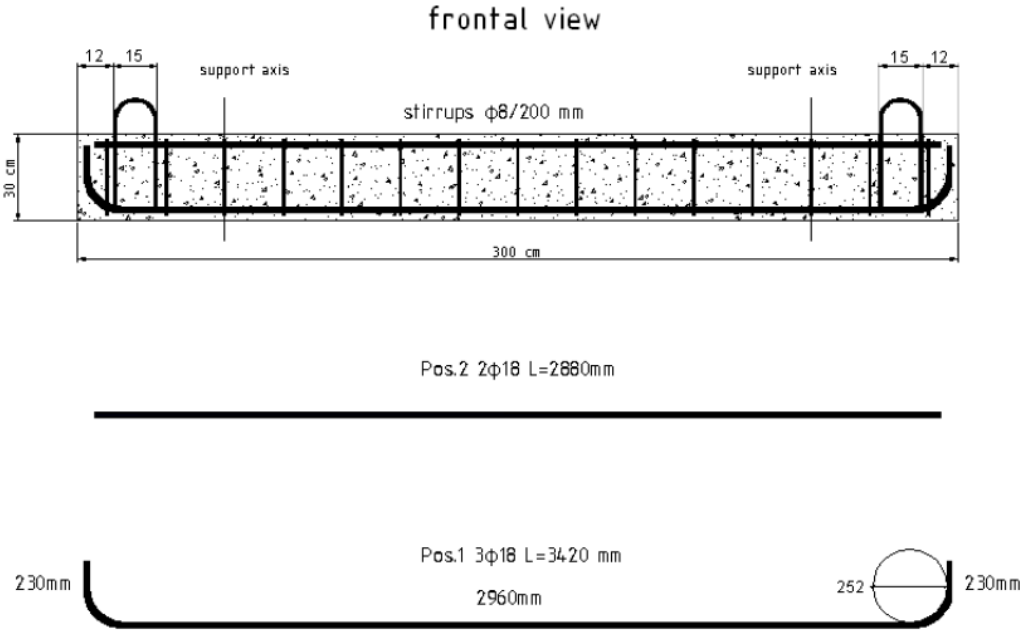

Figure 4-21. Disposition of steel bars in A2 beams.

B1 BEAMS

The third typology has no transversal reinforcement to ensure the failure for shear actions, whereas longitudinal reinforcement is medium high. Loads applied would develop high stresses at the support zones. In this case the influence of the compressed strut will be evidenced because of the missing of the tensile strength offered by the transversal reinforcement. This rebars' configuration has a particular importance in the analysis of the two different concretes structural behavior.

Geometrical data are the following ones:

w = width = 18.5 cm;
h = height = 30 cm;
L = effective span length = 200 cm;
c = concrete cover = 2 cm;
$d = H - c + \phi_{st} + \phi_l/2 = 25.4\ cm$;
Longitudinal reinforcement bars=
2Φ18 (508.68 mm^2) + *2Φ14* (307.72 mm^2) tense zone;
Lifting hooks = *2Φ12.*

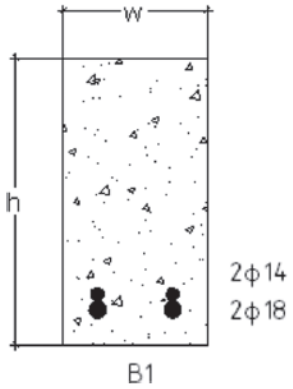

Figure 4-22. B1 - cross section.

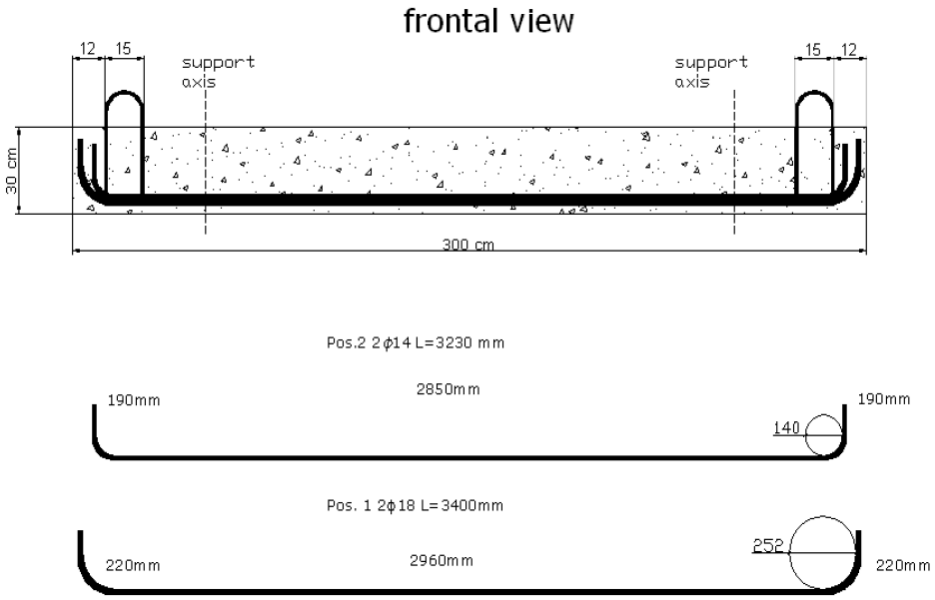

Figure 4-23. Disposition of steel bars in B1 beams.

B2 BEAMS

The last typology presents the higher reinforcement ratio, and it simulates a high-reinforced structural element. This high reinforcement ratio was necessary to prevent the failure for bending, and to allow the structure to fail for shear. Shear reinforcement is given by rectangular stirrups, which have the same step of the ones of "A" series (200 mm).

Geometrical data are the following ones:

w = width = 18.5 cm;
h = height = 30 cm;
L = effective span length = 200 cm;
c = concrete cover = 2 cm;
$d = H - c + \phi_{st} + \phi_l/2 = 24.6\ cm$;
Longitudinal reinforcement bars=
4Φ26 (2122.64 mm^2) tense zone + *2Φ20* (628 mm^2) compressed zone;
Shear reinforcement bars = stirrups *Φ8/200* mm;
Lifting hooks = *2Φ12.*

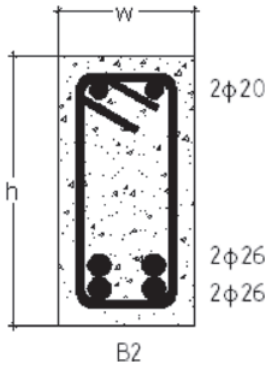

Figure 4-24. B2 - cross section.

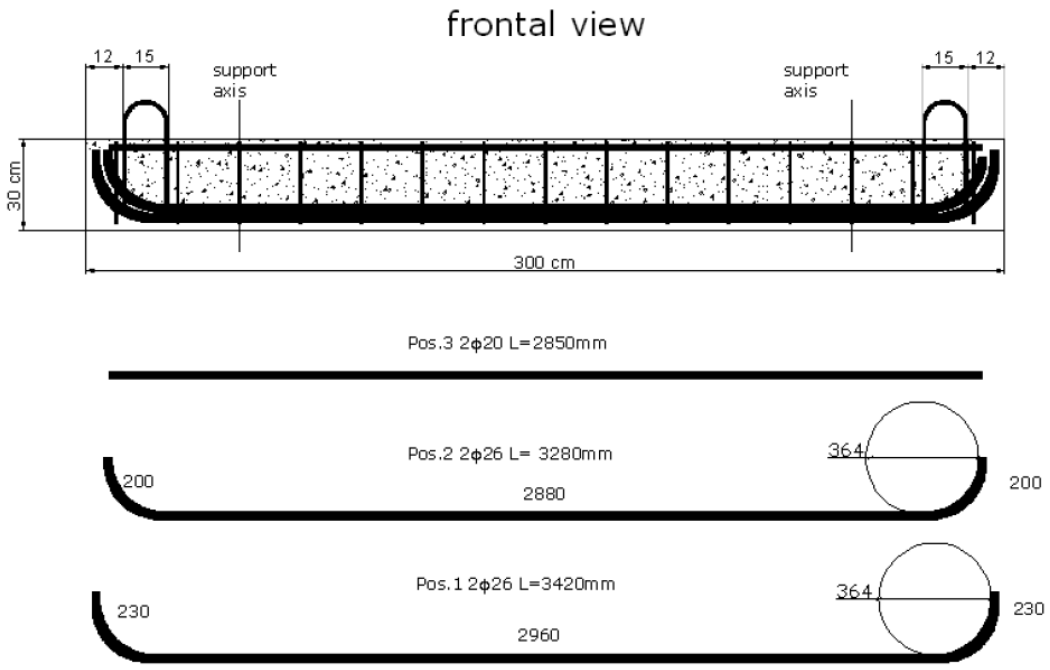

Figure 4-25. Disposition of steel bars in B2 beams.

4.8.2 Test Equipment

The experimental campaign, conducted at the Construction Materials Testing Laboratory of the University of Padova, was possible due to the following equipment:

• force application system: hydraulic actuator (with manual control) of 500 kN capacity with a jack (hydraulic cylinder) of ENERPAC typology, fixed at the frame;

• data acquisition system: dynamic data measurement system Spider 8, with graphical interface. It could work in parallel with other units, for a maxim number of 64 experimental channels, and more than 9600 analytical ones. Used for the acquisition of the applied load, displacement at the supports and in the mid-span section, cracks width;

• inductive displacement transducers LVDT (Linear Voltage Differential Transformers): used to measure displacements at the supports and at the mid-span section. Typology used are WA, and the precision is ± 0.01 mm;

• deformation transducers DD1, placed on a bar 100 mm long, used to evaluate displacements on the cracks after the cracking moment. The maximum elongation is ± 2.5 mm, and the precision is ± 0.001 mm. Negative values indicate contraction and positive an elongation.

The four-point bending tests were carried out as illustrated in Fig. 4-26.

Figure 4-26. Four-point bending test.

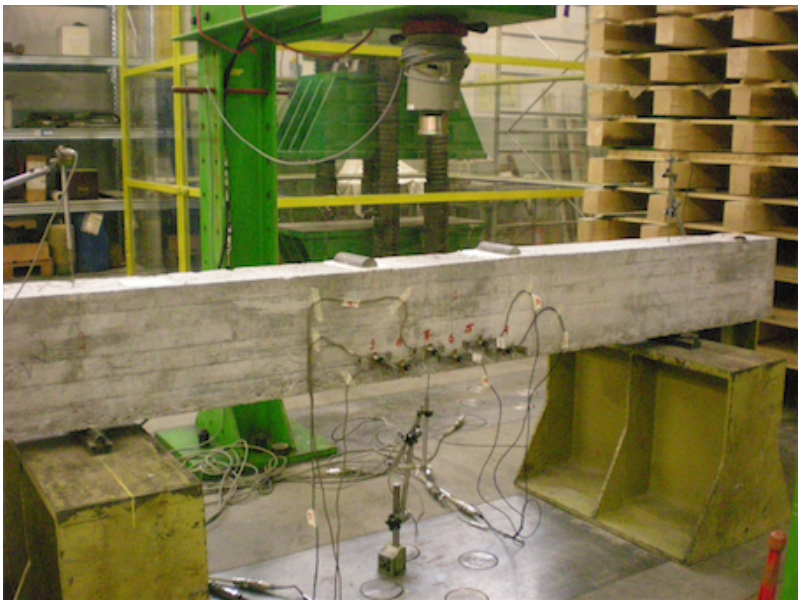

Figure 4-27. Instrumentation disposition - bending failure.

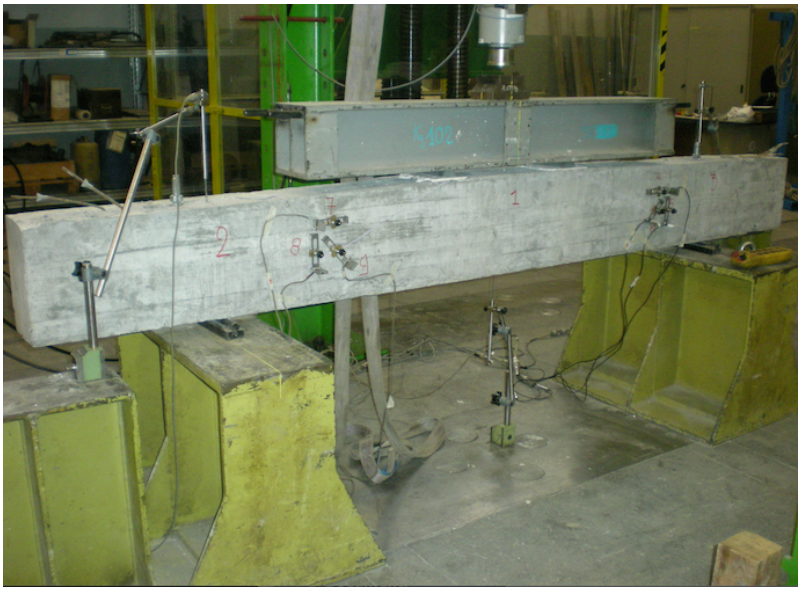

Figure 4-28. Instrumentation disposition - shear failure.

References

[4.1] Manso J.M., Polanco J.A.,Losanez M., Gonzalez J.J. Durability of Concrete Made with EAF Slag as Aggregate. Cement and Concrete Composites 2006; 28: 528-534.

[4.2] EN 1097-6. Tests for Mechanical and Physical Properties of Aggregates—Part 6: Determination of Particle Density and Water Absorption; CEN, Comité Europeen de Normalisation, Brussels, Belgium; 2000.

[4.3] Decreto Ministeriale N. 186 5/04/2006: Test di cessione, 2006 [in Italian].

[4.4] Pellegrino C., Gaddo V. Mechanical and durability characteristics of concrete containing EAF slag as aggregate. Cement and Concrete Composites 2009; 31(9): 663–671.

[4.5] Fuller W.B., Thompson E. The Laws of Proportioning Concrete. ASCE Transactions 1907; 59: 67-118.

[4.6] EN 206-1. Concrete – Part 1: Specification, Performance, Production and Conformity; CEN, Comité Europeen de Normalisation, Brussels, Belgium; 2006.

[4.7] EN 12390-4. Testing Hardened Concrete – Compressive Strength – Specification for Testing Machines; CEN, Comité Europeen de Normalisation, Brussels, Belgium; 2000.

[4.8] EN 12390-6. Testing Hardened Concrete – Tensile Splitting Strength of Test Specimens; CEN, Comité Europeen de Normalisation, Brussels, Belgium; 2009.

[4.9] UNI EN 6556. Tests of Concretes – Determination of Static Modulus of Elasticity in Compression; UNI, Ente Nazionale Italiano di Unificazione, Milan, Italy; 1976 (in Italian).

[4.10] EN 1992-1-1. Eurocode 2: Design of Concrete Structures – Part 1-1: General Rules and Rules for Buildings CEN, Comité Europeen de Normalisation, Brussels, Belgium; 2005.

[4.11] Al-Jabri K.S., Al-Saidy A.H., Taha R. Effect of Copper Slag as Fine Aggregate on the Properties of Cement Mortars and Concrete. Construction and Building Materials 2011; 25(2): 933-938.

[4.12] ACI Committee 318. Building Code Requirements for Structural Concrete (ACI 318-11) and Commentary. Farmington Hills, MI (U.S.): American Concrete Institute; 2011, 503 pp.

[4.13] Abu-Eishah S.I., El-Dieb A.S., Bedir M.S. Performance of Concrete Mixtures Made with Electric Arc Furnace (EAF) Steel Slag Aggregate Produced in the Arabian Gulf Region. Construction and Building Materials 2012; 34: 249-256.

5 Environmental impacts evaluation of EAF slag concrete

5.1 Abstract

A significant number of “green concrete” are developing to meet the growing request of reducing construction industry impacts, save raw materials and prevent industrial by-products’ discard. Between these, Black/Oxidizing Electric Arc Furnace (EAF) slag has been founded to be suitable for structural concrete applications when used as replacement of traditional coarse aggregate. However, a quantitative estimate of the environmental impacts’ assessment related to the production of concrete containing EAF slag is still missing. In this section a Life Cycle Analysis (LCA) framework using a cradle-to-gate approach is used aiming to quantify the emission reduction due to the use of EAF aggregates instead of natural gravel in structural concrete. Inventory data are mainly collected from experiments and refer to the considered materials. The definition of a proper functional unit to develop comparative LCA between concretes is discussed.

5.2 Introduction

The construction industry has an essential and priority role in the development of competitiveness and prosperity of the general economy of the country. Concrete is one of the most widely used building materials in roads, buildings, bridges and other infrastructures. On average, approximately 1 ton of concrete is produced each year for every human being in the world [5.1]. In particular, Italy is the first manufacturer of cement in Europe and the thirteenth in the world: it is estimated that in 2009 they produced 36 million tons of cement, equivalent to about 601 kg for every human [5.2]. In addition, the whole Italian cement and concrete manufacturing sector represents the 14% of EU-27 production [5.3]. Because of this global extensive use, it is imperative to evaluate the environmental impact of this material correctly, that should be equated, among the others, with its effect on greenhouse gas emissions and climate change. In 2007, a research report indicated that from 5 until 7% of the all anthropogenic CO_2 emissions were at the expense of the cement industry [5.4].

Since aggregates represent about 70% of concrete total volume, they play an important role in affecting the environmental impacts related to this

material. As an indicative data, European Environmental Agency has reported in 2008 that three billion tons of aggregate are produced each year in the countries of European Union [5.5], leading to the arising question concerning the availability of natural resources in the next future, in particular at local scale [5.6]. In this chapter, a procedure to evaluate the emissions related to the production of concretes including recycled aggregates will be shown, with a particular focus on the comparative assessment of the emissions between traditional and EAF concrete.

5.3 Life Cycle Assessment

In this chapter a comparative study related to the environmental emissions due to traditional and recycled concrete containing EAF slag is performed. The emissions assessment is evaluated through a LCA study, which consists of four phases: (1) the goal and scope definition phase, (2) the inventory analysis (LCI) phase, (3) the impact assessment (LCIA) phase, and (4) the interpretation phase. In the first step, a cradle-to-gate approach is used for the emissions assessment of both natural and recycled aggregates; then, the impacts related to whole concrete mixes are evaluated. Releases due to admixtures are here neglected because of the little amounts required in each mix. Regarding water contribution, the water footprint of the product has been only accounted since this last term has evolved independently from the discipline of LCA (both using Eco-indicator 99 and CML 2002 approaches), and there is not a clear relationship between water footprint and potential environmental harm [5.1].

LCA framework is generally accepted as a reliable assessment tool and allows comparing the environmental impact of a strength and durability/service life related functional unit (FU) of reference over its entire life cycle, within determined system boundaries. This tool is growing to be also applied to evaluate building materials sustainability, even though literature has mainly focused since now on cement products [5.7, 5.8]. In the present work Life Cycle Inventory (LCI) data were mainly obtained by means of experiments and, when this was not possible, collected from literature. Collected data are computed through a mass balance allocation procedure, and then the input/output (I/O) flows were translated into indicators associated with different pressures, such as climate change, acidification, or toxicity to plants, animals and people. All emissions contributing to each environmental problem are converted into common units (e.g., kg CO_2-equivalent for climate change, or kg SO_2-eq. for acidification) using conversion factors known as “characterization factors”

(e.g., for a climate change over a 100-year time frame, 1 kg of methane is equivalent to 25 kg of CO_2 [5.9]).

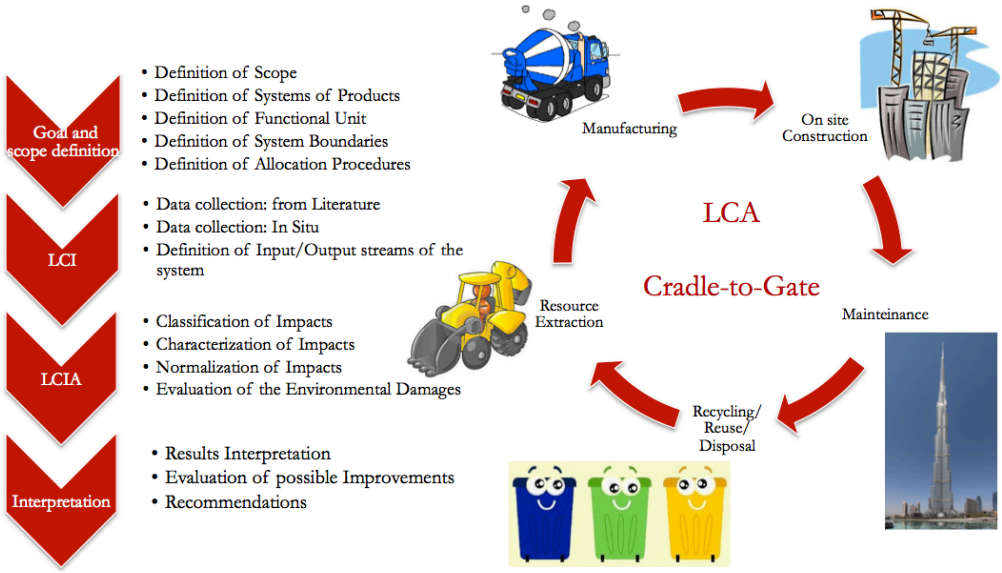

Figure 5-1. Stages of an LCA.

5.3.1 Goal and scope

The goal of this study is to provide a useful tool to compare the environmental impacts related to the production of two concretes: the first mix contains EAF slag as the whole part of coarse aggregates, and the second is the reference one entirely made with traditional aggregates. In order to obtain these results, firstly emissions were evaluated for the product “aggregates”. The EAF slag upstream impacts related to iron and steel production are not considered. Then the procedure could be also applied to concretes including recycled aggregates coming from construction and demolition waste, as done in Section 7. As a first attempt, the work focuses on a comparative study between EAF and traditional concrete, using as reference the mixes analyzed in the previous sections; some examples will be given to quantify the influences of the aggregates and cement dosage, and transportation on the total environmental burden due to concrete production.

The production system is considered from the extraction and processing of raw materials (“cradle”) through to actual production and assembly of the product (“gate”) at the company that places it on the market, taking into account all the production and transport fluxes inside

the system. The chosen functional unit FU is *1ton* of aggregate, to take into account the different specific weight of EAF slag (γ_d = 3900 kg/m^3) and natural aggregate (γ_d = 2736 kg/m^3). Concerning the conglomerate emissions assessment, FU is *1m^3* of concrete: this parameter should be influenced by mechanical properties, physical-chemical characteristics, durability and of course, it is related to the unit of mass.

As reported in the previous chapters, concrete containing EAF slag has better mechanical properties than the reference one, and similar characteristics from the durability point of view. Moreover, both the systems' boundary for natural and recycled concrete does not take into account transportation impacts outside the system. The choice is related to the clear difficulty of evaluating a significant transport scenario due to the specific complex system of natural and recycled aggregates plants location in Northern Italy that can significantly affect the correct evaluation of this phase [5.10]. In this respect it can be observed that the higher transportation costs related to the higher fresh EAF concrete specific weight could be compensated by its better mechanical properties that could involve less concrete volume to obtain the same performance when using EAF concrete with respect to traditional one [5.11, 5.12, 5.13]. Emission can be considered as at "*0-km*" and then, in a second step, transportation costs can be evaluated according to the model presented in [5.10]. This will be shown in the Example 3, section 5.5.3 of this thesis.

5.3.2 LCI - Life Cycle Inventory

The analysis of inventory includes the compilation and quantification of relevant input and output elements of a product during its life cycle. It develops in three phases: data collection, calculation procedure allowing to quantify the I/O elements of a relevant product system, and their allocation. Significance is determined by threshold for mass (more than 1% of inputs), energy and environmental significance (potential for harm) [5.14]. The collected data allow to define the input and output elements of the system, and in particular they can be classified into broad categories including:

- energy inputs, raw material inputs, ancillary inputs, other physical inputs;
- products, co-products and waste;
- emissions to air, discharges to water and soil;
- other environmental aspects.

All collected data must include the details of their collection, which are constituted by the period in which the data were collected and all the information on data quality indicators. The description of each stage unit must be made. It includes tracking of the flow charts that describe all unit processes included in the model, the detailed description of each process unit (specifying the factors that influence the inputs and output), a list of streams, the list of the units used, description of the data collection and calculation techniques, and at least the directives to document used and other issues associated with the data provided.

The calculation procedures are used to produce the results of inventory system defined, for each process unit and to define the functional unit of the system analyzed. The following operating steps must be done:

• validation of the data collected: during data collection there is the necessity to validate data, to confirm and provide evidences that the requirements of data quality for the intended application have been met. Among the available systems, mass and energy balances can be used;

• correlation of the data to the unit processes: quantitative input and output data of the process unit must be calculated in relation to an appropriate flow. All streams of unit processes must be connected to the reference flow;

• correlation of the flow of data to the reference functional unit: the result of the calculations should lead to report all system input and output data to functional unit;

• refining the system boundary: the data to be included must be chosen on the bases of a sensitivity analysis, and their significance must be evaluated. The initial system boundary shall be revised in accordance with the cut-off criteria established in the definition of the scope.

Allocation procedures are important to take into account multiple products and recycling systems: all input and output are allocated according to the different products. They should be defined and justified. The allocation procedure shall identify the processes shared with other product systems and it deals with them according to the stepwise procedure presented below:

• Step 1: Wherever possible, allocation should be avoided by: dividing the unit process to be allocated into two or more sub-processes and collecting the input and output data related to these sub-processes, or expanding the product system to include the additional functions related to the co-products;

• Step 2: Where allocation cannot be avoided, the inputs and outputs of the system should be partitioned between its different products or functions in a way that reflects the underlying physical relationships between them; i.e. they should reflect the way in which the inputs and outputs are changed by quantitative changes in the products or functions delivered by the system;

• Step 3: Where physical relationship alone cannot be established or used as the basis for allocation, the inputs should be allocated between the products and functions in a way that reflects other relationships between them. For example, input and output data might be allocated between co-products in proportion to the economic value of the products.

In general the procedures of allocation for recycling and reuse of materials should use in order [5.15, 5.16]:

• physical properties (e.g. mass);

• economic value (e.g. market value of the scrap material or recycled material in relation to market value of primary material);

• the number of subsequent uses of the recycled material (explained in ISO / TR 14049).

Hence in this work the allocation procedure for the environmental loads is based on physical/chemical causation per unit mass of aggregate produced. It should be remembered that the capital required for the system installation and in general the costs incurred are not part of the parameters considered in the model (mass allocation procedure). Figures 5.2 and 5.3 illustrate respectively the production systems of both natural aggregates (NA) and EAF slag treatment plant, which have the same daily production (~ 400 ton/d): hence they can be considered comparable. The NA plant characteristics considered in this study are typical of most NA extraction plants in Italy, and they are taken from [5.17], whereas EAF slag treatment plant data were collected in situ for a real plant. For each phase of treatment in both the systems, amount of I/O material, means used, energy and diesel consumption are used to calculate emissions. Releases are divided between direct and indirect: in particular, last ones refer to dust (PM_{10} release in atmosphere) and combustion gases due to energetic consumption (TSP, PM_{10}, CO, benzene, 1,3-butadiene, CO_2 and NO_x). This choice is done to allow a further homogenization and does not conduce separately a CED (Cumulative Energy Demand) analysis [5.18].

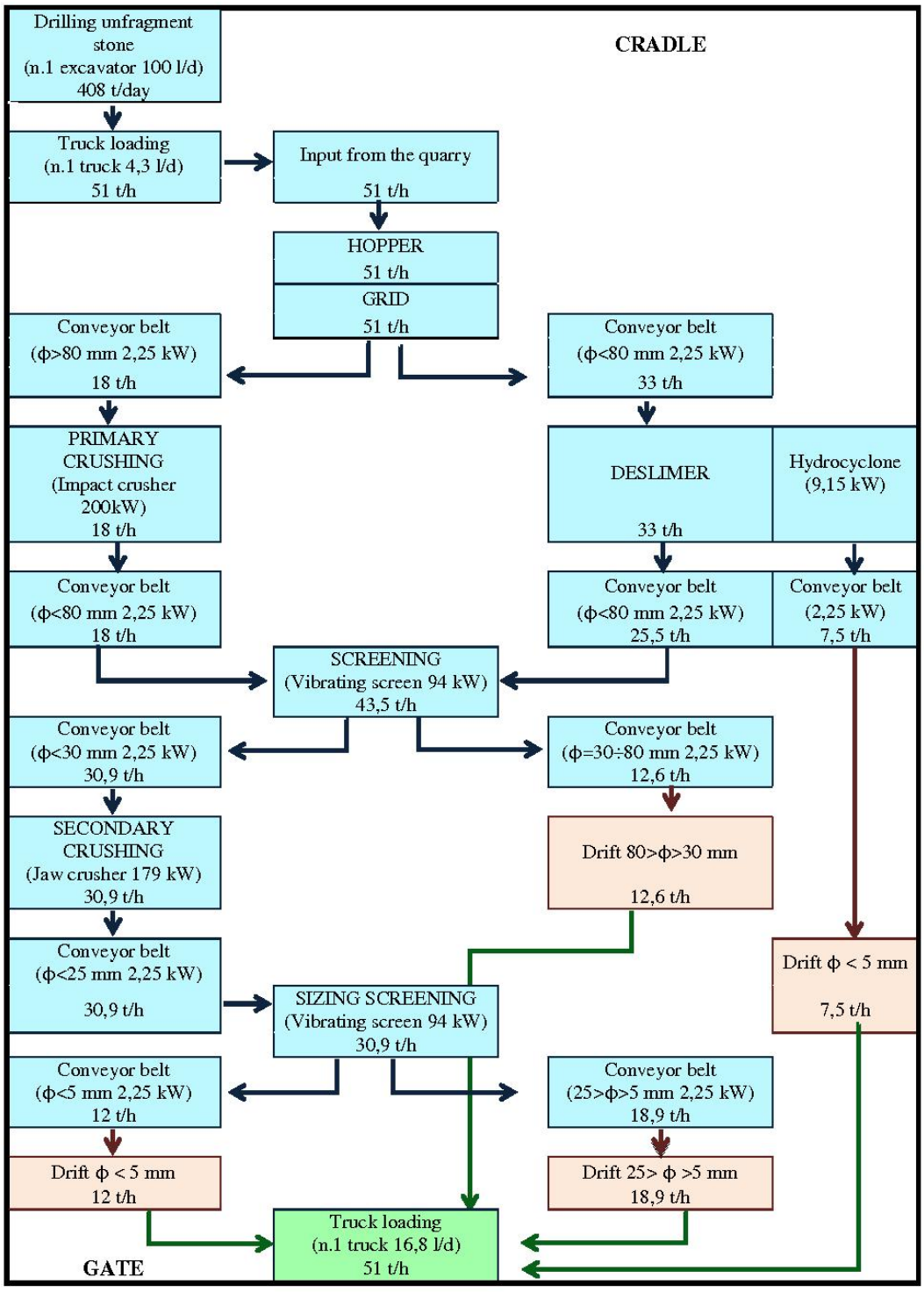

Figure 5-2. Block diagram of the activities in the natural aggregates extraction plant - analysis "Cradle-to-Gate".

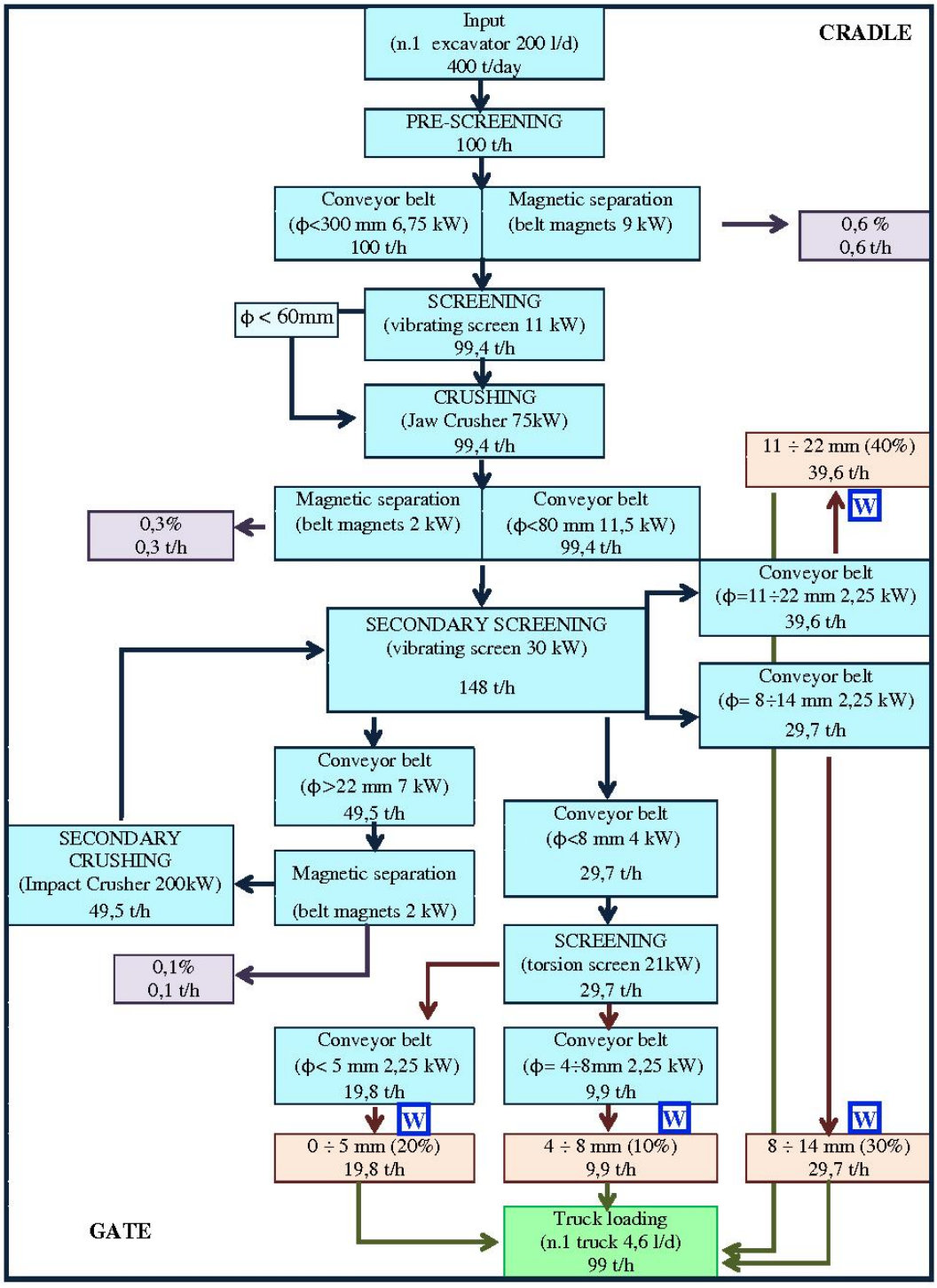

Figure 5-3. Block diagram of the activities in the EAF slag treatment plant - analysis "Cradle-to-Gate". The letter "W" refers to a washing process.

Air emissions related to each industrial process accounting in the system are calculated according to [5.19, 5.20, 5.21]. In particular, the main relations used for the evaluation of air pollutant emissions are listed below.

The general formula for the estimation of the air pollutant emissions according to [5.19], is:

$$E = A \cdot EF \cdot (1 - ER/100) \quad \textbf{5-1}$$

where *E* represents the emission, *A* is the activity rate expressed i.e. as [*ton material/y*], *EF* is the emission factor expressed as [*kg/ton material*] and *ER* is the overall emission reduction, expressed in [*%*]. The emission reduction mainly depends by the used devices' efficiencies and the control methods applied to limit the releases, such as the use of water sprays to limit dust releases. Emissions factors are evaluated according to [5.20, 5.21] respectively for direct and indirect releases; specific default *EF* values were used for some of the process operations, such as grinding, drying and crushing, according to [5.21]. Other releases, mainly concerning EAF treatment plants, were collected in situ after chemical analyses on water (I/O from inner wastewater plant) and leaching tests conducted on recycled aggregates (I/O aggregate treatment plant). In the present case, results from two experimental campaigns conduced in summer and winter 2012 were used.

Direct emissions

The following formulas can be used to estimate the particulate matters emissions.

PM_{10} EF Excavators/Shovels/Front-end loaders [*kg/ton*]:

$$PM_{10} = 0.35 \cdot 0.0016 \cdot (v_w/2.2)^{1.3} \cdot (w/2)^{-1.4} \quad \textbf{5-2}$$

where v_w is the mean wind velocity expressed in [*m/s*] and *w* is the mean moisture content expressed in [*%*].

PM_{10} EF for dust generation due to transport on unpaved roads [*kg/ton*]:

$$PM_{10} = 0.733 \cdot (s/12)^{0.8} \cdot [(g_v/3)^{0.4}]/[(w/0.2)^{0.3}] \quad \textbf{5-3}$$

where *s* is the mean silt content expressed in [*%*], g_v is the vehicle gross mass expressed in [*ton*].

PM_{10} EF for Scraper [*kg/ton*]:

$$PM_{10} = 1.32 \cdot 10^{-5} \cdot s^{1.4} \cdot g_v{}^{2.5} \quad \textbf{5-4}$$

where *s* is the mean silt content expressed in [*%*], g_v is the vehicle gross mass expressed in [*ton*].

PM_{10} EF for Bulldozer, expressed as [*kg/h*]:

$$PM_{10} = 0.34 \cdot v_b{}^{1.5} \cdot w^{-1.4} \quad \textbf{5-5}$$

where v_b is the mean vehicle speed expressed in [*km/h*] and *w* is the mean moisture content expressed in [*%*].

Indirect emissions

The general formula to estimate vehicle emissions factors as NO_x, PM_{10}, CO, HC (VOCs, including methane), benzene, 1,3-butadiene and CO_2, expressed as [*g/km*] is the following:

$$EF = (a + b \cdot v + c \cdot v^2 + d \cdot v^e + f \cdot ln(v) + g \cdot v^3 + h/v + i/v^2 + j/v^3) \cdot x \quad \textbf{5-6}$$

where *a*, *b*, *c*, *d*, *e*, *f*, *g*, *h*, *i* and *j* are NAEI vehicle emission factors coefficients, depending on the vehicle typology, on the used fuel and on the substance considered. The emission [*kg/d*] is then calculated as:

$$E = EF \cdot 10^{-3} \cdot f/100 \cdot n_h \cdot n_s \cdot n_v \quad \textbf{5-7}$$

where *f* is the use frequency expressed as [*%*], n_h is the number of hours per shift, n_s is the number of shift per day and n_v is the number of the vehicles of the same type used in each process phase. Indirect emission due to electricity consumption and to diesel consumption refers to default emission factors, and they are reported to the daily releases through the specific daily consumption of each device considered within system boundaries.

Water releases

Emissions acting on water and industrial soil compartment are evaluated by means of results from two experimental campaigns. First, chemical analyses on water (I/O from inner wastewater plant) and leaching tests conducted on recycled aggregates defined each analyzed substance

emission factor, expressed as EF [mg/l]. Then, the emission, expressed as [kg/ton] is evaluated trough:

$$E = EF \cdot 10^{-6} \cdot W/\rho_w \cdot n_d \quad \textbf{5-8}$$

where W is the monthly volume of water discharged expressed as [m^3], ρ_w is water density expressed as [kg/m^3] and n_d is the number of days per month of discharging.

5.3.3 LCIA – Life Cycle Impact Assessment

LCIA must be in accordance with the purpose and with the scope of the study and thus the data quality and results LCI has to verify this. The LCI results must be controlled so as to calculate the results of the indicators for the LCIA. The functional unit, the LCI, the aggregation and allocation methods should be suitably chosen to reduce the environmental relevance of the LCIA results. This phase is made by three mandatory elements:

- selection of impact categories, category indicators and characterization models;
- assignment of LCI results to the selected impact categories;
- calculation of category indicator results.

Optional elements can be used depending on the objective and scope of the LCA. They are:

- normalization: calculating the magnitude of category indicator results relative to reference information;
- grouping: sorting and possibly ranking of the impact categories;
- weighting: converting and possibly aggregating indicator results across impact categories using numerical factors based on value-choices. Data prior to weighting should remain available;
- data quality analysis: better understanding the reliability of the collection of indicator results, the LCIA profile.

Between these, in this work a normalization process was done [5.22] in which the results of each impact category are divided by a reference figure (for example, for the greenhouse effect, West Europe 1995 CO_2 year production was used). A problem-oriented methodology [5.23] is chosen for the impact assessment: this approach involves the environmental impacts associated with climate change, eutrophication, acidification, human toxicity, eco-toxicity, etc. In order to evaluate the environmental

burdens for the systems of natural and recycled aggregates, the evaluation procedure is performed in all the production phases, and it is based on the basic categories of CML 2002 Method [5.24]. In particular, this method is based on the list of best available practice impact categories drawn up by the Society of Environmental Toxicology and Chemistry (SETAC) Working Group on LCIA.

The environmental impact categories included in the present work are the following: Climate Change, Eutrophication, Acidification, Photo-Oxidant Formation, Human toxicity, Eco-toxicity and Ozone Layer Depletion. Assignment of LCI results to the impact categories is then performed, distinguishing the eventually parallel mechanisms acting (i.e. substance: 1,3-Butadiene acting on air compartment plays a parallel mechanism, affecting Photo-oxidant formation, Human toxicity and Eco-toxicity categories). Then, LCI results are converted to common units through characterization factors, and then they were aggregated within the same impact category.

Climate change There is not an evident and direct proof (even if the great part of the scientific world theorizes this cause-effect relationship) that links green-house gases (GHG) emissions to global climate change, but following the principle of prevention, several measures have been taken at the international level. Between these, the most famous one is the Kyoto Protocol, that states internationally the necessity to reduce GHG emissions. Recently the IPCC report of November 2014 on the GHG emissions stated the necessity to reduce the emissions from the current level until a value reduced by the 40-70% before the 2050. Emissions responsible for this problem are mainly nitric oxide, carbon dioxide and methane. In fact the increase of these gases are responsible for the greenhouse effect that is the atmosphere capacity to hold more or less heat. Climate change means changes in the Earth's climate or the variations at different spatial scales, historical and temporal parameters of one or more environmental and climate factors: temperature, precipitation, clouds, ocean temperatures, plants and animals development.

Eutrophication Eutrophication is caused by the emission of ammonia, nitrates, nitrogen oxides, phosphorus and nitrogen (nutrients). Nutrients are essential to life in ecosystems, but at the same time, when nutrient intakes increased disproportionately in relation to the ability to metabolize them by the aquatic environment, an environmental problem occurs. For instance, when the amount of nutrients in a lake is excessive, they cause the uncontrolled algae growth in the surface layers, because algae are able to assimilate the nutrients very quickly. When the algae will die, they will be the carbon source for the aerobic bacteria that will begin the

processes of decomposition using the dissolved oxygen. The birth of an anaerobic layer will lead to the gradual disappearance of the fauna and progressive wetland.

Acidification The acidification is due to the emission of ammonia, nitrogen oxides and sulphur dioxide. In particular, sulphur dioxide (SO_2) is due to the combustion of coal and oil, instead of nitrogen oxides (NO_x) are produced by all motor vehicles that work inside a plant and by other combustion processes that may be present. Acidifying compounds may fall to the ground with rain or snow (acid rain) as wet deposition, or in the form of particles or gases as dry deposition. Acid rain is caused by the interaction of these three substances with water, which are then converted into sulphuric acid (H_2SO_4) and nitric acid (HNO_3).

Photo-oxidant formation Benzene, 1,3-butadiene, sulphur dioxide, carbon monoxide, methane and non-methane volatile organic compounds (NMVOC), emitted to the atmosphere from many natural or anthropogenic processes, undergo a complex system of photochemical reactions induced by light in the ultraviolet sun rays, all leading to the formation of ozone (O_3), peroxyacetyl nitrate (PAN), peroxibenzoyl nitrate (PBN), aldehyde and hundreds of other substances. These substances are reactive (especially ozone) and they are harmful to human and ecosystems health. This problem is also referred to as "summer smog", easily identified by its color ranging from yellow-orange to brown and more common when solar radiation is more intense.

Human toxicity The industrial activities are responsible of the release of hazardous substances to human health. Toxicity can be defined as the relative ability of a substance to cause adverse effects in living organisms. There are several routes of exposure by which a substance may enter into the body, through processes such as ingestion, inhalation or through the skin. Once the chemical is absorbed into the body, three other processes are possible: metabolism, storage, and excretion. A substance becomes toxic when its concentration in the body is greater than a threshold value, which depends on a dose/response curve. Of course, the threshold value varies from the individual susceptibility and from substance to substance: the substance potential toxicity depends on its characteristic structure (small structural differences may correspond to large differences in toxic effects induced). The emissions from aggregates extraction and recycled aggregates treatment plants which may be toxic are benzene, 1,3-butadiene, PM_{10}, nitrogen oxides, sulphur dioxide and non-methane volatile organic compounds (NMVOC).

Eco-toxicity The pollutant toxicity depends on the biological effects it causes and by its concentration. Emissions of benzene, 1,3-butadiene and non-methane volatile organic compounds (NMVOC) may cause the problem appointed as ecotoxicity. The ecotoxicity may be aquatic or terrestrial. The substances responsible for ecotoxicity can damage the structure and the organization of an ecosystem, exerting toxic effects on organisms that inhabit it, until their death. The presence of persistent substances (those substance characterized by low biodegradability and which remain in the environment for long periods without undergoing any type of change) is responsible for toxic effects that occur for a long time (chronic toxicity). Therefore, this type of ecotoxicity is linked to the intrinsic substance toxicity, to its biodegradability and its ability to accumulate in tissues.

Ozone layer depletion Stratospheric ozone is a natural shield for the Earth, and it is able to filter the dangerous ultraviolet (UV) radiation that can be harmful to humans and other organisms. This layer is damaged by the most of industrial processes; in particular, in this case, the problems can be related to the energy sources used (electricity and diesel). The damage of this layer is known as the "ozone hole". It causes excessive human skin exposure to UV radiation, accelerates the cataract onset and interferes with photosynthesis putting at risk the plants growth.

5.4 LCA of EAF slag and NA

Main basic material consists in black EAF slag with high density and low water absorption, obtained from a local steel factory in North - Eastern part of Italy. This material, already used for the other experimental campaign during this research work, has been compared with a natural aggregate with carbonate origin and roundish shape. The main physical characteristics of the aggregates are reported in Table 5-1.

Table 5-1. Physical characteristics of aggregates.

	EAF aggregate	*NA coarse*	*NA fine*
Diameter range (mm)	*4-22*	*4-31.5*	*0-4*
Apparent specific gravity (kg/m³)	*3876-3900*	*2732*	*2724*
Water absorption (%)	*0.4-0.5*	*0.75*	*0.8*
Shape	*sharp-pointed*	*roundish*	*roundish*

The production processes of those materials are already described in Fig. 5-2 and Fig. 5-3. Each flow inside the production process is evaluated and quantified. The two materials were studied through LCA tool, considering the process from the production of the material to its use as "aggregate", whereas the phases that bear such material to landfills are not taken into consideration to simplify the analysis and due to lack of reliable data. This method allows to estimate the emissions associated with each phase of treatment and determine the environmental issues that generate these emissions. The impacts' comparison of the various systems is possible because the emissions are normalized and the quantities produced from each plant are similar (about 400 ton/d).

Table 5-2 and Table 5-3 show the emission values resulting from the processing of natural and EAF aggregates respectively, distinguishing direct and indirect ones. EAF slag emissions are significantly lower than emissions from natural aggregates, especially regarding the indirect impacts related to the energy demand. The higher simplicity of the recycled aggregates processing system promotes a more sustainable use of fossil resources and energy consumptions, hence reducing significantly greenhouse gases (GHG) releases. Table 5-4 lists the emissions reduction related to the production of *1ton* of EAF slag with respect to the production of *1ton* of NA. Applying the normalization, results are then divided by the West Europe annual production, to provide a measure of the contribution of the products in relation to the considered environmental categories. Fig. 5-4 and Fig. 5-5 represent results for NA and EAF slag aggregate respectively, where environmental impacts are divided by each process phase.

Table 5-2. Characterization of environmental emissions related to the selected category – natural aggregates (FU=*1ton*).

CATEGORY	*DIRECT EMISSIONS*	*INDIRECT EMISSIONS*	*TOTAL EMISSIONS*	*U.M.*
Climate Change	*4.65E-01*	*8.01E+00*	*8.47E+00*	*kg CO_2 eq.*
Eutrophication	*7.46E-04*	*2.18E-03*	*2.92E-03*	*kg PO_4 eq.*
Acidification	*2.87E-03*	*4.42E-02*	*4.71E-02*	*kg SO_2 eq.*
Photo-oxidant formation	*1.32E-04*	*2.64E-03*	*2.77E-03*	*kg ethylene eq.*
Human Toxicity	*2.14E-01*	*5.61E-01*	*7.75E-01*	*kg 1.4-DCB eq*
Eco-toxicity	*5.08E-09*	*4.12E+02*	*4.12E+02*	*kg 1.4-DCB eq*
Ozone layer depletion	*-*	*1.48E-05*	*1.48E-05*	*kg R11 eq.*

Table 5-3. Characterization of environmental emissions related to the selected category – EAF aggregates (FU=*1ton*).

CATEGORY	DIRECT EMISSIONS	INDIRECT EMISSIONS	TOTAL EMISSIONS	U.M.
Climate Change	3.30E-01	2.76E+00	3.09E+00	kg CO2 eq.
Eutrophication	8.66E-04	7.68E-04	1.69E-03	kg PO4 eq.
Acidification	3.13E-03	1.53E-02	1.86E-02	kg SO2 eq.
Photo-oxidant formation	1.73E-04	9.73E-04	1.15E-03	kg ethylene eq.
Human Toxicity	2.77E-01	1.97E-01	4.74E-01	kg 1.4-DCB eq
Eco-toxicity	2.24E-09	1.54E+02	1.54E+02	kg 1.4-DCB eq
Ozone layer depletion	-	3.82E-07	3.82E-07	kg R11 eq.

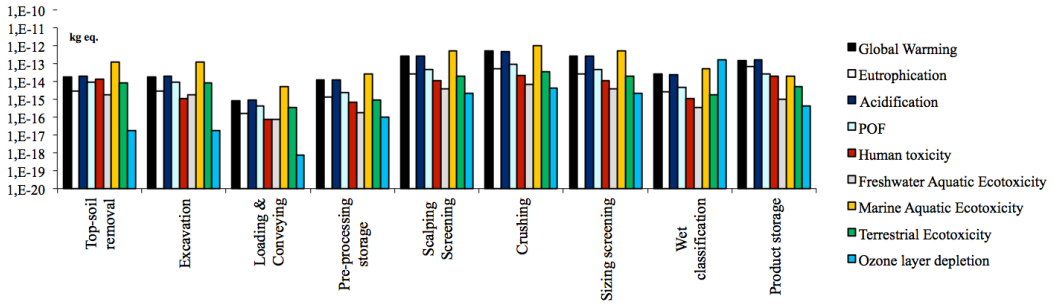

Figure 5-4. Normalized emissions due to NA.

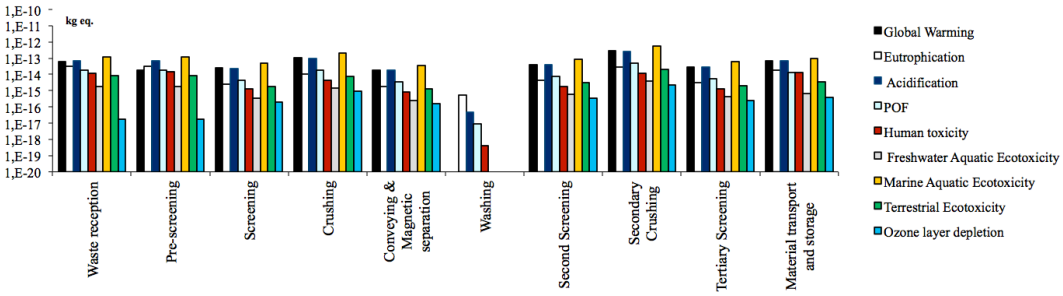

Figure 5-5. Normalized emissions due to EAF slag aggregates.

In addition, concerning the transport of the aggregates out of the system boundaries, both EAF and virgin ones, the range of CO_2 emissions produced during transport, due to the consumption of fossil fuels, is about 12.8-50.6 gCO_2/(ton·Km), depending on the truck typologies, according to [5.25].

5.5 LCA of EAF concretes

In this section, three case studies of the application of the LCA framework will be presented with the aim to highlight the importance of the definition of a proper functional unit for concretes comparison. The first example aims to analyze two concretes produced with the same mix-design, taking as constant the following parameters: aggregates volume and grading curve; water/cement ratio; cement content (there is a slight variation between the mixes). However, those concretes have different mechanical strength.

In the second example, two different concretes are compared with the aim to reach similar mechanical strength: in this case the cement content in the two mixes is changed, as also most of the mix details, i.e. w/c ratio, the aggregate grading curve, the plasticizer content. However those differences allow the concretes to have similar mechanical strength and workability and, for this reason, they are assumed to be comparable. This example is remarkable to highlight the influence of the cement content inside a mix against environmental emissions.

The last case aims to compute transportation burdens due to the different specific weight of the two analyzed concretes.

5.5.1 First example

Once recycled and natural aggregate emissions estimation has been performed, the assessment of the environmental impacts of the two experimental concrete mixes can be completed. As previously stated, in this case only impacts related to production of the materials are taking into account, thus neglecting both transportation and manufacturing of concrete. This choice is justified by the necessity of comparing only the influence of the main compounds of the mixes that affect environmental emissions, once the chosen functional unit allows comparing the two strength- and durability/service life- similar materials.

As a first attempt, the concretes used in the RC beams experimental campaign are used (Section 4 of this thesis): they have the same mix design, with almost constant w/c ratio, cement type and content, and aggregates volume and grading curve. However it is worth noting that, in reality, they do not have the same mechanical strength, but the better EAF slag performances are assumed to mitigate the higher specific weight effect on the results. Hence, in this case, the functional unit, assumed equal to $1m^3$ of concrete is not properly correct: a short focus about this problem is presented below in Section 5.5. A brief representation of the

mix design and mechanical properties of those concretes is given in Table 5-4 and Table 5-5.

Table 5-4. Mixtures details.

	EAF slag	*Reference*
D_{max} (mm)	*22.4*	*31.5*
$V_{aggregates}$ (l)	*762.7*	*746.34*
Cement content (kg/m^3)	*310*	*290*
Water (kg)	*164.3*	*159.5*
w/c	*0.53*	*0.55*
Total EAF slag s.s.d. (kg/m^3)*	*2041*	*-*
Total natural aggregate s.s.d. (kg/m^3)*	*617.24*	*2098.43*
Plasticizer agent (kg/m^3)	*1.24*	*1.16*
Aerating admixture (g/m^3)	*49.6*	*46.4*

* s.s.d. = saturated surface dry

Table 5-5. Mechanical properties of experimental concretes.

Mix type	*specific weight after 28 days (kg/m³)*	*slump (cm]*	*$f_{c,cube\ 7d}$ (MPa)*	*$f_{c,cube\ 28d}$ (MPa)*	*$f_{ctm,\ exp}$ (MPa)*	*$E_{cm,\ exp}$ (GPa)*
EAF slag	*3006*	*16.8*	*48.80*	*58.30*	*4.38*	*40.05*
Reference	*2447*	*21.2*	*27.20*	*34.50*	*3.54*	*37.40*

Cement data are taken from [5.7], and they are reported in Table 5-6, referring to *1 kg of Cement Portland type II*. These values are then multiplied by the quantity of cement inside each mixes, and then summed to the emissions due to respective quantities of NA and EAF slag in each concrete. It is noticeable that cement determines a huge quantity of emissions with respect to the ones deriving from the extraction/treatment of the aggregates: a nominal dosage of 300 kg/m^3 of cement CEM II in a concrete mix produces about 175 kg of CO_2, according to data reported in Table 5-6, whereas NA in the traditional mix (about 2 ton/m^3) is responsible of about 17.8 kg of CO_2.

Table 5-6. Characterization of environmental emission related to global and regional scale categories – cement (*FU=1kg*).

CATEGORY	TOTAL EMISSIONS	U.M.
Climate Change	5.86E-01	kg CO_2 eq.
Eutrophication	2.04E-04	kg PO_4 eq.
Acidification	1.22E-03	kg SO_2 eq.

The amount of cement required to produce the traditional concrete was 290 kg/m^3, whereas 310 kg/m^3 were used for EAF concrete elaboration. As a consequence, the two concretes are generally comparable from the environmental point of view since cement quantities are similar (slightly increased for concrete with EAF slag), even though EAF aggregates have lower impacts than NA. Table 5-7 lists the results derived from the environmental assessment of the concrete mixes considered in this work, involving Climate Change, Acidification, Eutrophication categories only (other data are not available for cement). Concrete with EAF slag, containing 20 kg/m^3 of additional cement than the traditional mix, showed a maximum increase in emissions on the Eutrophication category (+4.71%), whereas it presents less impacts on Acidification problem (-1.62%).

Table 5-7. Total environmental emission related to global and regional scale categories – NA concrete and EAF slag concrete (FU=1m^3).

CATEGORY	EMISSIONS FOR NA CONCRETE	EMISSIONS FOR EAF SLAG CONCRETE	U.M.	Δ EMISSIONS	U.M.
Climate Change	1.88E+02	1.93E+02	kg CO_2 eq.	+2.92	%
Eutrophication	6.53E-02	6.84E-02	kg PO_4 eq.	+4.71	%
Acidification	4.53E-01	4.45E-01	kg SO_2 eq.	-1.62	%

5.5.2 Second example

A second application of the comparative LCA procedure is applied to analyze two concretes designed to have similar mechanical performances. However, to reach the same strength characteristics, two completely different mixes were designed, with different cement content, w/c ratio, plasticizer type and content. Mix details are reported in Table 5-8, whereas the main mechanical properties are listed in Table 5-9. It should be re-called that this example just aims to show the influence of the cement

content on the concretes' emissions; as already stated, the latter is the main responsible of concrete environmental emissions.

The difference, in terms of cement content, is relevant: the reference mix has 90 kg/m^3 more than the EAF concrete, about 22.5% more than in the recycled specimens.

Table 5-8. Mixtures details.

	EAF slag	*Reference*
D_{max} (mm)	*22.4*	*22.4*
$V_{aggregates}$ (l)	*762.7*	*706.6*
Cement content (kg/m^3)	*310*	*400*
Water (kg)	*164.3*	*160*
w/c	*0.53*	*0.4*
Total EAF slag s.s.d. (kg/m^3)*	*2041*	*-*
Total natural aggregate s.s.d. (kg/m^3)*	*617.24*	*1839.00*
Plasticizer agent 1 (kg/m^3)	*1.24*	*-*
Super-plasticizer agent 2 (kg/m^3)	*-*	*5.8*
Air-entrainer admixture (g/m^3)	*49.6*	*-*

* s.s.d. = saturated surface dry

Table 5-9. Mechanical properties of experimental concretes.

Mix type	*specific weight after 28 days (kg/m³)*	*slump (cm)*	*$f_{c,cube\ 7d}$ (MPa)*	*$f_{c,cube\ 28d}$ (MPa)*	*$f_{ctm,\ exp}$ (MPa)*	*$E_{cm,\ exp}$ (GPa)*
EAF slag	*3006*	*16.8*	*48.80*	*58.30*	*4.38*	*40.05*
Reference	*2466*	*18.5*	*44.00*	*56.25*	*5.40*	*39.10*

The analyzed concretes have similar compressive strength at 7 and 28 days, and also elastic modulus. Tensile strength is slightly different, because as it is expected, the mechanical strength of the cementitious matrix is higher in the reference concrete (with 22.5% more cement) than in the EAF concrete. Concerning workability, the two mixes belong to the same consistency class (S4), and hence they can be considered comparable. On the other hand, it is worth noting that also in this case the specific weight of the two concretes is different, and this may determine higher emissions due to transportation. This item will be analyzed in the further example.

The cement emissions were taken from [5.7], as in the previous example, and then they are computed with the ones deriving by the production of the aggregates. Then the impacts related to the production of the two concretes could be obtained. In this example the influence of the cement for the emissions evaluation is remarkable: the amount of 90 kg/m^3 less in the EAF slag mixture determines a carbon saving of about 23%.

Table 5-10. Total environmental emission related to global and regional scale categories – NA concrete and EAF slag concrete (FU=1m^3).

CATEGORY	*EMISSIONS FOR NA CONCRETE*	*EMISSIONS FOR EAF SLAG CONCRETE*	*U.M.*	*Δ EMISSIONS*	*U.M.*
Climate Change	*2.49E+02*	*1.93E+02*	*kg CO_2 eq.*	*-22.71*	*%*
Eutrophication	*8.69E-02*	*6.84E-02*	*kg PO_4 eq.*	*-21.40*	*%*
Acidification	*5.74E-01*	*4.45E-01*	*kg SO_2 eq.*	*-22.51*	*%*

From this example it is possible to highlight the great influence that the cement content has with respect to the environmental emissions related to concrete production.

5.5.3 Third example

This example aims to analyze the influence of the different specific weight of the EAF concrete with respect to the reference mix on the environmental emissions. In general, it is possible to say that the use of EAF slag in concrete determines an increase of specific weight, which varies in relation to the replacement amount (look at Section 3 of this thesis). To take into account this difference, it is necessary to expand the system boundaries accounting also the transportation from the production site to the product placement on the market.

Firstly, the assessment of the transportation impacts in terms of carbon emissions is given for the products *aggregates*. From a first look it is possible to observe that transportation emissions in terms of carbon production have the same magnitude order than the emissions due to aggregates production life cycle: hence, transportation costs are relevant. In fact, a Euro II type fully loaded truck consumes about 1 liter of diesel per 3 km [5.20]: indirect emissions alone are responsible of about 900 g CO_2/km. In addition, direct emissions increase this number depending on the type and mass of the vehicle. They can be evaluated according to eq.

5-3, converting PM10 emissions to CO_2. Globally, CO_2 emissions due to transport can be estimated around 40g CO_2/km·ton$_{aggregate}$.

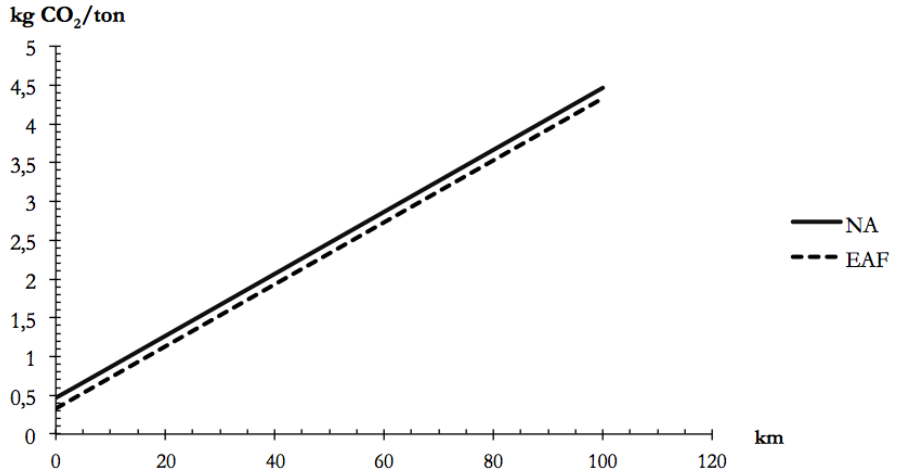

Figure 5-6. Carbon emissions due to aggregates transport [kg CO_2/ (ton · km)].

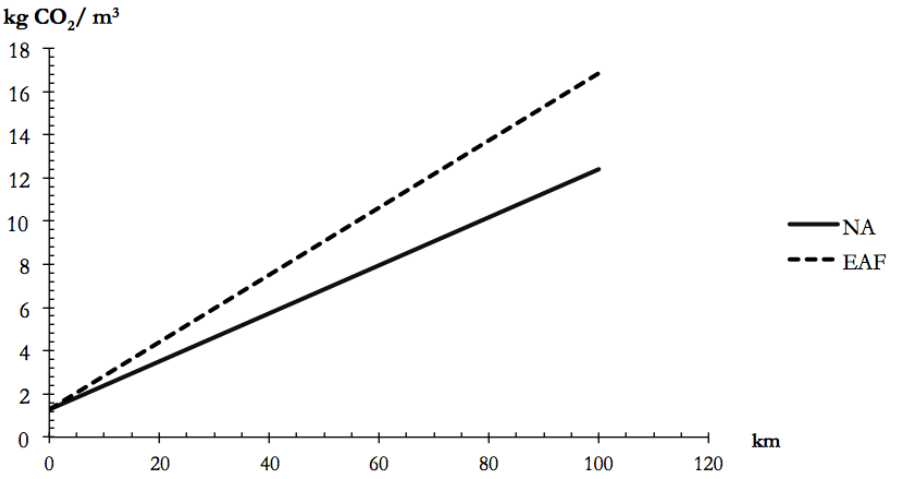

Figure 5-7. Carbon emissions due to aggregates transport [kg CO_2/ (m^3· km)].

Figs. 5-6 and 5-7 show the carbon production due to transport: the y-axis interception shows the "*km-0*" emissions, and as long as the distance increases, also the impacts increase. Fig. 5-6 represents the emissions in terms of carbon per weight unit, whereas Fig. 5-7 represents them in terms of carbon per volume unit. It appears clear that the functional unit influences the results, at least in terms of graphical interpretation of the results. As a matter of fact, the higher specific weight of the slag determines that, for the same maximum truck load, a reduced quantity of material can be transported. A focus about the importance in defining the proper functional unit is given in the next section.

When analyzing the effects of transport on the emissions due to concrete production, it is possible to observe that they do not contribute significantly on the overall emissions. In fact, concrete impacts are mainly due to cement manufacturing processes, which have great environmental burdens. Hence, from the next graph, it is possible to observe that emissions due to transportation can be neglected in most cases when comparing two different concretes. Results used to obtain Figs. 5-8 and 5-9 refer to the second example.

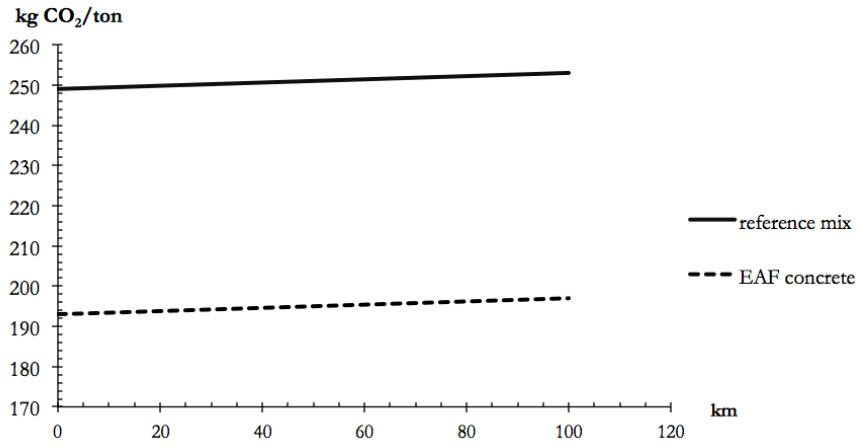

Figure 5-8. Carbon emissions due to concrete transport [kg CO_2/ (ton· km)].

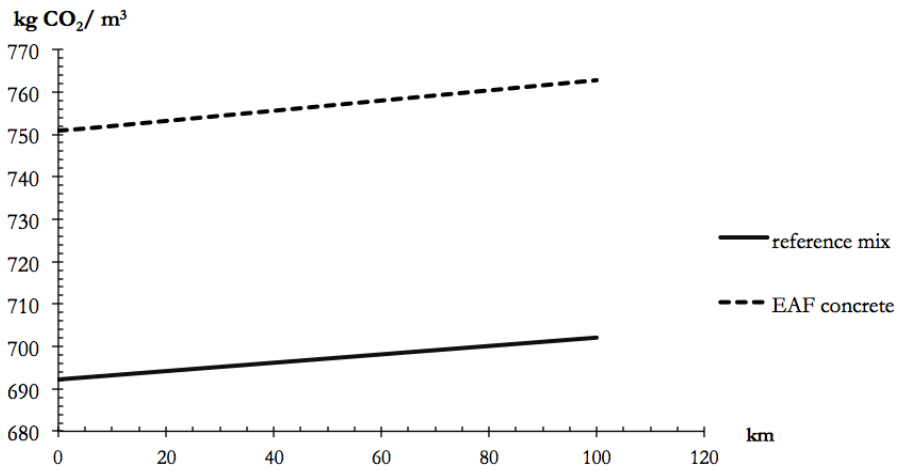

Figure 5-9. Carbon emissions due to concrete transport [kg CO_2/ (m^3· km)].

5.5.4 Functional Unit

An important result that has emerged from the application of the LCA framework to the above case studies deals with the definition of a proper functional unit when comparing different concretes.

The functional unit, already cited in Section 5.2, is the reference unit of the system for which the environmental impact will be calculated. It is the product, service or function on which to base the analysis and the comparison with possible alternatives. So it allows normalizing all input and output data so as to compare the results of the LCA. The functional unit is an arbitrary standardization parameter to describe all the final results and can be either a product or a service. Hence it is a necessary reference to ensure the comparability of LCA results. It is useful when different systems are evaluated, and when the comparison must be made on a common basis.

The functional unit for a concrete aggregate should be influenced by mechanical properties, physical and chemical characteristics, durability and of course, it is related to the unit of mass. However it is often difficult to define a proper FU when comparing different types of concrete. Looking at the first example, EAF slag compressive strength was almost the double of NAC strength: however, at the present case, there are no indications to how account this difference. Better mechanical properties of concrete with EAF slag as aggregate with respect to traditional concrete could involve less concrete volume (and hence less impacts) to obtain the same performances in real-scale structures. In the first example the compressive strength difference was assumed to balance the significant difference in specific weight between the two concretes, in absence of other indications. In the second example, this assumption was removed, because two concretes comparable from the mechanical and workability point of view are analyzed. However, cement content influence is highlighted: results show that cement is the major responsible of environmental emissions during concrete life cycle. This outcome is also confirmed by the results of the third example, where transportation costs are evaluated, by an expansion of the system boundaries. It has been shown that burdens du e to transportation are negligible with respect to the emissions at “km-0” if the functional unit refer to the product "concrete". This is not true when comparing just the aggregates manufacture process.

5.6 Conclusions

In this section a procedure to evaluate environmental impacts of different types of concrete is presented. In particular, the work deals with the comparative assessment of two concretes: the first contains only natural aggregates, the latter presents EAF slag as coarse aggregate. Although, the procedure can be generally applied for other types of concretes.

With regard to the examples shown in this section, the emissions related to the production of the aggregates were evaluated, by means of the developed LCA framework, with a cradle-to-gate approach, showing lower impacts for EAF slag aggregate. Reductions of impacts are both direct (linked to the direct use of the materials, such as leaching and air emissions) and indirect (due to energy and fossil resources use related to the productive system). Globally *1ton* of NA determines an increase in emissions of more than 35% with respect to EAF slag for each examined category. Improvements of results can be obtained taking into account the impacts saved by the expansion of EAF slag productive system, considering the different allocations linked to its actual application (i.e. asphalt layers and road sub-base), alternative to the landfilling of the material. In this respect, there is a huge lack of available data in literature concerning the end-of-life emissions of EAF slag. The development of a specific abiotic depletion study concerning bulk materials can also improve the precision of the environmental emission estimation of NA at the local scale.

Concerning concrete environmental assessment, three examples were developed to assess the impacts on the main global and regional scale environmental categories. Manufacture emissions have not been considered here; emissions are estimated taking into account the quantity of cement, NA and EAF slag aggregate present in each experimental mix; the used FU is $1m^3$ of concrete. Transportation costs were analyzed in the latter example, observing that they are negligible with respect to the emissions due to cement production, in the concrete LCA. On the contrary, they are relevant on the aggregates life cycle emissions.

In addition, a focus related to the estimation of a proper FU when comparing two different concrete mixes is given: it should take into account the same strength and durability/service life characteristics for both the experimental and traditional materials.

References

[5.1] Van den Heede P., De Belie N. Environmental impact and life cycle assessment (LCA) of traditional and 'green' concretes: Literature review and theoretical calculations. Cement and Concrete Composites 2012; 34(4): 431-442.

[5.2] Ministero dello Sviluppo Economico, Statistiche – Andamento della produzione di cemento anno 2009. Rome, Italy, 2009 [in Italian].

[5.3] European Commission, Eurostat, Cement and concrete production statistics 2009, NACE Rev.1.1.

[5.4] Metz B., Davidson O.R. , Bosch P.R., Dave R., Meyer L.A. Climate change 2007: mitigation. Contribution of working group III to the fourth assessment report of the IPCC. 2007.

[5.5] EEA Report. Effectiveness of environmental taxes and charges for managing sand, gravel and rock extraction in selected EU countries. Copenaghen, 2008.

[5.6] Habert G., Bouzidi Y., Chen C. & Jullien A. Development of a depletion indicator for natural resources used in concrete. Resources, Conservation and Recycling 2010; 54: 364-376.

[5.7] Josa A., Aguado A., Cardim A. & Byars E. Comparative analysis of the life cycle impact assessment of available cement inventories in the EU. Cement and Concrete Research, 2007; 37(5): 781-788.

[5.8] Damtoft J.S., Lukasik J., Herfort D., Sorrentino D. & Gartner E.M. Sustainable development and climate change initiatives. Cement and Concrete Research, 2008; 38: 115-127.

[5.9] IPCC 2006. 2006 IPCC Guidelines for National Greenhouse Gas Inventories. National Greenhouse Gas Inventories Programme, Eggleston H.S., Buendia L., Miwa K., Ngara T., Tanabe K. (eds). IGES, Japan.

[5.10] Marinkovic´ S., Radonjanin V., Malešev M. & Ignjatovic´ I. Comparative environmental assessment of natural and recycled aggregate concrete. Waste Management 2010; 30: 2255–2264.

[5.11] Pellegrino C. & Gaddo V. Mechanical and durability characteristics of concrete containing EAF slag as aggregate. Cement and Concrete Composites 2009; 31(9): 663-671.

[5.12] Pellegrino C., Cavagnis P., Faleschini F. & Brunelli K. Properties of concretes with Black/Oxidizing Electric Arc Furnace slag aggregate. Cement and Concrete Composites 2013; 37: 232-240.

[5.13] Pellegrino C. & Faleschini F. Experimental Behavior of Reinforced Concrete Beams with Electric Arc Furnace Slag as Recycled Aggregate. ACI Materials Journal 2013; 110(2): 197-206.

[5.14] Korre A. & Durucan S. Life Cycle Assessment of Aggregates. London: Waste & Resources Action Programme, 2009.

[5.15] Technical Committee ISO/TC 207 – "Environmental management", Environmental management - Life cycle assessment - Requirements and guidelines (ISO 14044:2006); European Committee for Standardization, 2006.

[5.16] Technical Committee ISO/TC 207 – "Environmental management", Environmental management - Life cycle assessment - Principles and framework (ISO 14040:2006); European Committee for Standardization, 2006.

[5.17] Barbaro A., Giovannini F. & Maltagliati S. Linee guida per la valutazione delle emissioni di polveri provenienti da attività di produzione, manipolazione, trasporto, carico o stoccaggio di materiali polverulenti. AFR Modeling Forecasting - Province of Florence and ARPAT - Regional Agency for Environmental Protection of Tuscany, 2009 [in Italian].

[5.18] Huijbregts M.A.J., Rombouts L.J.A., Hellweg S., Frischknecht R., Hendriks A.J., van de Meent D., Ragas A.M.J., Reijnders L. & Struijs J. Is Cumulative Fossil Energy Demand a Useful Indicator for the Environmental Performance of Products? Environmental Science &Technology, 2006; 40(3): 641-648.

[5.19] US-EPA. AP-42 Compilation of Air Pollutant Emission Factors. U.S. Environmental Protection Agency, 1995.

[5.20] UK NAEI. Vehicle speed emission factors. National Atmospheric Emissions Inventory, 2003, UK.

[5.21] NPI. Emission Estimation Technique Manual for Mining and Processing of Non-Metallic Minerals. Version 2.0. National Pollutant Inventory, 2000, Australia.

[5.22] Huijbregts M.A.J., Breedveld L., Huppes G., de Koning A., van Oers L. & Suh S. Normalisation figures for environmental life-cycle assessment - The Netherlands (1997/1998), Western Europe (1995) and the world (1990 and 1995). Journal of Cleaner Production, 2003; 11(7): 737-748.

[5.23] Bare J.C., Hofstetter P., Pennington D.W. & Udo de Haes H.A. Midpoints versus Endpoints: The Sacrifices and Benefits. The International Journal of Life Cycle Assessment 2000; 5(6): 319-326.

[5.24] Guinée J.B., Gorrée M., Heijungs R., Huppes G., Kleijn R., Koning A. de, Oers L. van, Wegener Sleeswijk A., Suh S., Udo de Haes H.A., Bruijn H. de, Duin R. van & Huijbregts M.A.J. Handbook on life cycle assessment. Operational guide to the ISO standards. IIa: Guide. IIb: Operational annex. Kluwer Academic Publishers, Dordrecht, 2002, 692 pp.

[5.25] Bossink B.A.G., Brouwers H.J.H. Construction waste: quantification and source evaluation. Journal of Construction Engineering Materials 1996; 122(5).

6 Workability of recycled concrete

6.1 Abstract

The use of recycled aggregates concrete (RAC) with coarse recycled aggregates (CRA) has been widely studied in literature. Several studies have already investigated mechanical and durability-related properties; however, the rheology of recycled concrete has not been extensively analyzed yet. Limited studies have discussed the influence of some recycled aggregate properties on slump, which is the most frequently used measure to evaluate workability. Since this measure is a single-value and also is often operator-sensitive, a more quantitative estimate can be derived in terms of fundamental physical quantities, such as plastic viscosity and yield stress. The higher heterogeneity in terms of experimental slump measure occurs when recycled aggregate concrete is tested. In this section, 16 recycled mixes were analyzed with two aggregates proportioning methods and results were compared with four controls: rheological parameters were measured with a ConTec BML Viscometer 3. The results represent a valid tool for better understanding of fresh RAC rheology.

6.2 Introduction

One of the most common solutions to improve sustainability in concrete production is given by the possibility to include recycled concrete aggregates in the place of virgin aggregates [6.1, 6.2, 6.3, 6.4], at least in limited replacement ratio. As recalled in Section 2, this possibility is also allowed by several International Codes and Recommendations [6.5, 6.6, 6.7], also for structural concrete applications, with the only prescriptions that recycled aggregate must comply with some minimum requirements [6.8], mainly concerning chemical stability and physical–mechanical characteristics. Literature research has widely studied the problems linked to the mechanical properties development in recycled aggregate concretes [6.9, 6.10, 6.11], within also some durability aspects related to RAC transport properties (chlorides and carbon diffusion) [6.12, 6.13, 6.14].

However, some limited information is reported by the scientific community about the properties of fresh recycled concretes, nevertheless it is often recognized that the introduction of recycled aggregate generally worsens workability. This problem arises significantly when recycled concrete is designed using a particular mix proportion method, called Equivalent Mortar Volume (EMV) [6.15], which produces generally stiffer

concretes with respect to the reference concretes produced with virgin aggregates. This problem can be overcome by the use of water-reducing admixtures in the mix [6.16] or by certain mixing procedures for RACs. The commonly named Mixing Water Compensation Method [6.17, 6.18] for elaborating concrete, based on added water which recycled aggregate absorbs to the total needed by the mix, allows acceptable workability to be achieved. In addition, an autogenous cleaning process can be applied [6.19], at least at lab scale, to remove part of the attached mortar from the recycled aggregates and hence improving the quality of the aggregates. This procedure allows both an improvement of workability and of mechanical properties of RAC.

Mix proportions can greatly influence the final performance of concrete, both in terms of workability and mechanical properties. In particular, the design of recycled aggregate concrete (RAC) is usually carried out by simply replacing the Natural Aggregate (NA) of a Natural Aggregate Concrete (NAC) with recycled material, and only taking into account some of the differences in physical properties among aggregates, such as surface texture and water absorption. In general terms, Recycled Aggregate (RA) is taken as NA, and this is the main cause of the poor mechanical performance often reported in the literature when different kinds of RAC mixes are tested [6.20, 6.21, 6.22]. On the other hand the EMV method is a suitable solution, as it considers RA as a two-phase material composed of NA and the mortar attached to it, which must be quantified and counted in the proportion. Since the physical properties of RA are affected by the attached mortar quantity and characteristics, this method can directly account for any deficiencies in low-quality aggregate, balancing the mix without affecting the mechanical and durability-related performance of the final concrete [6.15, 6.23, 6.24]. This allows the RAC mix to be prepared with a similar internal structure to that of NAC. In the case of EMV methodology, the parameters controlling workability should be carefully taken into account, due to the reduced amount of fresh mortar in the mix in favor of increased coarse aggregate volume. Knaack and Kurama [6.25], studying the rheological and mechanical behavior of RAC designed according to various methods – direct weight replacement (DWR), direct volume replacement (DVR), EMV methods – concluded that, compared with conventionally designed RAC (DWR, DVR), the workability of concrete mixes designed with the new method is significantly worsened. It should be noted that rheological behavior was analyzed according to the ‘‘mini slump’’ test, a variation on the conventional test described by the same authors [6.26]. This method may cause problems because it is a test with a single-number result, i.e., one which may be produced by two different samples of concrete with different rheological behaviors, as mentioned in [6.27, 6.28, 6.29, 6.30].

For the above reasons, the rheological properties of various concrete mixes produced with differing mixture proportioning methods (including EMV) were studied here. Basic rheological parameters were obtained with a ConTec BML Viscometer 3, with the aim of studying the flow behavior of concrete with different fresh mortar contents. The experimental campaign was conducted at the technical laboratories of the UPC of Barcelona, at the Departament d'Enginyeria de la Construcció.

6.3 Rheology background

6.3.1 Fresh concrete as a Bingham fluid

Concrete rheology has been extensively studied and the literature confirms that traditional concrete (with slump values higher than 8 cm and no segregation under gravity action) may be considered – with good accuracy – as a Bingham fluid [6.31, 6.32, 6.33]. The flow of a granular material, such as fresh concrete, can thus be viewed as a fluid, and should be described by at least two parameters, i.e., yield stress and plastic viscosity, as defined by the Bingham equation. This equation is the most commonly used, because its parameters can be measured independently, and also because the flow of real concrete follows it quite well. Other models can also be used to model fresh concrete flows (Fig. 6-1), such as the Herschel-Bulkley equation, which best describes the behavior of self-consolidating concrete [6.34]. With these assumptions, fresh concrete is represented as a viscoplastic fluid (for further information, look at the Appendix to this section), characterized by yield stress τ_0 [Pa], which must be exceeded before significant deformation can occur. After motion triggering, a linear relation associates shear stress τ with the applied shear rate $\dot{\gamma}$, called plastic viscosity μ [Pa·s]. Fig. 6-1 shows the flow curve of a Bingham fluid, which can also be described by the following equations (1), where $\eta(\dot{\gamma})$ represents shear viscosity, depending on the shear rate (Non-Newtonian fluid):

$$\begin{cases} \tau = \eta(\dot{\gamma})\dot{\gamma} = (\mu + \frac{\tau_0}{\dot{\gamma}})\dot{\gamma} = \mu\dot{\gamma} + \tau_0 & with\ \tau \geq \tau_0 \\ \dot{\gamma} = 0 & with\ \tau < \tau_0 \end{cases} \quad \textbf{6-1}$$

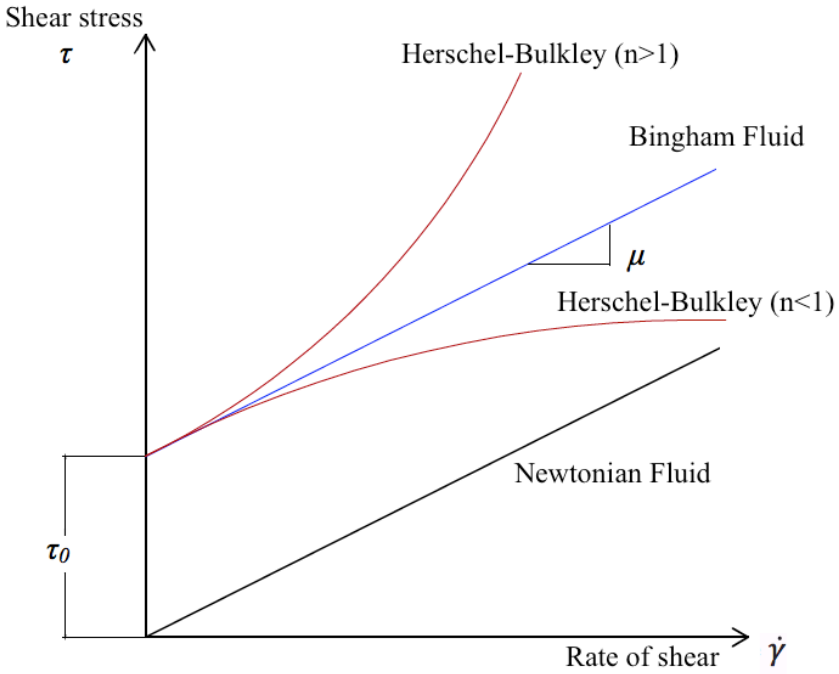

Figure 6-1. Concretes' flow curves.

6.3.2 Rheometer apparatus

Several test methods are currently available to estimate how various kinds of fresh concrete behave rheologically. Examples are the slump, L-box and V-funnel tests, the latter for highly flowable mixtures (S5 consistency class). For better evaluation of specific rheological parameters, viscometers can be used to obtain physical quantities; one of these, coaxial cylinder geometry for fresh concrete, has been used with good results since its first use in 1941 by Power and Wiler [6.35-6.36], followed by Tattersall and Banfill [6.28] and Wallevik [6.37-6.38], and can extract the Bingham model parameters, i.e., plastic viscosity μ and yield stress τ_0.

The apparatus used in the present experiments is a ConTec BML Viscometer 3 (Fig. 6-2), consisting of an outer cylinder (R_o=145 mm) rotating at an angular velocity of $\Omega=2\pi f$ [rad/s]; an inner cylinder unit (R_i=100 mm), to measure the torque applied, T [Nm]; and a special bottom unit, which eliminates shearing from the bottom to the outer walls. A schematic representation of the device is given in Fig. 6-3. The viscometer used here was designed to avoid slippage between cylinders and test material, due to protruding vanes in both upper and lower units [6.39, 6.40, 6.41]. In this work, each test involved a quantity of about 17 liters of fresh concrete, measuring 7 values of torque, with decreasing rotation speeds of the outer cylinder from a maximum of f_{max}= 0.44 rps to a minimum of f_{min}=

0.09 rps. After recording of the 7th point, a further increase in rotational velocity was given to check segregation, at f_{seg}= 2/3 f_{max}.

Figure 6-2. ConTec BML Viscometer 3.

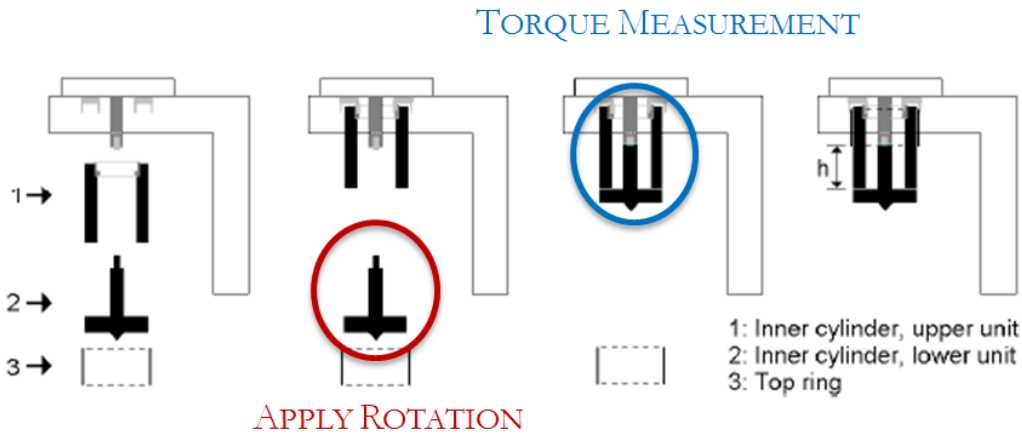

Figure 6-3. Configuration of a ConTec BML Viscometer 3.

6.3.3 Evaluation of rheological parameters

The physical rheological parameters of fresh concrete batches were calculated with the Reiner-Riwlin equation [6.42, 6.43, 6.44], analytically solving the inverse Couette problem for a Bingham fluid (for further information, look at the Appendix to this section). This equation is obtained by solving the velocity field (Eq. 6.2), under the following hypotheses:

- low Reynolds number *Re* (i.e., low rotational velocity and high apparent viscosity of fluid), allowing fluid stability and thus symmetry along the z-axis;
- no bottom effects, and thus z-independence of cylinder height;
- with circular flow, θ-independence occurs in both the velocity field and distribution of pressure p;
- time *t*-independence at each angular velocity step.

With the four above points, the general velocity profile:

$$\boldsymbol{v} = v_r(r,\theta,z,t)\boldsymbol{i_r} + v_\theta(r,\theta,z,t)\boldsymbol{i_\theta} + v_z(r,\theta,z,t)\boldsymbol{i_z} \quad \textbf{6-2}$$

was simplified into the following:

$$\boldsymbol{v} = v_\theta(r)\boldsymbol{i_\theta} \quad \textbf{6-3}$$

The velocity profile of Eq. 6-3, calculating both torque *T* and shear stress τ_0, with boundary condition $v_\theta(R_i)$=0, yields the following [6.45]:

$$v_\theta(r) = \frac{\hat{T}r}{4\pi\mu h}\left(\frac{1}{R_i^2} - \frac{1}{r^2}\right) - \frac{\tau_0 r}{\mu}\ln\left(\frac{r}{R_i}\right) \quad \textbf{6-4}$$

Thus, solving for torque *T* by applying boundary condition $v_\theta(R_0)= R_0\Omega$, and recalling that torque is measured directly by the apparatus for each angular velocity *Ω*, the above equation becomes:

$$\hat{T} = \frac{4\pi\mu h}{\left(\frac{1}{R_i^2}-\frac{1}{R_0^2}\right)}\Omega + \frac{4\pi\tau_0 h}{\left(\frac{1}{R_i^2}-\frac{1}{R_0^2}\right)}\ln\left(\frac{R_0}{R_i}\right) = H\Omega + G \quad \textbf{6-5}$$

Identification of the measured torque values for each angular velocity *Ω* means that a linear regression can be used to calculate relative viscosity *H* [Nm·s] and flow resistance *G* [Nm], which are then converted into Bingham parameters through Eq. 6-5. This equation, as here formulated, neglects the influence of plug flow [6.28,6.45] and gravel migration (see next section).

6.3.4 Plug flow and gravel migration

At high τ_0/μ ratios, a solid state may occur in the fresh concrete flow inside coaxial cylinder geometry viscometers. This phenomenon, called plug flow, starts from the outer cylinder and propagates towards the inner one, creating a layer which behaves as a rigid body. If not taken into consideration, plug flow leads to over-estimation of plastic viscosity μ and under-estimation of yield stress τ_0. Fig. 6-4 shows plug state.

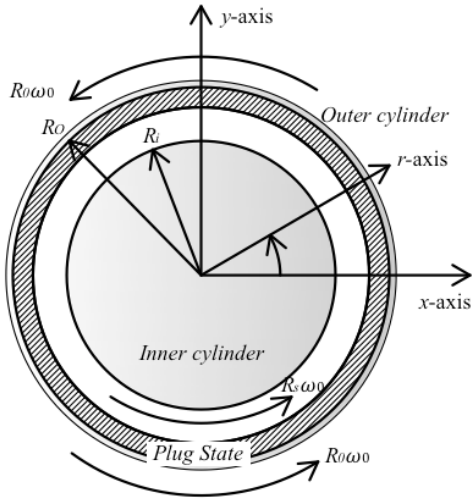

Figure 6-4. Plug state at R_s inside a coaxial cylinder geometry rheometer (from [6.40]).

When a solid layer occurs, the Reiner-Riwlin equation cannot be applied directly, because the outer boundary condition changes with plug radius $v_\theta(R_s) = R_s\Omega$. The first way of solving this problem is simply to remove the data included in the plug flow range by manually deleting $(\hat{T}_i, N_i)$ for every $N_i < N_s$ [6.41]. N_s is the speed below which plug flow occurs [6.28] and is evaluated in Eq. 6-6.

$$N_s = \frac{\tau_0}{\mu}\left[\frac{1}{2}\left(\frac{R_O^2}{R_i^2} - 1\right) - ln\left(\frac{R_o}{R_i}\right)\right] \cdot \frac{1}{2\pi} \qquad \textbf{6-6}$$

Alternatively, the Bingham parameters can be estimated more accurately. Here, we used an iterative procedure to calculate rheology parameters μ and τ_0, practically estimating plug radius and then deriving the above-mentioned quantities. The procedure is shown in Fig. 6-5, referring to the following equations:

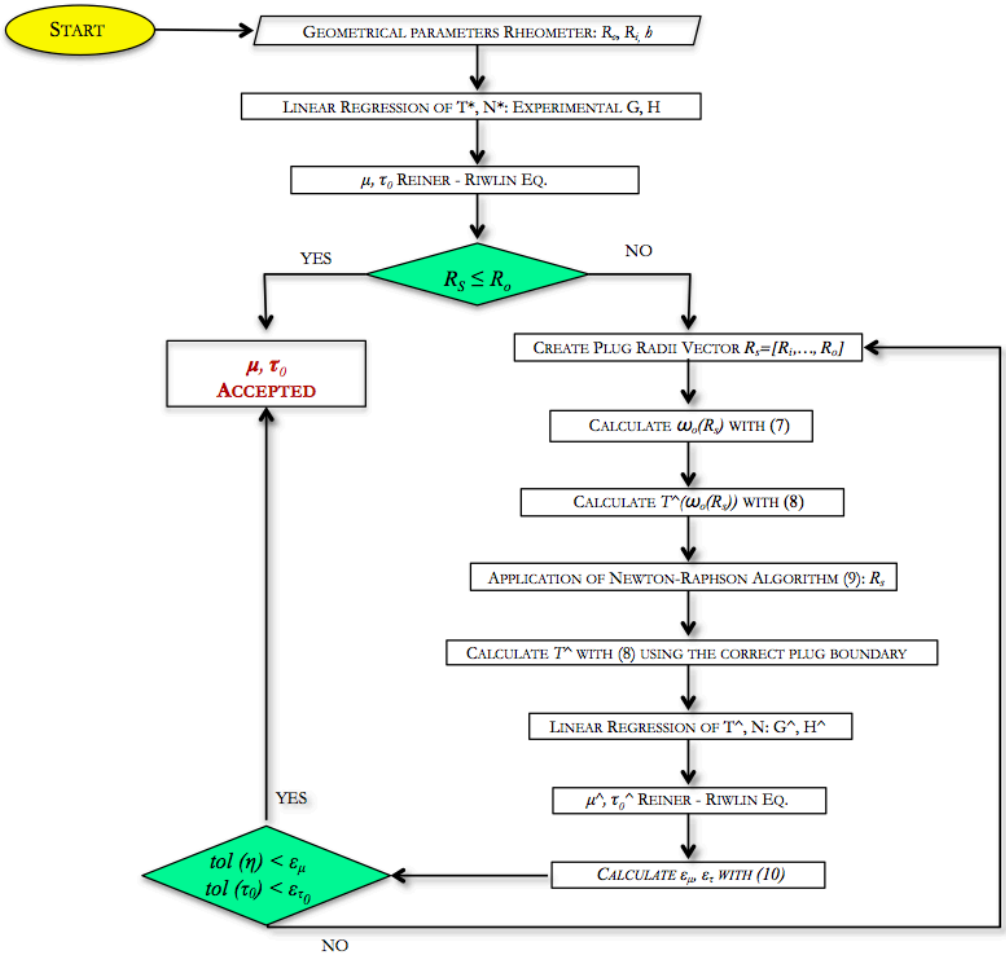

Figure 6-5. Iterative procedure applied to extract Bingham rheology with plug state at plug flow boundary (R_s).

$$\omega_0 = {}^{\tau_0}/_{\mu}\left[\frac{1}{2}\left(\frac{R_s^2}{R_i^2} - 1\right) - ln\left(\frac{R_s}{R_i}\right)\right] \qquad \textbf{6-7}$$

$$\hat{T} = \frac{4\pi\mu h}{\left(\frac{1}{R_i^2} - \frac{1}{R_s^2}\right)}\Omega + \frac{4\pi\tau_0 h}{\left(\frac{1}{R_i^2} - \frac{1}{R_s^2}\right)}\ln\left(\frac{R_s}{R_i}\right) \qquad \textbf{6-8}$$

$$\begin{cases} R_s : f(R_s) = {}^{\tau_0}/_{\mu}\left[\frac{1}{2}\left(\frac{R_s^2}{R_i^2} - 1\right) - ln\left(\frac{R_s}{R_i}\right)\right] - \omega_0 = 0 \\ Given\ an\ initial\ R_{s,0}, do\ until\ convergence \\ R_{s,k+1} = R_{sk} - \frac{f(R_{s,k})}{f'(R_{s,k})} \qquad with\ k \geq 0 \end{cases} \qquad \textbf{6-9}$$

$$\begin{cases} \varepsilon_{\mu} = \frac{\hat{\mu}-\mu}{\mu} \\ \varepsilon_{\tau_0} = \frac{\hat{\tau_0}-\tau_0}{\tau_0} \end{cases} \quad \textbf{6-10}$$

Another concomitant problem may occur at high rotational velocity, especially in concrete batches with low fresh mortar content and high aggregate volume. Coarse aggregate suspended in the fresh mortar matrix may migrate from high shear rate regions to low ones, i.e., in the present case, from the inner part of the rotating cylinder to the outer boundary. This phenomenon has been extensively reported in the literature [e.g., 6.45, 6.46] and was experimentally identified in most of the EMV samples: hence, the measured rheological parameters do not properly represent the tested mixes. However, the values can describe the remaining fat concrete, which does not rigidly move under shear rate gradient $-\nabla\dot{\gamma}$.

6.4 Materials and experimental methods

6.4.1 Materials

Several experimental mixes were prepared to study the rheological parameters of RAC, varying the w/c ratio, super-plasticizer (SP) content, recycled aggregate proportioning method, and coarse aggregate replacement ratio. Concrete mixes were prepared with calcareous sand, limestone and, in the case of RAC, locally available RA. The RA was composed of 37% clean aggregate, 59% aggregate with attached mortar, and 4% bituminous particles. Aggregates were all produced by crushing, but were not all from the same source (Fig. 6-6 - aggregate grading curve). The cement chosen was of CEM I 52.5 R type (Fig. 6-7), and the admixture was a polycarboxylate-based SP. Table 6-1 lists the main physical properties of both natural and coarse recycled aggregate used.

Table 6-1. Main physical characteristics of aggregates.

	Absorption (%)	*O.D. specific gravity (kg/m^3)*	*DR density (kg/m^3)*	*Mortar content (%)*	*D_{max} (mm)*
Sand	*1.2*	*2677*	*-*	*-*	*4*
Natural Aggregate	*0.5*	*2682*	*1501*	*-*	*12.5*
Recycled Aggregate	*6.3*	*2292*	*1288*	*34.6*	*12.5*

Twenty mixes were produced: 4 conventional concrete mixes, made entirely with natural aggregate; 8 RAC designed by simple replacement of a quantity of NA by RA, following conventional practices on design; and 8 RAC designed with the EMV method. The aggregate replacement ratios were 20% and 35%, the former representing the maximum RA content complying with the Spanish "Code on Structural Concrete" [6.48] and the latter being the maximum feasible content yielding at least an S4 slump class concrete, as defined in [6.49], obtained with the EMV method. The 35% limit was experimentally obtained during tests, and was closely associated with the high attached mortar content of the RA (Fig. 6-6 and Fig. 6-7). SP content was chosen in order to reach at least an S4 slump class for all concrete samples. The concrete strength class target for samples with w/c=0.4 was f_{ck}=*50MPa*, and for those with w/c=0.5 was f_{ck}=*40MPa*. Table 6-2 shows the mix design. Figure 6-10 explains why it was necessary to increase the SP content in the EMV batches: if designed with the same SP content of the RAC, the slump would result too low, even to test the specimens in the viscometer.

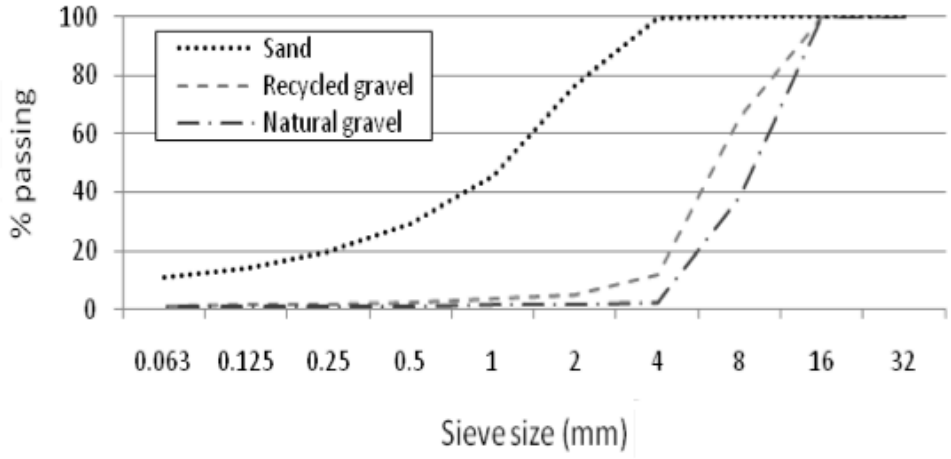

Figure 6-6. Aggregates' grading curves.

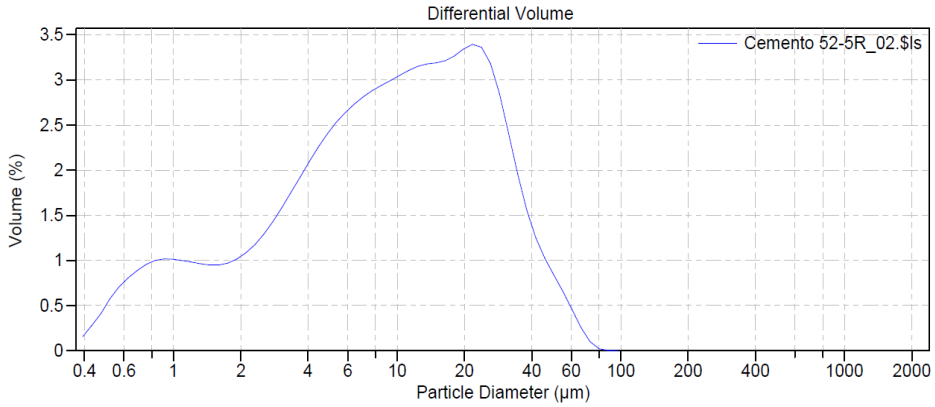

Figure 6-7. Particle grading curve of the cement.

Figure 6-8. RA with high attached mortar content.

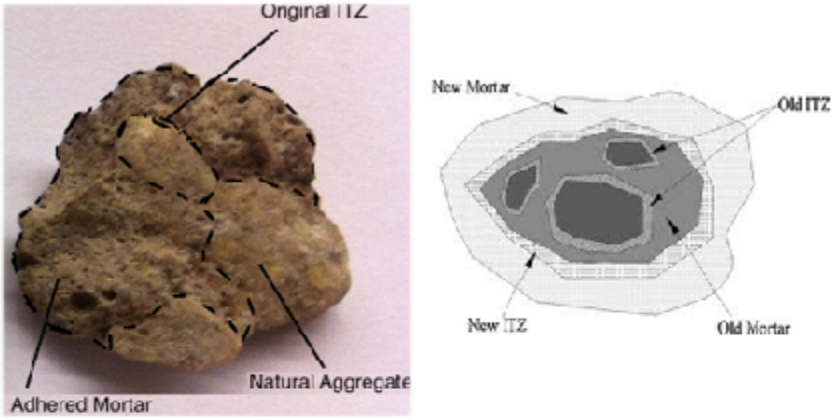

Figure 6-9. RA with attached mortar.

Figure 6-10. Left: RAC20/0.4-1 concrete; Right: EMV20/0.4-1 concrete (not rheologically investigated).

Table 6-2. Mix proportions of concrete samples [quantity per m^3].

	ID	RCA (%)	w/c	Water (kg)	Cement (kg)	Sand (kg)	Gravel (kg)	RCA (kg)	SP (kg)
BOLOMEY	NAC/0.4-1	0	0.4	182	455	835	1031	0	4.6
	NAC/0.4-1.2	0	0.4	182	455	835	1031	0	5.5
	NAC/0.5-1	0	0.5	182	364	880	1064	0	3.6
	NAC/0.5-1.2	0	0.5	182	364	880	1064	0	4.4
BOLOMEY RAC 20%	RAC20/0.4-1	20	0.4	182	455	835	794	203	4.6
	RAC20/0.4-1.2	20	0.4	182	455	835	794	203	5.5
	RAC20/0.5-1	20	0.5	182	364	880	820	209	3.6
	RAC20/0.5-1.2	20	0.5	182	364	880	820	209	4.4
BOLOMEY EMV 20%	EMV20/0.4-1.5	20	0.4	169	422	774	887	227	6.3
	EMV20/0.4-1.7	20	0.4	169	422	774	887	227	7.2
	EMV20/0.5-1	20	0.5	168	336	812	915	234	3.4
	EMV20/0.5-1.2	20	0.5	168	336	812	915	234	4.0
BOLOMEY RAC 35%	RAC35/0.4-1	35	0.4	182	455	835	633	340	4.6
	RAC35/0.4-1.2	35	0.4	182	455	835	633	340	5.5
	RAC35/0.5-1	35	0.5	182	364	880	649	355	3.6
	RAC35/0.5-1.2	35	0.5	182	364	880	649	355	4.4
BOLOMEY EMV 35%	EMV35/0.4-1.5	35	0.4	158	395	725	772	407	5.9
	EMV35/0.4-1.7	35	0.4	158	395	725	772	407	6.7
	EMV35/0.5-1.5	35	0.5	156	313	756	793	427	4.7
	EMV35/0.5-1.7	35	0.5	156	313	756	793	427	5.3

6.4.2 EMV aggregates proportioning method

The aggregates' proportioning method can highly influence the concrete performances, both in terms of mechanical strength, workability and durability-related properties. Generally, when recycled concrete is designed, the recycled aggregates are just take as the natural ones, replacing them or maintaining the same volume or weight proportion. The first method is called direct volume replacement (DVR), and the latter direct weight replacement (DWR). As already stated, this can cause losses in particular against mechanical strength, due to the worse characteristics of the recycled aggregates, which contain generally a high amount of adhered mortar.

The EMV method is based on the concept that the RAC mix should be proportioned to have the same total mortar volume as a reference concrete mix, made entirely with fresh NAs. The total amount of mortar is

defined by the new fresh mortar content plus the old adhered mortar onto the RCAs. Hence, the proportioning method essentially involves the proper determination of the amounts of RCA and the fresh mortar in RCA concrete, attached to the NAs. In addition, this method just take into account RA as CRA, whereas the fine recycled part is not analyzed. (Note: the notation used is according to the presented one in Section 2.1.1)

The procedure to design properly a concrete with the EMV method is herein reported.

First of all, the target fresh and hardened properties of the RCA are specified. Accordingly, a reference concrete is designed by means conventional proportioning methods: this is the NAC mix. The volume of natural aggregates inside this mix is defined as V_{NA}^{NAC}.

Then the RAC is designed. The first step is given by the definition of V_{NA}^{RAC}: it is the volume of natural aggregates inside the recycled mix.

The NA content ratio is defined as *R*:

$$R = \frac{V_{NA}^{RAC}}{V_{NA}^{NAC}} \quad \textbf{6-11}$$

If R=0: the coarse aggregate in the mix is 100% RCA; if R=1 the mix is made just by NA and no RCA is present.

In order to have the same hardened concrete properties, the EMV method proposes that two conditions must be satisfied (eq. 6-12, eq. 6-13): the volume of the total mortar in the two mixes must be the same, and the volume of the total natural aggregates in both the concretes should remain constant. This can also be expressed as follow:

$$V_{TM}^{RAC} = V_{M}^{NAC} \quad \textbf{6-12}$$

$$V_{TNA}^{RAC} = V_{NA}^{NAC} \quad \textbf{6-13}$$

The total volume of mortar (TM) in RAC is given by two contributions: the residual mortar V_{RM}^{RAC} and the new fresh mortar V_{NM}^{RAC}.

$$V_{TM}^{RAC} = V_{RM}^{RAC} + V_{NM}^{RAC} \quad \textbf{6-14}$$

The total volume of natural aggregates (TNA) inside RAC is given by the sum of the volumes of new coarse NA (V_{NA}^{RAC}) and the original NA present in the RCA (V_{OVA}^{RAC}):

$$V_{TNA}^{RAC} = V_{NA}^{RAC} + V_{OVA}^{RAC} \quad \textbf{6-15}$$

It should be noted that some differences in the final hardened properties of the two mixes can derived by the type of mortar and natural

aggregates: it is possible that the quality of recycled aggregates is lower than NA (i.e. higher RM porosity with respect to the new fresh mortar), hence some slight variations in the mechanical properties can be expected. The word slight has in this case a strong meaning: in fact, it is expected that even if the RCA comes from highly deteriorated concrete, the low-quality attached mortar could not survive to the crushing processes; hence, the quality of the adhered mortar is not expected to be highly worse than a new one.

According to the over-mentioned formula, the quantity of the old natural aggregates inside RAC (V_{OVA}^{RAC}) should be determined. It can be done knowing the residual mortar content (RMC) and the bulk specific gravity of OVA in RAC. RMC can be determined in a number of ways, including thermo-shock methods (as done in this work). Then the quantity of the old natural aggregates inside RAC (V_{OVA}^{RAC}) is:

$$V_{OVA}^{RAC} = V_{RCA}^{RAC} \cdot (1 - \mathrm{RMC}) \cdot \frac{{SG_b}^{RCA}}{SG_b^{OVA}} \quad \textbf{6-16}$$

where V_{RCA}^{RAC} is the quantity of RCA inside the RAC mix, ${SG_b}^{RCA}$ and ${SG_b}^{OVA}$ are respectively the bulk specific gravity of RCA and OVA.

Lastly, the required volumes V (and oven-dried weights W) of RCA and new NA in the RCA concretes can be evaluated as:

$$V_{RCA}^{RAC} = \frac{V_{NA}^{RAC} \cdot (1-R)}{(1-RMC) \cdot \frac{SG_b^{RCA}}{SG_b^{OVA}}} \quad \textbf{6-17}$$

$$V_{NA}^{RAC} = V_{NA}^{NAC} \cdot \mathrm{R} \quad \textbf{6-18}$$

$$W_{OD-RCA}^{RAC} = V_{RCA}^{RAC} \cdot SG_b^{RCA} \cdot 1000 \quad \textbf{6-19}$$

$$W_{OD-NA}^{RAC} = V_{NA}^{RAC} \cdot SG_b^{NA} \cdot 1000 \quad \textbf{6-20}$$

When properly defined the quantity of aggregates necessary in the RAC mix, water, cement and sand content should also be defined. The design starts from the definition of V_{RM}^{RAC}, which can be obtained as:

$$V_{RM}^{RAC} = V_{RCA}^{RAC} \cdot (1 - (1 - RMC) \cdot \frac{SG_b^{RCA}}{SG_b^{OVA}}) \quad \textbf{6-21}$$

Then the quantity of new fresh mortar inside RAC can be calculated (from eq. 6-13, 6-14 and 6-21):

$$V_{NM}^{RAC} = V_{M}^{NAC} - V_{RM}^{RAC} \quad \textbf{6-22}$$

Now, the quantity of the other components can be obtained by multiplying the ratio of the quantities present in the NAC. The further quantities of water, cement and sand (fine aggregates - oven dried), expressed in weight, can be respectively defined as:

$$W_w^{RAC} = W_w^{NAC} \cdot \frac{V_{NM}^{RAC}}{V_M^{NAC}} \quad \textbf{6-23}$$

$$W_c^{RAC} = W_c^{NAC} \cdot \frac{V_{NM}^{RAC}}{V_M^{NAC}} \quad \textbf{6-24}$$

$$W_{OD-FA}^{RAC} = W_{OD-FA}^{NAC} \cdot \frac{V_{NM}^{RAC}}{V_M^{NAC}} \quad \textbf{6-25}$$

RCA can hence be designed with the same TM and total NA volumes of the reference mix. If different replacement ratios are used (increasing), it will not result in different (higher) mortar content in RCA concrete compared to the companion NA, on the contrary of what can result if conventional proportioning methods are used.

However, a limit about the application of this method is given by the RMC: its effect determines a higher limit in replacement ratio (upper boundary). This limit is given by the R_{min} value [6.15]:

$$R_{min} = 1 - \frac{(1-RMC)}{V_{DR-NA}^{NAC}} \cdot \frac{SG_b^{RCA}}{SG_b^{NA}} \geq 0 \quad \textbf{6-26}$$

where V_{DR-NA}^{NAC} is the dry-rodded volume of NA in the NAC mix.

Rearranging eq. 6-26, it is also possible to define a maximum RMC value to design a RAC concrete with a fixed replacement ratio, i.e. fixing that R=100%, it is possible to determine a quality standard about the residual mortar content of the RCA. This can be obtained with:

$$\text{RMC}\ (\%) = [1 - V_{DR-NA}^{NAC} \cdot \frac{SG_b^{NA}}{SG_b^{RCA}}] \cdot 100 \quad \textbf{6-27}$$

The EMV-design procedure is reported in the next figure.

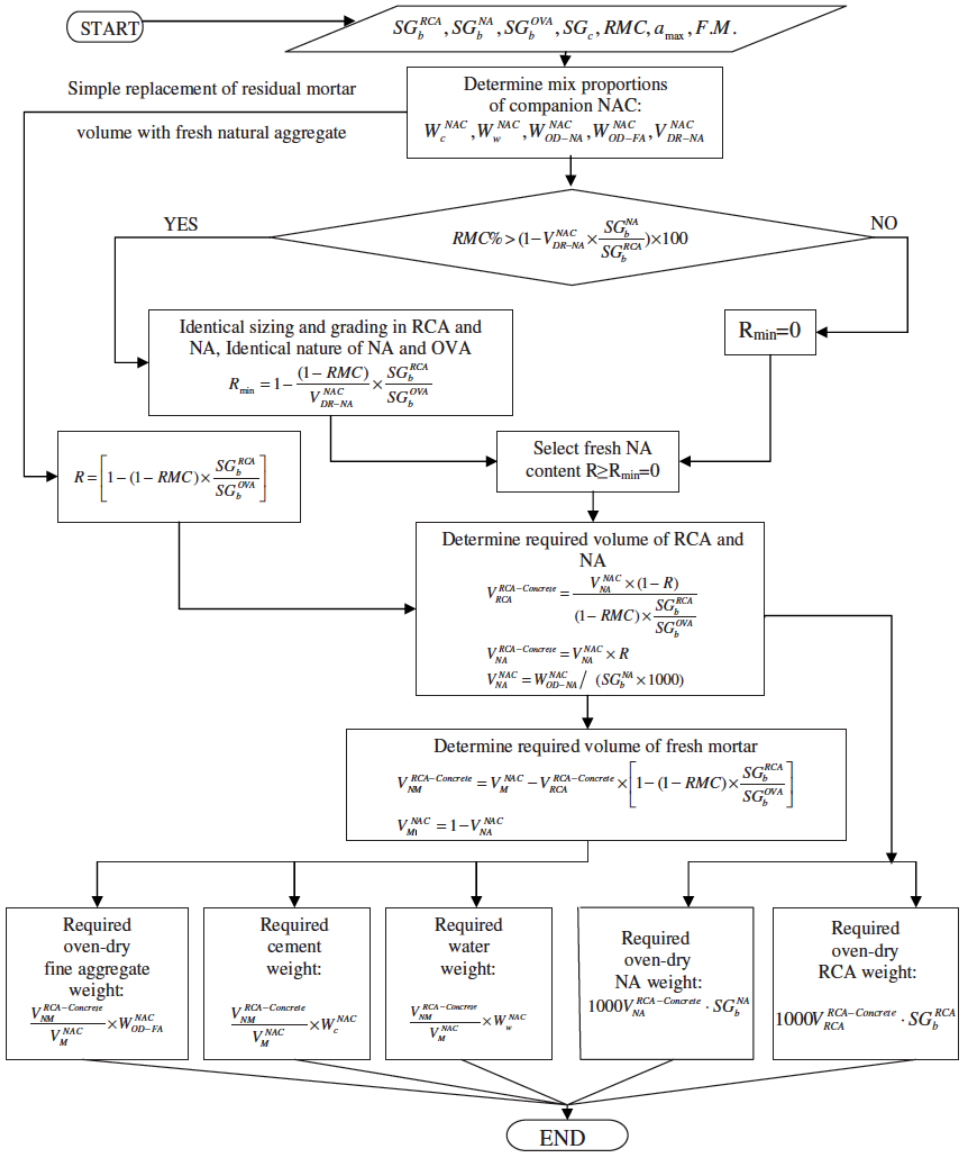

Figure 6-11. EMV design procedure (from [6.15]).

6.4.3 Mixing and rheology measurements

As rheological parameters are greatly influenced by temperature and humidity, all mixes were made at T= 20±2.5 °C and RH= 65±10%. The same mixing and measuring procedure was used for all concrete batches, as follows:

1) Dry mixing of 4-12.5 mm aggregate for about 10 seconds *t* [-10sec, 0min].

2) Wet mixing of 0-12.5 mm aggregate and cement in time interval t [0min, 3min]. Time t=0 min corresponds to the first addition of water.

3) Resting in time interval t [3min, 6min].

4) Mixing with SP in time interval t [6min, 8min]. The admixture was premixed with 0.5 l of water.

5) Slump value estimated at t=9 min, according to [46].

6) Rheological measurement at t_1= 16 min; t_2=20 min; t_3= 22 min; t_4=24 min.

It was not always possible to obtain all four measures expected for each batch, and only some were collected, so that the sampling times given above were slightly changed (see Results).

For each test, about 17 liters of fresh concrete were used, decreasing the rotation speed of the outer cylinder from max. f_{max}=0.44 rps to min. f_{min}=0.09 rps in 7 steps. For each velocity, 50 measures were taken in 3s; after the 7th step, increased speed was applied to the outer cylinder, reaching f_{seg}=2/3f_{max}. Between the 50 measures taken for each velocity step, the ten lowest were chosen and averaged to obtain a single value $\hat{T}$, as proposed in [6.38]. Fig. 6-12 shows the typical sampling profile.

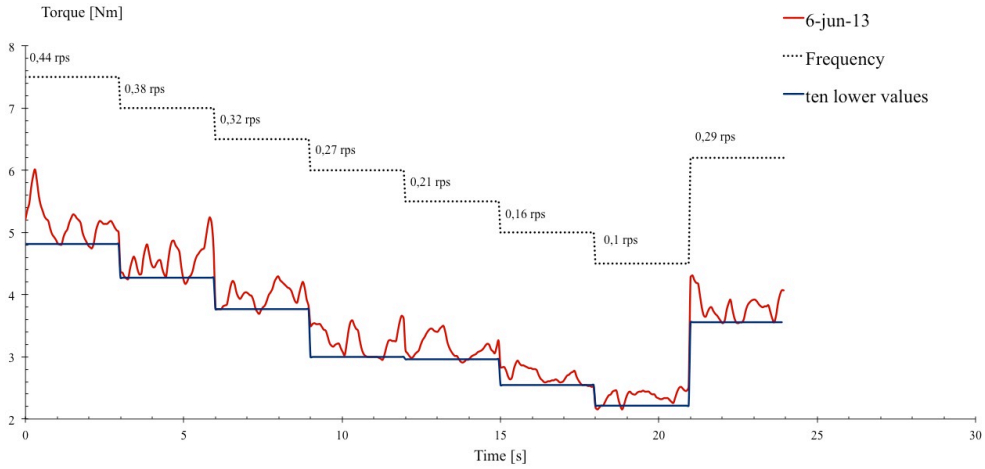

Figure 6-12. Rotation frequencies applied to the bottom disk of the rheometer.

6.4.4 Numerical reproduction of results

The Viscometric-ViscoPlastic-Flow 1.0 simulation software [6.37-6.38] is a GNU GPL licensed code, suitable for solving the velocity field inside a ConTec rheometer. This tool uses a finite difference model to solve the Cauchy equation of motion inside the apparatus:

$$\frac{\partial(\rho \boldsymbol{U})}{\partial t} + \nabla \cdot (\rho \boldsymbol{U}\boldsymbol{U}) = \nabla \cdot \boldsymbol{\sigma} + \rho \boldsymbol{g} \qquad \textbf{6-28}$$

where ρ is fresh concrete density, t is time, and g is gravity.

The above software has been used in several works, demonstrating its high accuracy in reproducing experimental results in both steady and transient states. Consistency, convergence and stability problems are extensively discussed in [6.38]. In the present work, numerical results were considered to be important in analyzing shear rate, shear stress and velocity field inside the rheometer, to understand the influence of gravel migration. Stationary analyses were conducted at various rotational speeds, comparing the analytical (calculated with Eq. 6-4) and numerical results of the velocity fields. Grid spacing in directions r and z was uniform and equal to Δr=Δz=1 mm (about 19500 grid points); Dirichlet boundary conditions were placed both on the whole inner cylinder and the outer one (including its bottom); a Neumann boundary condition was placed at the air-concrete interface (at the top of the tested batch). Regularization parameter δ was chosen according to the required approximation degree of the results and an acceptable computational cost (for further details of code, see [6.38]).

6.5 Results and discussion

For each tested mix, measured torque values $\hat{T}$ and angular velocity Ω were plotted to obtain relative viscosity H [Nm·s] and flow resistance G [Nm], to be converted into Bingham parameters. In all cases, the linear correlation was high ($0.980 \leq R^2 \leq 0.999$), confirming the hypothesis that fresh recycled concrete can properly be modeled as a Bingham fluid. Fig. 6-12 compares the behavior of two recycled samples with the same substitution ratio (20%), *w/c* ratio (0.4) and slump *s*= 20 cm, but proportioned with the two above methods. Measures refer to the same testing time, 16 minutes after the first addition of water. Here, the increased quantity of SP in the EMV batches (1.5%) lowered the yield stress, as in the RAC (1%) mixes. The ability of SP to reduce yield stress in the same manner for EMV and RAC batches was experimentally observed in all mixes at *w/c*= 0.4. Conversely, the EMV method caused a great increase in plastic viscosity, clearly seen in the slope of the two curves in Fig. 6-13.

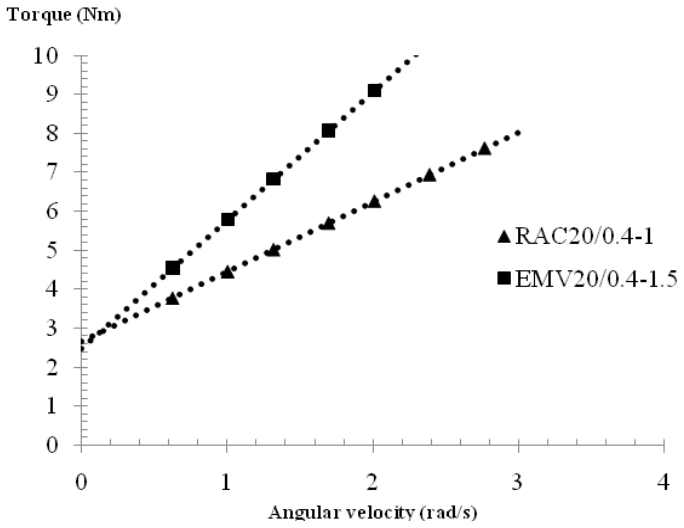

Figure 6-13. Bingham behavior of RACs.

Experimental results are listed in Table 6-3: rheological parameters were developed by both neglecting and considering plug flow. When τ_0 was too high for full shearing in the gap between the cylinders of the apparatus, large differences were found in the rheological measures computed with the two methods. These discrepancies were generally less than 5% for both estimated viscosity and yield stress, as also confirmed by other literature data [6.38]. Instead, in a few cases, plug flow could not be neglected, as it lasted even at higher rotational speeds, i.e., at higher values of the τ_0/μ ratio. Fig. 6-14 shows an example of the recalculation of Bingham parameters: mix NAC/0.5-1 is characterized by $\Delta\mu$= 8.77% and $\Delta\tau_0$= -7.5%, τ_0/μ= 5.79 and N_p= 0.16 rps.

Table 6-3. Rheological parameters evaluated with two methods.

	ID	t measure (min)	slump (cm)	no plug		iterative plug	
				μ (Pa·s)	τ_0 (Pa)	μ (Pa·s)	τ_0 (Pa)
BOLOMEY	NAC/0.4-1	17	21	37.60	147.40	37.62	147.29
	NAC/0.4-1.2	16	21	47.66	148.14	-	-
	NAC/0.5-1	15	21.5	20.72	140.99	22.54	130.42
	NAC/0.5-1.2	16	23	30.00	101.76	-	-
	NAC/0.5-1.2	20	23	28.90	95.05	-	-
	NAC/0.5-1.2	24	23	26.03	108.64	26.079	108.35
	NAC/0.5-1.2	26	23	28.42	102.52	28.42	102.51
BOLOMEY RAC 20%	RAC20/0.4-1	16	20	43.40	192.71	45.37	180.81
	RAC20/0.4-1	20	20	41.71	196.00	44.88	178.59
	RAC20/0.4-1.2	16	22	42.55	174.98	43.16	171.46
	RAC20/0.4-1.2	20	22	43.85	184.43	44.81	178.91
	RAC20/0.5-1	16	22	31.97	195.88	36.99	149.39
	RAC20/0.5-1	20	22	27.04	207.31	36.72	156.79
	RAC20/0.5-1	24	22	28.75	210.98	35.87	155.97
	RAC20/0.5-1.2	16	23	36.32	130.22	36.32	130.18
	RAC20/0.5-1.2	20	23	31.76	144.51	32.83	138.26
	RAC20/0.5-1.2	24	23	33.27	146.16	34.83	137.08
BOLOMEY EMV 20%	EMV20/0.4-1.5	16	20	91.86	185.17	-	-
	EMV20/0.4-1.5	24	20	85.75	216.66	-	-
	EMV20/0.4-1.7	16	21	90.62	152.66	-	-
	EMV20/0.4-1.7	22	21	65.52	165.01	-	-
	EMV20/0.4-1.7	24	21	76.06	155.97	-	-
	EMV20/0.5-1	16	20	55.66	259.68	59.07	240.08
	EMV20/0.5-1	20	20	57.29	274.06	64.16	256.17
	EMV20/0.5-1	24	20	72.57	200.79	-	-
	EMV20/0.5-1.2	16	21.5	50.04	226.13	52.41	212.42
	EMV20/0.5-1.2	20	21.5	51.46	215.44	52.04	211.88
	EMV20/0.5-1.2	24	21.5	45.63	238.04	50.09	212.15

	ID	t measure (min)	slump (cm)	no plug		iterative plug	
				μ (Pa·s)	τ_0 (Pa)	μ (Pa·s)	τ_0 (Pa)
BOLOMEY RAC 35%	RAC35/0.4-1	16	20.6	50.80	220.68	52.24	212.55
	RAC35/0.4-1	20	20.6	45.57	239.11	49.77	215.45
	RAC35/0.4-1	24	20.6	45.34	242.27	50.31	214.01
	RAC35/0.4-1.2	16	21	43.68	158.42	43.70	158.36
	RAC35/0.4-1.2	20	21	43.12	169.93	43.28	169.06
	RAC35/0.4-1.2	24	21	42.05	179.01	42.96	173.76
	RAC35/0.5-1	17	21.5	27.44	173.78	33.69	137.55
	RAC35/0.5-1	20	21.5	30.88	167.12	33.84	151.32
	RAC35/0.5-1	24	21.5	31.48	193.78	36.85	161.31
	RAC35/0.5-1.2	16	22.5	28.98	104.11	28.98	104.10
	RAC35/0.5-1.2	20	22.5	27.40	113.79	27.60	112.60
	RAC35/0.5-1.2	24	22.5	31.86	91.38	31.93	91.01
BOLOMEY EMV 35%	EMV35/0.4-1.5	16	19.5	81.36	233.54	-	-
	EMV35/0.4-1.5	20	19.5	81.14	253.34	-	-
	EMV35/0.4-1.5	24	19.5	86.71	214.80	-	-
	EMV35/0.4-1.7	16	22	71.19	89.60	-	-
	EMV35/0.4-1.7	20	22	65.18	99.33	-	-
	EMV35/0.5-1.5	16	19	65.88	271.13	67.43	262.23
	EMV35/0.5-1.5	20	19	66.82	254.64	66.89	254.22
	EMV35/0.5-1.5	24	19	63.07	255.66	63.51	253.03
	EMV35/0.5-1.7	16	19	86.34	301.23	-	-
	EMV35/0.5-1.7	20	19	72.51	298.27	73.18	294.37
	EMV35/0.5-1.7	24	19	82.63	242.70	-	-

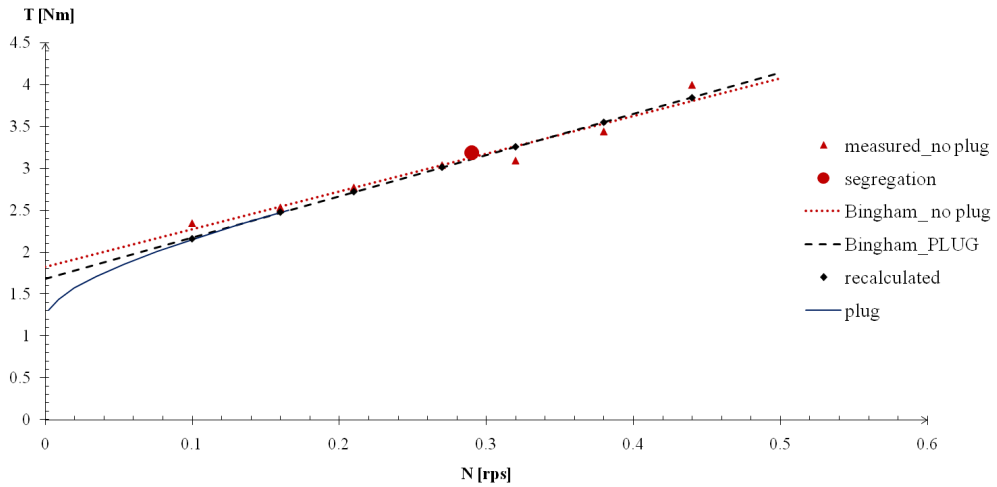

Figure 6-14. Torque vs. rotational frequency (Mix NAC/0.5-1 - test at 15 min).

Rheological parameters can also be shown in rheographs, which compare the various mixes in a simplified way, enabling evaluation of the effect of a single parameter on the complete rheological behavior of the samples [6.50]. Figs. 6-14 and 6-15 show Bingham parameters for batches with w/c = 0.4 and w/c = 0.5. Recycled concrete samples produced with the two aggregate proportioning methods clustered into two groups, showing significantly different rheological behavior. Recycled samples proportioned with direct aggregate volume substitution behaved like traditional mixes; instead, the EMV method gave rise to less fluid concretes, as also confirmed by the slump results (Table 6-3). As expected, the increased SP content reduced yield stress values in both cases; in particular, for w/c= 0.4, the increased SP content with the EMV method gave equivalent concretes in terms of yield stress. Comparison of Fig. 6-15 with Fig. 6-16 shows that the higher water content causes a general reduction in both viscosity and yield stress in all mixes.

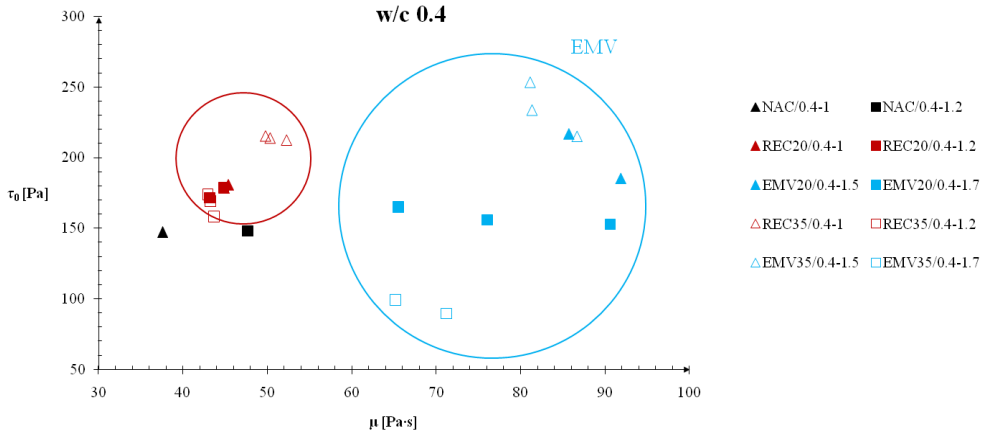

Figure 6-15. Effect of SP content, substitution ratio and aggregate proportion method (w/c=0.4).

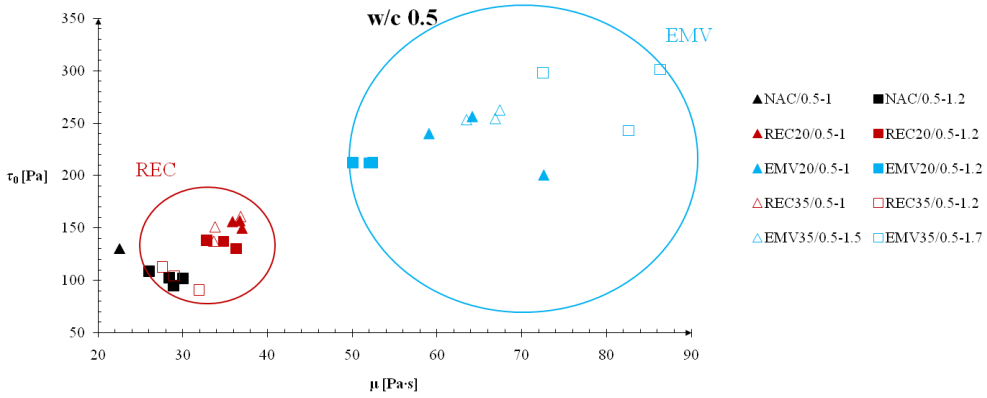

Figure 6-16. Effect of SP content, substitution ratio and aggregate proportion method (w/c=0.5).

Gravel migration still remains important, and was often seen during this research. It mainly occurred in the EMV mixes, with low fresh mortar contents, and this may have partially affected the results. Visual inspections during testing showed that the layer of packed gravel particles close to the outer cylinder was in the range 0-1.5 cm, becoming more solid as the substitution ratio increased. In this case, its influence could not be determined accurately, although Wallevik reported that gravel migration may give rise to under-estimation of yield stress and a poorly defined effect on plastic viscosity estimates [6.38].

Numerical results enabled us to determine potential gravel migration in some batches, by a comparison of the shear rate, velocity field and shear stress inside the test apparatus. Fig. 6-17 shows the computed velocity field (expressed in m/s) for the NAC/0.4-1.0 mix at f_{max}= 0.44 rps; the error between computed and analytical velocity, evaluated with Eq. 6-4 in the *z*-independence zone, where torque *T* was experimentally measured, is clear in the graph. Reducing the regularization parameter δ (Fig. 6-17: δ =10^{-3}) led to an improvement in fitting experimental results and reducing errors. However, the computational cost of the numerical simulation increased rapidly when δ was reduced.

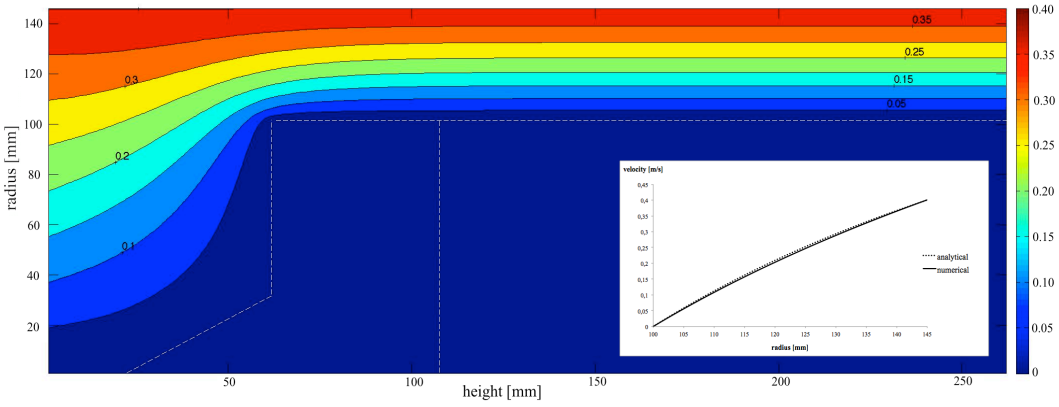

Figure 6-17. Computed velocity profile with f= 0.44 rps (NAC/0.4-1.0). Velocity expressed in [m/s].

Numerical results show that EMV batches generally have a high concentration of shear stress, due to the higher rheological parameter values. However, it is worth noting that the direction and potential of gravel migration are governed by the gradient of the shear rate, i.e., its spatial change. The gradient field of the shear rate is shown in Fig. 6-18, for the EMV/0.4-1.5 mix, at f_{max}= 0.44 rps: the isolines show the shear rate and the arrows the shear rate gradient. Their magnitude can be compared with the length of the reference vector, equal to 10^3 $m^{-1}s^{-1}$. Fig. 6-18 shows the

potential for gravel migration, which means that a zone filled by fat concrete may form near large vectors at the highest rotational speeds.

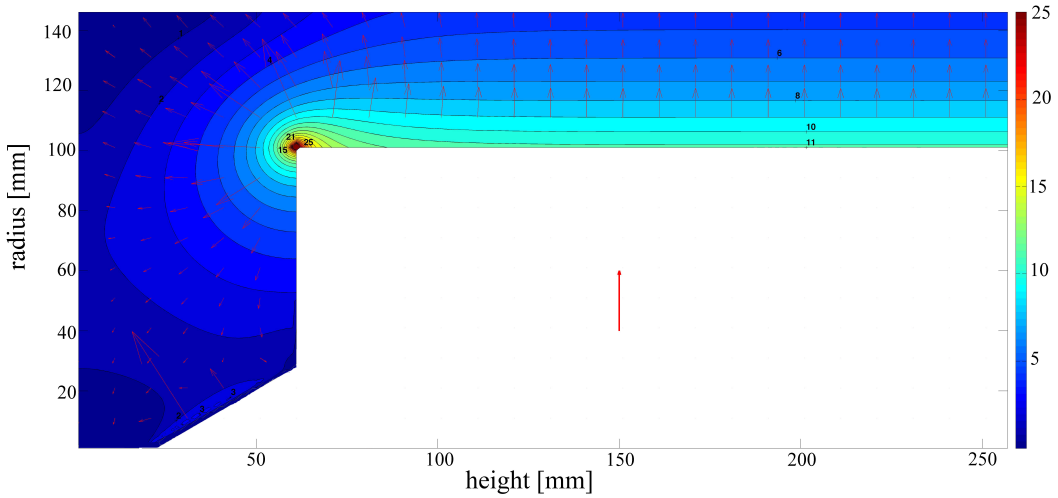

Figure 6-18. Computed gradient field of shear rate with f= 0.44 rps (EMV/0.4-1.5). Isolines: shear rate [s^{-1}]. Reference vector length: 10^3 $m^{-1}s^{-1}$.

6.6 Slump – yield stress relation

Once the rheological parameters were properly estimated, the relation between slump and yield stress was investigated. As previously said, the slump value is the result of one of the most simple rheology test: when the Abrams cone is lifted up, the concrete sample flows down under gravity action (Fig. 6-19). As fresh concrete is considered as a yield stress fluid (in this case, a Bingham fluid), it stops flowing downward just when the applied shear stress, induced by the gravity force, becomes less than the yield stress τ_0. Accordingly, it is expected that yield stress and the slump value are strictly correlated (look also at the Appendix to this section). Several authors attempted to determine a valid equation relating those two measures, also depending on the type of viscometer used. As a consequence a number of equations arose, empirically based on a number of experiments, with the aim to relate the slump, which measurement is simple, to physically-based measures, which evaluation could be done at lab-scale through viscometric tests. Tanigawa et al. [6.51] proposed a graph which correlates the slump with the yield stress, whereas the relation with the plastic viscosity was less significant, in agreement with the physical interpretation of the phenomenon. Another formulation was given by Murata and Kukawa [6.52], who proposed the following equation, where slump S is expressed in (mm):

$$\tau_0 = 714 - 473 \cdot log\ (S/10) \quad \textbf{6-29}$$

Then de Larrard [6.53] proposed to insert in the equation the specific weight of the concrete sample, arguing that the equation should be governed by the quantity $\tau_0/(g \cdot \rho_{sg})$, where g is gravity and ρ_{sg} is the specific gravity ρ/ρ_{ref}. The reference density is the density of a reference fluid which can be considered the water at 4°C (hence, $\rho_{ref} = 1000$ kg/m^3). Accordingly, in a NIST report, de Larrard himself with Ferraris [6.54] proposed the following equation, derived using a BTRHEOM viscometer, for ordinary concrete:

$$S = 300 - 0.347\frac{(\tau_0 - 212)}{\rho_{sg}} \quad \textbf{6-30}$$

This equation can be slightly modified to be applied for measurements with a ConTec BML rheometer [6.27], and it is reported below:

$$S = 300 - 0.416\frac{(\tau_0 - 394)}{\rho_{sg}} \quad \textbf{6-31}$$

The reason because those equations are different lies in the fact that those two viscometers measure differently yield stress: BTRHEOM gives a higher value of τ_0 than the ConTec BML rheometer. However, the relation between those systems is well-known, and reported also in [6.41].

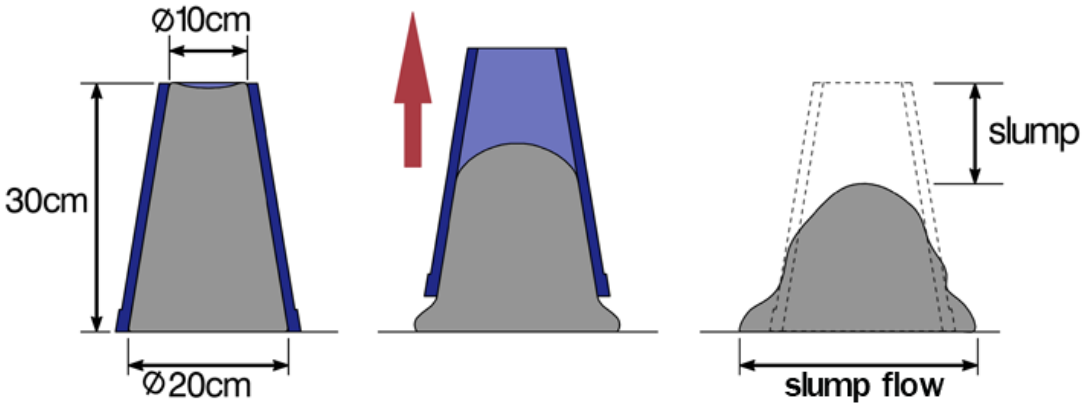

Figure 6-19. Slump test procedure.

When analyzing the results derived by the experimental campaign conducted in this thesis, the problem of the adaptation of the existing relation between slump and yield stress for recycled concrete has been emerged. In fact, the above relations were derived empirically for ordinary concrete and SCC; on the contrary, no validations for recycled concrete are present in literature. Hence, a dataset of experimental results was

collected (Table 6-4), using the results of two viscometric campaigns: the first, already described in this chapter, and a second one conducted at the UPC Laboratory (Barcelona, Spain). The latter results were furnished by a personal communication by Prof. Enric Vázquez and his collaborators [6.55], and consists in a further set of aerated recycled concretes.

Table 6-4. Experimental dataset.

#	method	w/c	air-entrainer (%)	SP (%)	REC (%)	slump (mm)	ρ	τ_0	μ
1	Bolomey	0.4	0	1	20	200	2350	180.8	45.4
2	Bolomey	0.4	0	1.2	20	220	2350	171.5	43.2
3	Bolomey	0.4	0	1	35	206	2300.9	212.6	52.2
4	Bolomey	0.4	0	1.2	35	210	2294.4	158.4	43.7
5	Bolomey	0.5	0	1	20	220	2330	149.4	37.0
6	Bolomey	0.5	0	1.2	20	230	2330	130.2	36.3
7	Bolomey	0.5	0	1	35	215	2259.9	137.6	33.7
8	Bolomey	0.5	0	1.2	35	225	2243.7	104.1	29.0
9	EMV	0.4	0	1.5	20	200	2350	185.2	91.9
10	EMV	0.4	0	1.7	20	210	2350	152.7	90.6
11	EMV	0.4	0	1.5	35	195	2350	223.6	81.4
12	EMV	0.4	0	1.7	35	220	2321.7	89.6	71.2
13	EMV	0.5	0	1	20	200	2324	240.1	59.1
14	EMV	0.5	0	1.2	20	215	2324	212.4	52.4
15	EMV	0.5	0	1.5	35	190	2337	262.2	67.4
16	EMV	0.5	0	1.7	35	190	2371	301.2	86.3
17	Bolomey	0.4	0.02	1	20	210	2115.5	199.2	31.6
18	Bolomey	0.5	0.02	1	20	220	2107.5	114.1	20.9
19	EMV	0.4	0.02	1.5	20	215	2172.5	77.9	23.7
20	EMV	0.5	0.02	1	20	210	2089.5	107.7	20.8
21	Bolomey	0.4	0.02	1	35	210	2121.5	154.7	26.3
22	Bolomey	0.5	0.02	1	35	220	2159.3	86.6	18.6
23	EMV	0.4	0.02	1.5	35	210	2165.5	109.7	37.5
24	EMV	0.5	0.02	1.5	35	215	2100	297.4	44.9

A non-linear regression model was used to develop a new relation between the slump and the yield stress, to maintain the same functional shape of eq. 6-29, 6-30 and 6-31, hence:

$$S = 300 - a1 \cdot \frac{(\tau_0 + a2)}{\rho} \qquad \textbf{6-32}$$

In the non-linear regression model the function *f* used to relate the response to the predictors is not necessarily linear:

$$y_i - f(\beta, x_i') + \varepsilon_i = 0 \quad \textbf{6-33}$$

where β is a vector of parameters, x_i' is the vector of the predictors, which are not necessarily of the same dimension, and $\varepsilon_i \sim N(0, \sigma^2)$.

The likelihood for non-linear models is:

$$L(\beta, \sigma^2) - \frac{1}{(2\pi\sigma^2)^{n/2}} \exp\left(-\frac{\sum_{i=1}^{n}[y_i - f(\beta, x_i')]^2}{2\sigma^2}\right) = 0 \quad \textbf{6-34}$$

which is maximized when the sum of the squared residuals is minimized:

$$\hat{\beta}^{NLS} = argmin(\sum_{i=1}^{n}[y_i - \hat{y}_i(\beta)]^2) = argmin(\sum_{i=1}^{n}[y_i - f(\beta, x_i')]^2) \quad \textbf{6-35}$$

Contrary to the linear model fitting, the solution of this optimization problem for a general function *f* cannot be expressed analytically. Hence, the solution should be obtained by numerical optimization: in this case the Gauss-Newton algorithm was applied. This method is designed specifically for the nonlinear least squares (NLS) estimator, by replacing the regression function $f(\beta, x_i')$ by its first-order Taylor expansion in eq. 6-35. The resulting iteration step is:

$$\hat{\beta}^{k+1} = \hat{\beta}^k - \left\{J\left(f, \hat{\beta}^k\right)^T J\left(f, \hat{\beta}^k\right)\right\}^{-1} J\left(f, \hat{\beta}^k\right)^T r(\hat{\beta}^k) \quad \textbf{6-36}$$

where $J(f, \beta) = \partial f(\beta)/\partial \beta_T$ is the Jacobian matrix of a vector function, and $r(\beta) = |y_i - f(x_i, \beta)|_{i=1}^{n}$ is the vector of the residuals.

The new relation obtained on the dataset of recycled concretes is the following:

$$S = 300 - 0.277 \frac{(\tau_0 + 557.0.16)}{\rho} \quad \textbf{6-37}$$

Other formulations were also studied, trying to include in the equation further parameters, i.e. the replacement ratio or the aggregate proportioning method (as a qualitative parameter), without success. This was due to the lack of statistically significance of the analyzed parameters, which can be related to the limited number of experimental data available in the dataset.

Concerning the obtained formulation, four residual plots were developed: a normal probability plot, to verify that the data are normally distributed (the closer are the data to the straight line, the higher is the normality); a versus fits plot, to verify the homoscedasticity; a histogram,

also used to check the hypothesis of normality; a versus order plot, to check the independency of the data. In this case the histogram reveals that the number of data is few to obtain a proper normal distribution. However, in absence of other experimental data, this assumption is accepted, also in relation to the normal probability plot distribution.

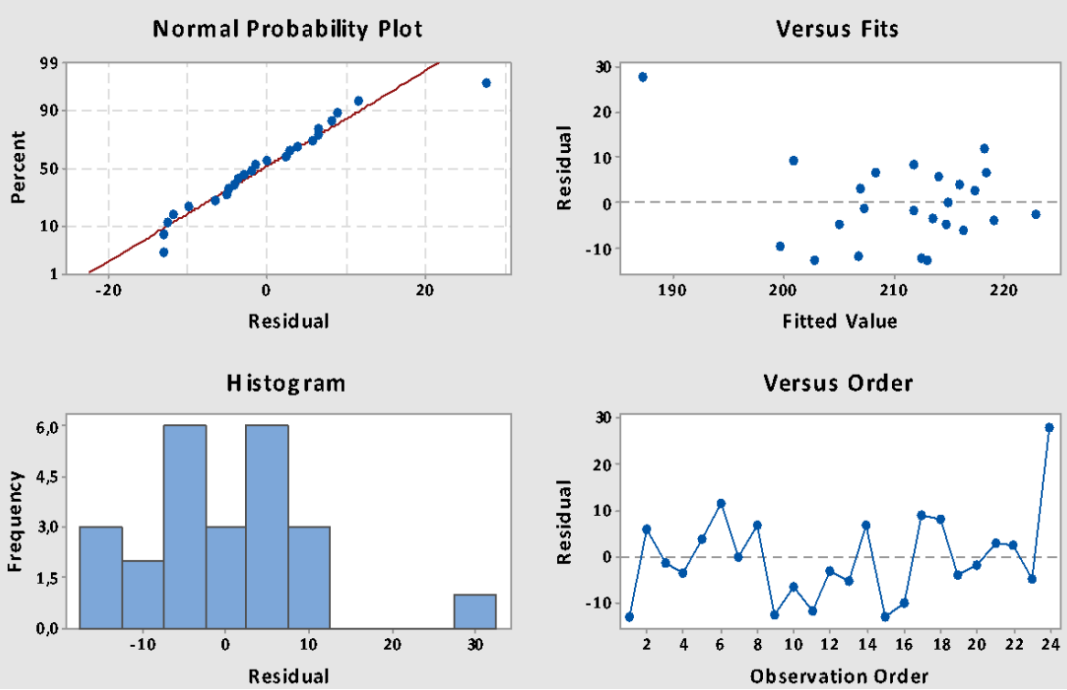

Figure 6-20. Residual plots.

A scatter plot was used to compare the results obtained using the new formulation (green marks; eq. 6-37), the existing one for the ConTec BML viscometer (red marks; eq. 6-31) and the experimental results (blue marks).

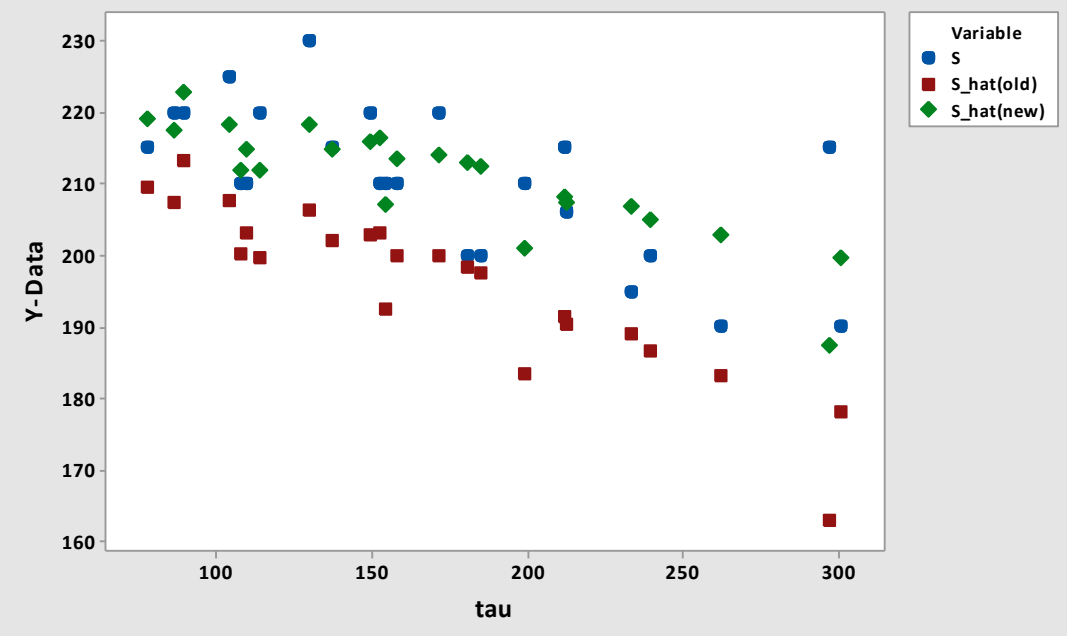

Figure 6-21. Scatter plot.

From this graph it is possible to conclude that eq. 6-31 determines a "systematic" underestimation of the slump values, with respect to the experimental results. On the contrary, the new formulation allows a better fit of the slump values. In addition, the new formulation is able to describe properly the decreasing trend between the slump and the yield stress, due to its functional shape.

A surface plot was also reported to show the influence of both the parameters included in the formulation (Fig. 6-22): the yield stress and the fresh concrete density. From this graph also the influence of the density could be observed, even though it does not present a monotonic trend as for the yield stress; on the contrary, it seems that it has a local maximum at about ρ=2200-2300 kg/m^3.

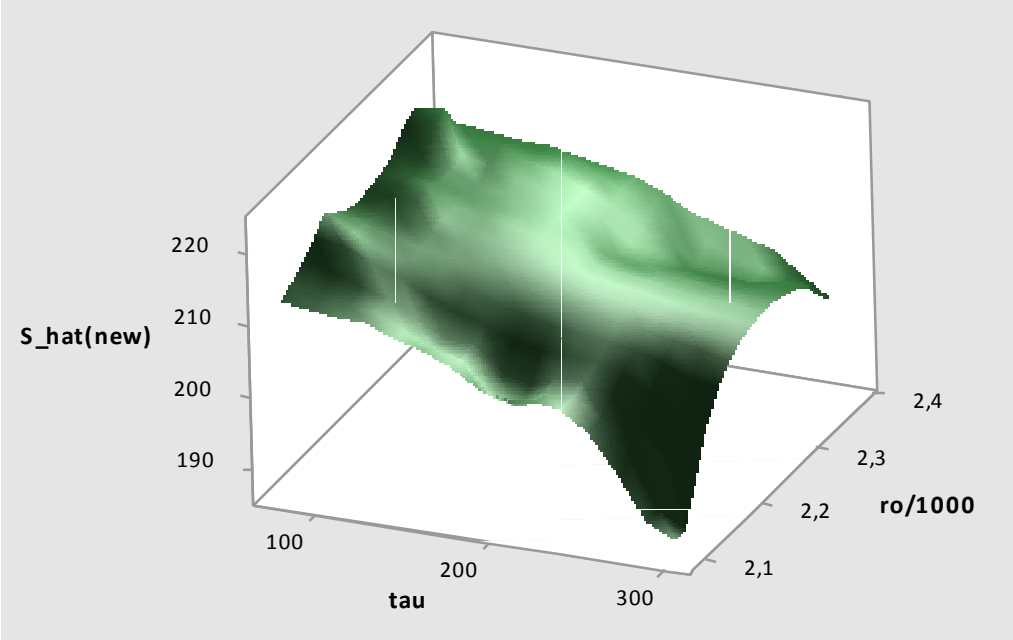

Figure 6-22. Surface plot.

6.7 Conclusions

The work described in this section is based on the first experimental campaign available in literature about rheology of fresh recycled concretes, proportioned with two methods. The test results allow the following conclusions to be drawn:

1. Recycled aggregate concrete (RAC) can be modeled as a Bingham fluid, and viscosity μ and yield stress τ_0 can properly describe its rheological behavior.

2. The mix proportioning method greatly affects rheological parameters. In particular, the EMV method strongly reduces slump and thus causes an increase in yield stress. The method also affects plastic viscosity. However, the EMV method allows savings in the required amount of cement, depending on mix, of up to 14 % in the cases examined here, and at the same time the required strength class can be reached (see section 6.4.1).

3. The increased SP content in EMV batches may not be sufficient to allow rheological behavior similar to that of RAC, although the same slump values may be reached. Further research with other admixtures, such as

air-entrainers, may help to reach the same rheological behavior of conventionally proportioned concrete for EMV samples.

4. The rheological measures of recycled aggregate are subject to two concomitant phenomena, plug flow and gravel migration. The former may be treated by varying the boundary position when analytically solving the inverse Couette problem for a Bingham fluid. Plug flow generally caused errors of ±5% in both μ and τ_0; this error may increase for mixes with high yield stress. Gravel migration mainly occurred in the EMV batches, with low fresh mortar content.

5. Gravel migration still remains an open question, which must be carefully taken into account when analyzing experimental results. In order to reduce the possibility of migration during viscometer measurements, reduced rotational speed applied to the outer cylinder of the apparatus will be considered in further experimental campaigns. This solution may have beneficial effects in lowering the shear rate gradient inside the viscometer.

6. A new formulation for relating slump to yield stress of fresh recycled concretes is derived. This equation solves the systematic underestimation of the slump values of recycled concretes obtained using the existing relation. However, as the dataset used for its derivation is limited, it is recommended to validate this equation also for other concrete batches.

6.8 Appendix

6.8.1 Flow of fresh cementitious materials

In this thesis the viscoplastic state of fresh concrete has been analyzed.

Fresh concrete can be identified as a single fluid, i.e. a continuum homogeneous medium, where the solid particles consist of a broad range in mass, dimension, shape and surface texture. Those particles are treated in the same manner, even they are coarse (i.e. gravel) and small (i.e. water molecules). When dealing with the motion of a huge number of solid particles, the concept of continuum particle (CP) can be introduced. In the case of fresh concrete, the CP consists of a collection of aggregates, cement grains, water molecules and so on, and it is designated by a volume Ω and a boundary ∂Ω (Fig. 6-23). With this approach, the elementary volume defined allows us to study the range of the macroscopic variations of the physical quantities we want to study (for instance, the velocity field gradient inside a formwork, or as in this case, inside a viscometer).

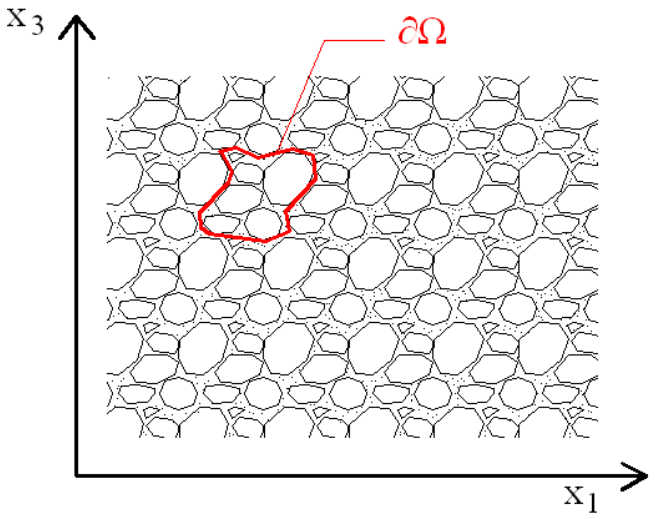

Figure 6-23. A cross section of a particle suspension with CP definition.

From a macroscopic scale of observation, most of the cementitious materials may show, at the steady state, either Newtonian, shear thinning and shear thickening behavior. Newtonian fluids are characterized by a constant apparent viscosity, shear thinning fluid have a decreasing apparent viscosity with the shear rate, whereas the shear thickening have an increasing apparent viscosity with the shear rate (Fig. 6-1).

A pure viscous fluid can self level under the effect of gravity: the viscosity of the material plays role on the time needed to obtain a horizontal surface. In addition, cementitious materials often display a yield stress that should be overcome before the flow can start, and below which the flow stops during casting. Yield stress is correlated with slump test.

Another important aspect of rheology of cementitious materials is the dependence of the flow history of the material on rheological parameters. For instance, the yield stress of a material which is left in rest can increase in time: this is what is generally known as “workability loss”. Some of these structural changes are reversible (can be recovered with mixing) and others are not reversible (they are associated mainly to the hydration of cement). The first ones are generally described as thixotropy.

The last aspect we will focus on concerns the segregation problems: the density of numerous components which constitutes cementitious materials can be very different, varying from 1000 (water) to 3200 kg/m^3 (cement grains). Those heterogeneities can determine two problems: bleeding (i.e. water migrations) and segregation (i.e. movement of coarse aggregates). The latter in particular is a multi-phase phenomenon, where at least two phase are involved, the suspending fluid and the inclusions. Segregation (or stability property) is often associated to static segregation (due to gravity force), but can also be related to a dynamic segregation when the material is flowing (i.e. gravel migration in a viscometer test).

The CP approach implies that various interactions play role in defining the complex macroscopic behavior of fresh cementitious materials. Four types of interaction can at least be identified, and one or several of them dominate in relation to the size of the particles in the cementitious mix analyzed:

- Brownian forces;
- Surface forces (or colloidal interactions);
- Hydrodynamic forces;
- Various contact forces between particles.

Between these, Brownian motion is the main responsible of the cement particles diffusion through the liquid, which may get close enough to lead van der Waals attractive forces (surface forces) to increase and dominate the electrostatic repulsion. However electrostatic repulsion is not able to separate the particles, and hence they agglomerate, giving origin to the yield stress. This network of particles may be very strong and may prevent the mixture to flow properly. The water-reducing admixtures work exactly to prevent this situation to occur: they can be seen as molecules which get adsorbed at cement grain surfaces, and via electrostatic effects,

they lead to the increase of the inter-particles distance, reducing the effect of the van der Waals forces.

At high shear rate, it is common that cementitious materials display a viscous behavior: for instance, concrete shows a viscosity called plastic viscosity in the Bingham model, over a certain yield stress. This viscosity has origin in the viscous dissipation in the interstitial fluid, which is a complex function of the volume fraction. The Krieger Dougherty equation [6.56] is the most famous equation which says that as the volume fraction Φ increases, energy dissipation progressively concentrates in strongly sheared fluid layers between neighboring particles. It can be written as:

$$\mu = \mu_0(1 - \frac{\phi}{\phi_m})^{-q} \quad \textbf{6-38}$$

where μ is the apparent viscosity of the suspension, μ_0 is the viscosity of the suspending fluid, Φ_m is the dense packing fraction, which is a geometric property of packing of non-interacting rigid particles, and q depends on the particle shapes (can be assumed as 2 for spheres, and >2 for non-spherical particles).

As above said, two main parameters can describe the macroscopic rheology of a viscoplastic material: yield stress τ_0 and plastic viscosity μ. Yield stress is relevant when the flow starts or stops to flow, and it is linked to the colloidal interactions of the particles, whereas the plastic viscosity dominates the behavior at higher shear rate. One common way to quantify the relative contribution of the colloidal interactions and hydrodynamics contribution is the computation of the Bingham number, a dimensionless number which is the ratio between yield stress and viscous contribution:

$$\mathcal{B}_n = \frac{\tau_0}{\mu_p \dot{\gamma}} = \frac{\tau_0}{\mu_p \cdot v/D} = \frac{\tau_0 \cdot D}{\mu_p \cdot v} \quad \textbf{6-39}$$

where τ_0 is the yield stress of the cementitious material, μ_p is the plastic viscosity, D is the typical dimension of the flow and v is the flowing velocity.

Whereas the Bingham number describes which is the main influencing parameter between yield stress (this occurs in ordinary rheology concrete) and plastic viscosity (in SCC), the Reynolds number can be used to define the ratio of the kinetic energy to the viscous energy. When Reynolds number is low, the flow is considered as laminar, which means that the kinetic energy of the system can be neglected with respect to the other sources of dissipation. It can be written as:

$$\mathcal{R}_e = \frac{\rho v D}{\mu} \quad \textbf{6-40}$$

where ρ is the density of the material, μ is the viscosity, D is the typical dimension of the flow and v is the flowing velocity. In the case of a yield stress fluid, such as fresh concrete, the apparent viscosity can be written as:

$$\mu_{app} = \frac{\tau_0}{\dot{\gamma}} + \mu_p \qquad \textbf{6-41}$$

where τ_0 is the yield stress of the cementitious material, μ_p is the plastic viscosity and $\dot{\gamma}$ is the shear rate. Hence the Reynolds number becomes:

$$\mathcal{R}_e = \frac{\rho v D}{\mu} = \frac{\rho v D}{\frac{\tau_0}{\dot{\gamma}} + \mu_p} = \frac{\rho v D}{\frac{\tau_0}{v/D} + \mu_p} = \frac{\rho v^2 D}{D\tau_0 + \mu_p v} \qquad \textbf{6-42}$$

6.8.2 Governing Equations

The casting processes of concrete represent an important stage to ensure structures to have the required mechanical and durability properties, to ensure properly finishing, joints and encapsulation of reinforcement. The simplest assumption that one can use when analyzing fresh concrete velocity field during casting is to treat it as a Newtonian fluid, subjected to a laminar flow. However, as previously seen, fresh concrete is generally considered as a Non-Newtonian fluid, i.e. with a non-linear relation between shear stress and shear rate. Fluid flow problems, such as the one analyzed in this thesis (the velocity field inside a coaxial cylinder rheometer) can be solved using computation flow dynamics (CFD) approach.

The equation of motion is the primary law to be used, and it is based on the Newton's 2nd law applied on a large set of solid particles. For Newtonian fluid it is the well-known Navier-Stokes equation (for incompressible fluids):

$$\rho\left(\frac{\partial \boldsymbol{v}}{\partial t} + \boldsymbol{v}\cdot\nabla\boldsymbol{v}\right) = -\nabla p + \mu\nabla^2\boldsymbol{v} + \boldsymbol{f} \qquad \textbf{6-43}$$

where $\boldsymbol{v}$ is the flow velocity, ρ is the fluid density, p is the pressure, μ is the fluid viscosity, $\boldsymbol{f}$ are the body forces (per unit of volume) acting on the fluid and t is the time. This equation derives from the general form, valid also for Non-Newtonian fluids, known as Cauchy equation of motion, which is more complex:

$$\rho\left(\frac{\partial \boldsymbol{v}}{\partial t} + \boldsymbol{v}\cdot\nabla\boldsymbol{v}\right) = -\nabla\cdot\boldsymbol{\sigma} + \boldsymbol{f} \qquad \textbf{6-44}$$

where $\boldsymbol{v}$ is the flow velocity, ρ is the fluid density, $\boldsymbol{\sigma}$ is the total stress tensor, $\boldsymbol{f}$ are the body forces (per unit of volume) acting on the fluid and t is the time. The body forces can be written as:

$$\boldsymbol{f} = \rho\boldsymbol{g} \qquad \textbf{6-45}$$

The total stress tensor can be written as:

$$\boldsymbol{\sigma} = -p\boldsymbol{I} + \boldsymbol{T} \qquad \textbf{6-46}$$

hence the total stress tensor can be decomposed in an isotropic pressure term p and a deviatoric component of the stress tensor $\boldsymbol{T}$. $\boldsymbol{I}$ is the unit dyadic. We will turn back in defining the functional form of the deviatoric component of the stress tensor.

The continuity equation is also used, using the incompressibility constraint:

$$\frac{\partial p}{\partial t} = -(\nabla\cdot\rho\boldsymbol{v}) \qquad \textbf{6-47}$$

$$\nabla\cdot\boldsymbol{v} = \boldsymbol{0} \qquad \textbf{6-48}$$

The constitutive equation is represented by eq. 6-46, and the definition of the deviatoric component of the stress tensor represents one important issue, objective of a relevant rheology branch [6.57]. The tensor $\boldsymbol{T}$ used in this thesis can be written as:

$$\boldsymbol{T}(\boldsymbol{x},t) = 2\eta(\boldsymbol{x},t)\dot{\boldsymbol{\varepsilon}}(\boldsymbol{x},t) \qquad \textbf{6-49}$$

where η is the shear viscosity (also known as apparent viscosity) and $\dot{\boldsymbol{\varepsilon}}(\boldsymbol{x},t)$ is the strain rate tensor, which can be expressed as:

$$\dot{\boldsymbol{\varepsilon}}(\boldsymbol{x},t) = \frac{1}{2}(\nabla\boldsymbol{v} + (\nabla\boldsymbol{v})^T) \qquad \textbf{6-50}$$

The apparent viscosity function depends on the model used: it can be constant if a Newtonian model is used, or can follow a Non-Newtonian model (i.e. Bingham or Herschel-Bulkley models). In this case a Bingham model was used:

$$\eta = \mu + \frac{\tau_0}{\dot{\gamma}} \qquad \textbf{6-51}$$

where, as we have previously seen, η is the apparent viscosity, μ is the plastic viscosity and τ_0 is the yield stress. The term $\dot{\gamma}$ represents the shear rate, and is function of the strain rate tensor $\dot{\boldsymbol{\varepsilon}}$:

$$\dot{\gamma} = \sqrt{2\dot{\boldsymbol{\varepsilon}}:\dot{\boldsymbol{\varepsilon}}} \qquad \textbf{6-52}$$

6.8.3 Reiner-Riwlin Equation

The equation used to make the conversion from *H* and *G* (look at section 6.3.3) into μ and τ_0 respectively is called Reiner-Riwlin equation [6.42]. We have seen a set of hypotheses that can be used to reduce eq. 6-2 into eq. 6-3: $\boldsymbol{v} = v_\theta(r)\boldsymbol{i_\theta}$, hence producing a set of analytical results. From this equation, the velocity gradient tensor $\nabla\mathbf{v}$ can be evaluated, in order to obtain the strain rate tensor:

$$\dot{\boldsymbol{\varepsilon}} = \frac{1}{2}\left(\frac{dv_\theta(r)}{dr} - \frac{v_\theta(r)}{r}\right)(\boldsymbol{i_r i_\theta} + \boldsymbol{i_\theta i_r}) \qquad \textbf{6-53}$$

Using this result into eq. 6-52, one can obtain the shear rate that applied inside the fresh concrete sample:

$$\dot{\gamma} = \left|\frac{dv_\theta(r)}{dr} - \frac{v_\theta(r)}{r}\right| \qquad \textbf{6-54}$$

Now, using the constitutive equation of the viscoplastic state (eq. 6-49) and eq. 6-53, the deviatoric stress tensor can be written as:

$$\boldsymbol{T} = \eta(\dot{\gamma})\left(\frac{dv_\theta(r)}{dr} - \frac{v_\theta(r)}{r}\right)(\boldsymbol{i_r i_\theta} + \boldsymbol{i_\theta i_r}) \qquad \textbf{6-55}$$

Hence the component $T_{r\theta}$ is extracted from eq. 6-55:

$$T_{r\theta} = \eta(\dot{\gamma})\left(\frac{dv_\theta(r)}{dr} - \frac{v_\theta(r)}{r}\right) \qquad \forall r \in [R_i, R_s] \qquad \textbf{6-56}$$

which is valid in the viscoplastic zone, hence in the zone between the inner radius R_i and the plug radius R_s, beyond which a solid state occurs and the constitutive equation to be used can be for instance the Hook law. If no plug occurs, R_s is equal to R_o, the outer radius.

Now, consider the fresh concrete sample to be divided into cylindrical shells of δR thickness. The equation of rotational motion for each shell is:

$$I_R\frac{d\boldsymbol{\omega}(r,t)}{dt} = \widehat{\boldsymbol{T}} = \hat{T}(r + \delta R/2, t)\boldsymbol{i_z} - \hat{T}(r - \delta R/2, t)\boldsymbol{i_z} \qquad \textbf{6-57}$$

where I_R is the inertia moment of each shell, $\widehat{\boldsymbol{T}}$ is the sum of the torques applied to the shell, and ω is the angular velocity:

$$\boldsymbol{\omega} = \boldsymbol{i_r} \times \frac{v_\theta(r,t)\boldsymbol{i_\theta}}{r} = \frac{v_\theta(r,t)}{r}\boldsymbol{i_z} \qquad \textbf{6-58}$$

At the steady state we have that $\frac{d\boldsymbol{\omega}}{dt} = 0$, hence eq. 6-57 reduces to:

$$\hat{T}\left(r + \frac{\delta R}{2}\right) = \hat{T}(r - \frac{\delta R}{2}) \qquad \textbf{6-59}$$

which means that, during each measurement at a fixed rotational velocity, where steady state is assumed, the torque is constant inside the concrete sample, at each radius $r \in [R_i, R_o]$. This result applied independently from the plug occurrence (note that we do not have a R_s).

The torque applied on a cylindrical shell can be calculated according to Cauchy's stress principle:

$$\widehat{\boldsymbol{T}} = \hat{T}\boldsymbol{i_z} = \int_0^h \int_0^{2\pi} r\boldsymbol{i_r} \times (\boldsymbol{i_r} \cdot \boldsymbol{\sigma}(r) r d\theta dz) = 2\pi r^2 h T_{r\theta}(r)\boldsymbol{i_z} \qquad \textbf{6-60}$$

where h is the height of the shell. From this equation one can derive the torque applied from the sample to the inner cylinder of the rheometer apparatus:

$$\hat{T} = 2\pi R_i^2 h T_{r\theta}(R_i) \qquad \textbf{6-61}$$

Now combining eq. 6-60 with eq. 6-56 it is possible to obtain the following:

$$\eta(\dot{\gamma})\left(\frac{dv_\theta(r)}{dr} - \frac{v_\theta(r)}{r}\right) = T_{r\theta}(r) = \frac{\hat{T}}{2\pi r^2 h} \qquad \forall r \in [R_i, R_s] \qquad \textbf{6-62}$$

With the hypothesis that the outer cylinder rotates counterclockwise, giving $v_\theta(r) > 0$, then $\hat{T}$ in eq. 6-61 should be positive. This determines $T_{r\theta} \geq 0 \ \forall r \in [R_i, R_s]$, which also determines that is possible to rewrite eq. 6-54 without the absolute sign. Now, with the Bingham model (eq. 6-51) used for defining the apparent viscosity, eq. 6-62 becomes:

$$\frac{dv_\theta(r)}{dr} - \frac{v_\theta(r)}{r} + \frac{\tau_0}{\mu} = \frac{\hat{T}}{2\pi\mu r^2 h} \qquad \forall r \in [R_i, R_s] \qquad \textbf{6-63}$$

Now the shear rate can be obtained as follows:

$$\dot{\gamma} = \frac{dv_\theta(r)}{dr} - \frac{v_\theta(r)}{r} = \frac{\hat{T}}{2\pi\mu r^2 h} - \frac{\tau_0}{\mu} \qquad \forall r \in [R_i, R_s] \qquad \textbf{6-64}$$

Lastly, we can obtain the Reiner-Riwlin equation using the no-slip condition at the boundary between solid and viscoplastic state, and the Dirichlet boundary conditions cited in section 6.3.3: $v_\theta(R_i) = 0$ and $v_\theta(R_s) = R_s\omega_0$. Now we will divide eq. 6-63 by *r*, obtaining the following:

$$\frac{1}{r}\frac{dv_\theta(r)}{dr} - \frac{v_\theta(r)}{r^2} + \frac{\tau_0}{\mu r} = \frac{\hat{T}}{2\pi\mu r^3 h} \qquad \textbf{6-65}$$

which is:

$$\frac{d(v_\theta/r)}{dr} = \frac{\hat{T}}{2\pi\mu r^3 h} - \frac{\tau_0}{\mu r} \qquad \textbf{6-66}$$

Now we can integrate eq. 6-66, obtaining:

$$\frac{v_\theta}{r} = -\frac{\hat{T}}{4\pi\mu r^2 h} - \frac{\tau_0}{\mu} ln(r) + C \qquad \textbf{6-67}$$

where *C* is the integration constant. Using the boundary condition to obtain C, it is possible to write:

$$v_\theta(r) = \frac{\hat{T}r}{4\pi\mu h}\left(\frac{1}{R_i^2} - \frac{1}{r^2}\right) - \frac{\tau_0 r}{\mu}\ln\left(\frac{r}{R_i}\right) \qquad \forall r \in [R_i, R_s] \qquad \textbf{6-68}$$

Then with the other Boundary condition, and solving for the torque:

$$\hat{T} = \frac{4\pi\mu h}{{}^1\!/_{R_i^2} - {}^1\!/_{R_p^2}}\omega_0 + \frac{4\pi\tau_0 h}{{}^1\!/_{R_i^2} - {}^1\!/_{R_p^2}}\ln\left(\frac{R_s}{R_i}\right) \qquad \textbf{6-69}$$

If plug does not occur, R_s can be substituted with R_o (a constant value), and eq. 6-69 can be re-arranged into the following:

$$\hat{T} = \frac{4\pi\mu h}{{}^1\!/_{R_i^2} - {}^1\!/_{R_o^2}}\omega_0 + \frac{4\pi\tau_0 h}{{}^1\!/_{R_i^2} - {}^1\!/_{R_o^2}}\ln\left(\frac{R_o}{R_i}\right) = H\omega_0 + G \qquad \textbf{6-70}$$

Plotting the measured torque $\hat{T}$ as a function of the angular velocity ω_0, it is possible to obtain the values of *H* and *G* of eq. 6-70, which now can be related to the plastic viscosity and the yield stress through the following formulas, obtained from eq. 6-70:

$$\mu = \frac{H\left({}^1\!/_{R_i^2} - {}^1\!/_{R_o^2}\right)}{4\pi h} \qquad \textbf{6-71}$$

$$\tau_0 = \frac{G\left({}^1\!/_{R_i^2} - {}^1\!/_{R_0^2}\right)}{4\pi h ln\left(\frac{R_o}{R_i}\right)} \qquad \textbf{6-72}$$

Lastly, if we combine eq. 6-64 with eq. 6-69, the shear rate equation can be derived:

$$\dot{\gamma} = \frac{2}{r^2}\left(\frac{1}{R_i^2} - \frac{1}{R_p^2}\right)^{-1}\left[\omega_0 + \frac{\tau_0}{\mu}\ln\left(\frac{R_s}{R_i}\right)\right] - \frac{\tau_0}{\mu} \qquad \forall r \in [R_i, R_s] \qquad \textbf{6-73}$$

from which the shear rate gradient (useful in the analysis of gravel migration problems) can be calculated:

$$\frac{d\dot{\gamma}}{dr} = -\frac{4}{r^3}\left(\frac{1}{R_i^2} - \frac{1}{R_p^2}\right)^{-1}\left[\omega_0 + \frac{\tau_0}{\mu}\ln\left(\frac{R_s}{R_i}\right)\right] \qquad \forall r \in [R_i, R_s] \qquad \textbf{6-74}$$

References

[6.1] Marinkovic´ S., Radonjanin V., Malešev M., Ignjatovic´ I. Comparative environmental assessment of natural and recycled aggregate concrete. Waste Management 2010; 30: 2255–2264.

[6.2] Lima C., Caggiano A., Faella C., Martinelli E., Pepe M., Realfonzo R. Physical properties and mechanical behaviour of concrete made with recycled aggregates and fly ash. Construction and Building Materials 2013; 47: 547–559.

[6.3] Xiao J., Li W., Fan Y., Huang X. An overview of study on recycled aggregate concrete in China (1996–2011). Construction and Building Materials 2012; 31: 364-383.

[6.4] Vázquez E. Progress of Recycling in the Built Environment, Final Report of the RILEM Technical Committee 217-PRE. Springer, 2013.

[6.5] Comisión Permanente Del Hormigón: Instrucción de Hormigón Estructural, EHE-08. Ministerio de Fomento, Madrid, 2011.

[6.6] Italian Ministry of Infrastructure. Technical Standards for Construction, NTC 2008 (in Italian).

[6.7] DAfStb Beton, rezyklierte Gesteinskörnung: 2010-09. DAfStb-Richtlinie Beton nach DIN EN 206-1 und DIN 1045-2 mit rezyklierten Gesteinskörnungen nach DIN EN 12620, Germay, 2010 (in German).

[6.8] European Committee for Standardization. EN 12620 Aggregates for Concrete. Belgium: Brussels; 2013.

[6.9] Koenders E.A.B., Pepe M., Martinelli E. Compressive strength and hydration processes of concrete with recycled aggregates. Cement and Concrete Research 2014; 56: 203-212.

[6.10] Tabsh S.W., Abdelfatah A.S. Influence of recycled concrete aggregates on strength properties of concrete. Construction and Building Materials 2009: 23(2): 1163-1167.

[6.11] Poon C.S., Shui Z.H., Lam L. Effect of microstructure of ITZ on compressive strength of concrete prepared with recycled aggregates. Construction and Building Materials 2004; 18(6): 461-468.

[6.12] Sim J., Park C. Compressive strength and resistance to chloride ion penetration and carbonation of recycled aggregate concrete with varying amount of fly ash and fine recycled aggregate. Waste Management 2011; 31(11): 2352-2360.

[6.13] Vázquez E., Barra M., Aponte D., Jiménez C., Valls S. Improvement of the durability of concrete with recycled aggregates in chloride exposed environment. Construction and Building Materials 2013; 67: 61-67.

[6.14] Otsuki N., Miyazato S.-I., Yodsujai W. Influence of recycled aggregate on interfacial transition zone, strength, chloride penetration and carbonation of concrete. Journals of Materials in Civil Engineering 2003; 15(5): 443-451.

[6.15] Fathifazl G., Abbas A., Razaqpur A.G., Isgor O.B., Fournier B., Foo S. New mixture proportioning method for concrete made with coarse recycled concrete aggregate. Journals of Materials in Civil Engineering 2009: 601–11.

[6.16] Barbudo A., de Brito J., Evangelista L., Bravo M., Agrela F. Influence of water reducing admixtures on the mechanical performance of recycled concrete. Journal of Cleaner Production 2013; 59: 93–98.

[6.17] Ferreira L., de Brito J., Barra M. Influence of the pre-saturation of recycled coarse concrete aggregates on concrete properties. Magazine of Concrete Research 2012; 63(8): 617–627.

[6.18] de Brito J., Saikia N. Recycled Aggregate in Concrete, Green Energy and Technology, Springer-Verlag, London 2013.

[6.19] Pepe M., Toledo Filho R.D., Koenders E.A.B., Martinelli E. Alternative processing procedures for recycled aggregates in structural concrete. Construction and Building Materials 2014; 69: 124:132.

[6.20] Kou S., Poon C.-S., Agrela F. Comparisons of natural and recycled aggregate concretes prepared with the addition of different mineral admixtures. Cement and Concrete Composites 2011; 33–8: 788–795.

[6.21] Schubert S., Hoffmann C., Leemann A., Moser K., Motavalli M. Recycled aggregate concrete: experimental shear resistance of slabs without shear reinforcement. Engineering Structures 2012; 41: 490–497.

[6.22] Kou S., Poon C.-S., Etxeberria M. Influence of recycled aggregates on long term mechanical properties and pore size distribution of concrete. Cement and Concrete Composites 2011; 33(2): 286–291.

[6.23] Abbas A., Fathifazl G., Isgor O.B., Razaqpur A.G., Fournier B., Foo S. Durability of recycled aggregate concrete designed with equivalent mortar volume method. Cement and Concrete Composites 2009; 31: 555–63.

[6.24] Jiménez C., Aponte D., Vázquez E., Barra M., Valls S. Equivalent mortar volume (EMV) method for proportioning recycled aggregate concrete: validation under the Spanish context and its adaptation to Bolomey methodology for concrete proportioning. Materiales de Construcción 2013; 63(311): 341–360.

[6.25] Knaac A.M., Kurama Y.C. Rheological and mechanical behavior of concrete mixtures with recycled concrete aggregates. Structures congress 2012. Chicago (US): American Society of Civil Engineers; 2012. p. 2257–2267.

[6.26] Knaack A.M., Kurama Y.C. Design of normal strength concrete mixtures with recycled concrete aggregates. Structures congress 2011. Las Vegas (US): American Society of Civil Engineers; 2011. p. 3068–3079.

[6.27] Wallevik J,E. Relationship between the Bingham parameters and slump. Cement and Concrete Research 2006; 36(7): 1214–1221.

[6.28] Tattersall G.H., Banfill P.F.G. The rheology of fresh concrete. Great Britain: Pitman Books Limited; 1983.

[6.29] Neville A.M. Chairman's summary, fresh concrete: important properties and their measurement. Proceedings of RILEM Seminar. Great Britain: University of Leeds; 1973.

[6.30] Ferraris C.F., Obla K.H., Hill R. The influence of mineral admixtures on the rheology of cement paste and concrete. Cement and Concrete Research 2001; 31(2): 245–255.

[6.31] Feys D., Verhoeven R., De Schutter G. Fresh self compacting concrete, a shear thickening material. Cement and Concrete Research 2008; 38: 920–929.

[6.32] Mahmoodzadeh F., Chidiac S.E. Rheological models for predicting plastic viscosity and yield stress of fresh concrete. Cement and Concrete Research 2013; 49 :1–9.

[6.33] Ferraris C.F. Measurement of rheological properties of high performance concrete: state of the art report. NISTIR 5869. Gaithersburg, MD, US: National Institute of Standards and Technology; 1996.

[6.34] Hu C., de Larrard F. The rheology of fresh high-performance concrete. Cement and Concrete Research 1996; 26(2): 283–294.

[6.35] Powers T.C., Wiler E.M. A device for studying the workability of concrete. Proc. of the ASTM 41, American Society for Testing and Materials, 1003–1015, Philadelphia, US; 1941.

[6.36] Powers TC. The Properties of Fresh Concrete, John Wiley & Sons, Inc., US; 1968.

[6.37] Wallevik O.H, Gjørv O.E. in: Wierig HJ, editor. 10th Proc. of the Rilem Colloquium: Properties of Fresh Concrete; London: Chapman & Hall; 1990, p. 213–224.

[6.38] Wallevik O.H. The Rheology of Fresh Concrete and its Application on Concrete with and without Silica Fume. The Norwegian Institute of Technology, Dr. Ing. thesis no. 1990:45, Trondheim, Norway; 1990.

[6.39] Wallevik J.E. Minimizing end-effects in the coaxial cylinders viscometer: Viscoplastic flow inside the ConTec BML Viscometer 3. Journal of Non-Newtonian Fluid Mechanics 2008; 155: 116–123.

[6.40] Wallevik J.E. Rheology of Particle Suspensions, Fresh Concrete, Mortar and Cement Paste with Various Types of Lignosulfonates. Department of Structural Engineering, The Norwegian University of Science and Technology, Ph.D. Thesis, Trondheim, Norway; 2003.

[6.41] Ferraris C.F., Brower L.E. Comparison of concrete rheometers: International tests at LCPC (Nantes, France) in October, 2000. NISTIR 6819; 2001.

[6.42] Reiner M. Deformation and Flow; An Elementary Introduction to Theoretical Rheology. H. K. Lewis & Co. Limited, Great Britain; 1949.

[6.43] Heirman G., Vandewalle L., Van Gemerta D., Wallevik O. Integration approach of the Couette inverse problem of powder type self-compacting concrete in a wide-gap concentric cylinder rheometer. Journal of Non-Newtonian Fluid Mechanics 2008; 150: 93-103.

[6.44] Heirman G., Hendrickx R., Vandewalle L., Van Gemert D., Feys D., De Schutter G., Desmet B., Vantomme J. Integration approach of the Couette inverse problem of powder type self-compacting concrete in a wide-gap concentric cylinder rheometer. Part II. Influence of mineral additions and chemical admixtures on the shear thickening flow behaviour. Cement and Concrete Research 2009; 39: 171-181.

[6.45] Feys D., Wallevik J.E., Yahia A., Khayat K.H., Wallevik O.H. Extension of the Reiner–Riwlin equation to determine modified Bingham parameters measured in coaxial cylinders rheometers, Materials and Structures 2013; 46: 289–311.

[6.46] Leighton D., Acrivos A. The shear-induced migration of particles in concentrated suspensions, Journal of Fluid Mechanics 1987; 181: 415-439.

[6.47] Lecompte T., Perrot A., Picandet V., Bellegou H., Amziane S. Cement-based mixes: Shearing properties and pore pressure. Cement and Concrete Research 2012; 42-1: 139-147.

[6.48] Comisión Permanente Del Hormigón: Instrucción de Hormigón Estructural, EHE-08. Ministerio de Fomento, Madrid.

[6.49] EN 206-1, Concrete – Part 1: Specification, Performance, Production and Conformity. Comité Européend de Normalisation, Brussels, Belgium; 2006.

[6.50] Wallevik O.H., Wallevik J.E. Rheology as a tool in concrete science: The use of rheographs and workability boxes. Cement and Concrete Research 2011; 41: 1279-1288.

[6.51] Tanigawa Y., Mori H. Analytical study on deformation of fresh concrete. Journal of Engineering Mechanics 1989; 115 (3): 493–508.

[6.52] Murata J., Kukawa H. Viscosity equation for fresh concrete, ACI Materials Journal 1992; 89 (3): 230–237.

[6.53] de Larrard F. Concrete Mixture Proportioning, A Scientific Approach 1999; F & FN Spon, New York.

[6.54] Ferraris C.F., de Larrard F. Testing and Modelling of Fresh Concrete, NISTIR 6094. Gaithersburg, MD, US: National Institute of Standards and Technology; 1998.

[6.55] Vázquez E. Dataset of rheological parameters: aerated recycled concrete. Personal communication; 2013.

[6.56] Krieger I.M., Dougherty T.J. A mechanism for Non-Newtonian flow in suspensions of rigid spheres. Transaction of the society of rheology 1959; III: 137-152.

[6.57] Barnes H.A., Hutton J.F., Walters K. An introduction to rheology. Elsevier Science B. V. 1989; Netherlands.

7 Sustainability of recycled concrete

7.1 Abstract

In this section the main available environmental tools were used to assess the environmental impacts of recycled concrete aggregates (RCA) when used in recycled concrete, i.e. through life cycle assessment (LCA) and the abiotic depletion indicator (DP_i). Special attention was paid to the influence of transportation scenarios and technological solutions used in the extraction and recycling plants. The procedure developed in this work can be applied to determine an integrated model for a sustainable production of aggregates, which couple both the extraction of virgin raw material and the recycling of construction and demolition waste.

7.2 Introduction

In the recent years a number of strategies have been introduced to allow the concrete industry to reduce its high environmental burdens. One of the main result is the growth of several types of recycled concrete, including recycled components which aim to replace, at least partially, the main constituents of concrete, i.e. cement [7.1, 7.2] and virgin aggregates [7.3, 7.4]. This will lead to improve the sustainability of this fundamental sector of the global economy. But what do we mean with sustainability? According to the Word Commission of Environment and Development of the United Nations, *sustainability* can be defined by “meeting the needs of the present without compromising the ability of the future generations to meet their own needs” [7.5]. This concept is often associated with the aim to do not increase, and even reduce, the emissions in atmosphere of the well-known greenhouse gases (GHGs), and in particular of CO_2. But one of the further aspects necessary to promote sustainability in concrete industry is related to the consumption of raw materials, and in particular of limestone, which availability is limited, especially in some geographical regions [7.6, 7.7]. In addition, when a new green concrete is developed, often its sustainability is addressed, but few proofs of the real embodied energy of the product are described. This rarely happens also for the evaluation of the environmental impacts associated to the production of the material, for a properly defined functional unit, according to the LCA protocols [7.8, 7.9]. Some examples of the exact definition of the sustainability of recycled concretes or of some of their components are shown in [7.10, 7.11, 7.12]. Accordingly, concretes designed for

sustainability should not only use recycled materials, but also have low energy costs, high durability, and display at least equivalent mechanical properties then their reference. A recent work developed by Marinkovic et al. [7.13] showed that often mechanical and durability-related properties of recycled aggregate concrete (RAC) with coarse recycled aggregates are lower than the properties of the reference natural aggregate concrete (NAC), due to the generally recognized worse properties of RCA. This determines a limitation on the utilization of RCA in structural concrete at high replacement ratio. Hence, to obtain the same strength class, which is necessary for a proper comparison of a reference functional unit of the products, an increase in cement content was necessary for RAC mixtures, resulting in that RAC was not sustainable as expected. In fact, $1m^3$ was responsible of about +11% of CO_2 with respect to the reference NAC, and about + 22% of energy used for its production. However, for non-structural applications, or when alternative aggregates proportioning methods are used [7.14, 7.15, 7.16], RCA use becomes competitive both from an economical and environmental point of view, as no further cement additions are required.

In this context, the proper evaluation of the emissions due to the production of the aggregates to be used in the concrete industry represents a fundamental starting point to show the effective sustainability of a building material, whether the materials are made of NA or RCA. Therefore in this section some tools are used to assess the environmental impacts due to the production of both NA and RCA, through Life Cycle Assessment (LCA), and using the Abiotic Depletion Indicator (DP_i). Those indicators are able to demonstrate quantitatively the impacts over the environment due to the production of the above materials, i.e. in terms of CO_2 emissions, or consumption of non-renewable resources. The results obtained by this analysis will be used for the proposal of a sustainable model of aggregates production, applied to the Veneto region in Italy. The model includes both the extraction of virgin materials and the recycling of construction and demolition waste (C&DW), taking into account the effective market demand of those products.

7.3 Sustainability indicators

The word “Indicator” identifies the instrument which allows the policy makers to take better decisions and more effective actions, by means of simplifying, clarifying and making aggregate the available information. They also can help in incorporating physical and social science knowledge into decision-making, and they can help measure and calibrate progress toward sustainable development goals. Accordingly, they have been introduced by the United Nations Conference on Environment and

Development in 1992 to help Countries to make informed decisions concerning sustainable development [7.17]. Chapter 40 of Agenda 21 [7.18], which is the action plan adopted in 1992 at the United Nations Conference on Environment and Development in Rio de Janeiro, has in fact called on countries, as well as international, governmental and non-governmental organizations, to develop indicators of sustainable development that can provide a solid basis for decision-making at all levels. The first draft results in a set of 134 indicators, divided into various themes, which was later modified several times, until arriving to the newly revised Commission on Sustainable Development (CSD) indicators. They are divided in a core of 50 indicators, plus other 46, which enable countries to do a more comprehensive and differentiated assessment of sustainable development. Between these, just a limited number refer to environmental sustainability, whereas also a great number concerns to social, economical and institutional themes. Between the environmental indicators, some of the core ones are herein reported:

- carbon dioxide emissions: this indicator measures the emissions of carbon dioxide, which is known to be the most important, in terms of impact on global warming, anthropogenic greenhouse gas (GHG);
- consume of ozone depleting substances: this indicator depicts the progress towards the phase out of ozone depleting substances (ODSs) by the countries which have ratified the Montreal Protocol on Substances that Deplete the Ozone Layer and its Amendments;
- ambient concentration of air pollutants in urban areas: this indicator provides a measure of the state of the environment in terms of air quality, in terms of particulate matter (PM_{10}, PM_{25}) and is an indirect measure of population exposure to air pollution of health concern in urban areas;
- arable and permanent crop land: this indicator shows the amount of land available for agricultural production and, inter alia, the cropland area available for food production;
- proportion of total water resources used: it shows the degree to which total renewable water resources are being exploited to meet the country's water demands and represents thus a measure of water scarcity.

Between the non-core indicators, some relevant ones are herein listed:

- emission of greenhouse gases: this indicator measures the main six greenhouse gases (GHGs) emissions, carbon dioxide (CO_2), methane (CH_4), nitrous oxide (N_2O), hydrofluorocarbons (HFCs), perfluorocarbons (PFCs), sulphur hexafluoride (SF_6). Emissions are then converted into equivalent CO_2 through the so-called global warming potentials (GWPs)

provided in assessments of the Intergovernmental Panel on Climate Change (IPCC);

• land degradation: this indicator measures the extent of land degradation, which is an impediment to sustainable development in general, and to sustainable agriculture in particular. The degradation refers to soil erosion, deterioration of the physical, chemical and biological or economic properties of soil and/or long-term loss of natural vegetation;

• fertilizer use efficiency: this indicator shows the potential environmental pressure from inappropriate fertilizer application. Data on the quantities of fertilizers used are converted into the three basic nutrient components (nitrogen N, phosphorous P_2O_5 and potassium K_2O) and aggregated.

Hence, if we want to determine how an activity or a production process participates into the sustainable development of a country, from the environmental point of view, at least some of these indicators should be evaluated. One common way to assess sustainability is given by the use of Life Cycle Analysis, which is a systems-based approach for quantifying the human health and environmental impacts associated with a product's life from “cradle to grave.” A well-established set of methods is already applied into LCA tools, which enable a direct comparison of alternatives associated with the analyzed product or technology. Despite being a mature tool with well-established data, including extensive data quality procedures, some limitations occurs: LCA usually models “average” systems, and may not capture the impacts of policies that cause indirect changes or significant (non-marginal) changes in the market. In addition, gaps in the availability of inventory data may represent a barrier to LCA practice.

Near to LCA, also other alternatives are available, such as environmental footprint analysis (EFA), cumulative energy demand (CED) or some indexes referring to a particular environmental problem, such as the abiotic depletion indicator (DP_i). EFA is an accounting tool which measures human demand on ecosystem services required to support a certain level and type of consumption by an individual, product, or population. CED is a screening impact indicator to provide information on potential product environmental impacts and estimation of energy resource depletion by capturing direct and indirect energy use/demand during the complete life cycle. Lastly, DP_i is an indicator which assesses the depletion of non-renewable abiotic natural resources.

In this work, two tools were applied to assess some of the environment sustainability indicators: LCA and DP_i. They were applied first to determine the environmental impacts associated to the production of natural and recycled aggregates, and then to assess how to reduce their impacts by

means of technical solution in the production process and transportation into the market.

7.3.1 Life Cycle Assessment

As seen in Section 5, Life-Cycle Assessment is a systems-based approach which allow the quantification of the impacts (both on human health and environment) associated with a product's entire life, generally from “cradle to grave.” Hence, a full LCA addresses all stages of the product life-cycle, and it should take into account alternative uses as well as associated waste streams, raw material extraction, material transport and processing, product manufacturing, distribution and use, repair and maintenance, and wastes or emissions associated with a product, process, or service as well as end-of-life disposal, reuse, or recycling. LCA considers multiple environmental indicators, i.e. emission of greenhouse gases, consume of ozone depleting substances and water quality. According to the ISO standards [7.8, 7.9], it consists of four phases:

- Step 1—definition of the assessment goal and scope. The definition of the LCA goals should be chosen according to the specific product or process, and scope includes definition of “system boundaries” for the analysis, such as whether an analysis considers end-of-life management for a product or if transportation scenarios should be included or not in the analysis. Goal and scope in a sustainability context should be defined through stakeholder engagement and collaboration and identify which products and technologies are to be evaluated;
- Step 2—compilation of the life-cycle inventory (LCI). The inventory is a detailed account of all inputs, outputs and emissions that occur at each stage of the life-cycle scenario;
- Step 3—life-cycle impact assessment of the product/technology/process using the LCI data and one or more assessment methods that translate emissions into one or more impact categories, such as global warming potential (based on GHG emissions), water quality impacts, human health impacts, or many others;
- Step 4—interpretation of the results. This discussion should transparently communicate the limitations and uncertainties associated with the LCA results, including uncertainties associated with data limitations, and with analytical (scenario and scope) assumptions. For further information about LCA, look at section 5.

7.3.2 Abiotic Depletion Indicator

The depletion of natural resources is one of the main category indicator of life cycle analysis. Although, the available methods generally focus on the depletion of biotic resources and, when referring to abiotic ones, they deal with minerals and energy resources, such as coal or oil. Resources can be divided into biotic resources such as biodiversity, sylvicultural products (wood, fish, etc.) and abiotic resources (that gathers all non biotic resources). Within abiotic resources, three categories can be defined: mineral resources, like metals; bulk materials, such as sand, gravel or lime; and energy resources, such as fossil fuels. Bulk materials are often excluded by the main Impact Assessment methods, i.e. CML [7.26], Ecopoint 97 [7.27], EcoIndicator 99 [7.28], Impact 2002+ [7.29], because the natural resources for those materials are considered infinitely available.

However, recent studies [7.6,7.7] have highlighted how this statement is incorrect, especially al local scale. Hence, an abiotic indicator for natural bulk resources was introduced in [7.6]:

$$DP_i = \frac{DMC-PR}{(R+PR)^2} \times \frac{(R_{Sb})^2}{DR_{Sb}} \quad \textbf{7-1}$$

where:

DMC is the Domestic Material Consumption in [ton/y];
PR refers to the Recycling in [ton/y];
I refers to the Imports [ton/y];
RS_b is the antimony reserve in [ton];
DRS_b is the extraction rate of antimony in [ton/y];
R refers to the potential reserve in [ton] and it is calculated as.

$$R = \int_{t_0}^{t_{exhaust}} DMC(t) \cdot (1 - \frac{I}{DMC}(t))\, dt \quad \textbf{7-2}$$

The exhaustion time of the resource is then evaluated according to the extraction rate and trend in time. If a constant rate is assumed, exhaustion time is rapidly obtained by eq. 7-3 and it expressed in years:

$$t_{ex} = \frac{R}{DMC-PR-I} \quad \textbf{7-3}$$

7.4 Aggregates production

The production processes of natural and recycled aggregates are analyzed to properly estimate the emissions produced from their manufacture until their conversion into a readily applied market-product. A great number of plants for the extraction and processing of virgin aggregates is present in North-Italy, especially in the Veneto region (Fig. 7-1). Fig. 7-2 shows the geographical distribution of the active quarries of sand and gravel in the region, which is mainly concentrated in the districts of Treviso (about 68%), Verona (about 20%) and Vicenza (about 12%). Overall, the extraction of virgin aggregates in Veneto accounts for about 6,000,000 m^3/y, which corresponds to about 10,000,000 ton/y [7.30].

Figure 7-1. Veneto region location in Italy.

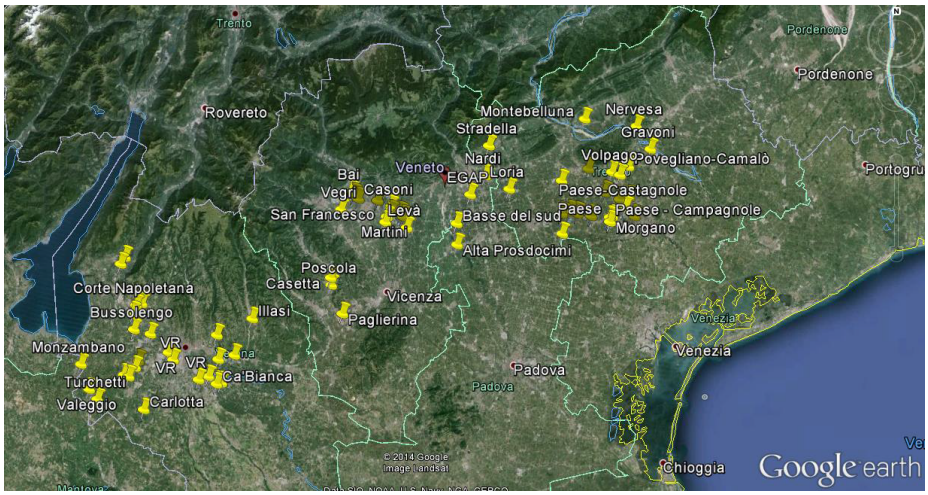

Figure 7-2. Quarries geographical distribution in Veneto, Italy.

The extraction of virgin aggregates in the last 20 years has been subjected to a decreasing trend, which is mainly influenced by the

economical crisis. The use of recycled aggregates in the market is not enough mature in the Italian market to have a significant influence in this trend, according to a recent survey made by ATECAP, the Italian Association for the Precast Concrete, but it could be in the next years. According to ATECAP [7.31], just the 9% of the C&DWs is actually reutilized and valorized into construction market, mainly due to the lack of production plants and the uncertainty about the technical characteristics of the recycled aggregates, which lead to a general mistrust around their applicability.

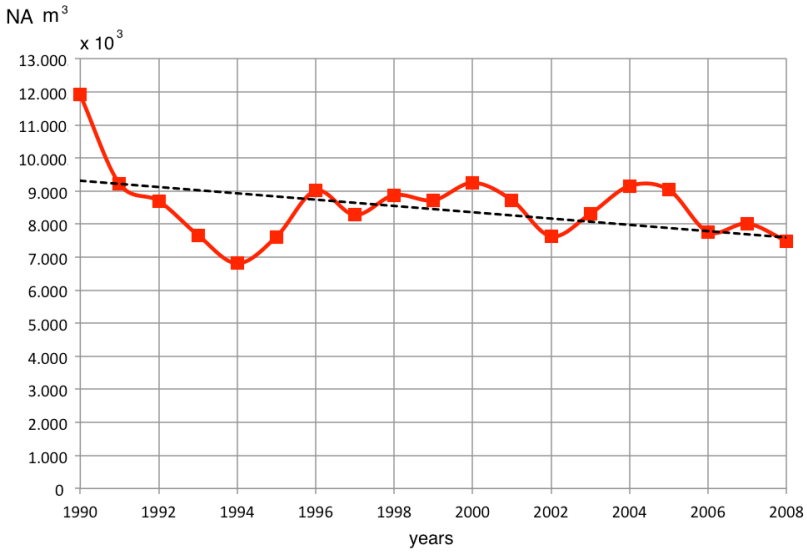

Figure 7-3. Extraction quantities from 1990 until 2008, Veneto, Italy.

According to the Regional Plan about the Extraction Activity [7.30], the active concessions allow the extraction of 106.431.675 m^3 in 2008 (R_{2008}), which is the last available datum to assess the reserve of natural aggregates. With the hypothesis of a constant extraction between the 2008 and 2014 (extraction rate E_R = 7.000.000 m^3), and knowing that no further concessions were given from 2008, the actual reserves of natural aggregates (R_{2014}) are estimated into:

$$R_{2014} = R_{2008} - E_R \cdot \Delta t = 64.431.675\ m^3 \qquad \textbf{7-4}$$

Of course, the effective resources' reserve are greater than this number; however, the actual legislation policy aims to preserve aggregate reserve, and new long-term concession are not easily allowed. Hence, the result obtained with eq. 7-4 is assumed as the basis for the DP_i indicator evaluation.

In this thesis, an existing combined plant for virgin aggregates extraction and for inert waste treatment was analyzed. The plant is located

in Rosà (VI), and it occupies a surface of about 10 hectares, as illustrated in Fig. 7-4.

Figure 7-4. EGAP plant, Rosà (VI), Italy.

This plant produces mainly natural aggregates, which constitutes the 90% of its products, and a remaining 10% of recycled aggregates coming from C&DWs recycling. The mean production, evaluated on the last 4 years, is about 56.361 ton/y of NA, and 5.993 ton/y of RA. The facilities are furnished by a photovoltaic plant (PV) for the production of the electric energy, which produces in average 878 kW/d. In addition, an area is destined to landfilling operations of inert materials, which cannot be recovered after the C&DW recycling.

For the operations related to the extraction of NA and recycling of C&DWs, the following equipment is used:

- washing plant;
- crushing machinery;
- primary crusher;
- 2 mechanical shovels;
- 1 excavator with a gripper for volume reduction;

- 2 trucks.

The extraction of NA facility can be described by the block-diagram of Fig. 7-5. The actual available resources of EGAP in terms of natural aggregates are 404.839 m^3 (R_{2014}), according to the concession given by the Region.

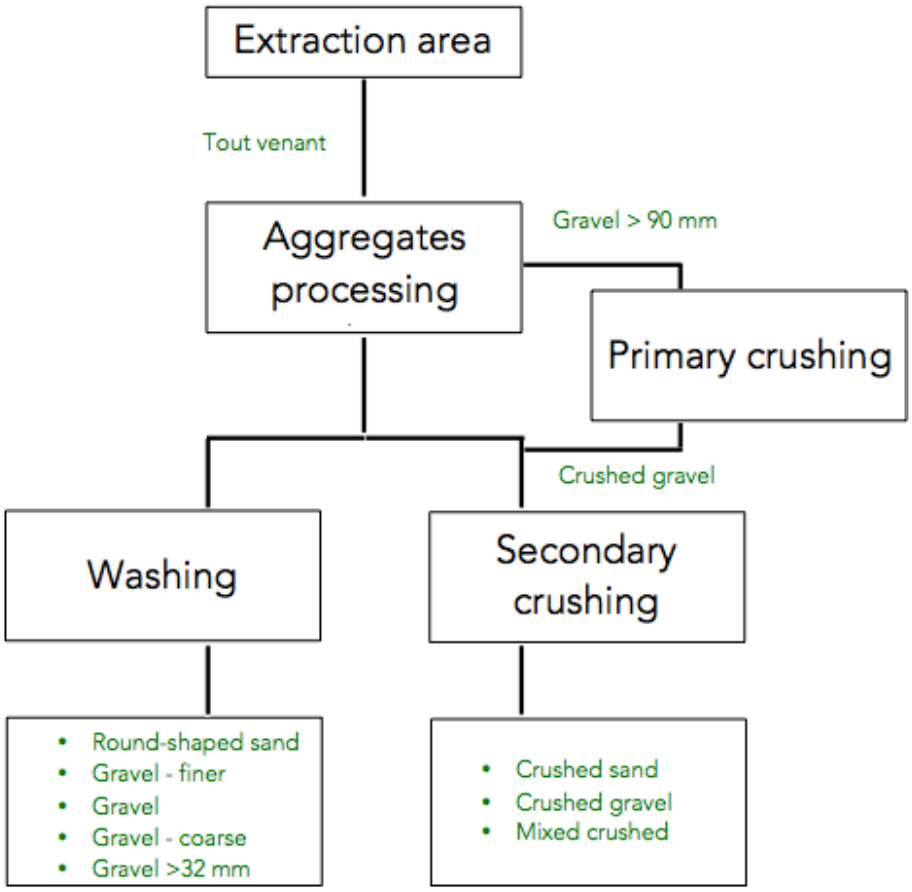

Figure 7-5. Block diagram of the production of NA at EGAP.

The RA production plant of the EGAP is authorized by the Region to treat about 18.000 ton/y of C&DW, and actually it operates at about 1/3 of its operative capacity, although the trend of its using is increasing. Its productive process is illustrated in Fig. 7-6.

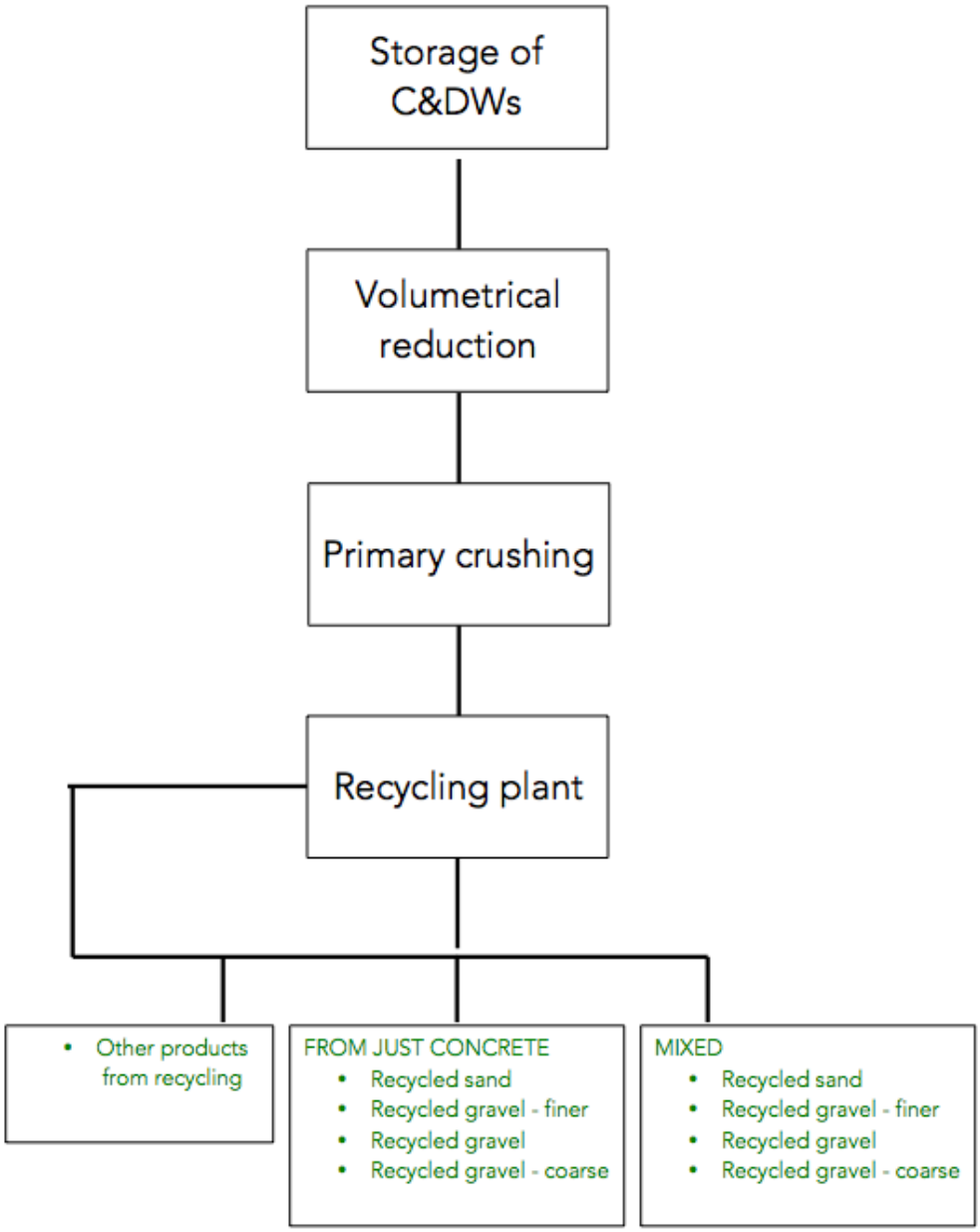

Figure 7-6. Block diagram of the production of RA at EGAP.

7.5 LCA of NA and RA

7.5.1 The "0-km" scenarios

Two scenarios are considered, one for the production of the product "natural aggregate" and the second, for the production of the "recycled aggregate". The production systems are considered from the extraction and processing of raw materials (“cradle”) through to the actual production and assembly of the product (“gate”) at the company that places it in the market, taking into account all the production and transport fluxes inside the system. The two facilities have different a productivity, which should be taken into account in the results. The chosen functional unit FU is *1ton* of aggregate. This system is defined as "0-km" scenario, i.e. it aims to comparatively assess the environmental impacts related to the production of natural aggregates and recycled aggregates (*goal*).

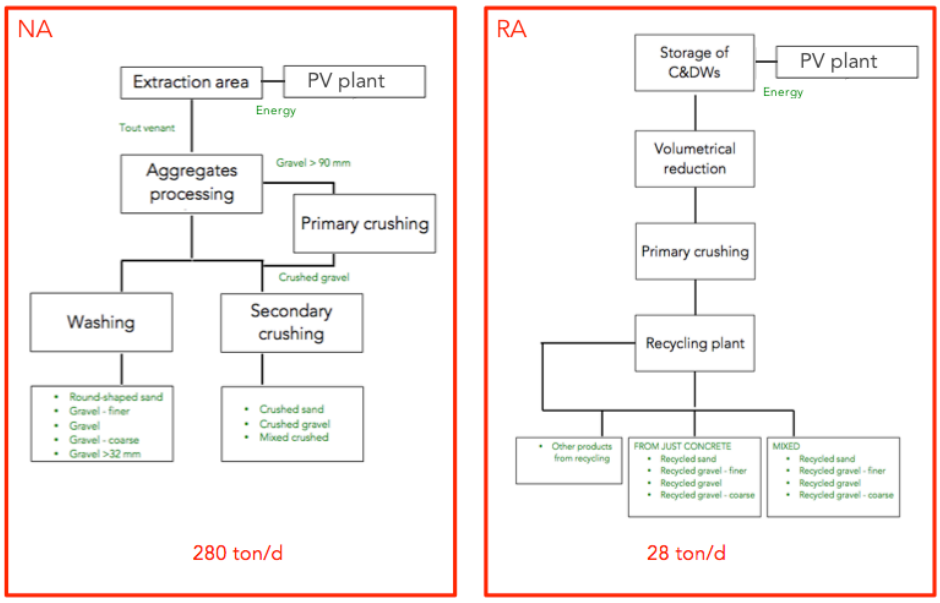

Figure 7-7. System boundaries for the NA and RA plants, at "0-km" scenarios.

Once established the system boundaries and the goal of the study, the data inventory was performed. The analysis of inventory includes the compilation and quantification of relevant input and output elements of a product during its life cycle. It develops in three phases: data collection, calculation procedure allowing to quantify the I/O elements of a relevant product system, and their allocation. Significance is determined by threshold for mass (more than 1% of inputs), energy and environmental significance (potential for harm) [7.32]. The collected data can be classified into broad categories including:

• energy inputs, raw material inputs, ancillary inputs, other physical inputs;
• products, co-products and waste;
• emissions to air, discharges to water and soil;
• other environmental aspects.

All collected data must include the details of their collection, which are constituted by the period in which the data were collected and all the information on data quality indicators. The data used should be validated, correlated with each unit process and to the functional unit and lastly refined on the basis of a sensitivity analysis. Also the allocation procedures are important to take into account multiple products and recycling systems: all input and output are allocated according to the different products. In this work the allocation procedure for the environmental loads is based on physical/chemical causation per unit mass of aggregate produced. It should be remembered that the capital required for the system installation and in general the costs incurred are not part of the parameters considered in the model (mass allocation procedure).

The data are collected for the two systems shown in Fig. 7-7, quantifying the amount of I/O material, energy and diesel consumption. Diesel fuel consumption of the last seven years and electricity consumption of the last four years and were used. Concerning the former, they could be estimated into 180 l/d, for all the activities inside the facility. Of these, about 90% are due to the NA processing, and the remaining to RA. Concerning the latter, the electricity consumption is calculated as:

$$E_{consumption} = (E_{PV} - E_N) + E_U \quad \textbf{7-5}$$

where E_{PV} is the energy produced by the PV plant, E_N is the energy which is supplied into the network, and E_U is the energy uptake from the network. Results are reported in Table 7-1.

Table 7-1. Electricity consumption.

	2011 (kW/y)	2012 (kW/y)	2013 (kW/y)	2014 (kW/y)	average (kW/y)	average (kW/d)
E_{PV}		133.049	253.190	293.548	193.120	878
E_N		93.662	191.262	218.414	142.462	648
E_{PV} - E_N		39.387	61.928	75.134	50.657	230
E_U	205.390	173.200	96.035	95.446	96.035	437
$E_{consumption}$	205.390	212.587	157.963	170.579	**191.980**	**873**

The emissions due to the consumption of the energy produced in the PV plant are not considered in this thesis, because their contribute is negligible with respect to the one of aggregates processing [7.33].

A diary of the consumption for each phase of the production process was created and compiled by the operators of the quarry in September 2014, to separate the consumption of the NA and RA facilities. From this, it was possible to obtain the following results: 2.96 kWh/ton of NA, and 0.97kWh/ton of RA.

When the inventory data was concluded, the emissions were evaluated, dividing them into direct and indirect: in particular, the latter refer to dust (PM_{10} release in atmosphere) and combustion gases due to energetic consumption (TSP, PM_{10}, CO, benzene, 1,3-butadiene, CO_2 and NO_x).

Air emissions related to each industrial process accounting in the system are calculated according to [7.34, 7.35, 7.36]. The main relations used for the evaluation of air pollutant emissions are listed below.

The general formula for the estimation of the air pollutant emissions according to [7-5], is:

$$E = A \cdot EF \cdot (1 - ER/100) \quad \textbf{7-6}$$

where *E* represents the emission, *A* is the activity rate expressed i.e. as [*ton material/y*], *EF* is the emission factor expressed as [*kg/ton material*] and *ER* is the overall emission reduction, expressed in [*%*]. The emission reduction mainly depends by the used devices' efficiencies and the control methods applied to limit the releases, such as the use of water sprays to limit dust releases. Emissions factors are evaluated according to [7.34, 7.35] respectively for direct and indirect releases; specific default *EF* values were used for some of the process operations, such as grinding, drying and crushing, according to [7.36]. Other releases were collected in situ after chemical analyses on water (I/O from inner wastewater plant) and leaching tests conducted on recycled aggregates (I/O aggregate treatment plant). The data were obtained from the ordinary chemical analyses done by the company in the last two years.

Direct emissions

The following formulas can be used to estimate the particulate matters emissions.

PM_{10} EF Excavators/Shovels/Front-end loaders [*kg/ton*]:

$$PM_{10} = 0.35 \cdot 0.0016 \cdot (v_w/2.2)^{1.3} \cdot (w/2)^{-1.4} \quad \textbf{7-7}$$

where v_w is the mean wind velocity expressed in [*m/s*] and *w* is the mean moisture content expressed in [*%*].

PM_{10} EF for dust generation due to transport on unpaved roads [*kg/ton*]:

$$PM_{10} = 0.733 \cdot (s/12)^{0.8} \cdot [(g_v/3)^{0.4}]/[(w/0.2)^{0.3}] \quad \textbf{7-8}$$

where *s* is the mean silt content expressed in [*%*], g_v is the vehicle gross mass expressed in [*ton*].

Indirect emissions

The general formula to estimate vehicle emissions factors as NO_x, PM_{10}, CO, HC (VOCs, including methane), benzene, 1,3-butadiene and CO_2, expressed as [*g/km*] is the following:

$$EF = (a + b \cdot v + c \cdot v^2 + d \cdot v^e + f \cdot ln(v) + g \cdot v^3 + h/v + i/v^2 + j/v^3) \cdot x \quad \textbf{7-9}$$

where *a*, *b*, *c*, *d*, *e*, *f*, *g*, *h*, *i* and *j* are NAEI vehicle emission factors coefficients, depending on the vehicle typology, on the used fuel and on the substance considered. The emission [*kg/d*] is then calculated as:

$$E = EF \cdot 10^{-3} \cdot f/100 \cdot n_h \cdot n_s \cdot n_v \quad \textbf{7-10}$$

where *f* is the use frequency expressed as [*%*], n_h is the number of hours per shift, n_s is the number of shift per day and n_v is the number of the vehicles of the same type used in each process phase. Indirect emission due to electricity consumption and to diesel consumption refers to default emission factors, and they are reported to the daily releases through the specific daily consumption of each device considered within system boundaries.

Water releases

Emissions acting on water and industrial soil compartment are evaluated by means of results from several experimental campaigns, conducted in the last two years by the company. First, chemical analyses on water (I/O from inner wastewater plant) and leaching tests conducted on recycled aggregates defined each analyzed substance emission factor, expressed as EF [mg/l]. Then, the emission, expressed as [kg/ton] is evaluated trough:

$$E = EF \cdot 10^{-6} \cdot W/\rho_w \cdot n_d \qquad \textbf{7-11}$$

where W is the monthly volume of water discharged expressed as [m^3], ρ_w is water density expressed as [kg/m^3] and n_d is the number of days per month of discharging.

7.5.2 The "time-0" scenario

Once defined the "0-km" scenario, a further scenario was analyzed, which aims to evaluate the actual-state of the plant emissions, i.e. the average emissions due to the whole activities inside the plant. Fig. 7-8 shows the system boundaries of this scenario. This analysis uses an average functional unit FU, which is *1ton of aggregate*, and it reflects a mean production of 90% of NA and 10% of RA. Those percentages are defined by the actual production of aggregates of the company. Emissions are evaluated as described in section 7.5.1.

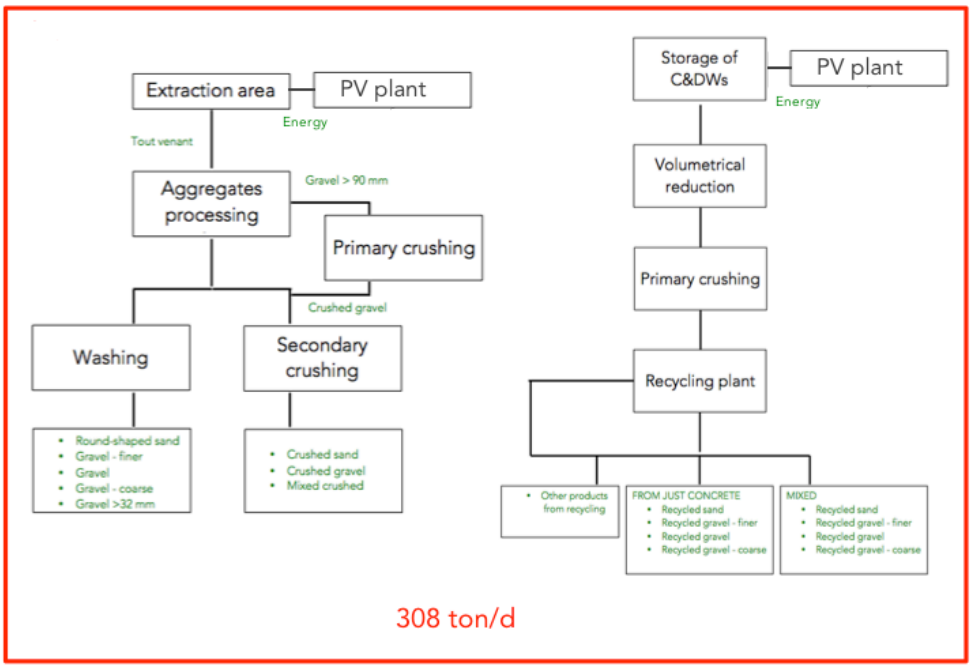

Figure 7-8. System boundaries - "time-0" scenario.

7.5.3 The "no-PV plant" scenario

Once further scenario was analyzed, to evaluate the effects of the PV plant, i.e. the technological solution which allows the plant to partially stand-alone from the energetic point of view. The new scenario, named as "no-PV plant" is used to be compared with the "time-0" scenario. The functional unit FU is *1 ton of aggregate*; also in this case it reflects a mean production of 90% of NA and 10% of RA. Fig. 7-9 shows the system boundaries. Emissions are evaluated as described in section 7.5.1.

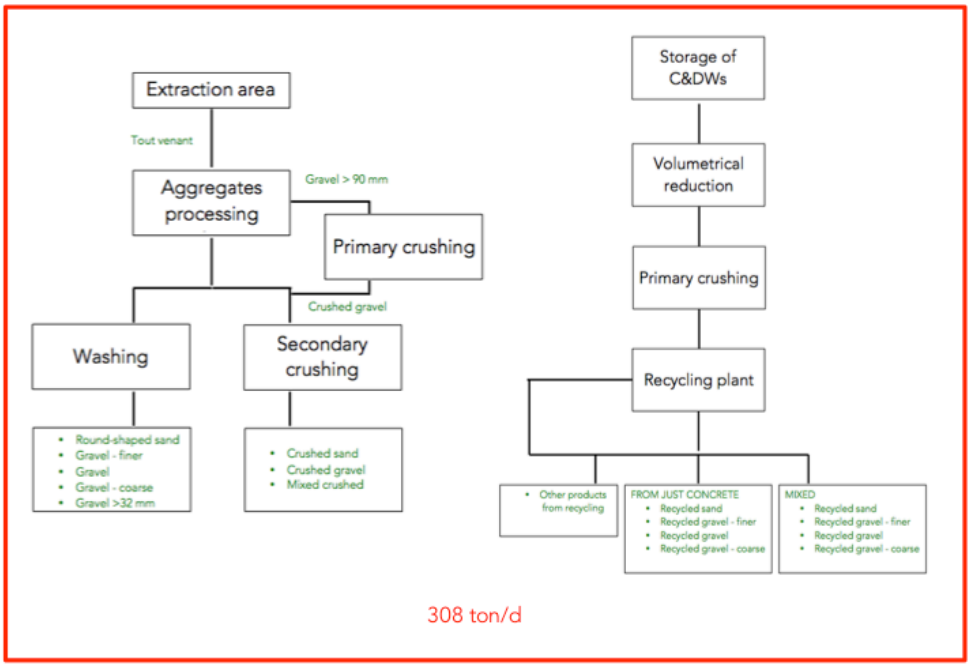

Figure 7-9. System boundaries at "no-PV plant" scenario.

7.5.4 The transportation scenarios

Six more scenarios were analyzed to take into account the effect of the transport of the product from the production site to its placement in the market, i.e. expanding the system boundaries until the effectively placement on the market of the product, namely its arrive at the consumer. Those analyses are made starting from the "time-0" scenario, from which the boundaries are expanded, taking into account the transportation outside the facilities, made by trucks on paved roads, on the increasing distances of: 10, 15, 20, 30, 40 and 50 km. These distances reflect the effective location of the buyers for the analyzed facility. The functional unit FU is *1 ton of aggregate*; also in this case it reflects a mean production of

90% of NA and 10% of RA. Fig. 7-10 shows the system boundaries. Emissions are evaluated as described in section 7.5.1. In addition, transport emission from the facility to the market placement is evaluated according to eq. 7-8 and 7-9.

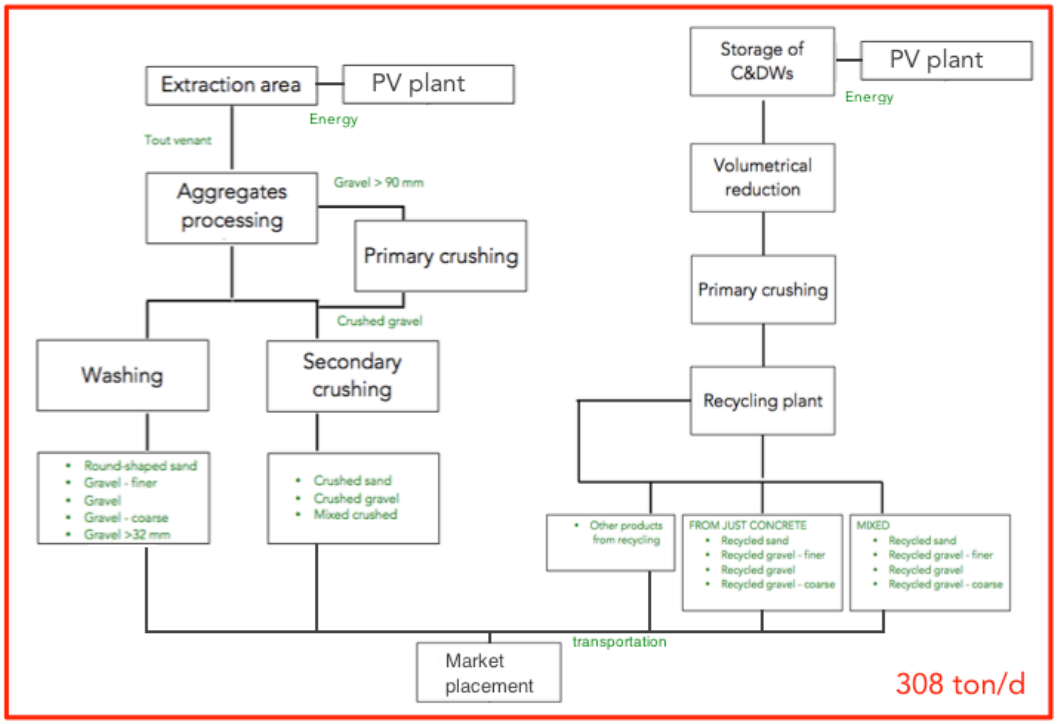

Figure 7-10. System boundaries at "transportation" scenarios.

7.6 LCA results

The results of the LCA are shown in the next tables, for each scenario and functional unit chosen. Table 7-2 and Table 7-3 show the LCA results for the "0-km" scenario, respectively for *FU= 1ton* of NA and *1 ton of RA*. The extraction activity is more complex than the recycling of C&DWs. Furthermore, its productivity is almost 10 times greater than the RA plant, which leads to an increase of the indirect emissions' amount in the NA line. On the contrary, the RA plant is responsible of higher direct emission, because of the high influence of the equipment ignition with respect to the FU. On the contrary, indirect emissions are lower with respect to the NA processing line, because they are due to the use of raw materials, i.e. energy and diesel consumption. Globally, the NA facility is responsible to higher emissions than the RA plant, for the production of 1 ton of material.

Table 7-2. Characterization of environmental emissions related to the selected category – NA aggregates (FU=*1ton*) - "0-km" scenario.

CATEGORY	*DIRECT EMISSIONS*	*INDIRECT EMISSIONS*	*TOTAL EMISSIONS*	*U.M.*
Climate Change	*2.41E-01*	*2.19E+00*	*2.43E+00*	*kg CO_2 eq.*
Eutrophication	*3.21E-04*	*6.22E-04*	*9.43E-04*	*kg PO_4 eq.*
Acidification	*1.23E-03*	*1.22E-02*	*1.34E-02*	*kg SO_2 eq.*
Photo-oxidant formation	*3.16E-05*	*8.17E-04*	*8.48E-04*	*kg ethylene eq.*
Human Toxicity	*2.14E-01*	*1.59E-01*	*1.93E-01*	*kg 1.4-DCB eq*
Eco-toxicity	*6.67E-10*	*1.31E+02*	*1.31E+02*	*kg 1.4-DCB eq*
Ozone layer depletion	*-*	*2.93E-07*	*2.93E-07*	*kg R11 eq.*

Table 7-3. Characterization of environmental emissions related to the selected category – RA aggregates (FU=*1ton*) - "0-km" scenario.

CATEGORY	*DIRECT EMISSIONS*	*INDIRECT EMISSIONS*	*TOTAL EMISSIONS*	*U.M.*
Climate Change	*5.72E-01*	*8.66E-01*	*1.44E+00*	*kg CO_2 eq.*
Eutrophication	*7.62E-04*	*2.70E-04*	*1.03E-03*	*kg PO_4 eq.*
Acidification	*2.93E-03*	*4.94E-03*	*7.87E-03*	*kg SO_2 eq.*
Photo-oxidant formation	*7.55E-05*	*4.06E-04*	*4.81E-04*	*kg ethylene eq.*
Human Toxicity	*6.27E-01*	*6.73E-02*	*1.30E-01*	*kg 1.4-DCB eq*
Eco-toxicity	*1.58E-09*	*6.72E+01*	*6.72E+01*	*kg 1.4-DCB eq*
Ozone layer depletion	*-*	*9.82E-08*	*9.82E-08*	*kg R11 eq.*

The "time-0" scenario shows the amount of the emission for the production of *1 ton of material* at the gate of the whole plant, i.e. it reflects the average production of the facility, about 90% of NA and 10% of RA (Table 7-4). As expected, the environmental indicators lie between the ones for NA and RA in the "0-km" scenario.

Table 7-4. Characterization of environmental emissions related to the selected category – mixed aggregates (FU=*1ton*) - "time-0" scenario.

CATEGORY	DIRECT EMISSIONS	INDIRECT EMISSIONS	TOTAL EMISSIONS	U.M.
Climate Change	2.72E-01	1.24E+00	1.51E+00	kg CO_2 eq.
Eutrophication	3.63E-04	3.68E-04	7.31E-04	kg PO_4 eq.
Acidification	1.40E-03	6.99E-03	8.38E-03	kg SO_2 eq.
Photo-oxidant formation	3.57E-05	5.18E-04	5.54E-04	kg ethylene eq.
Human Toxicity	3.75E-02	9.29E-02	1.30E-01	kg 1.4-DCB eq
Eco-toxicity	7.53E-10	8.44E+01	8.44E+01	kg 1.4-DCB eq
Ozone layer depletion	-	1.54E-07	1.54E-07	kg R11 eq.

Tables 7-5, 7-6 and 7-7 show the emissions assuming the "no-PV plant" scenario. The emission reduction is visible in the indirect emissions, where the source of the electricity can be defined. Hence, the reduction due to PV power use is higher in the RA facility, i.e. where the indirect emissions weight more (higher burden due to equipment ignition). Table 7-8 shows the total emission reduction, expressed in %, due to the PV plant for the "time-0" scenario.

Table 7-5. Characterization of environmental emissions related to the selected category – NA aggregates (FU=*1ton*) - "no-PV plant" scenario.

CATEGORY	DIRECT EMISSIONS	INDIRECT EMISSIONS	TOTAL EMISSIONS	U.M.
Climate Change	2.41E-01	2.48E+00	2.72E+00	kg CO_2 eq.
Eutrophication	3.12E-04	7.01E-04	1.02E-03	kg PO_4 eq.
Acidification	1.23E-03	1.38E-02	1.51E-02	kg SO_2 eq.
Photo-oxidant formation	3.16E-05	9.10E-04	9.42E-04	kg ethylene eq.
Human Toxicity	3.48E-02	1.79E-01	2.14E-01	kg 1.4-DCB eq
Eco-toxicity	6.67 E-10	1.45E+02	1.45E+02	kg 1.4-DCB eq
Ozone layer depletion	-	3.36E-07	3.36E-07	kg R11 eq.

Table 7-6. Characterization of environmental emissions related to the selected category – RA aggregates (FU=*1ton*) - "no-PV plant" scenario.

CATEGORY	DIRECT EMISSIONS	INDIRECT EMISSIONS	TOTAL EMISSIONS	U.M.
Climate Change	5.72E-02	2.16E+01	2.12E+01	kg CO_2 eq.
Eutrophication	7.62E-04	5.81E-03	6.58E-03	kg PO_4 eq.
Acidification	2.93E-03	1.19E-01	1.22E-01	kg SO_2 eq.
Photo-oxidant formation	7.55E-05	6.93E-03	7.01E-03	kg ethylene eq.
Human Toxicity	6.27E-02	1.50E+00	1.57E+00	kg 1.4-DCB eq
Eco-toxicity	1.58E-09	1.08E+03	1.08E+03	kg 1.4-DCB eq
Ozone layer depletion	-	3.13E-06	3.13E-06	kg R11 eq.

Table 7-7. Characterization of environmental emissions related to the selected category – mixed aggregates (FU=*1ton*) - "no-PV plant" scenario.

CATEGORY	DIRECT EMISSIONS	INDIRECT EMISSIONS	TOTAL EMISSIONS	U.M.
Climate Change	2.72E-01	2.26E+00	2.54E+00	kg CO_2 eq.
Eutrophication	3.63E-04	6.43E-04	1.01E-03	kg PO_4 eq.
Acidification	1.40E-03	1.26E-02	1.40E-02	kg SO_2 eq.
Photo-oxidant formation	3.57E-05	8.77E-04	8.77E-04	kg ethylene eq.
Human Toxicity	3.75E-02	2.01E-01	2.01E-01	kg 1.4-DCB eq
Eco-toxicity	7.53E-10	1.34E+02	1.34E+02	kg 1.4-DCB eq
Ozone layer depletion	-	3.04E-07	3.04E-07	kg R11 eq.

Table 7-8. Total emission reduction in (%) related to the selected category – aggregates (FU=*1ton*) - "time-0" scenario.

CATEGORY	1 ton aggr "time-0"
Climate Change	-40.41
Eutrophication	-27.31
Acidification	-40.24
Photo-oxidant formation	-36.85
Human Toxicity	-35.29
Eco-toxicity	-32.14
Ozone layer depletion	-49.37

Table 7-9 shows the transportation scenarios results: the boundaries are expanded until the market placement of the products.

Table 7-9. Characterization of environmental emissions related to the selected category – mixed aggregates (FU=*1ton*) - "transportation" scenario.

CATEGORY	*DIRECT EMISSIONS*	*INDIRECT EMISSIONS*	*TOTAL EMISSIONS*	*U.M.*
		10 km		
Climate Change	*4.89E-01*	*1.25E+00*	*1.75E+00*	*kg CO_2 eq.*
Eutrophication	*6.30E-04*	*3.71E-04*	*1.00E-03*	*kg PO_4 eq.*
Acidification	*2.42E-03*	*7.03E-03*	*9.45E-03*	*kg SO_2 eq.*
Photo-oxidant formation	*5.04E-05*	*5.24E-04*	*5.75E-04*	*kg ethylene eq.*
Human Toxicity	*5.17E-02*	*9.35E-02*	*1.45E-01*	*kg 1.4-DCB eq*
Eco-toxicity	*1.08E-09*	*8.55E+01*	*8.55E+01*	*kg 1.4-DCB eq*
Ozone layer depletion	*-*	*1.54E-07*	*1.54E-07*	*kg R11 eq.*
		15 km		
Climate Change	*5.96E-01*	*1.25E+00*	*1.85E+00*	*kg CO_2 eq.*
Eutrophication	*7.62E-04*	*3.72E-04*	*1.13E-03*	*kg PO_4 eq.*
Acidification	*2.93E-03*	*7.03E-03*	*9.98E-03*	*kg SO_2 eq.*
Photo-oxidant formation	*5.74E-05*	*5.27E-04*	*5.85E-04*	*kg ethylene eq.*
Human Toxicity	*5.86E-02*	*9.39E-02*	*1.52E-01*	*kg 1.4-DCB eq*
Eco-toxicity	*1.24E-09*	*8.60E+01*	*8.60E+01*	*kg 1.4-DCB eq*
Ozone layer depletion	*-*	*1.54E-07*	*1.54E-07*	*kg R11 eq.*
		20 km		
Climate Change	*7.03E-01*	*1.25E+00*	*1.96E+00*	*kg CO_2 eq.*
Eutrophication	*8.94E-04*	*3.74E-04*	*1.27E-03*	*kg PO_4 eq.*
Acidification	*3.44E-03*	*7.07E-03*	*1.05E-02*	*kg SO_2 eq.*
Photo-oxidant formation	*6.45E-05*	*5.30E-04*	*5.95E-04*	*kg ethylene eq.*
Human Toxicity	*6.55E-02*	*9.42E-02*	*1.60E-01*	*kg 1.4-DCB eq*
Eco-toxicity	*1.41E-09*	*8.65E+01*	*8.65E+01*	*kg 1.4-DCB eq*
Ozone layer depletion	*-*	*1.54E-07*	*1.54E-07*	*kg R11 eq.*

CATEGORY	DIRECT EMISSIONS	INDIRECT EMISSIONS	TOTAL EMISSIONS	U.M.
		30 km		
Climate Change	9.17E-01	1.26E+00	2.18E+00	kg CO_2 eq.
Eutrophication	1.16E-03	3.77E-04	1.53E-03	kg PO_4 eq.
Acidification	4.45E-03	7.11E-03	1.16E-02	kg SO_2 eq.
Photo-oxidant formation	7.86E-05	5.36E-04	6.15E-04	kg ethylene eq.
Human Toxicity	7.93E-02	9.48E-02	1.74E-01	kg 1.4-DCB eq
Eco-toxicity	1.73E-09	8.75E+01	8.75E+01	kg 1.4-DCB eq
Ozone layer depletion	-	1.54E-07	1.54E-07	kg R11 eq.
		40 km		
Climate Change	1.13E+00	1.27E+00	2.40E+00	kg CO_2 eq.
Eutrophication	1.42E-03	3.79E-04	1.80E-03	kg PO_4 eq.
Acidification	5.47E-03	7.15E-03	1.26E-02	kg SO_2 eq.
Photo-oxidant formation	9.27E-05	5.42E-04	6.35E-04	kg ethylene eq.
Human Toxicity	9.31E-02	9.55E-02	1.89E-01	kg 1.4-DCB eq
Eco-toxicity	2.05E-09	8.86E+01	8.86E+01	kg 1.4-DCB eq
Ozone layer depletion	-	1.54E-07	1.54E-07	kg R11 eq.
		50 km		
Climate Change	1.35E+00	1.27E+00	2.62E+00	kg CO_2 eq.
Eutrophication	1.68E-03	3.82E-04	2.07E-03	kg PO_4 eq.
Acidification	6.48E-03	7.19E-03	1.37E-02	kg SO_2 eq.
Photo-oxidant formation	1.07E-04	5.48E-04	6.55E-04	kg ethylene eq.
Human Toxicity	1.07E-01	9.62E-02	2.03E-01	kg 1.4-DCB eq
Eco-toxicity	2.37E-09	8.96E+01	8.96E+01	kg 1.4-DCB eq
Ozone layer depletion	-	1.55E-07	1.55E-07	kg R11 eq.

Results indicate an average increase of the emissions along the distance axis, for each selected category. Both the direct and the indirect emissions are influenced by the transportation, because of the increase in fuel consumption and due to the emissions on paved roads produced by trucks transit. It is possible to obtain an average emission production per

km, which in the case of CO_2 is about 882 g CO_2/(km) for a fully loaded truck (Euro II), i.e. about 30 g CO_2/(km · $ton_{aggregate}$).

Looking at Table 7-9, it is possible to observe that the total emissions in terms of CO_2 for the 50-km transportation scenario are the greater, with respect to the other scenarios analyzed, with except for the scenario "no-PV". This means that the introduction of the PV plant allows a saving of more than 50 km in terms of transport, leading to the definition of a "km-contraction" factor.

7.7 ADP

The Abiotic Depletion Indictor has been calculated with reference to the available resources of natural aggregates from the 1st January 2014, estimated with eq. 7-4 (R_{2014}=64.000.000 m^3). With a constant rate of extraction, equal to 6.000.000 m^3/y, the resources will be exhausted in $t_{exhaustion}$=11 years. According to the data collected from the Veneto Region [7.30], the domestic consumption *DMC* can be estimated in: 13.650.000 m^3/y. Furthermore, the rate of importation *I* is equal to 7.650.000 m^3/y. Using eq. 7-2, the potential reserve *R* are estimated into 1.088E0+11 kg of aggregates. Hence the DP_i indicator can be evaluated: 6.93E+11.

The DP_i was then calculated with reference to the analyzed case study of this thesis, with the aim to show the recycling impact on the potential reserve of the quarry, and hence on its service life. The resources available from the 1st January 2014 account for 404.839 m^3 of natural aggregates. Five scenarios were considered to evaluate the influence of the recycling activity on this indicator:

- 100% NA;
- 90% NA; 10%RA;
- 80% NA; 20% RA;
- 75% NA; 25% RA;
- 71% NA; 29% RA.

The upper boundary of 100% NA represents the scenario of no-recycling; the lower boundary represents the authorization limit given by the Region for the recycling facility.

Table 7-10. Abiotic Depletion Indicator results.

	100% NA	
ERate	*36.678 m^3*	*62.353 ton*
t exhaustion	*11 years*	*2025*
DPi	*4.66E-15*	
	90% NA – 10% RA	
ERate	*33.149 m^3*	*56.353 ton*
Recycling	*3.529 m^3*	*6.000 ton*
t exhaustion	*12 years*	*2026*
DPi	*4.21E-15*	
	80% NA – 20% RA	
ERate	*29.502 m^3*	*50.153 ton*
Recycling	*7.050 m^3*	*12.200 ton*
t exhaustion	*14 years*	*2028*
DPi	*3.75E-15*	
	75% NA – 25% RA	
ERate	*27.561 m^3*	*46.853 ton*
Recycling	*9110 m^3*	*15.500 ton*
t exhaustion	*15 years*	*2029*
DPi	*3.50E-15*	
	71% NA – 29% RA	
ERate	*26.090 m^3*	*44.353 ton*
Recycling	*10.580 m^3*	*18.000 ton*
t exhaustion	*16 years*	*2030*
DPi	*3.31E-15*	
R2014	*404.839 m^3*	*6.88E+06 kg*
Rsb	*4.63E+15 kg*	
DRsb	*60600000 kg/y*	

Results show a progressive decrease of the DPi indicator, which indicates an increase of the service life of the quarry with the increase of the recycling activity. The service life moves from 11 to 16 years, just reaching the upper boundary of the regional authorization about the inert waste treatment plant.

7.8 Conclusions

The analyses conducted in this section aimed to estimate quantitatively the effects of the use of recycled aggregates on the sustainability of building materials market. Results are derived for a specific plant of natural aggregates extraction where also an activity of recycling of C&DWs is performed, located in Veneto (Italy).

Different measures of sustainability can be given with reference to the used indicator: in this work the emissions are evaluated according to a life cycle approach. Also a focus about the depletion of abiotic natural resources is given. Results can be summarized in the following:

- a quarry, where an extraction of natural resources activity takes place, is responsible of direct environmental emissions, linked to the facility activity, and to indirect emissions, due to the consumption of non-renewable resources used in the plant;
- most of the indirect resources can be reduced by means of the use of renewable resources, i.e. if the electric energy is furnished by a PV plant;
- almost the same CO_2 emissions are produced in the scenario without the PV plant and the one including a transportation of 50 km, but where the facilities are furnished by renewable resources. This lead to define a “km-contraction” factor due to the introduction of this technological solution;
- the introduction of a C&DWs recycling plant inside the quarry plant allows to reduce the consumption of natural resources. Recycled aggregate have a proper market, where their characteristics comply with the Italian standards;
- the DP_i indicator is able to quantify the influence of recycling in the improvement of the service life of the quarry, leading to a reduction in the extraction rate of natural resources, given a fixed domestic consumption of the product "aggregates".

References

[7.1] Papayianni I. Investigation of the pozzolanicity and hydraulic reactivity of a high-lime fly ash. Magazine of Concrete Research 1987; 39(138): 231-235.

[7.2] Langley W.S., Carette G.S., Malhotra, V.M. Structural concrete incorporating high volumes of ASTM Class F fly ash. ACI Materials Journal, 1989; 86(5): 507-514.

[7.3] Evangelista L., de Brito J. Mechanical behaviour of concrete made with fine recycled concrete aggregates. Cement and Concrete Composites 2007; 29: 397-401.

[7.4] Manso J.M., Polanco J.A., Losañez M., González J.J. Durability of concrete made with EAF slag as aggregate. Cement and Concrete Composites 2006; 28: 528–534.

[7.5] UNFCCC COP9 Report. Delivering the Kyoto baby. Refocus, International Renewable Energy Magazine, 2004: 52-53.

[7.6] Naik T.R. Sustainability of concrete constructions. Practice periodical on structural design and construction, ASCE, 2008; 98-103.

[7.7] Habert G., Bouzidi Y., Chen C. & Jullien A. Development of a depletion indicator for natural resources used in concrete. Resources, Conservation and Recycling 2010; 54: 364-376.

[7.8] Technical Committee ISO/TC 207 – "Environmental management", Environmental management - Life cycle assessment - Requirements and guidelines (ISO 14044:2006); European Committee for Standardization, 2006.

[7.9] Technical Committee ISO/TC 207 – "Environmental management", Environmental management - Life cycle assessment - Principles and framework (ISO 14040:2006); European Committee for Standardization, 2006.

[7.10] Van den Heede P., De Belie N. Environmental impact and life cycle assessment (LCA) of traditional and 'green' concretes: Literature review

and theoretical calculations. Cement and Concrete Composites 2012; 34(4): 431-442.

[7.11] Zabalza Bribián I., Valero Capilla A., Aranda Usón A. Life cycle assessment of building materials: Comparative analysis of energy and environmental impacts and evaluation of the eco-efficiency improvement potential. Building and Environment 2011; 46(5): 1133-1140.

[7.12] Habert G., D'Espinose De Lacaillerie, J.B.; Roussel, N. An environmental evaluation of geopolymer based concrete production: Reviewing current research trends. Journal of Cleaner Production 2011; 19(11): 1229-1238.

[7.13] Marinkovic´ S., Radonjanin V., Malešev M., Ignjatovic´ I. Comparative environmental assessment of natural and recycled aggregate concrete. Waste Management 2010; 30: 2255–2264.

[7.14] Fathifazl G., Abbas A., Razaqpur A.G., Isgor O.B., Fournier B., Foo S. New mixture proportioning method for concrete made with coarse recycled concrete aggregate. Journals of Materials in Civil Engineering 2009: 601–11.

[7.15] Pepe M., Toledo Filho R.D., Koenders E.A.B., Martinelli E. Alternative processing procedures for recycled aggregates in structural concrete. Construction and Building Materials 2014; 69: 124:132.

[7.16] Ferreira L., de Brito J., Barra M. Influence of the pre-saturation of recycled coarse concrete aggregates on concrete properties. Magazine of Concrete Research 2012; 63(8): 617–627.

[7.17] United Nations publication. Indicators of Sustainable Development: Guidelines and Methodologies. United Nations, New York (US), 2007.

[7.18] Agenda 21, Programme of Action for Sustainable Development, adopted at the United Nations Conference on Environment and Development, Rio de Janeiro, Brazil, 1992.

[7.19] Rees W.E., M. Wackernagel. Ecological footprints and appropriated carrying capacity: Measuring the natural capital requirements of the human economy, in Jansson, A. et al.. Investing in Natural Capital: The Ecological Economics Approach to Sustainability, 1994, Island Press, Washington D.C. (US).

[7.20] Global Footprint Network. National Footprint Accounts. Global Footprint Network, Oakland (US), 2010.

[7.21] Kautsky N., Berg H., Folke C., Larsson J., Troell M. Ecological footprint for assessment of resource use and development limitations in shrimp and tilapia aquaculture. Aquaculture Research, 1997; 28: 753–766.

[7.22] Stöglehner G. Ecological footprint – a tool for assessing sustainable energy supplies. Journal of Cleaner Production, 2003; 11: 267–277.

[7.23] Chambers N., Simmons C., Wackernagel M. Sharing nature's interest. Ecological Footprints as an Indicator of Sustainability. Earthscan publications, 2000, London, UK, p. 185.

[7.24] Technical Committee ISO/TC 207 – "Environmental management", Carbon footprint of products - Requirements and guidelines for quantification (ISO 14067); European Committee for Standardization, 2013.

[7.25] Technical Committee ISO/TC 207 – "Environmental management", Environmental labels and declarations -- Type III environmental declarations - Principles and procedures (ISO 14025). European Committee for Standardization, 2006.

[7.26] Guinée J.B., Gorrée M., Heijungs R., Huppes G., Kleijn R., van Oers L., Sleeswijk A., Suh S., Udo de Haes H.A., de Bruijn H., van Duin R., Huijbregts M.A.J. Life cycle assessment: an operational guide to the ISO Standards. Dordrecht (NL): Kluwer Academic Publishers; 2002.

[7.27] Braunscheweig A., Bär P., Rentsch C., Schmidt L., Wüest G. Bewerung in Ökobilanzen mit der Methode der ökologischen Knappheit, Ökofaktoren 1997, Methodik für Oekobilanzen. Buwal Schriftemreihe Umwelt, 297. 100 pp.

[7.28] Goedkoop M., Spriensma R. The Eco-indicator 99, a damage oriented method for Life Cycle Impact Assessment, methodology report. PRé Consultants 2001, B.V. 132 pp. http://www.pre.nl.

[7.29] Jolliet O., Margni M., Charles R., Humbert S., Payet J., Rebitzer G., Rosenbaum R. IMPACT 2002+: A New Life Cycle Impact Assessment Methodology. International Journal of Life Cycle Assessment 2003; 10: 324–330.

[7.30] Regione del Veneto. Decreto della Giunta regionale n. 2015/2013 - Piano Regionale Attività di Cava (PRAC), 2013.

[7.31] ATECAP, Indagine sull'uso degli aggregati riciclati nel calcestruzzo, 2013.

[7.32] Korre A. & Durucan S. Life Cycle Assessment of Aggregates. London: Waste & Resources Action Programme, 2009.

[7.33] Tsoutsos T., Frantzeskaki N., Gekas V. Environmental impacts from the solar energy technologies. Energy Policy 2005; 33: 289-296.

[7.34] US-EPA. AP-42 Compilation of Air Pollutant Emission Factors. U.S. Environmental Protection Agency, 1995.

[7.35] UK NAEI. Vehicle speed emission factors. National Atmospheric Emissions Inventory, 2013, UK.

[7.36] NPI. Emission Estimation Technique Manual for Mining and Processing of Non-Metallic Minerals. Version 2.0. National Pollutant Inventory, 2000, Australia.

8 SCM-concrete with co-combustion fly ashes

8.1 Abstract

The use of Supplementary Cementing Materials (SCMs) is one of the most suitable solution for improving concrete sustainability. The purpose of this section is to compare the effects of two different SCMs on mechanical and durability-related properties of structural concrete. Three mixes were produced, where coal and co-combustion fly ashes were used as partial substitute of cement (20% in volume) and compared with a control/reference concrete. Performances investigated included fresh concrete properties, compressive and tensile strength, elastic modulus, permeability, capillarity and drying/wetting resistance. Results indicate that both the SCMs can be classified as low-carbon fly ashes, and their use in concrete improves the workability of the mixes. A slight reduction of mechanical strength was observed for the concretes including both the SCMs. In addition, concrete transport properties were also slightly reduced when co-combustion fly ash was used. Wetting-drying cycles affected significantly the durability of all the mixes: compressive strength after these cycles was significantly lowered, and the cracks occurred due to the thermal stress applied, appeared to be filled by needle-shape crystals of ettringite.

8.2 Introduction

The use of secondary fuels in coal-fired power plants plays an important role to reduce the emissions of carbon in the atmosphere due to energy industry. A number of experiments with different supplementary fuels are reported in literature, i.e. with municipal sewage sludge, biomass, and refuse-derived fuels [8.1, 8.2, 8.3, 8.4]. Between these, Refuse-Derived Fuels (RDFs), also known as Solid Recovered Fuels (SRFs), are already applied in full-scale coal-fired power plants, such as at the “Andrea Palladio” plant at Fusina, owned by Ente Nazionale per l'Energia eLettrica (ENEL), the major Italian energy provider, and located close to the petrochemical facility of Porto Marghera within the Venice lagoon (Italy). In this plant two thermoelectric units are equipped with a RDF storage, dosage and feeding system; each line is designed for a maximum throughput of 9 ton/hour, corresponding to 70.000 ton/year and about 5% of the whole thermal input. RDF is obtained from the separation of the high

calorific fraction from municipal solid waste, through a mechanical-biological treatment, and it mainly consists in paper and plastics, with minor content of wood and textile. This material has a relatively high lower heating value (LHV) with respect to other supplementary fuels, which makes it particularly suitable for the intended application: it is characterized by an average LHV of 17 MJ/kg, greater than residual waste (10.617 MJ/kg) and paper sludge (2.537 MJ/kg) [8.4, 8.5]. According to the production data of 2013, this plant produces about 49.000 ton/y of coal-fly ash (CFA), and about 155.000 ton/y of co-combustion fly ash (CCFA).

Figure 8-1. The "Andrea Palladio" plant at Fusina, owned by ENEL.

A fundamental issue that should be investigated when using supplementary fuels relates to the quality of fly ash produced during the combustion, as it may be a valuable resource in concrete industry. Coal fly ash has been successfully used in concrete industry since more than 50 years, primarily as mineral admixture in Portland cement concrete and also as a component of blended cement [8.6]. Concerning its first use, fly ash can either partially substitute Portland cement or be applied as an addition into ready-mix concrete at the batch plant [8.7, 8.8]. Usual structural and durability-related properties were widely analyzed in literature [8.9, 8.10, 8.11]. In addition, several authors have attempted to relate some properties of SCM-concretes with parameters such as fly ash fineness [8.12], glass phase content [8.13] soluble and reactive silica content [8.14], water to powder ratio [8.15] and curing conditions [8.16]. Despite a wide literature concerning coal fly ash use as mineral admixture, up to now few works analyzed the application of fly ashes from co-combustion processes in concrete industry, and they are generally focused on a limited number of properties, i.e. cement setting time and

compressive strength [8.17, 8.18], concrete slump and mechanical strength [8.2].

According to the above concepts, the work shown in this section aims to characterize the fly ash produced by the full scale power plant of Fusina (Italy), where coal is co-combusted with RDF, and analyzing some mechanical and durability-related properties of concretes, including fly ash as 20% of replacement of cement. Results are compared with a control/reference concrete without any mineral addition, and another concrete including coal-fly ash produced in another line of the same plant.

8.3 Fly Ashes' Characterization

Two types of fly ashes are used in this work: a light-brown coal-fly ash (CFA) and a dark-grey co-combustion fly ash (CCFA), both produced at the Fusina power plant (Italy). The ashes were subjected to a physical-chemical, mineralogical and morphological characterization.

The particle size distributions of both the FAs were determined by means of laser diffraction particle size analyses. Fig. 8-2 shows the grain size distribution of the considered FAs. CFA has a two-modal distribution, and it is characterized by the following percentile values of the distribution: d_{10}= 4.305µm; d_{50}=12.481µm; d_{90}=55.506µm. CCFA has a Gaussian monomodal distribution, with: d_{10}= 4.589µm; d_{50}=14.494µm; d_{90}=52.43µm. Both the FAs have very small dimension, with about 35% of particles with less than 10µm dimension (PM_{10}), which is particularly advantageous for the reactivity of the material. The cumulative particles grading curve are shown in Figs. 8-3 and 8-4. The specific surface areas are 632 m^2/kg and 582 m^2/kg respectively for CFA and CCFA.

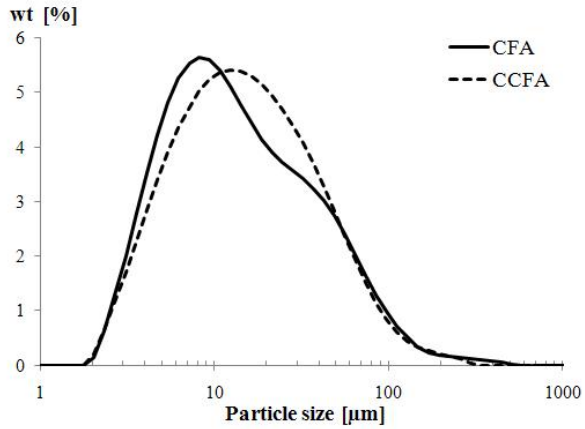

Figure 8-2. Particles size distribution of CFA and CCFA.

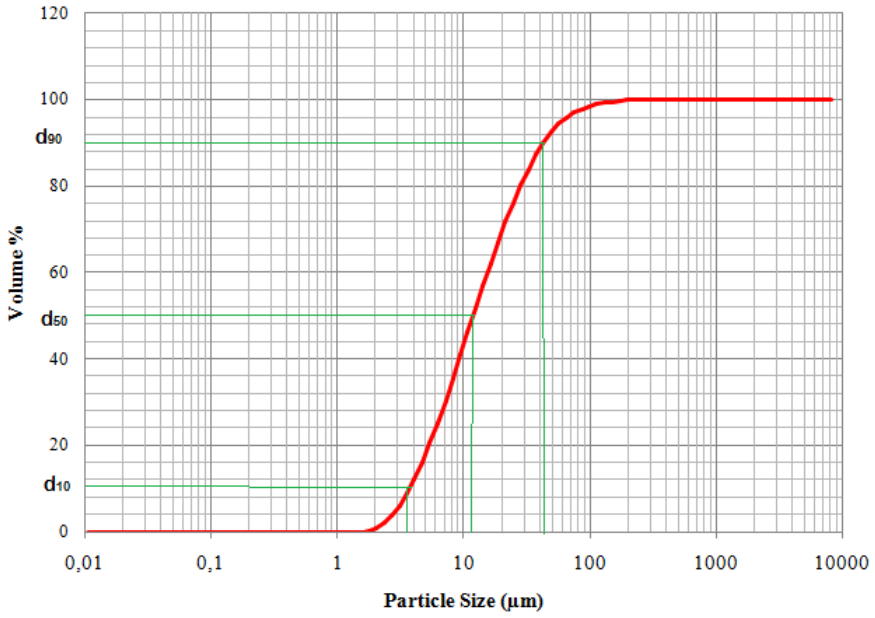

Figure 8-3. Cumulative particles size distribution of CFA.

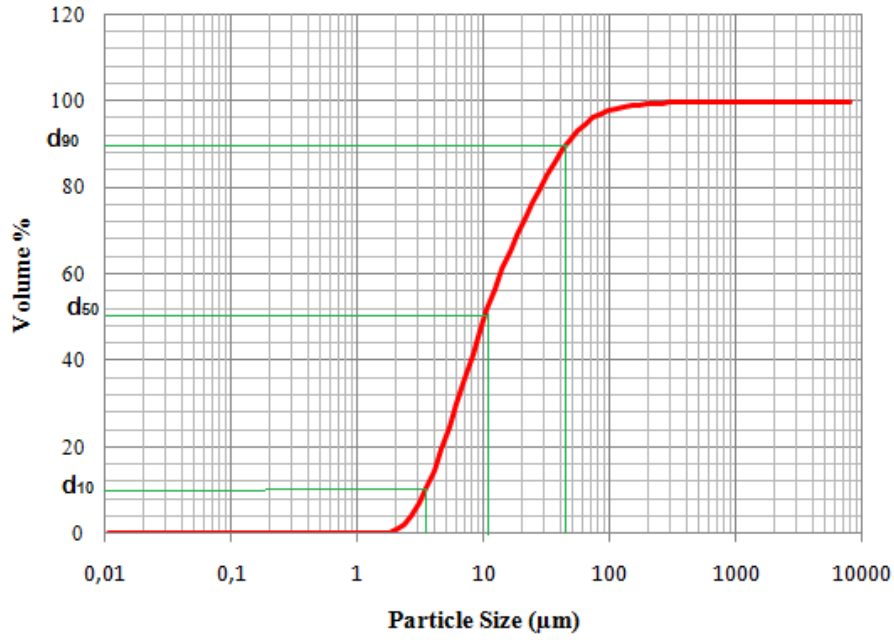

Figure 8-4. Cumulative particles size distribution of CCFA.

The true density was obtained with the pycnometer method, where kerosene was used as fluid, and it results in the range of 2035-2140 kg/m^3 for both the FAs.

Chemical composition was obtained by means of X-Ray Fluorescence spectrometry (XRF), using an Automated XRF Thermo Scientific ARL Advant'X, and major compounds of FAs are listed in Table 8-1. Accordingly, both FAs can be classified as low-calcium fly ashes [8.19].

Loss on ignition (LOI) of solid combustion residues was determined according to [8.20]: this value indicates that CCFA has a relatively high unburned carbon content. During the test, due to coal burning, CCFA changed color from dark grey to brown.

Figure 8-5. Automated XRF Thermo Scientific ARL Advant'X.

Table 8-1. Major chemical compounds of FAs.

Compound	*CFA*		*CCFA*	
	%	*error %*	*%*	*error %*
Na_2O	*2.04*	*± 0.19*	*1.18*	*± 0.17*
MgO	*1.971*	*± 0.06*	*1.693*	*± 0.054*
Al_2O_3	*21.36*	*± 0.07*	*28.48*	*± 0.08*
SiO_2	*52.77*	*± 0.10*	*48.48*	*± 0.09*
SO_3	*1.158*	*± 0.006*	*0.5598*	*± 0.0036*
K_2O	*1.872*	*± 0.013*	*0.8597*	*± 0.0094*
CaO	*2.978*	*± 0.014*	*4.863*	*± 0.017*
TiO_2	*1.030*	*± 0.006*	*1.530*	*± 0.007*
Fe_2O_3	*7.690*	*± 0.015*	*3.422*	*± 0.009*
LOI	*3.63*	*-*	*6.50*	*-*

Fly ashes bulk composition is represented in Fig. 8-6, within the data of other ashes reported in [8.21].

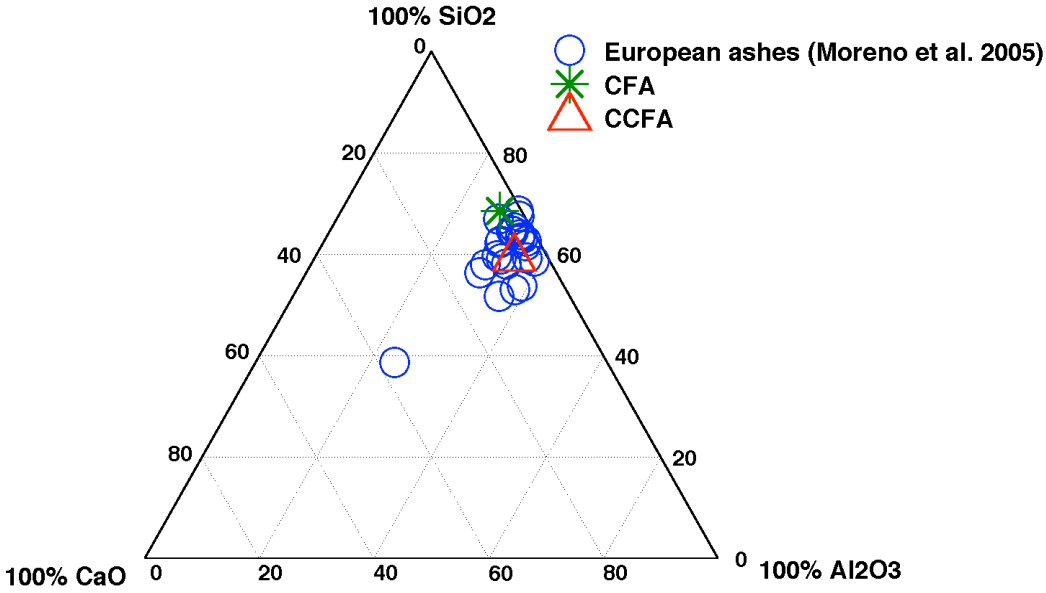

Figure 8-6. Ternary diagram of the average bulk composition of CFA and CCFA.

X-Ray Diffraction (XRD) technique was used to qualitatively identify the crystalline phases of the FAs (look at the Appendix of Section 3 for further information about XRD technique). A diffractometer with nickel-filtered CuKα (λ = 1.5405 Å), at 40 kV and 30 mA, was used. Results are represented in Fig. 8-7: the major non-reactive phases in both the FAs are hematite (Fe_2O_3), mullite ($Al_6Si_2O_{13}$) and quartz (SiO_2). Those phases usually characterize low-calcium ashes (Dhole et al. 2013). In addition, peaks corresponding to magnetite (Fe_3O_4) and kyanite (Al_2SiO_5) were found in CFA, whereas sillimanite (Al_2SiO_5) is present in CCFA. The glass content, which is visible in the XRD patterns as a background, is about the 70 wt% for CFA according to the semi-quantitative estimation of mineral phases made in [8.21].

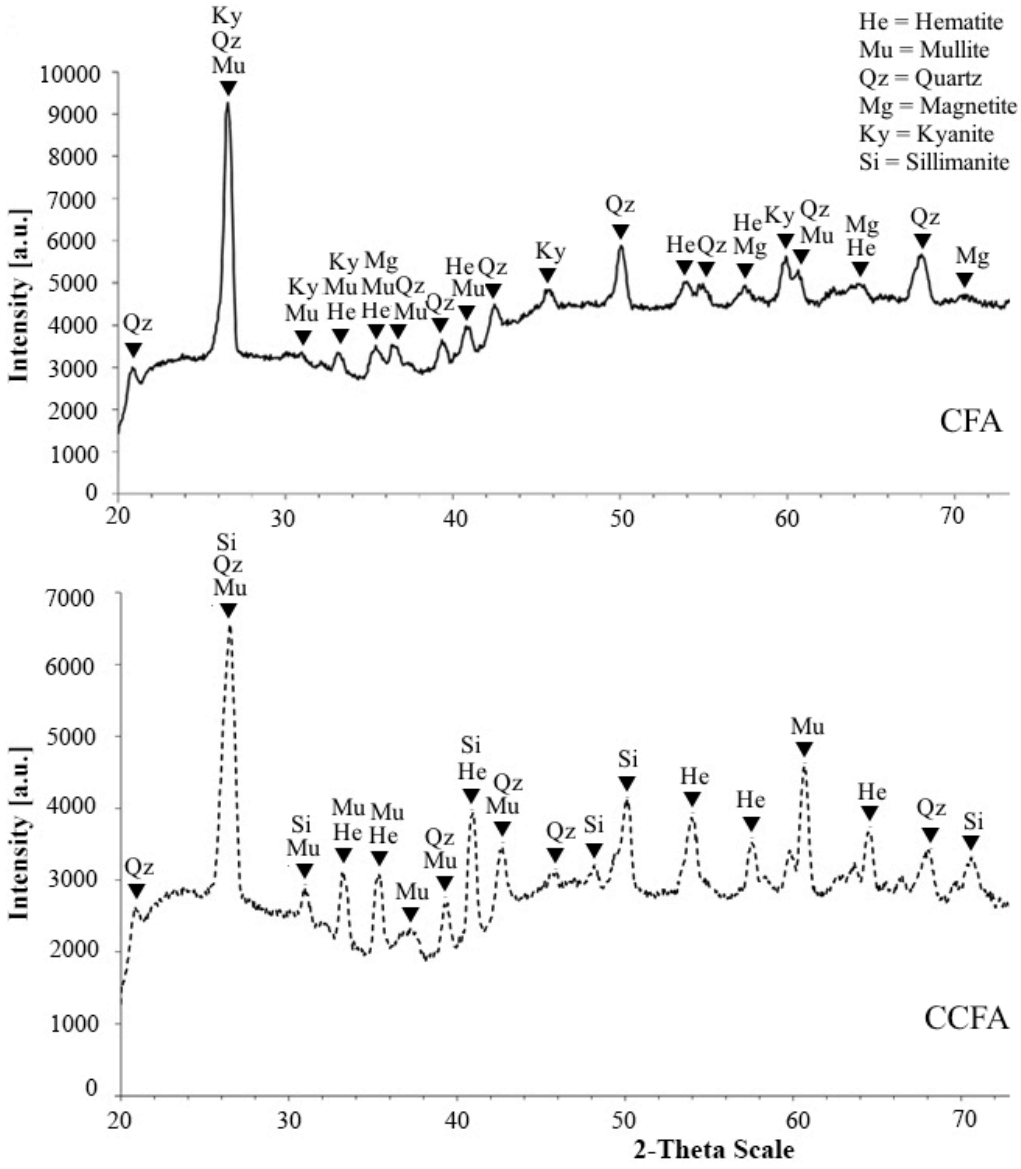

Figure 8-7. Comparison of XRD patterns of CFA (upper) and CCFA (lower).

Scanning Electron Microscope (SEM) images were taken both in the secondary-electrons (SE) mode, with an acceleration voltage of 15 kV, and in the backscattered electrons (BSE) mode, using an accelerating voltage of 25 kV (for further information about SE- and BSE- SEM technique, look at the Appendix of section 3). A Stereoscan equipped with an Energy Dispersive X-Ray spectroscopy (EDS) system was used, and samples were sputtered with gold before the analyses. Figs. 8-8 and 8-9 show images of CFA and CCFA: based on EDS spectra, samples appear as composed of small spherical particles, with medium-size conglomerate

particles formed by alumino-silicate matter, and medium-to-small compact heavy metal-rich particles (mostly Fe), which appears brighter. The texture of both the FAs appears smooth, despite the relative high LOI value, indicating that they underwent an incomplete burning. A pleroshere filled by microsphere is also shown in a CCFA sample (Fig. 8-10).

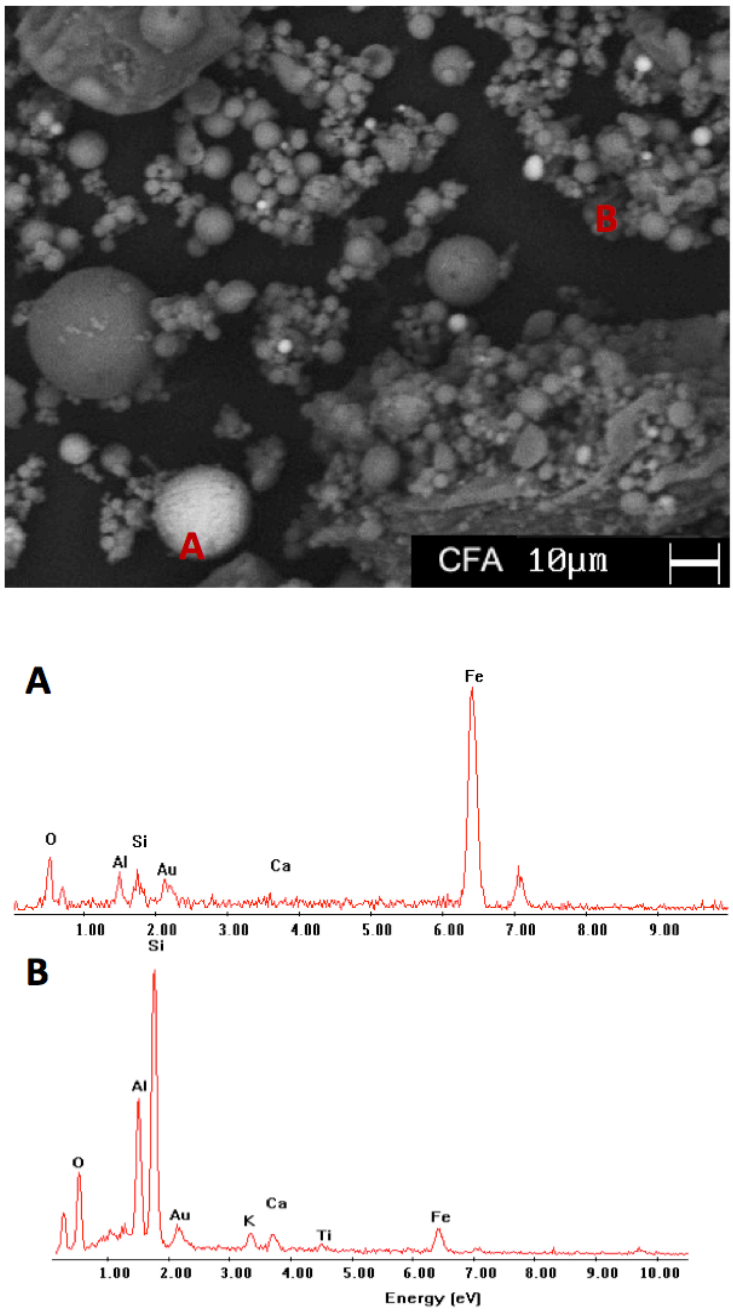

Figure 8-8. BSE-SEM images of CFA.

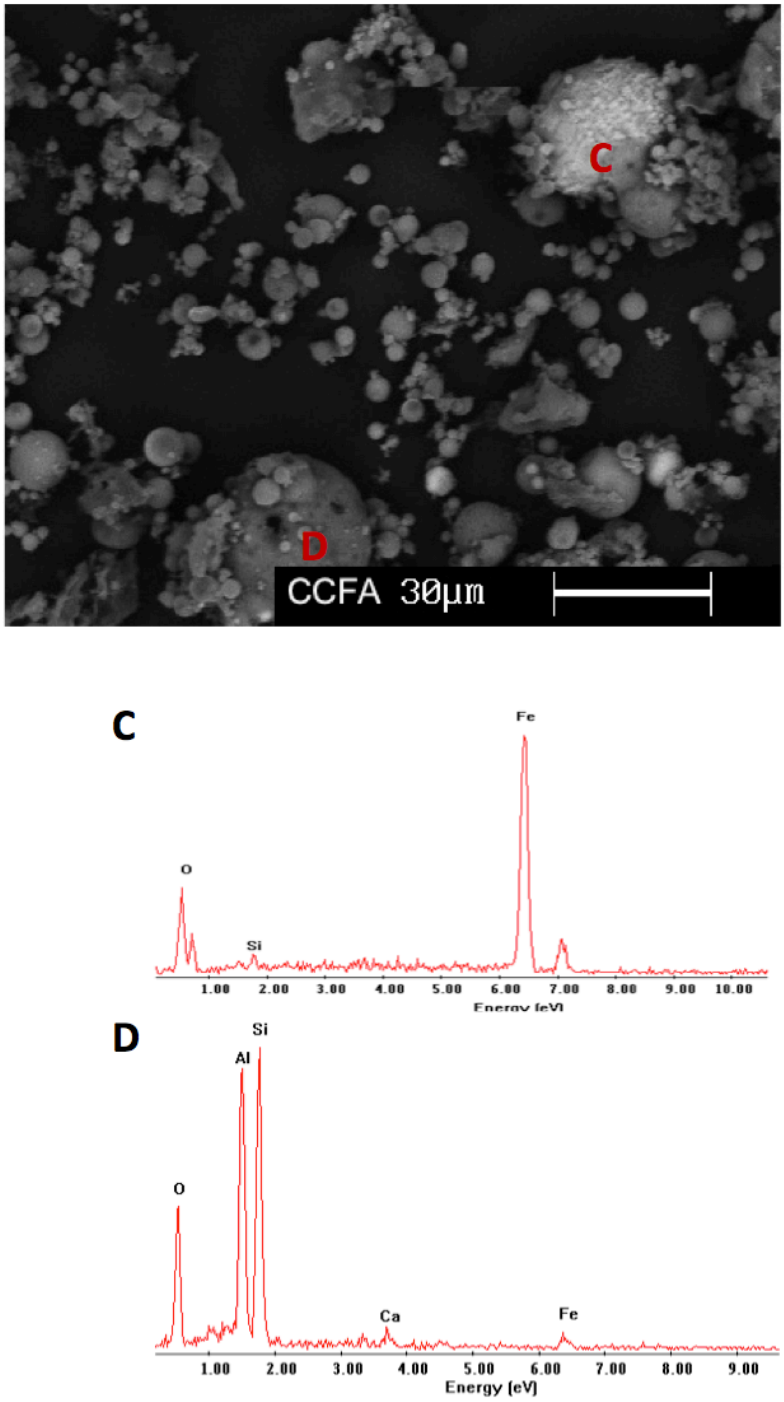

Figure 8-9. BSE-SEM images of CCFA.

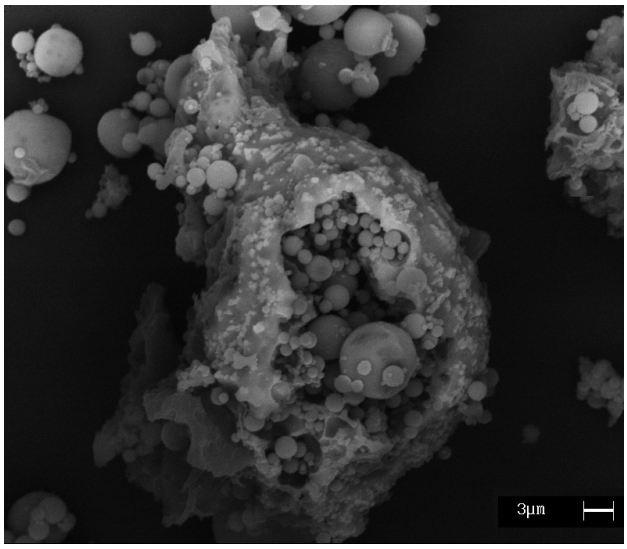

Figure 8-10. BSE-SEM image of a pleroshere in a CCFA sample.

8.4 Experimental Investigation on SCM-Concrete

8.4.1 Materials

The materials used for all the mixes are: Ordinary Portland Cement type I 52.5R class, as defined in [8.22]; natural sand with a 6.3 mm maximum size as fine aggregate; natural coarse aggregates with a 22.4 mm maximum size; a super-plasticizing sulphonated naphtalene admixture; CFA and CCFA described in the previous section.

8.4.2 Mixtures Details

Three different concretes were produced: the first was used as control, and it does not contain any mineral admixture. The others contained CFA and CCFA respectively, with a cement replacement ratio equal to 20% by volume. Water-to-binder ratio, Bolomey aggregates grading curve, super plasticizing admixture content were kept almost constant for all the batches. Table 8-2 illustrates the details of the mix proportions, chosen to reach the following concrete performances: water-to-binder ratio less or equal to 0.5, S4 consistency class according [8.23], cylindrical/cubic compressive strength after 28 days greater than 30/35MPa. During the production of CCFA mix, the water content was slightly reduced because of the high workability reached by the fresh concrete.

Table 8-2. Mix design.

	Control mix	*CFA mix*	*CCFA mix*
Cement [kg/m^3]	*300*	*240*	*240*
CFA [kg/m^3]	*-*	*48*	*-*
CCFA [kg/m^3]	*-*	*-*	*48*
W/(C+FA)	*0.5*	*0.5*	*0.47*
Coarse Aggregates [kg/m^3]	*1030*	*1030*	*1030*
Fine Aggregates [kg/m^3]	*1030*	*1030*	*1030*
SP [kg/m^3]	*3*	*3*	*3*

8.4.3 Experimental methods

After mixing, specimens were properly compacted (Fig. 8-11), covered to limit evaporation, demolded 24 hours after casting, and then cured in standard temperature (20 ± 2°C) and humidity (RH ≥ 95%) conditions until the time of testing.

Compressive strength was measured after 7, 28 and 90 days on cubic specimens with 150 mm side [8.24]. Cylindrical specimens with 100 mm diameter and 200 mm length were used for measuring tensile strength by means of splitting test [8.25]. Secant modulus of elasticity was evaluated according to [8.26]. Load cycles are shown in Fig. 8-12.

Figure 8-11. Specimens casting.

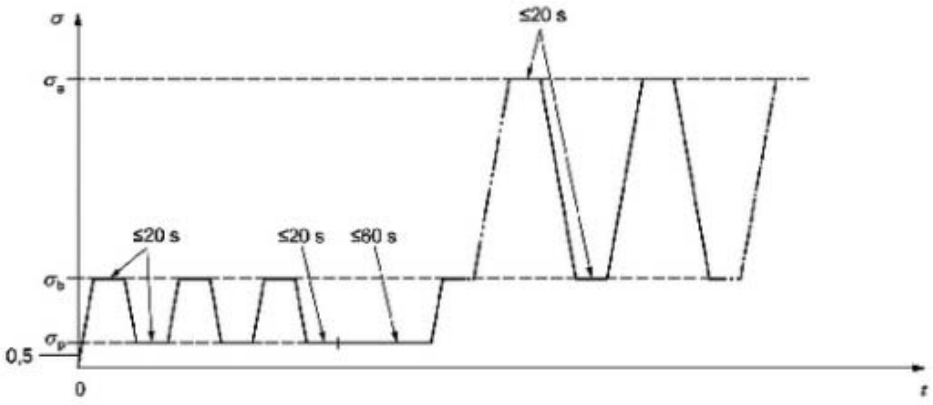

Figure 8-12. Load cycles for evaluating secant elastic modulus.

Durability-related properties were analyzed using the following tests performed after a 28 days standard maturation: water absorption test under atmospheric condition [8.27], water depth penetration under pressure [8.28], and compressive strength tests after wetting/drying cycles. Water absorption was evaluated on 100mm (diameter) x 200mm (height) cylindrical specimens, preliminary dried at 110°C in an electric oven for 24 hours. Then they were dipped in water, with a 5 mm emerging side in the first 24 hours; subsequently, they were completely submerged for other 6 days. Specimens weight is measured after 1, 3, 8, 24 hours, 3, 7 days and then water absorbed is expressed as its percentage on the dried weight. Water depth penetration is measured on 100x100mm cylindrical specimens subjected to a water pressure of 500 ± 50kPa for 72 hours. Then the specimens were cut, and the water profile was measured on the splitting surfaces. Detrimental cycles were performed on 100x200mm cylindrical specimens: the test consisted in 30 daily cycles, in which the specimens were completely immersed in potable water at room temperature for 16 hours, and then dried at 110° C in electric oven for the remaining 8 hours.

For each test, at least three specimens were used and the mean value of these is reported.

8.5 Results and discussion

8.5.1 Mechanical strength and fresh concrete properties

The concretes produced in this experimental campaign belong to the S4 consistency class, with a slump value equal to s=19±1cm (Fig. 8-14). Fresh concrete properties are listed in Table 8-3 together with the results of mechanical strength tests, including compressive, tensile strength and elastic modulus. The use of FA improves the workability of both the SCM-concretes, due to the small round-shape and smooth texture of the particles observed by SEM images, which could be advantageous from the water demand point of view [8.29]. Regarding compressive strength, its evolution in time is plotted in Fig. 8-15.

Figure 8-13. Slump test.

Table 8-3. Fresh concrete properties and mechanical strength at 28 days.

	Control mix	*CFA mix*	*CCFA mix*
Fresh concrete properties			
Density [kg/m^3]	*2438*	*2380*	*2438*
Slump [mm]	*180*	*200*	*200*
Mechanical strength - 28 days			
Density [kg/m^3]	*2436*	*2428*	*2434*
$f_{cm,cube}$ [MPa]	*40.7*	*38.97*	*39.80*
f_{ctm} [MPa]	*3.66*	*3.59*	*3.94*
E_{cm} [GPa]	*31.96*	*30.64*	*30.20*

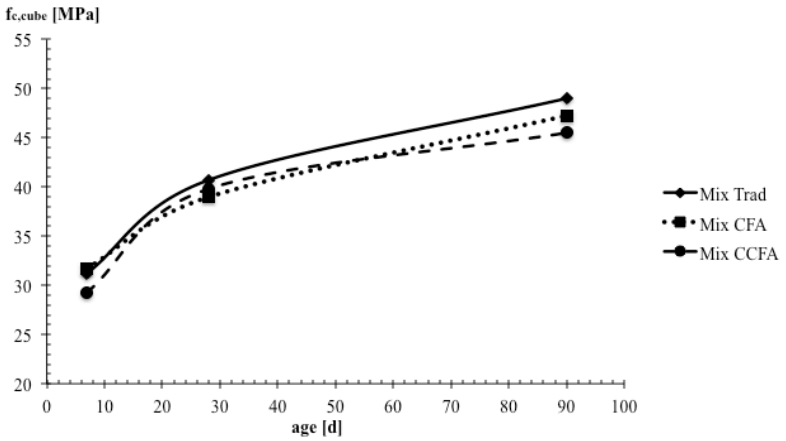

Figure 8-14. Compressive strength evolution with concrete age.

As expected, when SCM partially replaces cement, strength slightly reduces if compared with that of the traditional mix, mainly due to the lower cement content rather than for slower hydration and pozzolanic reactions, occurring for low calcium fly ashes [8-30]. The strength loss is generally similar at each concrete age: the reduction of the gap between control/traditional and FA concrete in time, often reported in literature, is not observed in this work. This can be due to their lower content in available active silica with respect to most of the FAs used in literature, and also to the relatively high water content used in this work. The use of FAs is highly sensible to W/(C+FA) ratio: it is demonstrated that strength reductions are recovered only when low water-to-binder ratios are used [8-31]. In addition, tensile strength is improved of 7.65% when CCFA is used as partial cement replacement. Elastic modulus is slightly reduced in SCM-concretes, with a maximum loss of 5.5% for the CCFA mix.

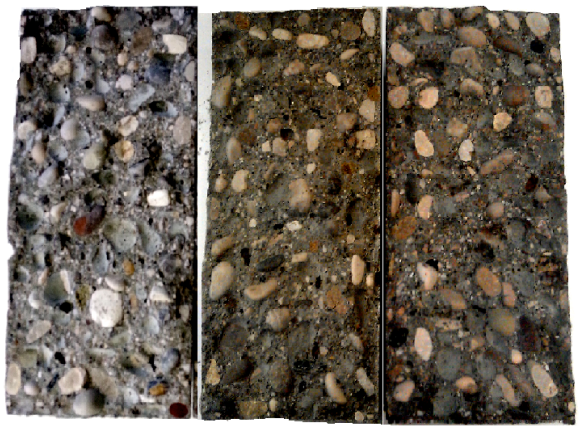

Figure 8-15. Concrete surfaces after splitting failure: Control, CFA and CCFA mix.

8.5.2 Concrete transport properties

Water absorption at atmospheric pressure is the increase in mass of the specimens, expressed as a percentage of the oven-dried mass, due to the quantity of the water absorbed per unit of concrete volume. It can be expressed as:

$$W_i = \frac{M_i - M_0}{M_0} \cdot 100 \qquad \textbf{8-1}$$

where W_i is the absorption at time i, M_i is the mass at time i, and M_0 is the mass oven-dried of the specimen. The cumulative water absorption in time is plotted in Fig. 8.16: the effect of the FAs is beneficial in both the SCM concretes.

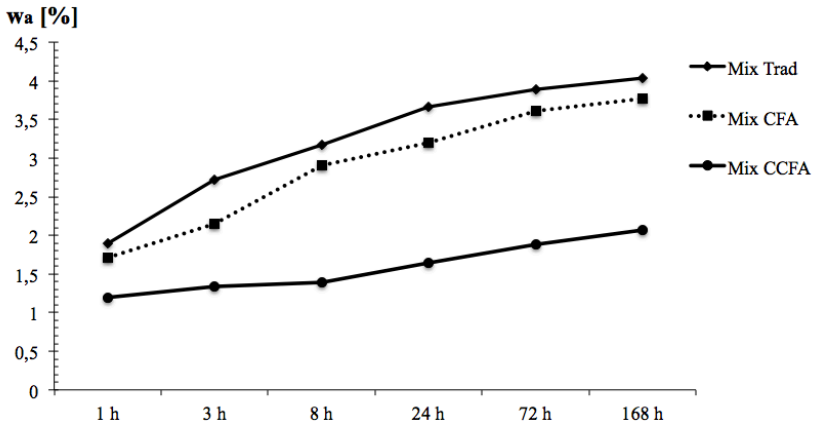

Figure 8-16. Water absorption in time.

Water penetration depth was measured on specimens subjected to a hydraulic pressure equal to 500kPa (Fig. 8-17): results indicate that the partial substitution of the traditional binder slightly increase the water depth profile, for both the analyzed fly ashes, as shown in Fig 8-18. Fig. 8-19 shows a typical water depth profile, measured in a control mix specimen. According to the results of water absorption and water penetration tests it is possible to state that SCM-concretes have a lower porosity matrix, i.e. the volume of pore space in these concretes seems less than in the control/reference mix. Conversely, as the permeability is a measure of the capillary porosity, it is possible to assume that the pores seem more connected in the SCM-concretes. This outcome could be also confirmed by the slight reduction of compressive strength at 28 and 90 days, which depends on the capillary porosity, obtained by the concretes with FAs as partial substitution of cement. However, a proper verification of this result should be confirmed by an analysis of the specimens' microstructure.

Figure 8-17. Water depth penetration test.

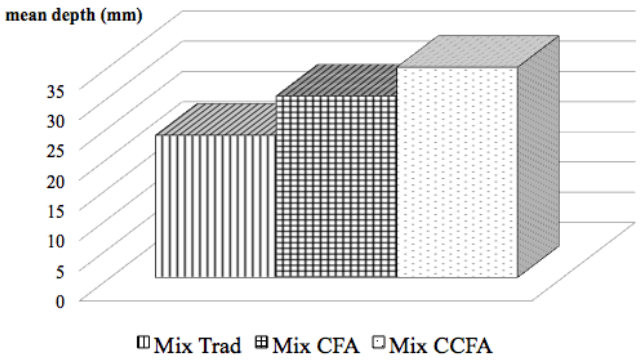

Figure 8-18. Mean water penetration depth.

Figure 8-19. Water penetration depth profile, Control Mix.

8.5.3 Resistance against wetting/drying cycles

Alternate wetting/drying cycles are very detrimental for concrete: they accelerate the damage due to salts crystallization in the pores of the conglomerates, and determine deterioration due to thermal stress. The main effect is the decrease of concrete mechanical strength, i.e. the loss of compressive strength, which occurred for each mix tested. In addition, a gain of weight of the dry-surface specimens was observed for each concrete, which was more significant for the CCFA mix. This could be caused to the cracks' opening, through which water can enter into the specimen. Results after the 30 daily cycles applied to the analyzed specimens are reported in Table 8-4.

Table 8-4. Strength loss due to wetting/drying cycles.

	Control mix	CFA mix	CCFA mix
Mechanical strength - 28 days			
Density [kg/m^3]	2436	2428	2434
$f_{cm,cube}$ [MPa]	40.7	38.97	39.80
Mechanical strength - W/D cycles			
Density [kg/m^3]	2452	2434	2530
$f_{cm,cube}$ [MPa]	32.20	30.72	28.38
$\Delta f_{cm,cube}$ [%]	-20.88	-21.17	-28.69

Concrete surfaces exposed to environmental cycles were analyzed by means of SEM test to check the potential of delayed ettringite formation (DEF), and analyze the paste-aggregates bond surface after the compressive strength test. The extent of damage observed during this work leads to the assumption that another damaging action could be involved, such as the one caused by massive ettringite formation. Often DEF (also known as secondary ettringite) has been found in concretes exposed to heat treatment at high temperature, generally above 70°C [8.32, 8.33]. Its formation has been associated to several causes, including pre-damage of concrete, sulfates and alkali content. In general it is possible to state that DEF occurs in concretes with particular compositional characteristics (SO_3 content in cement around 4% or more), that have undergone heating until 70°C or more, and which have been exposed to a moisture environment [8.34]. According to Batic et al. [8.35] wetting/drying cycles cause large expansion and concrete cracking, and this phenomenon can be attributed mainly to two causes. On one side, there is the action of the water inside the pores and the cracks, especially

in the smallest ones, due to the orientation of water dipoles, which determine significant pressure inside concrete matrix. On the other side, massive ettringite formation participates in concrete damage, even if it is not already clear if it represents the cause or the effect of the expansion. It should be noted that the presence of ettringite does not mean that a damage has occurred, and the simple presence of ettringite in cracks is not diagnostic of DEF-related damage [8.36].

Concerning the influence of fly ash, it generally decreases the expansion due to DEF, and this is partially due to the increased Al_2O_3 content in the binder, available for sulfoaluminate formation [8.37].

On those bases, SEM images were taken in the SE mode with an acceleration voltage of 15 kV, on samples obtained after compressive strength test, which were sputtered with gold. Energy Dispersive X-Ray spectroscopy (EDS) system was used for the microanalysis. The traditional concrete, when not subjected to any detrimental treatment, was not damaged and it appeared rather dense (Fig. 8-20): cracks mainly occurred between the cement paste and the aggregate, and developed through the less resistant part of the matrix, i.e. air voids.

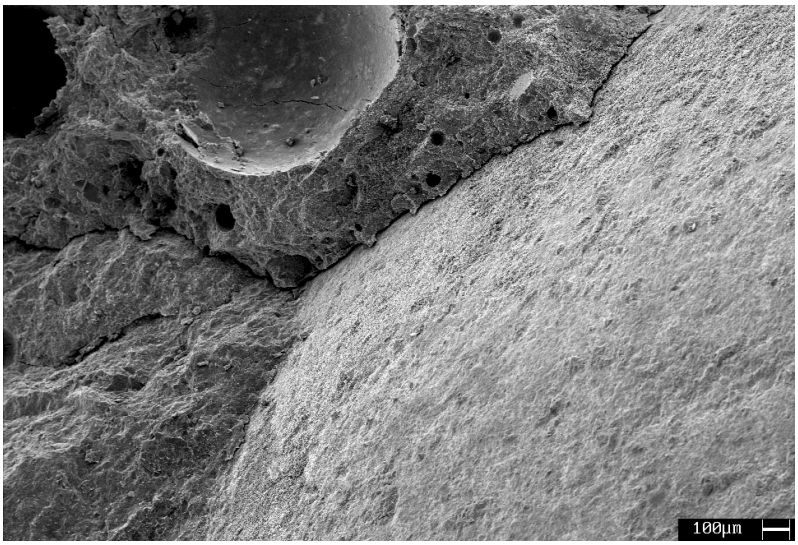

Figure 8-20. SE-SEM magnified view of a crack between aggregate and cement paste (Control mix).

When the specimens were subjected to wetting/drying cycles, the matrix appeared, from a visual inspection, more brittle than the case without cycles. This occurred for all the mixes: SEM images shows micro-cracks with a width of 2-5µm on the surface of the binder matrix (Fig. 8-21), which is directly related to the strength reduction shown in Table 8-4. Cracks appeared to be filled by needle-shape crystals, which were also abundant on concrete surface. Based on EDS analysis, those needles can

be identified as ettringite (Fig. 8-11): the presence of traces of gold are just due to the specimen preparation procedure. Strength reduction can be also associated to the heterogeneous expansion due to secondary ettringite formation in the hardened concrete, which is mainly located in the cracks or in the existing weakness produced by the thermal stress applied with the treatment. The source of sulfates, which determines an internal attack as defined by Collepardi [8.38], can be imputed to the relatively high SO_3 content of the cement used in this work, which is about 3.84% of cement weight. The use of fly ash did not exhibit any additional benefits in wetting/drying resistance, probably due to the high water-to-binder ratio used in this work, which results in a high rate of water transport in the matrix.

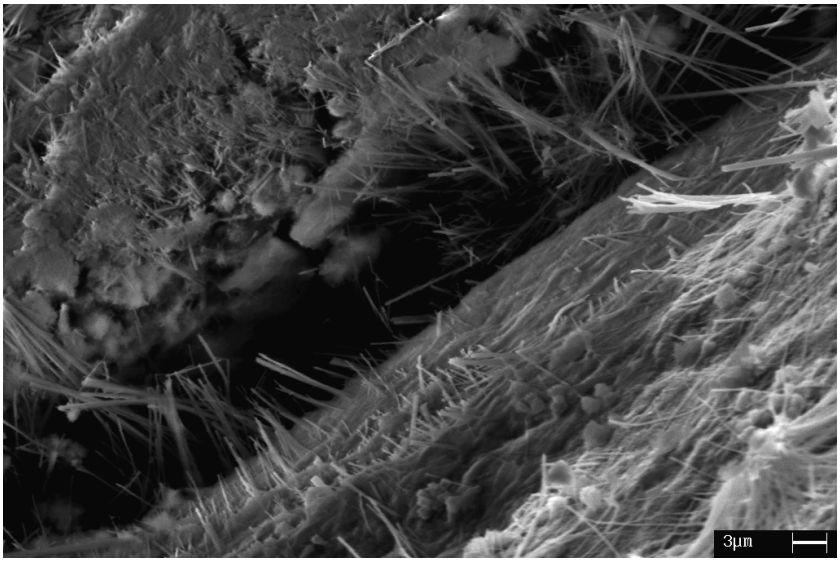

Figure 8-21. SE-SEM image of needle-shape crystals filling a micro-crack (CFA mix).

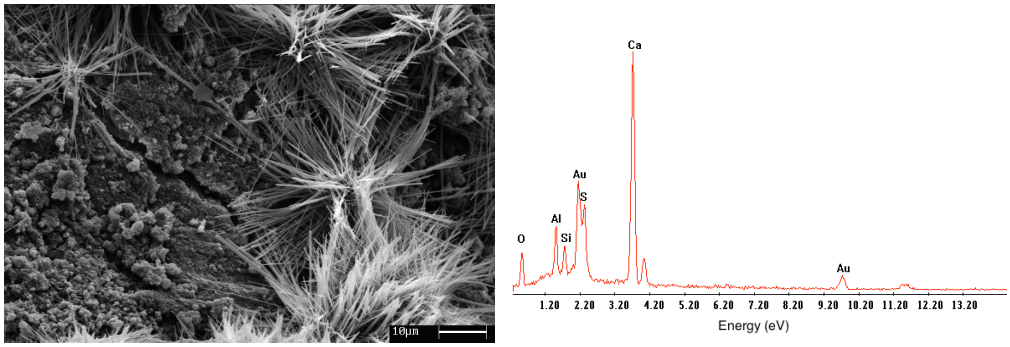

Figure 8-22. On the left: Needle-shape crystals. On the right: EDS spectrum.

8.6 Conclusions

The use of RDF in the Fusina thermal plant allows saving of about 5% of non-renewable resources, contributing to reduce the environmental impacts of the energy industry. When supplementary fuels are used, the quality of the ashes should be analyzed to use them in building materials, because they can be a valuable resource.

According to the results obtained in this section, the following conclusions can be drawn with reference to this specific CCFA:

- The fineness, the small round shape and the smooth texture of FAs improve concrete workability;
- The use of SCMs as 20% replacement in weight of cement allows a saving of 60 kg/m^3 of cement, i.e. about 35 kg CO_2/m^3 according to Table 5-6 of this thesis;
- The use of the SCMs in partial replacement of cement results in a slight decrease in compressive strength of concretes. This gap is not reduced with the curing age, as expected, because of the high W/(C+FA) content used in this experimental campaign. Nevertheless, this reduction does not exceed the 5% in all the analyzed cases, and the produced concretes satisfy the minimum requirements defined in section 8.4;
- The use of CCFA slightly decreases transport properties of the concrete: on one side, the overall porosity of the matrix is reduced, but on the other side the pores appear to be more connected and, as a consequence, its permeability is higher;
- Wetting/drying cycles are very detrimental for the tested concrete: the compressive strength, measured after the treatment, was 20% lower than without any cycles for all the mixes (including control/reference mix). The extent of the damage lead to state that, within the micro-cracking due to the high thermal stress, massive ettringite formation could be involved. Micro-cracks were found to be filled by needle-shape ettringite crystals. The effect of the SCMs was not relevant against wetting/drying resistance.

This work gives some elements for encouraging the use of potentially huge quantities of CCFA for concrete engineering applications and can pave the ground for a more complete assessment of the potential application of various types of fly ashes from co-combustion processes in concrete industry. A particular attention should be paid to fly ash fineness, texture, unburned carbon and glassy phase content, within bulk oxides composition, which are parameters affecting fresh and hardened concrete

properties. In addition, their elemental composition should be analyzed to check the environmental compatibility.

8.7 Appendix

8.7.1 Compressive strength results

For each mixture, three samples were tested to evaluate compressive strength at 28 days. When possible, also at 7 days three samples were tested. Results are listed in Table 8-5 and Table 6-6.

Table 8-5. Compressive strength at 7 days.

#	Density [kg/m^3]	$f_{c.cube}$ [MPa]	Ultimate Load [kg]	Mix	Density [kg/m^3]	$f_{cm.cube}$ [MPa]
Trad 1	2453	32.00	72000	Trad	2457	31.75
Trad 2	2462	31.50	71000			
Mix CFA 1	2349	33.40	73000	Mix CFA	2337	32.80
Mix CFA 2	2326	32.20	72500			
Mix CCFA 1	2462	29.80	67000	Mix CCFA	2454	29.90
Mix CCFA 2	2447	30.00	67500			

Table 8-6. Compressive strength at 28 days.

#	Density [kg/m^3]	$f_{c.cube}$ [MPa]	Ultimate Load [kg]	Mix	Density [kg/m^3]	$f_{cm.cube}$ [MPa]
Trad 1	2433	40.20	90500	Trad	2436	40.70
Trad 2	2465	42.40	95500			
Trad 3	2410	39.5	89000			
Mix CFA 1	2412	39.40	91000	Mix CFA	2428	38.97
Mix CFA 2	2415	39.00	90000			
Mix CFA 3	2457	38.50	89000			
Mix CCFA 1	2442	40.10	92500	Mix CCFA	2434	39.80
Mix CCFA 2	2400	39.40	91000			
Mix CCFA 3	2460	39.80	92000			

8.7.2 Tensile strength results

For each mixture, three samples were tested to evaluate tensile strength at 28 days. Results are listed in Table 8-7.

Table 8-7. Tensile strength results.

#	Density [kg/m^3]	f_{ct} [MPa]	Ultimate Load [kg]	Mix	f_{ctm} [MPa]
Trad 1	2458	3.66	11500	Trad	3.66
Trad 2	2424	3.66	11500		
Mix CFA 1	2407	3.51	11000	Mix CFA	3.59
Mix CFA 2	2402	3.29	10300		
Mix CFA 3	2458	3.99	12500		
Mix CCFA 1	2484	3.94	12300	Mix CCFA	3.62
Mix CCFA 2	2458	4.09	12800		
Mix CCFA 3	2470	3.87	11900		

8.7.3 Elastic modulus results

For each mixture, three samples were tested to evaluate the secant modulus of elasticity. Results are listed in Table 8-8.

Table 8-8. Elastic modulus results.

#	E_c [Mpa]	Mix	$E_{cm.}$ [Mpa]
Trad 1	32650		
Trad 2	30700	Trad	319625
Trad 3	31900		
Trad 4	32600		
Mix CFA 1	29580		
Mix CFA 2	30170	Mix CFA	30640
Mix CFA 3	32180		
Mix CCFA 1	26870		
Mix CCFA 2	31130	Mix CCFA	30200
Mix CCFA 3	32620		

8.7.4 Compressive strength results after wetting/drying cycles

For each mixture, three samples were tested to evaluate compressive strength after wetting/drying cycles. Results are listed in Table 8-9.

Table 8-9. Compressive strength after wetting/drying cycles.

#	Density [kg/m^3]	$f_{c.cube}$ [MPa]	Mix	Density [kg/m^3]	$f_{cm.cube}$ [MPa]
Trad 1	2453	32.30	Trad	2452	32.20
Trad 2	2450	32.00			
Mix CFA 1	2471	33.05	Mix CFA	2434	30.72
Mix CFA 2	2401	30.72			
Mix CFA 3	2429	28.40			
Mix CCFA 1	2532	30.72	Mix CCFA	2530	28.38
Mix CCFA 2	2529	26.05			

References

[8.1] Wolski N., Maier J., Hein K.R.G. Fine particle formation from co-combustion of sewage sludge and bituminous coal. Fuel Processing Technology 2004; 85: 673-686.

[8.2] Sarabèr A.J. Co-combustion and its impact on fly ash quality; full-scale experiments. Fuel Processing Technology 2014; 128: 68-82.

[8.3] Wu H., Pedersen A.J., Glarborg P., Frandsen F.J., Dam-Johansen K., Sander B. Formation of fine particles in co-combustion of coal and solid recovered fuel in a pulverized coal-fired power station. Proceedings of the Combustion Institute 2011; 33: 2845-2852.

[8.4] Rigamonti L., Grosso M., Biganzoli L. Environmental assessment of Refuse-Derived Fuel Co-Combustion in a Coal-Fired Power Plant. Journal of Industrial Ecology 2012: 16(5): 748-760.

[8.5] Wan H-P., Chang Y-H., Chien W-C., Lee H-T., Huang C.C. Emissions during co-firing of RDF-5 with bituminous coal, paper sludge and waste tires in a commercial circulating fluidized bed co-generation boiler, Fuel 2008; 87(6): 761-767.

[8.6] Bouzoubaâ N., Zhang M-H., Malhotra V.M., Golden D.M. Blended Fly Ash Cements - A Review. ACI Materials Journal 1999; 96(6): 641-650.

[8.7] Siddique R., Khatib J.M. Abrasion resistance and mechanical properties of high-volume fly ash concrete. Materials and Structures 2010; 42(5): 709–718.

[8.8] Siddique R. Performance characteristics of high-volume Class F fly ash concrete. Cement and Concrete Research 2004; 34(3): 487–493.

[8.9] Papadakis V.G., Tsimas S. Supplementary cementing materials in concrete. Part I: efficiency and design. Cement and Concrete Research 2002; 32: 1525-1532.

[8.10] Papadakis V.G., Antiohos S., Tsimas S. Supplementary cementing materials in concrete. Part II: A fundamental estimation of the efficiency factor. Cement and Concrete Research 2002; 32: 1533-1538.

[8.11] Aponte D.F., Barra M., Vàzquez E. Durability and cementing efficiency of fly ash in concrete. Construction and Building Materials 2012; 30: 537-546.

[8.12] Bentz D.P., Garboczi E.J. Simulation Studies of the Effects of Mineral Admixtures on the Cement Paste-Aggregate Interfacial Zone. ACI Materials Journal 1991; 88(5): 518-529.

[8.13] Aughenbaugh K. L., Chancey R.T., Stutzman P., Juenger M.C., Fowler D.W. An examination of the reactivity of fly ash in cementitious pore solutions. Materials and Structures 2013; 46: 869-880.

[8.14] Ranganath R.V., Bhattacharjee B., Krishnsmoorthy S. Influence of size fraction of ponded ash on its pozzolanic activity. Cement and Concrete Research 1998, 28(5): 749-761.

[8.15] Siddique R., Aggarwal P., Aggarwal Y. Influence of water/powder ratio on strength properties of self-compacting concrete containing coal fly ash and bottom ash. Construction and Building Materials 2012; 29: 73-81.

[8.16] Eren O. Strength development of concretes with ordinary Portland cement, slag or fly ash cured at different temperatures. Materials and Structures 2002; 235: 536-540.

[8.17] Sarabèr A.J. Co-combustion and its impact on fly ash quality; pilot-scale experiments. Fuel Processing Technology 2012; 104: 105-114.

[8.18] Tkaczewska E., Mróz R., Łój G. Coal–biomass fly ashes for cement production of CEM II/A-V 42.5R. Construction and Building Materials 2012; 28: 633-639.

[8.19] ASTM C618-12a. Standard Specification for Coal Fly Ash and Raw or Calcined Natural Pozzolan for Use in Concrete. American Society for Testing and Materials, Annual book of ASTM Standards, Vol. 04.02, West Conshohocken, PA; 2012.

[8.20] EN 196-2. Method of testing cement - Part 2: Chemical analysis of cement. Comité Européen de Normalisation, Brussels, Belgium; 2013.

[8.21] Moreno N., Querol X., Andrés J.M., Stanton K., Towler M., Nugteren H., Janssen-Jurkovicová M., Jones R. Physico-chemical characteristics of European pulverized coal combustion fly ashes. Fuel 2005; 84: 1351-1363.

[8.22] EN 197-1. Cement - Part 1: Composition, specification and conformity criteria for common cements. Comité Européen de Normalisation, Brussels, Belgium; 2006.

[8.23] EN 206-1. Concrete - Part 1: Specification, performance, production and conformity. Comité Européen de Normalisation, Brussels, Belgium; 2006.

[8.24] EN 12390-4. Testing hardened concrete – compressive strength – specification for testing machines. Comité Européen de Normalisation, Brussels, Belgium; 2000.

[8.25] EN 12390-6. Testing hardened concrete – tensile splitting strength of test specimens. Comité Européen de Normalisation, Brussels, Belgium; 2009.

[8.26] EN 12390-13. Testing hardened concrete – Determination of secant modulus of elasticity in compression. Comité Européen de Normalisation, Brussels, Belgium; 2013.

[8.27] UNI 7699. Testing hardened concrete - Determination of water absorption at atmospheric pressure. Ente Nazionale Italiano di Unificazione, Milano, Italia; 2005 [in Italian].

[8.28] EN 12390-8. Testing hardened concrete - Depth of penetration of water under pressure. Comité Européen de Normalisation, Brussels, Belgium; 2009.

[8.29] Chindaprasirt P., Homwuttiwong S., Sirivivatnanon V. Influence of fly ash fineness on strength, drying shrinkage and sulfate resistance of blended cement mortar. Cement and Concrete Research 2004; 34: 1087-1092.

[8.30] PapadakisV.G. Effect of fly ash on Portland cement systems: Part I. Low-calcium fly ash. Cement and Concrete Research 1999; 29: 1727-1736.

[8.31] Dunstan M.R.H. Fly Ash as the 'Fourth Ingredient' in Concrete Mixtures. ACI SP 1996; 91: 171-200.

[8.32] Diamond S. Delayed Ettringite Formation - Process and Problems. Cement and Concrete Composites 1996; 18: 205-215.

[8.33] Odler I., Chen Y. On the Delayed Expansion of Heat Cured Portland Cement Pastes and Concrete. Cement and Concrete Composites 1996; 18: 181-185.

[8.34] Pavoine A., Brunetaud X., Divet L. The impact of cement parameters on Delayed Ettringite Formation. Cement and Concrete Composites 2012; 34: 521-528.

[8.35] Batic O., Milanesi C.A., Maiza P.J., Marfil S.A. Secondary ettringite formation in concrete subjected to different curing conditions. Cement and Concrete Research 2000, 30(9): 1407-1412.

[8.36] Scrivener K., Skalny J.P. Conclusions of the International RILEM TC 186-ISA Workshop on Internal Sulfate Attack and Delayed Ettringite Formation (4-6 September 2002, Villars, Switzerland). Materials and Structures 2005; 38: 659-663.

[8.37] Taylor H.F.W., Famy C., Scrivener K.L. Delayed ettringite formation. Cement and Concrete Research 2001; 31: 683-693.

9 Conclusions

In the last decade the pursuit of sustainable development in concrete industry has widely grown. A number of initiatives arose to meet the request to produce building materials reducing environmental emissions and natural resources exploitation. The most important concrete and cement producers are implementing identified good practices at their operating facilities to reach the goal of “zero-emission” products. However, just a limited number of technical solutions have been widely analyzed in literature and are currently included in standardized normative, guidelines and codes.

This thesis aimed to investigate the potential application of some recycled materials to be used for structural concrete production: it covers the use of EAF slag and recycled coarse aggregate as substitute of natural gravel, and the use of co-combustion fly ashes as partial cement replacement. A thorough review of the available scientific literature about recycled component utilization in concrete has been carried out. From this initial survey, the necessity to study in deep some particular features of recycled concrete has emerged, in particular concerning the use of metallurgical slag as concrete aggregate, and about rheology of fresh recycled concrete, which are just limited studied in literature.

The first part of this thesis was devoted to analyze the mechanical and durability-related properties of concretes with EAF slag as aggregate for structural concrete. The principal results indicate that the proposed pre-treatment to the slag allows its safe use in concrete, both in terms of dimensional stability and environmental compatibility. The use of EAF slag as coarse aggregate increased the mechanical strength of the concrete; on the contrary, its use is not recommended as sand replacement. The typical rough texture and the angular shape of the slag allow the development of very strong interlocking properties with the cementitious matrix, improving the mechanical strength of the concrete. RC elements were also produced and tested to analyze the ultimate bending and shear capacities. The predicting equations of the Eurocode 2 and ACI code were applied to the experimental results, obtaining that the code predictions for the ultimate shear are overly conservative, also for the reference beams. The high specific weight of this concrete may represent a limit for its application, however there are a number of possible applications where it can be considered a pro, i.e. for retaining walls, foundations, and in concretes with radiation shielding properties. Furthermore, a tool for evaluating environmental emissions of aggregates and concretes with a life-cycle approach was developed, and it was applied to quantify the

emissions reduction due to the use of EAF slag. It was observed that the principal responsible of concrete emissions is the cement content in the paste: hence, if it is possible to reduce it, even in a small amount, without decreasing the mechanical properties of the mix, the environmental burdens are highly reduced.

In the second part of this thesis the problem of rheology of fresh recycled concrete was investigated. In this case recycled aggregates coming from construction and demolition waste (C&DW) were used. An extensive experimental campaign was carried out to derive yield stress and plastic viscosity of a number of mixtures, aiming to correlate the recycled aggregate proportioning method to the behavior of the fresh concrete. In addition, an empirical formula was proposed to correlate concrete slump to the yield stress of recycled concrete. The LCA tool was also applied to recycled aggregate coming from C&DW to estimate the environmental benefit coming from their use. A further environmental indicator was used to analyze the abiotic depletion problem: for instance, it has been shown that for an existing quarry, the service life of the plant can be extended of about the 40%, reducing the extraction of the natural aggregates and increasing the productivity of the C&DW recycling plant.

Lastly, the use of supplementary cementitious material was analyzed: this alternative solution allows to directly save cement, reducing the impacts of the concrete. In this case, a co-combustion fly ash was used, obtaining positive results in terms of mechanical and durability properties.

10 Ongoing work and future developments

The results derived in this thesis may pave the ground for further studies related to the use of recycled aggregates coming both from construction and demolition waste and metallurgical by-products in structural concrete for several engineering applications. Currently there is a lack of knowledge about many durability-related properties of concretes with EAF slag, and few studies about their use in RC structures are reported in literature. In addition, no guidelines are available for a correct design of concretes' mixtures with EAF slag, thus representing the main limit to its application in real-scale structures.

Accordingly, further tests are needed to analyze the transport properties of EAF slag concrete, and in particular an extensive experimental campaign about the diffusion of chlorides and the corrosion of steel bars in RC structures made by EAF concrete has already started. Those results will be used to predict service life of structures produced with this material, exposed in chloride environment.

Furthermore, tests on real-scale beam-column joints will be conducted, with the aim to verify the potential application of this concrete in structures subjected to seismic loads. The high specific weight of the concrete may represent a limit which can hinder this application, and hence it should be accurately examined. Although the high specific weight can be a limit for several applications in RC structures, some recent scientific studies have highlighted also the possibility to apply EAF slag in heavy-weight concrete, due to its high density. Hence, its application may be suitable to produce panels with radiation shielding properties, with a reduced thickness with respect to the traditional ones obtained with baritic concretes. This will be another interesting research topic that could give promising results to provide alternative uses of the slag in the concrete industry.

Concerning the use of recycled aggregates coming from C&DWs, there are still a number of properties of recycled concrete which are not completely understood. The use of mesoscale models can be suitable to understand the influence of recycled aggregates properties on the damage behavior and durability properties of recycled concrete. As a matter of fact, concrete has a highly heterogeneous microstructure, which should be accounted with the properties of its individual component, for properly deriving its macroscopic constitutive behavior. In the case of recycled concrete, heterogeneities increase, because recycled aggregates can be considered as a two-phase material, made by the virgin aggregate and the adhered mortar. Numerical simulations of concrete at mesoscopic level are considered to be an important tool for understanding recycled concrete

properties, when coupled with experimental campaigns. Hence, the effect of the adhered mortar on the ITZ zone properties, and consequently on the overall behavior of concrete can be investigated.